Identification and Characterization of Proteins Involved in *C. elegans* EGF-Receptor Localization

---

Dissertation

zur

Erlangung der naturwissenschaftlichen Doktorwürde
(Dr. sc. nat.)

vorgelegt der

Mathematisch-naturwissenschaftlichen Fakultät

der

Universität Zürich

von

Peter Gutierrez

aus

Inkwil BE

Promotionskomitee

Prof. Dr. Alex Hajnal, Universität Zürich (Vorsitz)

Prof. Dr. Monica Gotta, Université de Genève

Prof. Dr. Nancy Hynes, Friedrich Miescher Institut Basel

Dr. Gino Poulin, University of Manchester

Zürich, 2009

TO THOSE I HOLD DEAR

TABLE OF CONTENTS

Zusammenfassung **7**

Summary **9**

Abbreviations **11**

1. General introduction **13**

1.1 The ErbB signalling network 13

1.2 Trafficking of ErbBs and its influence on signalling 14

1.3 PDZ-domains are interaction modules found in plasma membrane scaffold proteins 15

1.4 FERM-domain proteins: linkers between the membrane and the cytoskeleton 16

1.5 The model organism *Caenorhabditis elegans* 16

1.6 The EGFR system in *C. elegans* 17

1.7 Vulval development 18
1.7.1 Vulval induction and patterning 18
1.7.2 The LET-23 EGFR pathway promotes the 1° vulval cell fate 18
1.7.3 The LIN-12 Notch pathway promotes the 2° vulval cell fate 19
1.7.4 GAP-1 is an inhibitor of LET-60 19
1.7.5 LIP-1 is a negative regulator of MPK-1 20
1.7.6 DEP-1 is a negative regulator of LET-23 20
1.7.7 The synMuv genes negatively regulate vulval development 21
1.7.8 The small GTPase RHO-1 is a positive regulator of 1° cell fate specification 21
1.7.9 Execution of the vulval fates 21
1.7.10 LET-23 expression and localization during vulval development 22
1.7.11 The ternary complex LIN-7/LIN-2/LIN-10 22

1.8 Chapter figures 24

2. Objectives of this study **27**

3. Part I: A reverse genetics approach to identify regulators of LET-23 localization **28**

3.1 Characterization of *frm-8* 28
3.1.1 Preliminary data 28
3.1.2 Isolation of the *frm-8(zh67)* allele 28
3.1.3 *frm-8(zh67)* appears to mislocalize LET-23 in the VPCs 28
3.1.4 *frm-8(zh67)* shows a weak genetic interaction with the LET-23 pathway 29
3.1.5 Downregulation of FERM genes in *frm-8(zh67)* does not result in a synthetic vulval phenotype, nor in enhanced mislocalization of LET-23 30
3.1.6 Expression pattern of *frm-8* 30

3.2 Characterization of *tag-60* 31
3.2.1 General gene information and alleles 31
3.2.2 TAG-60 is the putative *C. elegans* orthologue of EBP-50/NHE-RF1 32
3.2.3 TAG-60 is a putative regulator of LET-23 localization 33
3.2.4 *tag-60(zh93)* genetically interacts with mutants of the LET-23 pathway 33
3.2.5 *egl-17::cfp* expression is reduced in the 1° cells of *tag-60(zh93)* 35
3.2.6 *zh93* is a dominant allele of *tag-60* 36
3.2.7 Expression analysis of *tag-60* 37
3.2.8 Investigation of the cellular focus of *tag-60* 38
3.2.9 αTAG-60-1 recognizes a putative novel TAG-60 isoform of ~80kDa 40

3.3 Characterization of *erm-1* 42
3.3.1 ERM-1 is the orthologue of Ezrin, Radixin and Moesin 42
3.3.2 *erm-1* is an essential gene involved in tubular morphogenesis 43
3.3.3 ERM-1 is necessary for TAG-60 localization in *C. elegans* 44
3.3.4 LET-23 appears to be mislocalized in *erm-1(tm677)* animals 44
3.3.5 *erm-1(tm677)* genetically interacts with the LET-23 pathway 45
3.3.6 ERM-1::CFP is localized to the basolateral membrane of the VPCs 46
3.3.7 ERM-1::CFP associates with LET-23 47

3.4 Discussion 48
3.4.1 *frm-8* is unlikely a regulator of the LET-23 pathway 49
3.4.2 TAG-60 may be the *C. elegans* orthologue of EBP-50 and NHE-RF2 50
3.4.3 TAG-60 might be involved in LET-23 retention at the basolateral membrane of the VPCs 50
3.4.4 The *tag-60(zh93)* allele interacts genetically with the LET-23 pathway 51
3.4.5 *zh93* is a dominant allele of *tag-60* 53
3.4.6 A cell non-autonomous role of TAG-60 during vulval development? 54
3.4.7 TAG-60a::YFP fusion proteins localize to plasma mebrane compartments 56
3.4.8 The *tag-60* locus encodes more than 5 isoforms 57
3.4.9 ERM-1 and TAG-60 might form a complex 58
3.4.10 ERM-1 is a putative regulator of LET-23 retention or recycling at the basolateral membrane of the VPCs 58
3.4.11 ERM-1 is a novel negative regulator of vulval development 59
3.4.12 ERM-1::CFP is localized to the basolateral membrane of the VPCs 60
3.4.13 Putative mechanisms for ERM-1 function during vulval development 60
3.4.13.1 Models for *C. elegans* ERM-1 activation 61
3.4.13.2 Putative ERM-1 effectors 61

3.5 Methods 63
3.5.1 General methods and alleles 63
3.5.2 Buffers 63
3.5.3 RNA-interference 65
3.5.4 Purification of polyclonal TAG-60 antibodies 65
3.5.5 Whole-mount immunostaining 66
3.5.6 Scoring the VPC induction index 67
3.5.7 Generation of *C. elegans* gene knockout libraries 68
3.5.8 Screening the *C.elegans* gene knockout-libraries 70
3.5.9 Genotyping PCR assays 71

3.5.10 DNA constructs 75
3.5.11 Quantification of *egl-17::cfp* expression 76
3.5.12 Lifespan assay 77
3.5.13 Protein alignments 77
3.5.14 Western Blot 77

3.6 Chapter figures 79

4. Part II: A forward genetic screen for *gap-1(lf)* interactors 102

4.1 Introduction 102
4.1.1 GAP-1 is a negative regulator of the EGFR/Ras/MAPK pathway 102
4.1.2 Rationale of the forward genetic screen 103

4.2 Results 104
4.2.1 Isolation of six mutant alleles 104
4.2.2 *zh96* is a novel allele of *lin-2* 105
4.2.3 *zh98* is a novel allele of *lin-7* 105
4.2.4 *zh94* is a novel allele of the Ras inhibitor *gap-3* 106
4.2.5 *zh95* is a putative allele of *lin-13* 108
4.2.6 *zh99* affects the gene encoding LET-19, a mediator subunit 111
4.2.7 *zh78* is a putative allele of *lin-1* 112
4.2.8 Summary 113

4.3 Discussion 114
4.3.1 A *gap-1(lf)* enhancer screen can reveal factors involved in LET-23 localization 114
4.3.2 *zh94* is a mutant allele of the conserved RasGAP gene *gap-3* 115
4.3.3 *zh95* is a putative allele of *lin-13* 116
4.3.4 *zh99* is most likely an allele of *let-19/mdt-13* 117
4.3.5 *zh78* might be an allele of *lin-1* 118
4.3.6 Concluding remarks 119

4.4 Methods 121
4.4.1 Mutagenesis procedure for the forward genetic screen 121
4.4.2 Organization of mutagenized worms and screening 121
4.4.3 Automated FLP mapping 121
4.4.4 Manual SNP-mapping 122
4.4.5 Alleles 123
4.4.6 Whole-mount immunostaining 123

4.5 Chapter figures 124

5. Part III: A preliminary genome-wide RNAi screen in a *gap-1(lf)* background 138

5.1 Introduction 138
5.1.1 RNAi is a powerful reverse genetics tool 138
5.1.2 Rationale of the preliminary genome-wide RNAi screen presented in this study 138

5.2 Results 140

5.2.1 Thirty-six candidates constitute the high confidence class....140
5.2.2 The *rrf-3(pk1426); gap-1(ga133)* background results in many false positives....141

5.3 Discussion....142
5.3.1 The candidate gene *cdc-37*....143
5.3.2 The candidate gene F43G9.1....143
5.3.3 Screening the remaining three chromosomes IV, V and X....144

5.4 Methods....146
5.4.1 RNAi screen setup....146

5.5 Chapter figures....147

6. General discussion....148

6.1 The candidate based approach to find regulators of LET-23 localization....149

6.2 The forward genetic approach to find regulators of LET-23 localization....156

6.3 The large-scale RNAi screen in a *gap-1(lf)* background....157

6.4 Chapter figures....158

7. References....160

8. Acknowledgements....168

9. Curriculum Vitae....170

Zusammenfassung

Während der Entwicklung von mehrzelligen Organismen reagieren Zellen auf Signale in ihrer Umgebung, welche in das Innere der Zellen geleitet werden und in verschiedene biologische Antworten übersetzt werden, wie zum Beispiel Zellproliferation und Differenzierung. Entwicklungsbiologische Prozesse werden von konservierten, komplexen Signal-Netzwerken reguliert, welche in verschiedenen Modellorganismen studiert werden können. Die Entwicklung des Reproduktionsorganes von *C. elegans* Hermaphroditen dient als ein etabliertes Modellsystem um diese komplexen Signalwege zu analysieren.

Die Vulva der *C. elegans* Hermaphroditen entsteht aus drei von sechs äquipotenten Vulvavorläuferzellen (P3.p-P8.p). Die Ankerzelle in der Gonade produziert den epidermalen Wachstumsfaktor (EGF), welcher den konservierten EGF-Rezeptor/RAS/MAPK Signalweg in P6.p aktiviert und somit das primäre Zellschicksal ausführt. Um das Signal der Ankerzelle zu empfangen, muss der EGF-Rezeptor in P6.p auf der der Ankerzelle zugewandten basolateralen Plasmamembran lokalisiert sein. Die basolaterale Lokalisierung des EGF-Rezeptors ist essentiell für eine effiziente Aktivierung des Signalweges und somit für die Initiierung der Vulvaentwicklung. Ein Proteinkomplex mit den PDZ (PSD-95/Dlg/ZO-1)-Proteinen LIN-7, LIN-2 und LIN-10 wird für die basolaterale Lokalisierung des EGF-Rezeptors benötigt. Interessanterweise sind PDZ-Proteine oft Adaptoren, welche die subzelluläre Lokalisierung und Aktivität von Plasmamembranproteinen regulieren. Proteine mit FERM (Band 4.1/Ezrin/Radixin/Moesin)-Domänen sind bekannt dafür mit PDZ-Proteinen zu interagieren um gemeinsam die Lokalisierung und die Aktivität von Transmembranproteinen zu regulieren.

Mutationen im EGF-Rezeptor, welche zu einer Überexpression, konstitutiver Aktivität oder Misslokalisierung führen, können zum Beispiel zu Krebs führen. Während meiner Doktorarbeit identifizierte und charakterisierte ich zuvor unbekannte Proteine, welche die Lokalisierung des *C. elegans* EGF-Rezeptors regulieren. Somit war es mir möglich, den Zusammenhang zwischen der Rezeptorlokalisierung und dem Zellschicksal zu erforschen.

Ein im Voraus durchgeführter kandidatenbasierter Ansatz mit Hilfe von RNA Interferenz war die Basis für ein Projekt dieser Studie. RNA Interferenz gegen die Gene *frm-8* und *tag-60* supprimierte den *let-60 ras(gf)* Multivulva Phänotyp und mislokalisierte den EGF-Rezeptor zu den “Junctions” und intrazellulären Kompartimenten. In dieser Studie wurden die Deletionsmutanten *frm-8(zh67)* und *tag-60(zh93)* generiert. Dabei zeigte *tag-60(zh93)* starke und *frm-8(zh67)* schwache genetische Interaktionen mit dem EGF-Rezeptor Signalweg. Die

Charakterisierung der *tag-60(zh93)* Mutante zeigte, dass TAG-60 ein neuer Regulator der Vulvaentwicklung sein könnte, welcher im Prozess der EGF-Rezeptor Lokalisierung in den Vulvavorläuferzellen involviert sein könnte.

ERM-1 in *C. elegans* ist das einzige orthologe Protein von Ezrin, Radixin und Moesin in *H. sapiens*. ERM-1 wurde untersucht, weil es ein potentieller Interaktionspartner von TAG-60 ist. In dieser Studie zeigen wir, dass ERM-1 ein neuartiger Inhibitor der Vulvaentwicklung ist, der möglicherweise die EGF-Rezeptor Lokalisierung an der basolateralen Plasmamembran der Vulvavorläuferzellen reguliert.

In einem zweiten Ansatz wurde ein klassischer genetischer Screen für Multivulva Tiere in einem *gap-1(ga133)* Hintergrund durchgeführt, um entweder Mutanten mit apikal mislokalisiertem EGF-Rezeptor, oder Mutanten von Inhibitoren des EGFR/RAS/MAPK Signalweges zu finden. In diesem Screen wurden zwei fertile Mutanten mit apikal mislokalisiertem EGF-Rezeptor gefunden, welche neue Allele von *lin-2* und *lin-7* darstellen. Zusätzlich wurden zwei Allele von den zuvor charakterisierten Genen *let-19* und *gap-3* isoliert. Die Kartierung der zwei verbleibenden Mutanten *zh78* und *zh95* ist noch nicht abgeschlossen. Die Lokalisierung des EGF-Rezeptors in diesen Mutanten scheint normal zu sein, was darauf hindeutet, dass die Mutationen negative Regulatoren des EGF-Rezeptor Signalweges beeinträchtigen.

Um die Kartierung der isolierten Mutanten vom klassischen genetischen Screen zu erleichtern, wurde ein gross angelegter RNAi Screen von den Klonen der Chromosomen I, II und III in einem *gap-1(lf)* Hintergrund durchgeführt. Sechsunddreissig Kandidatengene wurden gefunden, welche einen synthetischen Multivulva Phänotyp in Kombination mit *gap-1(lf)* zeigen. Dabei wurden zuvor charakterisierte negative Regulatoren wie *puf-8*, *fbf-1* und *fbf-2*, aber auch neue genetische Interaktoren von *gap-1* identifiziert. Diese Kandidaten müssen noch genauer analysiert werden und könnten sowohl Regulatoren der EGF-Rezeptor Lokalisierung oder Inhibitoren der Vulvaentwicklung sein.

Summary

During the development of multicellular organisms, cells respond to extracellular signals, which are transduced into the cells and result in biological outcomes such as proliferation and differentiation. Developmental processes are controlled by conserved complex signalling networks, which can be studied in model organisms. The development of the egg-laying organ of the *C. elegans* hermaphrodite serves as a model system, in which these complex signalling cascades can be analyzed.

The *C. elegans* hermaphrodite vulva is formed from the descendants of three out of six equipotent vulval precursor cells (VPCs, P3.p-P8.p). The gonadal anchor cell (AC) produces the epidermal growth factor (EGF) that activates in P6.p the conserved EGF receptor (EGFR)/RAS/MAPK pathway to specify the primary cell fate. In order to receive the AC signal, the EGFR has to be kept on the basolateral surface of the VPCs facing the AC. The basolateral localization of the EGFR is essential for the efficient activation of the RAS/MAPK signalling pathway and consequently for correct vulval induction. A ternary complex formed by the PDZ domain proteins LIN-7, LIN-2 and LIN-10 is required for EGFR localization to the basolateral compartment of the VPCs. Interestingly, PDZ domains are often found in adaptor proteins that regulate the subcellular localization and activity of plasma membrane proteins. Proteins with FERM (Band 4.1/Ezrin/Radixin/Moesin)-domains are known to associate with PDZ-proteins and have been shown to regulate the localization and activity of transmembrane receptors in other model organisms.

In humans, mutations in the EGFR that lead to overexpression, constitutive activity or missorting lead to malignancies such as cancer. During my thesis, I identified and characterized novel factors involved in *C. elegans* EGFR localization and explored the connection of receptor trafficking with cell fate specification. For this purpose, different genetic approaches were used.

A candidate-based approach involving RNAi had been used in a preceding screen. RNAi against *frm-8* and *tag-60* suppressed the *let-60 ras(gf)* Multivulva phenotype and mislocalized EGFR to the junctional region and to intracellular punctae. In this study, the deletion mutants *frm-8(zh67)* and *tag-60(zh93)* were generated, which showed that *tag-60(zh93)* had strong, and *frm-8(zh67)* weak genetic interactions with the inductive EGFR signalling pathway. Characterization of the *tag-60(zh93)* mutants indicated that TAG-60 is a novel regulator of vulval development, which might be involved in EGFR localization in the VPCs.

erm-1 is the only ortholog of Ezrin, Radixin and Moesin in *C. elegans*. ERM-1 was studied because it is a putative binding partner of TAG-60. In this study, we present evidence that ERM-1 is a novel attenuator of vulval development, possibly by regulating the localization of EGFR at the basolateral plasma membrane of the VPCs.

In a second approach, a forward genetic screen for synthetic Multivulva animals in a *gap-1(lf)* background was performed to find mutants that display mislocalized EGFR or mutants in inhibitors of the EGFR/RAS/MAPK pathway. In this screen, we isolated two fertile mutants with apically mislocalized EGFR, which represent novel alleles of *lin-2* and *lin-7*. Additionally, we isolated two alleles of the previously characterized genes *let-19* and *gap-3*. The two remaining mutants *zh78* and *zh95* are still in the mapping process. EGFR localization seems to be normal in these mutants, indicating that the mutations affect negative regulators of the EGFR pathway.

A preliminary genomewide RNAi screen of chromosomes I, II and III in a *gap-1(lf)* background was performed in order to facilitate the mapping process of the mutants isolated in the forward genetic screen. Thirty-six high confidence candidate genes were found, which showed a synthetic Multivulva phenotype in combination with *gap-1(lf)*. The candidates include not only formerly characterized negative regulators such as *puf-8*, *fbf-1* and *fbf-2*, but also many novel genetic interactors of *gap-1*. These candidates have yet to be analyzed in more detail and could either encode regulators of EGFR localization or attenuators of vulval development.

Abbreviations

1°	primary
2°	secondary
3°	tertiary
AC	anchor cell
CFP	cyan fluorescent protein
Chr.	chromosome
CSL	CBF1/Su(H)/LAG-1
DNA	desoxyribonucleic acid
Dpy	dumpy: shortened body
EBP-50	ERM binding phosphoprotein 50kDa
EGF	epidermal growth factor
EGFR	epidermal growth factor receptor
EMS	ethane methyl sulfonate
ERM	Ezrin / Radixin / Moesin
EtOH	ethanol
F1	first filial generation
F2	second filial generation
FERM	4.1 protein / Ezrin / Radixin / Moesin
FLP	fragment length polymorphism
GAP	GTPase activating protein
GEF	guanine nucleotide exchange factor
gf	gain of function
GFP	green fluorescent protein
GPCR	G protein coupled receptor
GTP	guanosine -5'-triphosphate
hyp	hypodermis
IPTG	isopropyl β-D-1-thiogalactopyranoside
JA	Julie Ahringer
L1 – L4	larval stages 1 - 4
LET	lethal
lf	loss-of-function
LG	linkage group
LIN	lineage defective
MAGUK	membrane associated guanylate kinase
MAPK	mitogen activated protein kinase
Muv	multivulva
N2	*C. elegans* wild-type strain
Nf	neurofibromatosis
NGM	nematode growth medium
NHE-RF	Sodium/Hydrogen exchanger regulatory factor
P0	parental generation
PCR	polymerase chain reaction
PDZ	PSD-95 / Dlg / ZO-1
PI3K	phosphoinosite-3-kinase
PLC	phospho lipase C
Pvl	protruding vulva
Q-H_2O	Mili-Q filtered water / sterile water
RAS	rat sarcoma

rf	reduction-of-function
RNA	ribonucleic acid
RNAi	RNA interference
RT	room temperature
RTK	receptor tyrosine kinase
SNP	single nucleotide polymorphism
SWL	single worm lysate
synMuv	synthetic multivulva
TAG	temporary assigned gene name
Unc	uncoordinated
VPC	vulval precursor cells
Vul	Vulvaless
WLB	worm lysis buffer
WT	wild-type
YFP	yellow fluorescent protein

1. General introduction

1.1 The ErbB signalling network

Organs, which perform diverse highly specialised functions in the body of higher eukaryotes, are formed from many differently specified cells. Organogenesis during animal development is partly controlled by signals originating from the cellular environment surrounding the future organ. These intercellular signals are sensed by membrane localized receptors on the surface of the undifferentiated cells. The receptors transduce the signals into the cell and finally into the nucleus, where specific gene programs are activated to establish the corresponding cell fate.

The ErbB family of receptor tyrosine kinases (RTK) consists of four members, namly EGFR (epidermal growth factor receptor)/ErbB1, ErbB2, ErbB3 and ErbB4 (Holbro and Hynes, 2004). Each receptor type encodes an extracellular ligand binding domain, two cystein rich domains, a transmembrane domain, an intracellular tyrosine kinase domain and a carboxy-terminus with several tyrosine residues, which serve as substrates for autophosphorylation events. These receptors have been implicated in various biological processes depending on the cellular context, including proliferation, differentiation, cell shape and contact establishment and motility. The ErbBs have been subject for extensive investigation for almost three decades, first of all because of their tumerogenic properties. It has been shown that in various types of cancer, ErbBs are overexpressed or harbour a mutation that renders them constitutively active (Yarden and Sliwkowski, 2001).

In higher vertebrates, the ErbB signalling network is a sophisticated system composed of multiple levels that provide signal specificity and duration. First, different ligands harbouring EGF (epidermal growth factor)-like domains have various binding specificities towards the four ErbB receptors, meaning that the spacial and temporal control of ligand expression determines which receptor types are being activated (Riese and Stern, 1998). Second, the ErbBs have been shown to homo- or heterodimerize with each other upon ligand binding (Heldin 1995).

Upon receptor activation, the intracellular kinase domain phosphorylates tyrosine residues on the C-terminus, which provides docking sites for a plethora of adaptor proteins or enzymes harbouring SH2 (Src-homology domain) or PTB (Phosphotyrosin binding)-domains (Sudol 1998). The proto-oncogene Ras and the downstream MAPK (Mitogen activated protein kinase) cascade are almost invariant targets of all ErbB receptor combinations, but many other

signalling cascades have been associated with the ErbB network (Yarden and Sliwkowski, 2001).

1.2 Trafficking of ErbBs and its influence on signalling

In addition to the signal specificity, the duration of the signalling event is an important determinant for the various biological outcomes. The major process for EGFR/ErbB1 inactivation is initiated through receptor internalization *via* clathrin-coated vesicles (Hanover et al. 1984). Depending on the receptor-ligand combination (Muthuswamy et al. 1999), the pH of specialized endosomes results in dissociation of the ligand and subsequent recycling of the receptor to the cell surface (French et al. 1995). Persisting ligand-receptor complexes are thought to be ubiquitinated and targeted for lysosomal degradation in a Cbl (E3 ubiquitin ligase)-dependent manner (Levkowitz et al. 1998). ErbB2, ErbB3 and ErbB4 receptors were found to be endocytosis impaired and more often recycled back to the plasma membrane compared to EGFR/ErbB1 (Sorkin and Goh 2008). Trafficking of ErbB2-4 is much less understood but is believed to be based on clathrin-independent mechanisms (Baulida et al. 1996). In general, the receptors undergo constant cycling between the cell surface and intracellular compartments. In the absence of the ligand, the EGFR is slowly internalized but quickly recycled back to the plasma membrane. In contrast, upon activation by EGF, the EGFR undergoes rapid internalization and is more frequently targeted to lysosomes for degradation (Wiley 2003). The dynamic distribution and the turn over of transmembrane proteins are in general dictated by specific trafficking motifs, which are typically found in the cytoplasmic domains (Mellman 1996).

Importantly, receptor internalization is not a negative regulatory event *per se*. An interesting hypothesis emerged from different sources, which propose the existence of “signalling endosomes” (Sorkin and Von Zastrow, 2002). Experiments using conditional dynamin mutants with impaired receptor endocytosis showed that Ras can be activated from EGFR at the plasma membrane and endosomes, in contrast to PLC-γ (Phospholipase C γ) and PI3K (Phosphatidylinsoitole-3 kinase), which are only activated by EGFR at the plasma membrane. Thus, the distribution of EGFR might modulate the specificity and duration of the signalling (Wiley 2003).

In most human polarized epithelia cells, EGFR is predominantly displayed at the basolateral plasma membrane compartment, where it senses ligands originating from the underlying mesenchyme. However, mislocalization of the EGFR has direct consequences, as its ligands and substrates also show apical-basolateral polarity features. For example, the mislocalization

of EGFR to the apical membrane of renal tubular epithelial cells has been associated with autosomal dominant polycystic kidney disease (ADPKD or short PKD). The expansion of the renal tubules and the formation of multiple cysts is thought to be caused by overproliferation of the epithelia cells and by enhanced fluid secretion into the lumen. It was found that the cyst fluids possess high mitogenic potential towards renal epithelial cells (Du and Wilson 1995). The model suggests that these cells produce and secrete EGF into the lumen and that EGF is possibly necessary for epithelial repair and regeneration mechanisms (Du and Wilson 1995). Taken together, apically missorted EGFR is associated with ADPKD, where it is activated by autocrine EGF, leading to overproliferation of the epithelial cells (Du and Wilson 1995).

1.3 PDZ-domains are interaction modules found in plasma membrane scaffold proteins

Multiple PDZ (PSD-95/Dlg/ZO-1)-domain containing proteins function in the establishment and maintenance of epithelial apical-basolateral polarity (Fanning and Anderson, 1999). This polarity is maintained mainly by tight junctions, protein complex barriers that prevent passive translocation of transmembrane proteins and lipids from one plasma membrane compartment to the other (Tsukita et al. 2008).

The polar distribution of transmembrane receptors or channels also require PDZ-scaffolds. This distribution is based on sorting mechanisms such as retention, recycling and targeting for lysosomal degradation mediated thorough PDZ proteins (Fanning and Anderson, 1999). In the case of ErbB2, it was shown that the PDZ protein ERBIN is a direct binding partner of the receptor *in vitro* and *in vivo* and is essential for basolateral restriction of the receptor in Caco-2 (human colon carcinoma) and MDCK (Madin-Darby Canine Kidney) cells (Borg et al. 2000). Interestingly, ErbB2 is the only member of the ErbB family that associates and depends on ERBIN (Borg et al. 2000).

Another PDZ protein that has been shown to influence the localization of ErbB2 is called hLin-7/Veli. The N-terminal kinase interaction domain of hLin-7 directly binds to the kinase domain of ErbB2 and thereby promotes the basolateral targeting of the receptor (Shelly et al. 2003). Moreover, the C-terminal PDZ domain of hLin-7 binds directly to the C-terminal tail (PDZ binding motif) of ErbB2, which stabilizes the receptor at the basolateral membrane, presumably by recruiting retention and/or recycling components (Shelly et al. 2003).

The distribution of the transmembrane proteins has direct impact on their activity. Furthermore, PDZ domain proteins can also function as docking sites for receptor effectors or regulators (Brône and Eggermont 2005).

1.4 FERM-domain proteins: linkers between the membrane and the cytoskeleton

The FERM (4.1 protein, Ezrin, Radixin, Moesin) family is essential for the attachment of transmembrane proteins or PDZ scaffolds at the cell periphery through its characteristic FERM domain (Bretscher et al. 2002). The subfamily of ERM-like proteins, which consist of Ezrin, Radixin and Moesin and the closely related tumor suppressor Nf2(Neurofibromastosis 2)/Merlin, are believed to link plasma membrane proteins to the peripherical actin cytsokeleton and thus regulate the membrane distribution and activity of various receptors and channels (Chishti et al. 1998, Bretscher et al. 2002). Merlin was shown to be an important regulator of cellular proliferation in various model systems (Bretscher et al. 2002). However, the mechanism of its tumor suppressive function is not known in detail. Shaw et al. (2001) proposed that Merlin acts to negatively regulate Rac function, which was shown to have oncogenic properties. Curto et al. (2007) recently showed that Merlin functions in contact-dependent inhibition of EGFR-signalling, which results in an attenuation of cell proliferation.

1.5 The model organism *Caenorhabditis elegans*

Evolutionarily distant organisms seem to share developmental mechanisms and underlying sigalling networks. This makes it possible to study developmental processes in lower organisms such as *Caenorhabditis elegans*. The Nobel Assembly awarded the Nobel prize in Physiology or Medicine for 2002 to Sydney Brenner, Robert Horvitz and John Sulston for their discoveries concerning genetic regulation of organ development and apoptosis in this nematode.

C. elegans is a small nematode, measuring approximatively 1.5 mm in length and serves as a model organism to study animal development and behaviour (Brenner 1974). The wild-type strain (N2) was originally collected from a mushroom compost near Bristol, England (Brenner 1974). *C. elegans* is a predominantly hermaphroditic species and therefore, most populations in the wild consist of clones from one animal. The gender of *C. elegans* is defined by the ratio of autosomal to sex-chromosomes, hermaphrodites possess two X-chromosomes and males exhibit one (X0), which are generated by nondisjunction of the X-chromosome. The frequency of the appearance of males is about 0.1 %.

There are many advantages in using *C. elegans* as an organism for genetic analysis. One hermaphrodite can give rise to 300 - 350 progeny and their life cycle is relatively rapid, taking only three days at 25°C. Before reaching the adult stage, the newly hatched *C. elegans* larvae undergo four larval stages (L1 to L4) that are separated by molting. The worms grow on agar plates and feed on genetically modified *E. coli* (OP-50).

The simplistic anatomy and the translucent nature of *C. elegans* make this nematode amenable to microscopical manipulations and analyses. Interestingly, there is very little variation in the cell lineage between wild-type individuals. Every division and migration of these invariant lineages is well known and described (Sulston and Horvitz, 1977). *C. elegans* can be stored long-term in liquid nitrogen or at –80°C. Therefore, it is possible to maintain a collection of genetically modified worms as stocks in a laboratory.
Lastly, the complete sequencing of the *C. elegans* genome serves as an efficient tool for genetic analysis (The *C. elegans* Genome Sequencing Consortium, 1998).

1.6 The EGFR system in *C. elegans*

In contrast to four ErbB receptors in humans, *C. elegans* only encodes one EGFR like molecule called LET-23 (Aroian et al. 1991), which is essential for the development of many tissues and processes in *C. elegans* such as viability, vulval development, P12 fate determination, fertility and male spicule formation (Moghal and Sternberg, 2003). Many *let-23* alleles have reduced viability and have tissue-specific defects. For example, the allele *sy1* displays only vulval defects but does not affect the other tissues (Aroian et al. 1994). The *sy1* allele results in a C-terminal truncated form of LET-23, which disallows the interaction with the vulval specific component LIN-7 essential for vulval development (Kaech et al. 1998). The activation of LET-23 is thought to happen by the sole *C. elegans* epidermal growth factor (EGF) called LIN-3 (Moghal and Sternberg, 2003). However, the downstream signalling cascade is cell-context dependent. The small GTPase Ras for example acts downstream of LET-23 during the mechanisms involved in viability, vulval development, P12 fate determination and male spicule formation, but not during ovulation (Moghal and Sternberg, 2003).
Vulval development as a model system for LET-23 signalling has obvious advantages, as mutants of the LET-23 pathway have easily detectable phenotypes that are already observable under the dissecting microscope. Overactivation of the LET-23 pathway leads to ectopic induction of cells, normally determined to be fused with surrounding cells (Moghal and Sternberg, 2003). These ectopically induced cells lead to ventral protrusions called “pseudovulvae” and the phenotype referred to as “Multivulva” (Muv). In contrast, reduction of LET-23 signalling can lead to a partially or non-induced vulval tissue, resulting in a malformed or an absent vulva, which prevents the animal from laying the fertilized eggs (Moghal and Sternberg, 2003). Thus, underinduced animals exhibit the Vulvaless (Vul)

phenotype. Some Vul mutant strains are viable, as the animals bloat with eggs, which hatch inside the mother animal (“bag of worms”).

1.7 Vulval development

The development of the *C. elegans* hermaphrodite vulva can be divided into three steps. First, the epithelial VPCs (Vulval Precursor Cells) are generated. Second, vulval patterning and development is triggered by a specialized gonadal cell called the Anchor Cell (AC). Third, the execution of the cell fates includes eversion after divisions along cell fate specific axis and morphogenesis forming the mature vulva (Sternberg 2005).

1.7.1 Vulval induction and patterning

Vulval cells are derived from the P cell lineage (Sulston and Horvitz, 1977). A total of 12 P cells migrate from the lateral sides of the worm to the ventral side during the L1 stage. Following cell migration, the P cells divide along the anterior-posterior axis. As a result, 12 anterior P cells (Pn.a) divide and differentiate into neuronal cells, while 12 posterior P cells (Pn.p) form epidermal cells (Sulston and Horvitz, 1977). During the L2 stage, the 12 epidermal Pn.p cells are aligned along the ventral midline. From these cells, P3.p to P8.p form equipotent Vulval precursor cells (VPCs) and the remaining cells, P1.p, P2.p and P9-12.p, fuse with the surrounding hypodermal syncitium hyp7. The six VPCs gain their potential to adopt a vulval fate by expressing the Hox factor LIN-39, which blocks their fusion to hyp7 (Clark et al. 1993). Vulval development is triggered by a secreted signal originating from the somatic gonadal AC in the form of LIN-3 EGF (Hill and Sternberg 1992).

1.7.2 The LET-23 EGFR pathway promotes the 1° vulval cell fate

The AC is located dorsally of P6.p and produces the epidermal growth factor (EGF) orthologue LIN-3 (Hill and Sternberg 1992), which binds and activates the epidermal growth factor receptor (EGFR) orthologue LET-23 (Aroian et al. 1991). While LET-23 is expressed in all VPCs, P6.p (the VPC closest to the AC) receives the highest level of LIN-3 ligand (figure 1.1). LIN-3 is sequestered primarily by P6.p, but is also thought to be distributed gradually in the extracellular space, thus activating LET-23 in the remaining VPCs to a lesser extent (Sternberg and Horvitz, 1986; Katz et al. 1995). Binding of LIN-3 to LET-23 activates the evolutionary conserved Ras/MAPK pathway by similar mechanisms as found in mammalian systems (figure 1.1). Firstly, ligand binding leads to the dimerization and autophosphorylation of the receptor. This generates docking sites for the adaptor proteins like

SEM-5 Grb2 (Clark et al. 1992). Subsequent recruitment of SOS-1 (Chang et al. 2000), the RasGEF, leads to the activation of LET-60 RAS (Beitel et al. 1990) at peripherical membranes. As a result, the phosphorylation cascade of LIN-45/Raf (Han et al. 1993), MEK-2/MEK (Wu et al. 1995, Kornfeld et al. 1995) and MPK-1/ERK (Lackner et al. 1994) is triggered. Activated MPK-1 translocates to the nucleus, where it phosphorylates different targets, including transcription factors, which control the expression of genes underlying the primary (1°) vulval fate (Sundaram, 2006). Two well characterized targets of MPK-1 are LIN-1, a transcription factor of the Ets family (Beitel et al. 1995) and LIN-31, a member of the forkhead family of transcription factors (Miller et al. 1993).
Transcriptional targets of the LET-23 pathway include the gene *egl-17*, which encodes the *C. elegans* orthologue of the fibroblast growth factor FGF (Burdine et al. 1998) and *lag-2*, which represents a Delta-like Notch ligand (Chen and Greenwald 2004).

1.7.3 The LIN-12 Notch pathway promotes the 2° vulval cell fate

One of the downstream targets of LET-23 pathway is the gene *lag-2* (Chen and Greenwald 2004) that encodes a transmembrane ligand specific for LIN-12/Notch (figure 1.1 and Greenwald, 2005). Shortly after P6.p is induced, the LAG-2 ligand activates LIN-12 on the flanking VPCs P5.p and P7.p (Greenwald, 2005). Activated LIN-12 is proteolytically processed at the plasma membrane and the intracellular domain subsequently translocates into the nucleus. In the nucleus it controls the expression of a variety of target genes together with the protein LAG-1 CSL (Greenwald, 2005). The LIN-12 target genes are believed to encode either factors responsible to adopt the secondary (2°) vulval fate or inhibitors of the LET-23 pathway (figure 1.1 and Berset et al. 2001, Yoo et al. 2004). As mentioned above, the LET-23 pathway is responsible for the establishment of the primary vulval fate. The LIN-12 pathway is also called the lateral inhibitory pathway, as it is crucial to inhibit the LET-23 pathway and therefore the primary vulval fate in P5.p and P7.p.

1.7.4 GAP-1 is an inhibitor of LET-60

The activity of the LET-23-pathway is tightly regulated, since aberrant signalling can lead to malformation of the vulval tissue and hence impairs the mating and egg-laying function of this organ. For example *gap-1* encodes a RasGAP (GTPase activating protein), a negative regulator of LET-60 RAS (figure 1.1 and Hajnal et al. 1997). This small GTPase Ras switches from the active GTP-bound state to the incactive GDP-bound state (and vice versa). The hydrolysis of this step is performed by Ras itself, but is greatly enhanced by the GAP proteins

(Bollag and McCormick 1991, Boguski and McCormick 1993). *gap-1* loss-of-function animals exhibit a wild-type phenotype but are thought to have elevated LET-60 signalling (Hajnal et al. 1997, Yoo et al. 2004). Interestingly, some combinations of loss-of-function alleles of *gap-1* and other negative regulators (from which both are superficially wild-type) show a synthetic Muv phenotype (Gupta et al. 2006, Walser et al. 2006, Stetak et al. 2008). It is believed that by additionally removing the activity of another negative regulator, the signalling level overcomes a threshold, which leads to ectopic inductions.
So far, three different RasGAPs with different tissue specificity have been identified: *gap-1*, *gap-2* and *gap-3* (Stetak et al. 2008). However, genetic analysis shows that only *gap-1* and *gap-3* act as negative regulators of vulval development. Consistently, double mutants of *gap-1(lf)* with *gap-3(lf)* result in a Multivulva phenotype (Stetak et al. 2008, this study).

1.7.5 LIP-1 is a negative regulator of MPK-1

As mentioned above, the LIN-12 pathway is activated in P5.p and P7.p to inhibit the primary vulval fate in these cells. One of the key players in this lateral inhibition is LIP-1 (Lateral induced phosphatase) (Berset et al. 2001). Transcription of *lip-1* is regulated by the LIN-12 pathway (figure 1.1; Berset et al. 2001). It has been shown that LIP-1 interacts directly with and dephosphorylates MPK-1, which renders it inactive (Berset et al. 2001). The main focus of LIP-1 are the secondary VPCs, where it inhibits the LET-23 pathway at the level of MPK-1 and consequently the 1° vulval fate (Berset et al. 2001). Transcription of other negative regulators of the LET-23 pathway have been found to be regulated by LIN-12, such as *ark-1*, *dpy-23*, *lst-1*, *lst-2*, *lst-3* and *lst-4* (Yoo et al. 2004). These studies show that a sophisticated crosstalk between the LET-23 and the LIN-12 pathway controls the patterning of the vulval cells.

1.7.6 DEP-1 is a negative regulator of LET-23

The existence of negative regulators of the inductive pathway within the 2° VPCs, whose transcription is independent from the LIN-12 pathway, was shown through the identification of *dep-1* (figure 1.1; Berset et al. 2005). DEP-1 (Density enhanced phosphatase) is a receptor tyrosine phosphatase, which is thought to dephosphorylate activated LET-23. Interestingly, the subcellular localization of a DEP-1::GFP reporter is in peripherical intracellular punctae (Berset et al. 2005), suggesting internalized LET-23 is dephosphorylated by DEP-1. Presently, it is unknown which signals are responsible to transcribe and regulate the *dep-1* gene product. However, it was shown that DEP-1 expression is negatively regulated by SUR-

2 in the 1° cells. SUR-2 is a component of the mediator complex that acts downstream of the EGFR/RAS/MAPK pathway to induce LIN-12 down-regulation (Berset et al. 2005).

1.7.7 The synMuv genes negatively regulate vulval development

The synMuv (synthetic Multivulva) genes ensure that the distal VPCs P3.p, P4.p and P8.p adopt the tertiary (3°) nonvulval fate (Fay and Yochem, 2007). The synMuv genes are grouped into three classes: A, B and C. Most of single mutants of the synMuv genes do not exhibit defects in vulval development. But a loss-of-function combination of a synMuv class A with a synMuv class B leads to a highly penetrant synthetic Muv phenotype (Fay and Yochem, 2007). Combining either two mutants of class A or class B does not have any impact on vulval development. The class C synMuvs elicit a Muv phenotype only in combination with mutants of either class A or class B (Fay and Yochem, 2007). Two kinds of mechanisms are proposed to fulfil the inhibitory function of the synMuv genes. Firstly, the repression of *lin-3* transcription in hyp7 (Cui et al. 2006) and secondly, the repression of *lin-39* in the distal VPCs, which promotes their fusion to hyp7 (Chen and Han 2001a).

1.7.8 The small GTPase RHO-1 is a positive regulator of 1° cell fate specification

Canevascini et al. (2005) demonstrated that Rho signalling positively regulates vulval development. Gain-of-function of *ect-2*, a gene encoding a RhoGEF (Guanine nucleotide exchange factor), exhibits a Multivulva phenotype in combination with a loss-of-function allele of *gap-1*. The ubiquitous expression of a dominant negative form of RHO-1 was sufficient to neutralize the effects provoked by the *ect-2(gf)* allele. Furthermore, it was found that ECT-2 most likely represents the GEF for RHO-1 and that this pathway feeds either upstream or at the level of the RasGEF SOS-1 (Canevascini et al. 2005).

1.7.9 Execution of the vulval cell fates

Both primary and secondary vulval lineages undergo three rounds of cell divisions (henceforth called 1-, 2-, 4- and 8-cell stage) (figure 1.2). P6.p gives rise to 8 descendants and P5.p and P7.p each give rise to 7 descendants. In the early L4 stage, the primary vulval cells detach from the cuticule and migrate dorsally, which induces the invagination of the vulval tissue. The secondary vulval cells facing the primary cells follow their neighbouring primary cells, resulting in the mid L4 stage structure called the “Christmas Tree” (figure 1.2 F). It is a symmetrical structure, where the primary cells constitute the upper building block of the “tree” and the secondary cells form the lateral branches of the “tree”. Subsequent homotypic

fusion of the vulval cells lead to a stack of vulval rings (toroids) that form a tubular structure connecting the uterine tissue with the outside space (Sharma-Kishore et al. 1999).
Vulval development is very sensitive to changes in gene function and these aberrations can be quantified by scoring the vulval induction index at the L4 stage, which ranges from 0 to 6. Additionally, hybrid inductions can occur when a VPC divides once and one daughter cell continues proliferating, while the other daughter cell arrests. This event is scored as an induction of 0.5.

1.7.10 LET-23 expression and localization during vulval development

As mentioned above, LET-23 is expressed in all VPCs at the time of induction and later on upregulated in P6.p and descendants, but downregulated in all remaining VPCs (Kaech et al. 1998). The VPCs are polarized, much like all epithelial cells, with their plasma membrane divided into an apical and basolateral compartment by a large protein complex structure called apical junctions (Cox and Hardin, 2004). The *C. elegans* apical junctions represent one electrodense structure, which can be divided into 2 subcomplexes; First the HMR-1A (Cadherin)/HMP-1 (α-Catenin)/HMP-2 (β-catenin) complex and second the more basal DLG-1 (Disks large) - AJM-1 (novel coiled-coil protein) complex (Cox and Hardin 2004). One of their function is to hinder membrane components from diffusing between different compartments. Since the AC faces the basolateral membrane of P6.p, LET-23 must be expressed on this side in order to process the inductive signal (Kaech et al. 1998). Immunostaining experiments show a predominant basolateral localization of LET-23 at the time of induction (figure 1.3 A, B), which is enhanced during vulval development (Kaech et al. 1998). Minor localization is found in intracellular punctae and in a sub apical compartment (Whitfield et al. 1999). Furthermore, correct basolateral targeting of LET-23 is crucial for proper vulval induction by the AC (Kaech et al. 1998, Whitfield et al. 1999).

1.7.11 The ternary complex LIN-7/LIN-2/LIN-10

Some of the first mutants with vulval phenotypes were isolated and published by Horvitz and Sulston in 1980. The mutants of the genes *lin-2*, *lin-7* and *lin-10*, exhibit aberrant vulval lineages and were positionally mapped and characterized (Hoskins et al. 1996, Simske et al. 1996). They have been shown to act as positive regulators of the LET-23 pathway as loss-of-function mutants of these genes show a highly penetrant Vulvaless phenotype (Hoskins et al. 1996, Simske et al. 1996). Visualization of LET-23 in these mutants revealed that the receptor was fully mislocalized to the apical compartment of the VPCs (figure 1.3 C, D) (Kaech et al.

1998, Whitfield et al. 1999). Similar localization of LET-23 was found in the *let-23(sy1)* hypomorphic allele (Kaech et al. 1998), encoding a LET-23 variant which lacks the five distal C-terminal amino acids (Aroian et al. 1994). The distal 3 amino acids represent the PDZ-binding motif TCL, which constitutes a binding interface for the PDZ domain of LIN-7 (Kaech et al. 1998).

Sequence analysis of LIN-2, LIN-7 and LIN-10 showed that all three proteins harbour PDZ (PSD-95/Dlg/ZO-1) domains, known protein interaction modules (Kaech et al. 1998). Kaech et al. (1998) furthermore showed that LIN-2 directly binds both LIN-7 and LIN-10 simultaneously *in vitro*. Altogether these results lead to the model in which the ternary complex, consisting of LIN-7, LIN-2 and LIN-10, binds to the C-terminus of LET-23 *via* LIN-7, thus targetting the receptor to the basolateral membrane of the VPCs (figure 1.3 E) (Kaech et al. 1998, Whitfield et al. 1999).

Another positive regulator of LET-23 is EPS-8, a protein that is required for proper retention of LET-23 at the basolateral membrane (Stetak et al. 2006). Consequently, removal of EPS-8 results in mislocalization of LET-23 to intracellular punctae (Stetak et al. 2006). Additionally, Stetak et al. (2006) showed that overexpression of EPS-8 in all six VPCs resulted in persisting LET-23 expression in these cells, indicating that EPS-8 functions to block degradation of the receptor. Lastly, it was found that EPS-8 function is dependent on LIN-2 but not on LIN-7 (Stetak et al. 2006).

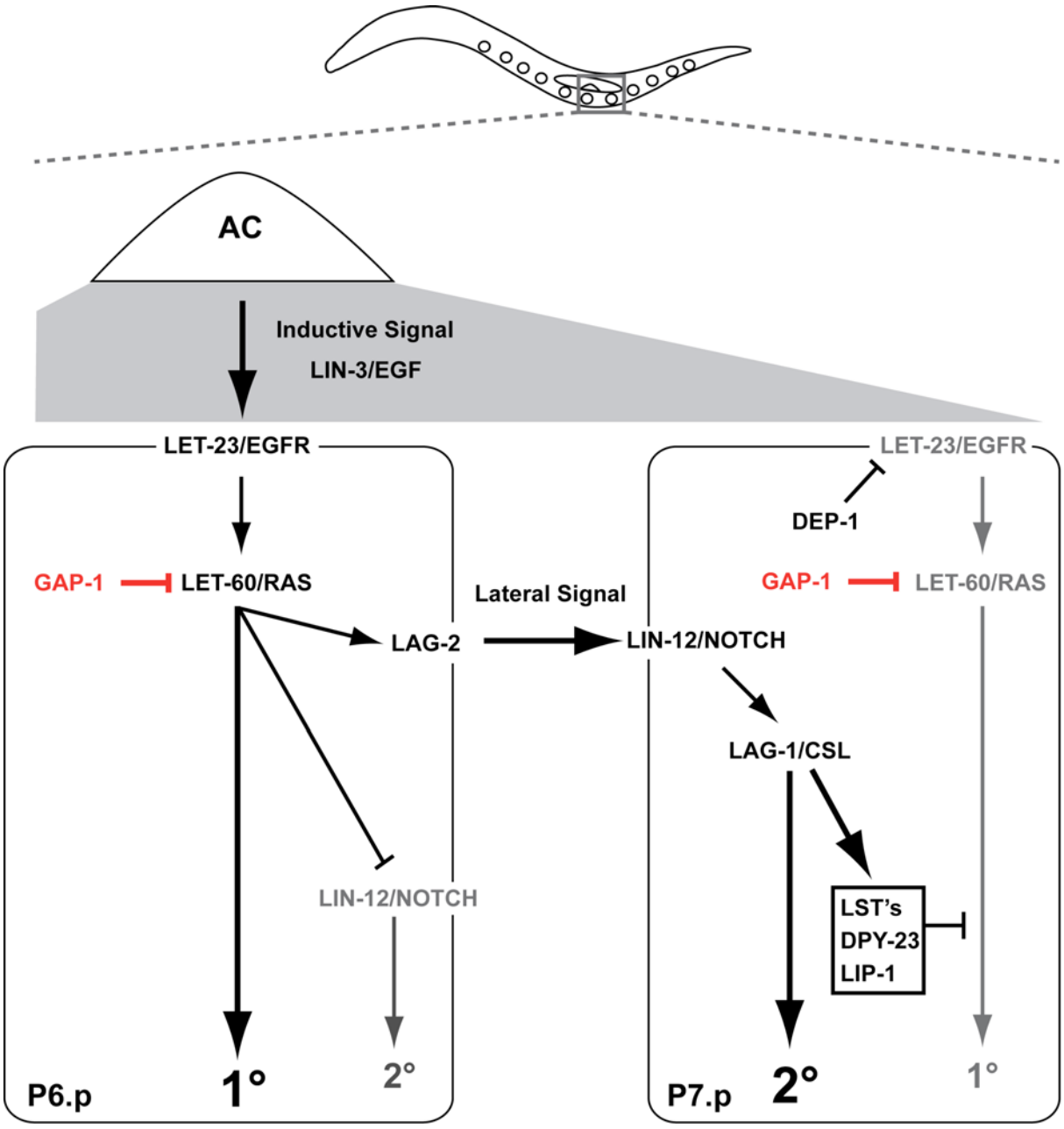

Fig. 1.1: The inductive and the lateral signal define the 2°1°2° pattern of vulval cell fates.
The scheme displays the crude signaling events between the vulval cells P6.p and P7.p. The same lateral interaction occurs between P6.p and P.5p. The AC secretes the growth factor LIN-3/EGF (grey area). This leads to maximal LET-23/EGFR and LET-60/RAS signaling in the nearest vulval cell, P6.p. As a consequence P6.p adopts the 1° cell fate. Moreover, P6.p produces the lateral signal, consisting of the DSL ligand LAG-2. Thereby, the LIN-12/Notch pathway is activated in the flanking vulval cells. LIN-12/Notch activates its transcription factor LAG-1/CSL. The LIN-12/Notch pathway has two effects. On one hand, it drives transcription of negative regulators of the LET-23/EGFR pathway and thereby inhibits acquisition of the 1° cell fate. On the other hand, LIN-12/Notch signaling induces the 2° cell fate by an unknown mechanism. The activity of the attenuators GAP1 and DEP-1 are believed to be LIN-12/Notch-independent. For simplicity reasons not all pathway components and regulators mentioned in the text are shown. Figure provided by Ivo Rimann.

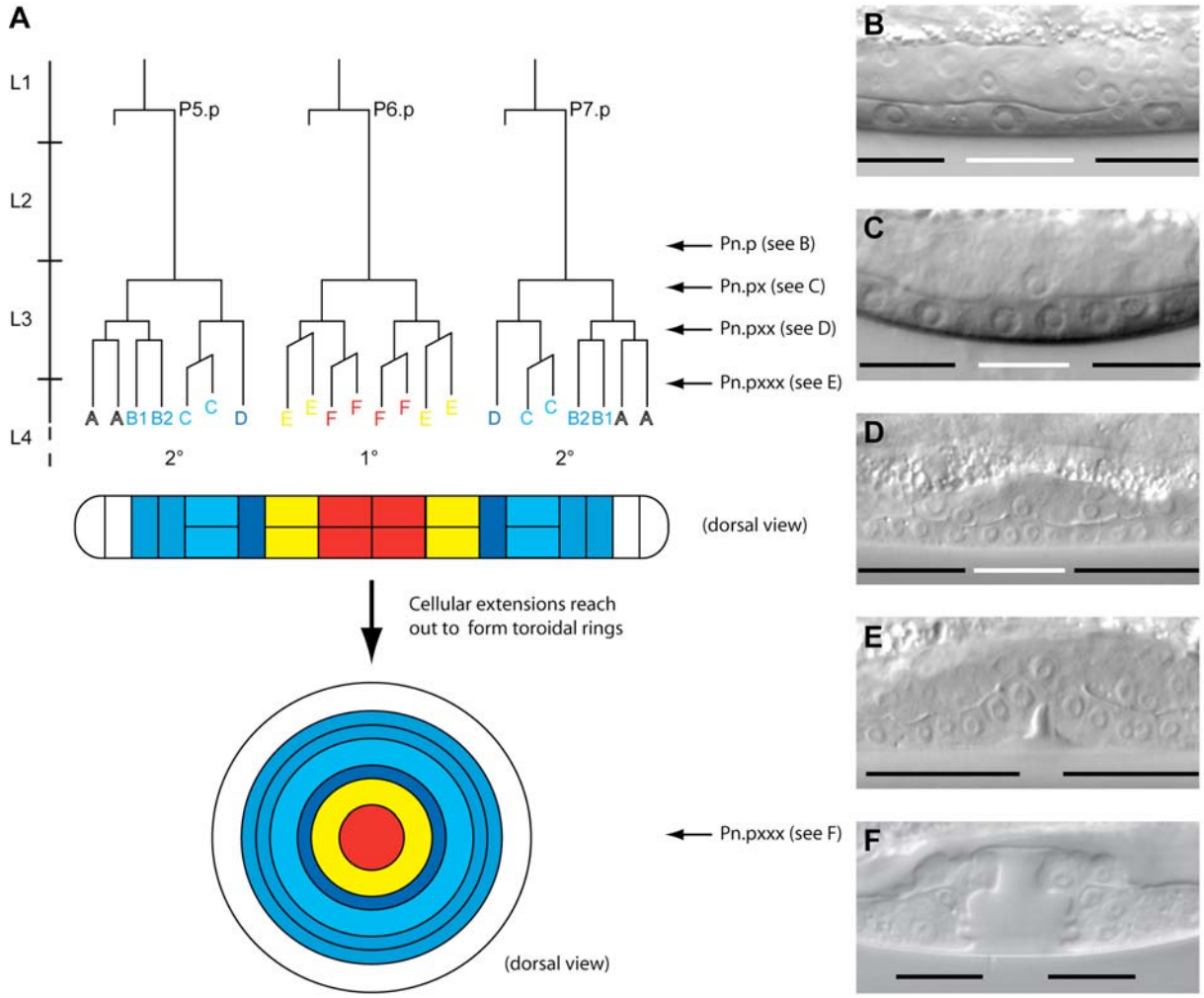

Fig. 1.2: Execution of the vulval fates.
A) Following vulval induction at the beginning of the L3 stage, P6.p adopts the 1° and P5.p and P7.p adopt the 2° fate. P6.p undergoes 3 rounds of cell divisions and gives rise to 8 descendants. The P5.p and P7.p lineages result in 7 descendants due to asymmetric cell divisions. Subsequent cell migration events during invagination give rise to the toroid structure at the L4 stage ("Christmas tree" stage). B to F) Normarski pictures show the nuclei of the vulval cells at the indicated developmental stages. P6.p and descendants are marked with a white bar and P5.p/P7.p descendants are marked with a black bar. B) P6.p or 1-cell stage. C) Pn.px or 2-cell stage. D) Pn.pxx or 4-cell stage. E) Pn.pxxx or 8-cell stage. Vulval cells just started to invaginate and 1° cells are out of focus. F) "Christmas-tree" structure at the L4 stage. 1° cells are out of focus. Figure provided by Ivo Rimann.

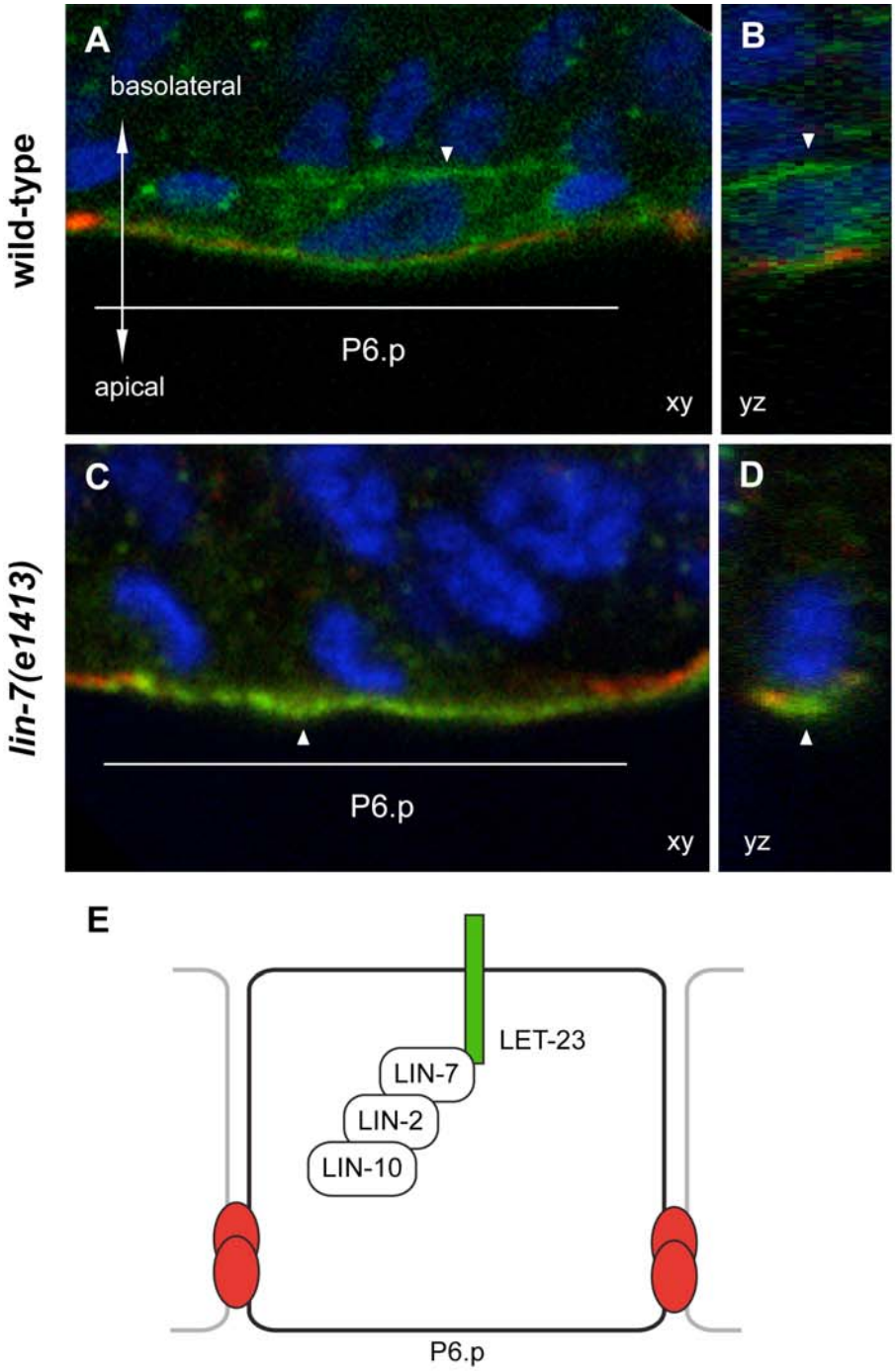

Fig. 1.3: LIN-7 is required for basolateral LET-23 localization.
A and B) Immunostaining of LET-23 (green), AJM-1 (red) and DNA (blue) in P6.p of wild-type animals, showing predominant basolateral localization of LET-23 (arrowheads). Lateral view is shown in the xy section (A) and one corresponding yz section (B). C and D) Immunostaining of LET-23 (green), AJM-1(red) and DNA (blue) in P6.p of *lin-7(e1413)* animals, showing apically mislocalized LET-23 (arrowheads). Lateral view indicated as xy section (C) and one corresponding yz section (D). E) Schematic model for basolateral LET-23 localization (Kaech et al. 1998). LIN-7, LIN-2 and LIN-10 form a trimeric complex, which binds to the C-terminus of LET-23. Removal of either LIN-7, LIN-2 or LIN-10 results in apically missorted LET-23 (C, D, Kaech et al. 1998). LET-23 is shown in green and apical junctions are shown in red.

2. Objectives of this study

The aim of my thesis was to identify and characterize novel proteins involved in the trafficking of the *C. elegans* EGF-receptor LET-23. It is the general belief that the localization of a receptor tyrosin kinase is directly coupled to the duration and specificity of the signalling. Therefore the targeting of EGFR LET-23 to specific membrane compartments has consequences in cell fate determination. In this study, *C. elegans* vulval development was used as a system to identify regulators of LET-23 localization by different genetic approaches.

Our lab is especially interested in genes encoding PDZ-domains and FERM-domains. In a preceding candidate-based RNAi screen, genes encoding PDZ or FERM-domains were downregulated in *let-60(gf)* Multivulva animals to find genetic interactors of the LET-23 pathway. RNAi experiments, which modulated the Muv phenotype, were repeated in wild-type animals and LET-23 localization was assessed using immunostaining. The genes *frm-8* and *tag-60* were found as candidate regulators of LET-23 localization (A. Stetak, unpublished results). The main project of my thesis was to generate deletion mutants of *frm-8* and *tag-60* and to characterize their role in LET-23 localization and vulval development. ERM-1 was found to be a putative binding partner of TAG-60 and was as well part of the investigations presented in this study.

In a second approach I performed a forward genetic screen for animals exhibiting a Muv phenotype in a *gap-1(lf)* sensitized background. In this screen I was hoping to find not only other negative regulators of the EGFR/Ras/MAPK pathway, but also proteins that are involved in the targeting of LET-23 to the basolateral membrane. Six mutants strains were isolated and the goal of this side project was to positionally map the mutations and to characterize one interesting candidate.

3. Part I: A reverse genetics approach to identify regulators of LET-23 localization

3.1 Characterization of *frm-8*

3.1.1 Preliminary data

frm-8 is located on chromosome III and encodes a protein with one PDZ, one WW and one FERM-domain (Figure 3.1). A genetic interaction was previously found between *frm-8* and *let-60 Ras* (A. Stetak, personal communication). RNAi against *frm-8* was found to suppress the Muv phenotype of the *let-60(n1046gf)* mutant in a candidate based RNAi screen (A. Stetak, personal communication). *frm-8* RNAi suppressed the Muv phenotype of *let-60(n1046gf)* from 5.4 to an average of 4.9 induced VPCs. In a subsequent experiment, downregulation of *frm-8* by RNAi in the *rrf-3(pk1426)* RNAi hypersensitive background (Simmer et al. 2003) seemed to mislocalize LET-23 in the primary VPCs to the apical junctions and intracellular punctae (A. Stetak, personal communication).

3.1.2 Isolation of the *frm-8(zh67)* allele

In order to examine the function of *frm-8*, it was indispensable to generate a deletion mutant. Deletion libraries were screened as described in the Methods section, which led to the isolation of the *frm-8(zh67)* deletion allele that was subsequently backcrossed 8 times with wild-type. As shown in figure 3.1, the *zh67* deletion removes 1'677bp, which contains exons 4, 5 and parts of 6th exon of the a-isoform. The deleted sequence encodes parts of the predicted PDZ and FERM domains. Therefore, the *zh67* allele is likely to encode a hypothetical protein with reduced or impaired function with respect to the PDZ and/or the FERM domains. Assuming that exon 3 would be spliced with exon 7, this would lead to a frameshift and hence *zh67* is predicted to introduce a premature STOP codon. Nevertheless, *frm-8(zh67)* was found to be superficially wild-type. A closer look into vulval development confirmed that the vulva was formed as in wild-type animals.

3.1.3 *frm-8(zh67)* appears to mislocalize LET-23 in the VPCs

As previously discussed, LET-23 is predominantly localized on the basolateral plasma membrane of primary VPCs (Figure 3.2 A), whereas *frm-8(zh67)* mutants seemed to show intracellular accumulation of LET-23 (Figure 3.2 B). At the 2- and 4-cell stage in *frm-8(zh67)*

animals, LET-23 seemed to be enriched predominantly on the basolateral membrane, which is facing the respective sister cell and in intracellular punctae (30-40% of the cases, n=18, figure 3.2 D arrow compared to the arrowheads), whereas in the control animals the distribution of LET-23 appeared more uniformly on the basolateral membrane (figure 3.2 C). At the 4-cell stage, 50% (n=20) of the analyzed *frm-8(zh67)* animals had a higher expression level of LET-23 in the 2 inner VPCs (Figure 3.2 F, P6.pap and P6.ppa, arrows) than the two outer VPCs (Figure 3.2 F, P6.paa and P6.ppp, arrowheads), whereas most wild-type animals showed equal expression levels in all 4 primary VPCs (Figure 3.2 E, G). In 5% (n=20) of the analyzed animals, LET-23 was expressed in 3 cells (instead of 4), which could represent VPCs with slightly aberrant timing of cell-division, where one P6.px cell already finished division and the sister cell did not complete the cell cycle yet (Figure 3.2 H). Altogether, the general feature of *frm-8(zh67)* animals seemed to be the intracellular accumulation of LET-23 in the VPCs. These results were consistent with what was observed in the candidate based RNAi screen and supported the assumption that *frm-8* might be involved in the regulation of LET-23 localization.

3.1.4 *frm-8(zh67)* shows a weak genetic interaction with the LET-23 pathway

Since RNAi of *frm-8* suppressed the Muv phenotype of *let-60(n1046gf)* in the RNAi screen, the genetic interaction between *frm-8(zh67)* and mutants of the EGFR/Ras/MAPK pathway was tested. *frm-8(zh67)* was combined with either *let-60(n1046gf)* or *lin-2(n105rf)*. The average induced VPCs of *frm-8(zh67); let-60(n1046gf)* was 3.4 (n=41) and therefore not significantly different from the induction of *let-60(n1046gf)*, which was 3.5 (n=46) (Table 3.1, rows 3, 4). Additionally, *frm-8(zh67); lin-2(n105)* animals showed an induction index of 1.1 (n=27) compared to *lin-2(n105)* single mutants which had 0.9 (n=25) induced VPCs in average. Although weak, the suppression of the *lin-2(n105)* was significant ($P<0.05$) (Table 3.1, rows 5, 6).

GFP-reporter expression analysis was next used to assay the activity of the LET-60 RAS pathway, using a previously established downstream target of the LET-23 cascade. EGL-17 is the orthologue of the human fibroblast growth factor and is transcriptionally regulated by the LET-23 pathway in the primary VPCs during the early steps of vulval development (Burdine et al. 1998, Yoo et al. 2004, Stetak et al. 2006). The expression of a transcriptional CFP reporter for *egl-17* (integrated transgene *arIs92*, Yoo et al. 2004) was quantified at the 1-cell stage of either wild-type or *frm-8(zh67)* animals (Figure 3.3 A, B). However, the mean intensity CFP signal of the analyzed *frm-8(zh67)* animals was not significantly different from

the wild-type samples (Figure 3.3 C). These epistasis results obtained with the *zh67* allele are inconsistent with the data from the RNAi screen where frm-8 RNAi clearly suppressed the *let-60(gf)* phenotype. A possible explanation for these conflicting results is that the *zh67* allele represents a weak reduction-of-function mutation, which would give a weaker effect compared to *frm-8* RNAi. Another possibility is that *frm-8* RNAi in the screen was not specific for *frm-8* alone, resulting in a simultaneous downregulation of a gene of similar sequence.

3.1.5 Downregulation of FERM genes in *frm-8(zh67)* does not result in a synthetic vulval phenotype, nor in enhanced mislocalization of LET-23.

In order to test the possibility of functional redundancy with other FERM encoding genes similar to *frm-8*, all FERM-domain encoding genes (including *frm-8* itself) were downregulated by RNAi in a *frm-8(zh67)* background. None of the tested RNAi clones resulted in a synthetic phenotype (data not shown). Additionally, the same set of RNAi experiments was subjected to immunostaining of LET-23 and its localization was assessed. No obvious change in LET-23 localization was observed following RNAi in the *frm-8(zh67)* background (data not shown).

3.1.6 Expression pattern of *frm-8*

To assess the expression pattern of *frm-8*, two transcriptional GFP reporters were constructed. Approximatively 9kb of the upstream sequence from the second exon of the *frm-8a* isoform and 6kb of the upstream sequence from the ATG of the *frm-8b* isoform were used as putative promoters, respectively. Reporters showed expression in the nervous system (head region and ventral nerve cord), the excretory cell and some unidentified cells in the tail region. The only difference between the expression pattern of the two constructs was for the *frm-8b* isoform reporter, which showed additional expression in the intestinal cells and some unidentified cells surrounding the pharynx (data not shown). In all analyzed animals, no expression was detected in the vulval cells.

The results presented in this section led to the conclusion that *frm-8* effects were generally weak and therefore the project was not continued. Instead I concentrated on the characterization of other candidate regulators of LET-23 localization.

3.2 Characterization of *tag-60*

3.2.1 General gene information and alleles

A genetic interaction between *tag-60* and *let-60 Ras* was previously found in a candidate-based RNAi screen (A. Stetak, personal communication). RNAi against *tag-60* was found to suppress the Muv phenotype of the *let-60(n1046gf)* mutant (A. Stetak, personal communication). In a subsequent experiment, downregulation of *tag-60* by RNAi in the *rrf-3(pk1426)* RNAi hypersensitive background (Simmer et al. 2003) seemed to mislocalize LET-23 in the primary VPCs to the apical junctions and intracellular punctae (A. Stetak, personal communication).

tag-60 is a gene encoded on chromosome IV at the genetic position of 4.05cM. There are presently 5 different isoforms confirmed by cDNA(s). Isoform a, c and d encode proteins with two PDZ domains and isoforms b and e with one PDZ domain (figure 3.5 B). All isoforms encode a putative ERM binding domain (EBD) at the C-terminus. *tag-60* does not have any paralogues in the *C. elegans* genome.

At the beginning of this study, only the *tag-60* allele *ok297* was available. *ok297* is a 724bp deletion which is located approximatively 500bp upstream of the ATG of the e isoform (figure 3.5 A). *ok297* does not remove any predicted regulatory or coding sequences. The *ok297* animals were received from the *C. elegans* knockout consortium but were not backcrossed. Interestingly they show a Pvl (Protruding vulva) phenotype, but no defects regarding vulval induction nor LET-23 localization were found (data not shown). Therefore, the first step of this project was to generate another deletion mutant of *tag-60*. The *zh93* allele was isolated following screening of six deletion libraries. This allele produces an in-frame deletion of 1’565bp that has its left breakpoint in exon 5a and its right breakpoint in exon 8a. *zh93* does not remove any predicted protein domains and it is the main allele used in this study (figure 3.5 A). *tag-60(zh93)* animals are superficially indistinguishable from wild-type worms.

The *tag-60(tm3501)* deletion was just recently generated by the Japan National Bioresource Project. tag-60(*tm3501)* animals harbour a 953bp deletion which begins in the exon 8a and ends within the predicted 3’UTR (figure 3.5 A). Therefore, the *tm3501* allele is likely a strong reduction-of-function allele. Further genetical experiments have to be done in the future to support this notion. However, also *tag-60(tm3501)* animals look superficially wild-type.

The *tag-60(ok2292)* deletion was recently generated by the *C. elegans* knockout consortium. The *ok2292* deletion has a size of 1’117bp and covers the ATG plus the exons 1, 2 and 3 of

the *tag-60e* isoform (figure 3.5 A), that encodes the PDZ 2 domain. Therefore, it is likely that *ok2292* represents a "null" allele of the *tag-60e* isoform. Regarding the other *tag-60* isoforms, the *ok2292* allele represents an "in-frame" deletion that removes the whole second PDZ domain. The phenotype of *tag-60(ok2292)* has not been investigated yet, although it is already known that they are viable and fertile.

3.2.2 TAG-60 is the putative *C. elegans* orthologue of EBP-50/NHE-RF1

There are 2 different human genes that encode a protein with the same domain architecture as TAG-60: EBP-50/NHE-RF1 (ERM binding phosphoprotein 50 / Sodium/Hydrogen exchanger regulatory factor 1) and NHE-RF2/E3KARP (Sodium/Hydrogen exchanger regulatory factor 2 / Exchanger isoform 3 protein kinase A regulatory protein). Both genes encode scaffolding proteins with a tandem PDZ domain and a large C-terminus, which does not harbour any predicted domains. As shown in figure 3.4, the alignment of the TAG-60a protein with EBP-50 and NHE-RF2 shows high degrees of similarity in the predicted PDZ domains and the C-terminus. Interstingly, the 30 distal amino acids of the EBP-50 C-terminus have been reported to bind ERM proteins in crystal structure analysis (Finnerty et al. 2004). The conserved domain architecture with 2 PDZ proteins and the similar C-terminus indicates that TAG-60 is the putative orthologue of EBP-50/NHE-RF1 and NHE-RF2/E3KARP. Since there are no other predicted genes that encode similar proteins in *C. elegans*, *tag-60* may be the sole gene encoding a EBP-50/NHE-RF1 or NHE-RF2/E3KARP homologue.

The N-terminal PDZ domain of EBP-50 has been shown to bind a plethora of different transmembrane proteins such as NHE-3 (Sodium/Hydrogen exchanger isoform 3), CFTR (Cystic fibrisis conductance transmembrane receptor), β2-adrenergic receptor, PDGF-R (Platelet derived growth factor receptor) and EGFR and regulate their localization and activation (Bretscher et al. 2000 and Weinman et al. 2006). Furthermore, the C-terminus of EBP-50 can bind the FERM-domains of Ezrin and Merlin, two related proteins of the FERM superfamily (Bretscher et al. 2002). EBP-50 has been suggested as a candidate tumor suppressor gene in human breast cancer, as it was found to be associated with the two tumor suppressors Merlin/Nf2 and SYK (spleen tyrosin kinase). Loss of heterozygosity (LOH) at the EBP-50 locus was associated with breast cancer initiation and/or progression and the mutations affected the SYK and Merlin/Nf2 binding sites within EBP-50 (Le Dai, 2004). EBP-50 is proposed to act as a scaffold protein that organizes signal transduction complexes at the plasma membrane. Lazar et al. (2004) showed that EBP-50 inhibits ligand induced internalization of EGFR. Curto et al. (2007) and Cole et al. (2008) demonstrate that Merlin

and EBP-50 mediate contact-dependent EGFR inhibition. In contrast to these retention functions, EBP-50 was found to be a necessary component of the endocytic recycling of the β2-adrenergic receptor (Cao et al. 1999).

3.2.3 TAG-60 is a putative regulator of LET-23 localization

The *tag-60(zh93)* mutant was used to confirm the genetic interaction observed in the initial RNAi screen of A. Stetak. Monitoring the localization of LET-23 in the primary VPCs was performed by immunostaining and subsequent epifluorescence or confocal laser scanning microscopy. In wild-type worms, LET-23 was expressed at the time of induction in all 6 VPCs (data not shown). Upon induction by the LIN-3 ligand, the receptor was upregulated in P6.p and degraded in all the other VPCs. As development proceeds, the expression levels of LET-23 were increased in the primary vulval lineage. In P6.p, LET-23 was predominantly localized at the basolateral membrane (figure 3.6 A). Additionally, LET-23 was localized to a lesser amount in the intracellular space and in an unidentified compartment facing the apical side of the cell (figure 3.6 A). In *tag-60(zh93)* animals, there seemed to be similar amounts of receptor in the VPCs, but the localization of LET-23 was slightly aberrant, as the basolateral localization was reduced and the accumulation of LET-23 in intracellular punctae enhanced (figure 3.6 B). This effect seemed to persist in the 2-cell stage (figures 3.6 D, F compared to 3.6 C, E). Immunostaining of LET-23 is variable, in which high levels of LET-23 intracellular signal compared to predominantly basolateral localization occurred with a penetrance of 10% and 90% (n=many) in wild-type, respectively (figure 3.6 C, E). The fraction of animals having intracellular accumulation of LET-23 was increased to approximatively 40% (n= 31) in *tag-60(zh93)* animals (figure 3.6 D). In the remaining 60% of cases, LET-23 seemed to have predominant basolateral localization similar to wild-type worms (figure 3.6 C). In conclusion, a significant fraction of the *tag-60(zh93)* worms appeared to have mislocalized LET-23 to unidentified intracellular compartments, relative to wild-type worms. Since VPC induction is unaffected in *tag-60(zh93)* animals, it is likely that LET-23 is delivered correctly to the basolateral membrane. Thus, TAG-60 rather plays a role in the retention of LET-23 at the plasma membrane or during post-endocytic LET-23 recycling.

3.2.4 *tag-60(zh93)* genetically interacts with mutants of the LET-23 pathway

The first criteria of the initial RNAi screen was the genetic interaction with *let-60(n1046gf)*. *tag-60* RNAi significantly suppressed the *let-60(gf)* Muv phenotype, which indicated that *tag-60* encodes a positive regulator of the inductive pathway (A. Stetak, personal

communication). Since the two genes *let-60* ras and *tag-60* are both located on chromosome IV and less than 1cM apart, the construction of the double mutant *tag-60(zh93); let-60(n1046gf)* was not attempted. Instead, a heat-shock inducible transgene combination of MPK-1 and MEK-2 (*gaIs36*, Lackner et al. 1994) was used to induce a Muv phenotype in a *tag-60(zh93)* background. However, *tag-60(zh93)* did not significantly alter the average number of induced VPCs of *gaIs36* animals after heat-shock treatment (figure 3.7).

Reduction-of-function alleles of positive regulators of the LET-23 pathway were also used to quantify the effects of *tag-60(zh93)* on vulval induction. The *lin-2(n105rf)* weak Vul mutant was used to test whether this phenotype was enhanced in combination with *tag-60(zh93)*. Surprisingly, *tag-60(zh93)* suppressed the *lin-2(n105)* Vulvaless phenotype (I=2.2) to wild type levels (I=3; figure 3.7). This result was reproduced with the stronger *lin-2(n397)* allele, where the average induction index was supressed from 0.2 to 1.8 in a *tag-60(zh93); lin-2(n397)* double mutant. In contrast, *tag-60(zh93)* was not able to significantly suppress the vulvaless phenotypes of *lin-7(e1413)*. In the double mutant with *lin-10(e1439)*, a certain degree of suppression was observed, which was not statistically significant (figure 3.7). Since *lin-2(n397)* is supposed to be a null allele (Hoskins et al. 1996), the genetic interaction with *tag-60(zh93)* indicates that it acts in parallel to or downstream of *lin-2*. On the other hand the strong loss-of-function alleles of *lin-7* and *lin-10*, did not show any statistically significant alteration of the induction index, indicating that either *tag-60* acts genetically upstream of *lin-7* and *lin-10*, or that the regulation mechanism of vulval development by TAG-60 is dependent on LIN-7 and LIN-10.

The combination of *tag-60(zh93)* with different reduction-of-function alleles of *let-23* uncovered interesting genetic interactions. The double mutant with *let-23(sy10)*, which encodes a receptor with a missense mutation in the first cystein-rich region of the extracellular domain (Aroian et al. 1994), showed a suppression of the Vulvaless phenotype (I=1.7) in comparison to the single mutant (I=0.5). In contrast, *let-23(sy1); tag-60(zh93)* did not show any suppression compared to the *let-23(sy1)* single mutant (figure 3.7). The *sy1* allele is a LET-23 variant, which lacks the last 6 amino acids and thereby fails to interact physically with LIN-7 and so it is mainly localized at the apical compartment of the VPCs (Aroian et al. 1994, Simske et al. 1996, Kaech et al. 1998). Thus, the C-terminus of LET-23 is probably involved in the regulation of vulval development by TAG-60.

Additionally, the Vulvaless reduction-of-function allele *sem-5(n2019)* (Clark et al. 1992) was suppressed by *tag-60(zh93)*. However, it is not clear if *tag-60* acts up- or downstream of *sem-*

5, since the *sem-5(n2019)* allele does not represent a null allele and null alleles of *sem-5* are lethal (figure 3.7).

Collectively, these results indicate that *tag-60(zh93)* mutants have augmented activity of the inductive and/or lateral signalling pathway, which is able to suppress the Vul phenotypes of *lin-2(lf)*, *let-23(sy10)* and *sem-5(n2019)*, but not of *lin-7(e1413)*, *lin-10(e1439)* and *let-23(sy1)*. However, the combination of *tag-60(zh93)* with mutants of previously characterized negative regulators of the inductive pathway, *gap-1(ga133)* (Hajnal et al. 1997), *sli-1(sy143)* (Jongeward et al. 1995), *unc-101(sy108)* (Lee et al. 1994), *dpy-23(e840)* (Pan et al. 2008) and *dep-1(zh34)* (Berset et al. 2005) did not result in a synthetic phenotype (figure 3.7).

3.2.5 *egl-17::cfp* expression is reduced in the 1° cells of *tag-60(zh93)*

To test whether *tag-60(zh93)* influences the inductive pathway, a transcriptional reporter for *egl-17* was used as a read-out. *egl-17* encodes the *C. elegans* fibroblast growth factor (FGF) homologue which is the attracting cue for the sex myoblasts, which later form the muscles for the whole egg-laying system (Burdine et al. 1998). *egl-17* has been shown to be transcriptionally regulated by the inductive pathway and is expressed in the 1° lineage of the vulva from the 1-cell stage to the 4-cell stage. The *arIs92[egl-17::cfp]* transcriptional reporter has repeatedly been used as a marker for the 1° VPCs and hence as an indicator for the activity of the inductive pathway (Yoo et al. 2004, Stetak et al. 2006). Worms harbouring the transgene *arIs92* in a wild-type or *tag-60(zh93)* background were synchronized and L1 larvae grown at 20°C for 28h, 32h and 36h. The timepoints represent 1-cell, 2-cell and 4-cell stage of vulval development. For each timepoint the worms were mounted on a microscope and the focal plane set to the approximate midplane of the nuclei of the VPCs. Pictures were taken in the DIC and the CFP filter and the average *egl-17::cfp* intensity was measured. Interestingly, the *tag-60(zh93)* mutant showed in average a significant reduction of 20-30% in *egl-17::cfp* expression in the 1° cells at the 2- and 4 cell stage (figure 3.8, P6.px and P6pxx respectively). This result suggests, that the LET-23 pathway activity is reduced in the primary vulval cells of *tag-60(zh93)* animals.

Previously characterized mutants of negative regulators of the inductive pathway, as for expample *puf-8*, showed as well a reduction of *egl-17::cfp* in the 1° lineage, but additionally display ectopic expression in the 2° lineage (Walser et al. 2006), which is not the case in wild-type nor in the *tag-60(zh93)* mutant backgrounds. In addition, reduction-of-function alleles of negative regulators like *puf-8*, show a synthetic Multivulva phenotype in combination with other mutants of negative regulators of the inductive pathway such *as gap-1* (Walser et al.

2006). The fact that *tag-60(zh93); gap-1(ga133)* showed wild-type vulval development (figure 3.7), can be interpreted in several ways. *tag-60* might encode a negative regulator of the inductive pathway (assuming that *zh93* is a reduction-of-function allele), which acts genetically upstream of *gap-1*. On the other hand, assuming that *tag-60* and *gap-1* act in parallel pathways, it is possible that in the double mutant LET-23 signalling is not sufficiently increased to bypass the threshold to produce ectopic inductions. Alternatively, that *tag-60* might not only regulate the inductive pathway but other signalling pathways involved in vulval development. Further genetic data is required to dissect the different functions of *tag-60* during vulval development.

3.2.6 *zh93* is a dominant allele of *tag-60*

As described before, the *zh93* allele is an in-frame deletion, which does not affect any predicted domains of TAG-60. In order to assess the nature of the *zh93* allele, different kinds of experiments were performed. For example, if a mutant phenocopies the effects observed in the corresponding RNAi experiment leads to the conclusion that the mutant allele represents a reduction-of-function allele. Following this idea, the defects associated with the *tag-60(zh93)* allele were compared to *tag-60 RNAi* experiments.

Hamilton et al. (2005) found *tag-60* to increase the average lifespan of *C. elegans* when downregulated by RNAi. *tag-60(zh93)* was therefore tested for its effect on lifespan. The idea behind this experiment was to test if *tag-60(zh93)* mimicks the “reduction-of-function” effect of the RNAi observed in the longevity screen. 100 L4 wild-type and *tag-60(zh93)* worms were observed and their lifespan scored. In my experiments, the *tag-60(zh93)* allele did not have a significant effect on the lifespan compared to the wild-type control (data not shown).

Alternatively, RNAi experiments were performed to examine whether *tag-60* RNAi phenocopies the suppressive effect of *tag-60(zh93)* with the *lin-2(n397)* Vulvaless phenotype. If *tag-60(zh93)* represented a gain-of-function allele, the *tag-60(zh93); lin-2(n397)* induction would be reduced by *tag-60* RNAi. Therefore, either *lin-2(n397)* or *tag-60(zh93); lin-2(n397)* worms were subjected to *tag-60* RNAi by feeding. The *tag-60* RNAi clone from the Vidal feeding library was used (Rual et al. 2004), which consists of the *tag-60a* cDNA flanked by T7 promoters. As shown in Table 3.2, both experiments resulted in no significant change in the VPC induction index. Nevertheless, the average induction of *tag-60(zh93); lin-2(n397)* was slightly reduced from 1.6 (RNAi vector control) to 1.2 or 1.1 respectively. It is notable that the P-Value for one of these comparisons was 0.057 (Table 3.2, row 6). Given the possibility that the RNAi of *tag-60* is not very efficient, maybe scoring a larger population of

worms would result in a significant change. If that were to be true, *zh93* would represent a gain-of-function mutation.

To further examine the nature of the *tag-60(zh93)* allele, the *tag-60(zh93)* mutation was placed in *trans* to the balancer nT1 in a *lin-2(n397)* background. Heterozygous *tag-60(zh93)* also suppressed the Vul phenotype of *lin-2(n397)* to the same extent as homozygous *tag-60(zh93)* (data not shown), strongly suggesting that *zh93* is a dominant mutation. This is consistent with the hypothesis posted after the RNAi results. Thus, *zh93* represents a dominant allele of *tag-60*, which might be a gain-of-function variant. Experiments using other *tag-60* alleles (*tm3501* and *ok2292*) are currently being performed to clarify this issue.

3.2.7 Expression analysis of *tag-60*

Given the complexity of the *tag-60* locus (figure 3.5), 3 different transcriptional GFP reporters were generated. The different putative promoters were fused with the coding sequence of NLS::GFP::LacZ by PCR fusion.

The first reporter harboured 2kb upstream sequence of the ATG of the *tag-60a* isoform and showed GFP expression in the pharynx, the intestine, one unidentified cell in the head region that could potentially be part of the excretory system and some unidentified cells in the tail (data not shown). The second reporter contains 2kb of upstream region of the b isoform ATG until the first cluster of exons of the a isoform. Three independent transgenic lines were analyzed, but no GFP expression was observed at all (data not shown). This can be interpreted as a non-functional reporter lacking important regulatory elements for expression. The third reporter consisted of the putative promoter of the *tag-60e* isoform, which contains 6kb from the ATG until the first exon of the *tag-60b* isoform. This reporter showed a very similar expression pattern as the reporter for the *tag-60a* isoform in three independent transgenic lines (data not shown).

Taken together, these results indicate that *tag-60* messages of the a, c, d and e isoforms might be generated in the pharynx, the intestine and some unidentified cells, but not in the developing vulva. Therefore, *tag-60* might acts cell-nonautonomously during vulval development, or the GFP reporters used did not contain all regulatory sequences for complete expression (including putative expression in the VPCs).

To further examine the expression of TAG-60 and to analyze its subcellular localization, two different polyclonal rabbit antisera were raised. Two peptides were used as epitopes for the generation of TAG-60 antibodies. The first peptide (TAG-60e amino acids 28-41 / NSAYQYKESSTAYD; referred to as “peptide 1”), is present in TAG-60a, b and e isoforms

only and is located within the *zh93* deletion (figure 3.9 A) The second peptide is located in the N-terminus of the TAG-60e isoform (TAG-60e amino acids 4-16 / LPRLAELNKGTPD; referred to as "peptide 2") and is present in all predicted TAG-60 isoforms (figure 3.9 B). Antibodies generated against peptide 1 and peptide 2 are referred to as αTAG-60-1 and αTAG-60-2, respectively.

Immunostaining of worms with αTAG-60-1 showed a similar expression pattern as observed with the transcriptional GFP reporters, with staining in the intestine, the pharynx and unidentified cells in the head and tail regions (figure 3.9 C). Additionally, signals were detected in the developing uterus and vulva originating from intracellular compartments at the early L4 stage (invagination of vulval tissue, figure 3.9 E, E'), which fades during the L4 stage (figure 3.9 F, F'). The function of TAG-60 in late vulval and early uterine development is not known to date. Curiously, TAG-60 expression was absent throughout the early inductive stages of vulval development. Interestingly, the intestinal cells show exclusive apical localization of TAG-60, as reported for its orthologue EBP-50 in mammals, where it forms a functional unit with Ezrin to link transmembrane proteins to the peripherical actin cytoskeleton (Bretscher et al. 2002).

Except for the pharynx, all signals observed following immunostainings with αTAG-60-1 were absent in *tag-60(zh93)* animals and hence, specific for TAG-60 (data not shown). Henceforth, the antibody αTAG-60-1 was used in other experiments of this study.

The immunostaining showed expression of TAG-60 during late vulval development much later than the vulva induction and patterning events. It is possible that TAG-60 is expressed at low levels during the time of induction, but not detectable by αTAG-60-1. Alternatively, it is known that adjacent tissues such as the hypodermis (Cui et al. 2006) and the nervous system (Battu et al. 2003) can influence vulval induction. No gene has yet been reported to influence VPC induction from the intestine or uterus.

Immunostaining with αTAG-60-2 showed expression in structures resembling the nerve ring (figure 3.9 D) and the ventral nerve cord (data not shown). The signal from the αTAG-60-2 was insensitive to the *zh93* deletion, as mixed stage *tag-60(zh93)* animals showed the same expression pattern as wild-type animals (data not shown).

3.2.8 Investigation of the cellular focus of *tag-60*

Tissue-specific rescue experiments were conducted to investigate the cell autonomy of TAG-60 during vulval development, owing to lack of expression of TAG-60 in the VPCs during induction (N.B. these experiments were performed prior to determining the dominant nature

of the *zh93* allele). Tissue specific promoters were used to construct translational YFP fusion proteins of the TAG-60a isoform. The TAG-60a isoform was chosen because it represented the predominant transcript, when analyzing the cDNAs originating from the *tag-60* locus (data not shown). The *opt-2* promoter was used for specific expression in the intestine (Nehrke 2003), the *vab-9* promoter for all epithelial cells (Simske et al. 2003) and the vulva specific element of the *lin-31* gene for exclusive VPC expression (Tan et al. 1998, A.Stetak, personal communication). These constructs were injected into *tag-60(zh93); lin-2(n397)* animals, analyzed for proper expression and the vulval induction index was scored. If *zh93* was a reduction-of-function allele, the average induction index would be expected to reduce to levels similar to *lin-2(n397),* as the transgene would rescue the effects of the *zh93* allele. Alternatively, if *zh93* represented a gain-of-function allele, the average induction index would be expected to increase, since the additional gene dosage would likely enhance the effect of *zh93*.

As shown in figure 3.10, all established transgenic lines did express the TAG-60a::YFP fusion protein in the expected tissues. Notably, the YFP signal from the construct with the *opt-2* promoter mimicked the apical localization of TAG-60 in the intestinal cells (figure 3.10 A, A'), observed in the immunostaining experiments (figure 3.9 C), indicating that the YFP did not interfere with the localization, and potentially the function, of the fusion protein.

In the construct with the *vab-9* promoter, no clear expression was observed in the VPCs, although a bias towards the apical compartment of the late vulval cells was observed (figure 3.10 B, B', arrowheads). In a few animals also basolateral (figure 3.10 B, B', arrow) localization was observed. The *vab-9* promoter is highly expressed in the developing uterus and hence masks the signal in the early VPCs. Therefore, the localization of the fusion protein driven by the *vab-9* promoter was not determinable at the time of induction.

The reporter with the *lin-31* promoter element showed very weak activity. By pushing the sensitivity of the camera, expression in the VPCs was seen and the fusion protein localized generally to the entire plasma membrane (figure 3.10 C, C', arrowheads) and to the junctions (figure 3.10 C, C' arrows) at the time of induction. Taken together, the TAG-60a::YFP fusion protein can localize to plasma membrane compartments and the junctions depending on the cellular context.

As shown in table 3.3, none of the established transgenic lines could suppress or enhance the induction index of the *tag-60(zh93); lin-2(n397)* animals (rows 2-9 compared with row 1). Different explanations could account for this finding: first, the YFP tag might not interfere with the localization but diminish the activity of the fusion protein. Second, the transgenes are

encoded on extrachromosmal arrays, which are transmitted randomly in the cell-lineages and therefore the established lines could represent mosaic animals. Therefore, it is possible that not all cells, which require TAG-60 function possess the transgene. Third, the cDNA of the *tag-60a* isoform was used to construct the fusion proteins because it seems to be the most abundant of all *tag-60* isoforms. It is possible that the wrong isoform was used for this experiment, or that different isoforms act in a cooperative manner and are thus all necessary for proper TAG-60 function. Lastly, the described suppression of the *lin-2(n397)* Vulvaless phenotype might be due to another mutation in the background of the *tag-60(zh93)* mutant strain.

In order to address these possibilities, a similar approach was used, where a 17kb genomic piece of the *tag-60* locus was amplified by PCR. Three different PCR products covering 5.8kb upstream of the ATG of the a isoform until 1kb downstream the STOP of all *tag-60* isoforms were fused together and injected into *tag-60(zh93); lin-2(n397)* animals. It was rationalized that the resulting extrachromosomal arrays would represent overexpressions of all endogenous *tag-60* isoforms. One out of five established lines enhanced the suppression of *tag-60(zh93)* towards *lin-2(n397)* from 1.77 to 2.60 average induced VPCs (table 3.3, rows 1, 10). The remaining four lines showed no significant change in the average number of induced VPCs (table 3.3, rows 1, 11-14). These results may indicate that the *zh93* mutation is a gain-of-function allele of *tag-60*, whose effect on the *lin-2(n397)* Vul phenotype was enhanced by providing additional *tag-60* gene copies on the extrachromosomal array.

3.2.9 αTAG-60-1 recognizes a putative novel TAG-60 isoform of ~80kDa

The purified TAG-60 antibodies described above were tested in Western Blot experiments. Mixed-staged wild-type or *tag-60(zh93)* animals were lysed in 2xSDS loading buffer and separated on a SDS-PAGE gel. In the case of αTAG-60-1, a band of the approximative size of 80kDa was present in the wild-type lysate (figure 3.11, red star), but was absent in the *tag-60(zh93)* sample. Since αTAG-60-1 recognizes an epitope within the *zh93* deletion, this 80kDa band is very likely to represent a TAG-60 isoform. Since TAG-60b is the isoform with the highest predicted molecular weight (68.2kDa), the higher band found in this experiment indicates that either TAG-60 proteins are being posttranslational modified or that larger TAG-60 isoforms are existing. It is unclear why no other bands sensitive to the *zh93* deletion were detected, as the confirmed cDNAs predict proteins of different molecular weights: 52kDa (a isoform), 68.2kDa (b isoform) and 37.1kDa (e isoform). More detailed analysis of different stages throughout development might uncover stage-specific expression of the TAG-60

isoforms. As already mentioned above, αTAG-60-1 might not recognize the isoforms c (47.5kDa) and d (50.1kDa).

To assess the possibility of the existance of a larger TAG-60 isoform, we hypothesized that an alternative a isoform, spliced with the first exon of the b isoform might be formed. This new isoform, "*tag-60a+b*", would account for the approximate 80kDa seen on the Western Blot. cDNA samples of whole wild-type RNA were generated and analyzed by PCR using one forward primer within the first exon of *tag-60a* and one reverse primer within the first exon of *tag-60b*. Indeed, the two primers could amplify a sequence harbouring the first 3 exons of *tag-60a* and the first exon of *tag-60b* (data not shown). This experiment indicated that the putative isoform "*tag-60a+b*" exists, although cloning of the whole cDNA still has to be performed.

The αTAG-60-2 antibody, which presumably recognized head neurons in immunostaining experiments (figure 3.9 D), produced multiple bands in wild-type lysates which were also present in the *tag-60(zh93)* lysates (data not shown). Truncated TAG-60 proteins were expected, assuming that the *tag-60(zh93)* deletion produces proteins of smaller molecular weight, which was not the case. Therefore, αTAG-60-2 might not be suitable for Western Blot analysis.

3.3 Characterization of *erm-1*

3.3.1 ERM-1 is the orthologue of Ezrin, Radixin and Moesin

C. elegans ERM-1 was investigated during this study, since it is a putative physical interactor of TAG-60 (see chapter 3.3.3). Ezrin, Radixin and Moesin are members of the FERM (4.1/Ezrin/Radixin/Moesin) superfamily. These family members share a FERM domain, which is a protein interaction module (Chishti et al. 1998, Bretscher et al. 2002). A subfamily is the ERM-like proteins, which consists of Ezrin, Radixin, Moesin and Merlin (Bretscher et al. 2002). These proteins have been shown to self-associate through intramolecular association of the distal termini (Pearson et al. 2000). One of the main differences between these proteins is that Ezrin, Radixin and Moesin contain an F-actin binding interface at the C-terminus, which is not present in Merlin. ERM proteins are known to be organizers at the plasma membrane, by linking the peripherical actin cytoskeletion with transmembrane proteins (Bretscher et al. 2002). It is thought that in this way, functionally distinct microdomains are formed at the plasma membrane. As shown in figure 3.12, the sole *C. elegans* orthologue of Ezrin, Radixin and Moesin is called ERM-1 (Göbel et al. 2004). The N-terminal FERM-domain is very well conserved (figure 3.12, red line), whereas the C-terminus displays lower levels of sequence conservation. *C. elegans* ERM-1 was investigated in this study, as it is a putative physical interactor of TAG-60 (see chapter 3.3.3).

Biochemical and structural analysis of proteins of the ERM family have revealed that they exist in two different states: a folded, globular (inactive) and an extended (active) state. Transition between these two states is thought to be regulated by the phosphorylation status of a C-terminal threonine (figure 3.12, red dot, Bretscher et al. 2002) and by binding of phospholipids to the FERM-domain (figure 3.13). It has been proposed that ERMs can homo- and heterodimerize, but also form oligomers in their active state (Berryman et al. 1995, Gautreau et al. 2000). The subcellular localization of ERMs is tissue-specific, but the generally localize to the periphery of most cells.

The FERM domain has been shown to bind transmembrane proteins directly, or indirectly via the scaffolding PDZ-domain proteins EBP-50/NHERF1 or E3KARP/NHERF2 (Bretscher et al. 2002, figure 3.13). This set up has been proposed to form functionally distinctive microdomains at the plasma membrane. However, the biological outcome of this interaction seems to be dependent on the cellular context, and also on its interacting transmembrane proteins and its associated factors. It has also been proposed that the linkage between the actin

cytoskeleton and the plasma membrane can influence the activity and the trafficking of certain transmembrane receptors (Bretscher et al. 2000, Bretscher et al. 2002).

ERM-like proteins have been demonstrated to influence EGFR activity in human tissue culture cells, as Merlin together with EBP-50, control the contact dependent inhibition of EGFR. The model is that association of EGFR with EBP-50 and Merlin renders the receptor to an inactive state, and shifts it to a microdomain, where its endocytosis is blocked (Curto et al. 2007, Cole et al. 2008).

Ezrin is a putative target of EGFR in human epidermoid carcinoma A431 cells (Krieg and Hunter 1992). After stimulation of A431 cells with EGF, Tyr145 and Tyr353 of Ezrin are phosphorylated. Subsequent *in vitro* expriments showed that EGFR directly phosphorylates Ezrin at the proposed tyrosine residues (Krieg and Hunter 1992). However, Ezrin Tyr145 and Tyr353 are not conserved with *C. elegans* ERM-1 (figure 3.12, blue dots).

3.3.2 *erm-1* is an essential gene involved in tubular morphogenesis

The *C. elegans erm-1* gene encodes the sole orthologue of the human proteins Ezrin, Radixin and Moesin. It is located in the middle of chromosome I (-0.18cM / 5291608bp) and encodes a protein of 563 amino acids. Göbel et al. (2004) showed that *erm-1* is an essential gene, as animals homozygous for the loss-of-function allele *erm-1(tm677)* are maternally rescued for the lethality but some animals show an enlarged intestinal lumen and a Pvl (protruding vulva) phenotype. These animals have reduced fertility, but most of the F2 progeny dies as early larvae. The *tm677* allele represents a 972bp deletion spanning from the 6th to the 7th exon of the a isoform (figure 3.15). *tm677* furthermore seemed to represent a “null” allele, as trans-heterozygotes with a deficiency did not result in enhanced defects. However, *erm-1(tm677)* animals undergo wild-type induction of the VPCs and only develop morphological defects at the stage where the vulva tissue starts to invaginate (migration and elongation of vulval cells).

Göbel et al. (2004) showed that *erm-1* is expressed in all tubular epithelia as the pharynx, intestine, excretory system, the uterus and the vulva. Since the *erm-1(tm677)* animals show severe morphological defects in these tissues, they proposed a cell-autonomous role of *erm-1* in lumen morphogenesis. Consistent with these results, they showed that a translational GFP reporter of *erm-1* was localized exclusively on the apical compartment (facing the lumen) of these polarized cells. These results suggested that ERM-1 is a valid orthologue of Ezrin, since this protein has been found to be expressed at the apical side of intestinal cells, where it is necessary for microvilli architecture by linking the cortical cytoskeleton to the plasma membrane. Importantly it was also shown that the *erm-1* mutation does not disturb the apico-

basolateral polarity *per se*, but affects the remodelling of the apical surface of intestinal cells (Göbel et al. 2004).

3.3.3 ERM-1 is necessary for TAG-60 localization in *C. elegans*

Some observations lead to the intriguing hypothesis that ERM-1 and TAG-60 form a complex in *C. elegans*. First, it has been shown that human EBP-50 binds to the FERM-domain of Ezrin via its 30 distal carboxy-terminal amino acids (Finnerty et al. 2004). As shown in figure 3.14 A, the alignment of the C-termini of TAG-60a, EBP-50 and NHERF2 shows low level of similarity and hence no good conclusion can be drawn from the sequence analysis. If *C. elegans* TAG-60 and ERM-1 physically associate, removal of one component may influence the localization of its respective partner. To examine this possibility, control and *erm-1* RNAi (Vidal RNAi clone, Rual et al. 2004) worms were immunostained with αTAG-60-1 to visualize TAG-60 localization. Control RNAi experiments showed the previously characterized apical localization of TAG-60 in the intestine (figures 3.9 C and 3.14 B, arrowheads). In contrast, the *erm-1* RNAi animals mislocalized TAG-60, with enrichment in subapical intracellular compartments (figure 3.14 C, arrows). Therefore, the proper localization of TAG-60 is dependent on the presence of ERM-1. Moreover, D. Kradolfer and E. Fröhli showed that the ERM-1::CFP fusion protein is coimmunoprecipitated with TAG-60 (unpublished results). Additionally, ERM-1 has been found to physically interact with TAG-60 in Yeast-2-Hybrid experiments (Li et al. 2004). Altogether, these results indicate that ERM-1 and TAG-60 might form a functional unit in *C. elegans* as demonstrated in other systems (Bretscher et al. 2002).

3.3.4 LET-23 appears to be mislocalized in *erm-1(tm677)* animals

While *erm-1(tm677)* animals display obvious defects in vulval morphogenesis, they exhibit wild-type induction of the VPCs. *erm-1* was a candidate in the initial RNAi screen of A. Stetak. The RNAi experiment (Ahringer clone, Kamath et al. 2003) did not cause any effects reminiscent to the phenotype of the allele *tm677*. Therefore, this particular mutant was analyzed in respect to vulval development and LET-23 localization. At this timepoint we obtained the strain VJ311 with the genotype *erm-1(tm677) / unc-63(x18) dpy-5(e61)*. The *erm-1(tm677)* was balanced over two markers visible under the dissecting microscope. This strain was subjected to immunostaining to visualize LET-23 and the apical junctions and optical sections were recorded by confocal microscopy. This strain had the disadvantage that *erm-1(tm677)* homozygous or *erm-1(tm677) / unc-63(x18) dpy-5(e61)* were theoretically

undistinguishable in fixed samples, unless the homozygous worms have a striking defect in terms of the visualized proteins. Indeed, some animals were found, which expressed LET-23 around the plasma membrane of intestinal cells (figure 3.16 F). In wild-type animals, LET-23 is found exclusively localized on the apical compartment of intestinal cells (figure 3.16 E), where it performs a yet unknown function. The animals with misexpressed LET-23 in the intestinal cells were analyzed for the LET-23 localization in the VPCs. Compared to wild-type LET-23 localization (figure 3.16 A, D), the receptor was found to be expressed not only on the basolateral membrane, but in intracellular punctae and the junctions (n=5, Figure 3.16 B). To confirm this result, another strain was constructed to facilitate the analysis of LET-23 localization. The *erm-1(tm677)* lethality was rescued with a large genomic DNA fragment (around 12kb) of the *erm-1* locus. This genomic fragment was introduced into the worms by microinjection and presence of the genomic DNA was observed by the coinjection marker *sur-5::gfp*, a ubiquitously expressed transgene (Yochem et al. 1998). The *sur-5::gfp* marker indicated the presence of the extrachromosomal array that rescued the lethality of the *erm-1(tm677)* deletion. This strain was subjected to immunostaining against LET-23. Worms which had no *sur-5::gfp* expression (and hence lost the genomic *erm-1* rescue transgene) were then analyzed using epifluorescence microscopy. Approximatively 50% (n=28) of the *sur-5::gfp* negative worms showed mislocalized LET-23 to intracellular punctae when compared to wild-type animals. Thus, the effects on LET-23 localization were similar in *erm-1(tm677)* compared to what was observed in *tag-60(zh93)* animals (figure 3.6). Since the human orthologues of ERM-1 and TAG-60 were shown to act together to regulate transmembrane proteins (Bretscher et al. 2002) and because both mutants showed similar phenotypes with regards to the localization of LET-23, it is a possibility that TAG-60 acts together with ERM-1 in the retention or recycling of LET-23 at the basolateral membrane of the VPCs.

3.3.5 *erm-1(tm677)* genetically interacts with the LET-23-pathway

The *erm-1(tm677)* mutant strain was next used for epistasis analysis with components of the LET-23 pathway. For this purpose, the strain *erm-1(tm677) / hT2 [gfp]; let-60(n1046)* was constructed. *hT2* is a chromosome translocation marked with pharyngeal *myo-2::gfp*. Animals with GFP positive (GFP^+) pharynx were therefore heterozygous for *tm677*, whereas GFP negative (GFP^-) animals were homozygous for *tm677*. The average vulval index was scored in both types of worms and was enhanced from 3.8 (n=39) in GFP^+ animals to 5.1 (n=26) in GFP^- animals ($P<0.001$) (Table 3.4, rows 4, 5). Since the *tm677* allele is considered to be a "null" allele (Göbel et al. 2004), these results strongly suggested that ERM-1 represents a

novel negative regulator of the inductive pathway. While the scoring of the vulval index in *erm-1(tm677)* is not precise due to severe vulval morphology defects, the enhanced number of invaginations of ectopic inductions was nonetheless striking. Interestingly, the combination of *erm-1(tm677)* with *gap-1(ga133)* did not result in a synthetic vulval phenotype despite both genes being negative regulators of the inductive pathway (table 3.4).

Loss-of-functions mutants of *lin-2*, *lin-7* and *lin-10* were next analyzed in combination with *erm-1(tm677)*. Due to the previously mentioned difficulties experienced while scoring the induction of *erm-1(tm677); let-60(n1046)* animals, worms were grouped into three distinct classes: Completely Vul (induction index I=0), partially induced (0<I<3) and wild-type (I=3). Approximatively 80% of both *lin-2(n397)* and *lin-7(e1413)* and 65% of *lin-10(e1439)* animals heterozygous for *erm-1(tm677)* were completely Vul, while in a homozygous *erm-1(tm677)* background the proportion of completely Vul animals was reduced to 11% (*lin-2*, *lin-7*) and 5% (*lin-10*), respectively (figure 3.17).

Further genetic experiments were performed by D. Kradolfer, who found that *erm-1(tm677)* was able to suppress the *let-23(sy1)* but not the *lin-3(e1417)* or *lin-45(sy96)* Vulvaless phenotypes (unpublished results). Interestingly, the regulation of the LET-23 pathway by ERM-1 seems to be independent on the C-terminal PDZ binding motif of LET-23, which is missing in the LET-23 variant encoded by the *sy1* allele. The results with *lin-3(e1417)* might indicate that the inhibitory role of ERM-1 is dependent on the activation of LET-23. Since the *lin-45(sy96)* allele does not represent a “null” allele, *erm-1* does not necessarily act genetically upstream of *lin-45 raf*. The finding that *erm-1(tm677)* does not alter the average number of induced VPCs of *lin-45(sy96)* could mean that the negative regulation of the LET-23 pathway by ERM-1 is dependent on LIN-45 Raf activity. Altogether, these results support the notion of ERM-1 being a negative regulator of the LET-23 pathway.

However, *erm-1(tm677)* suppressed the Vulvaless phenotype of *lin-7(e1413)*, *lin-10(e1439)* and *let-23(sy1)*, whereas *tag-60(zh93)* did not. In the last paragraph, a model of TAG-60 and ERM-1 as a functional unit in the regulation of LET-23 (localization) was proposed, which was challenged by the genetic data collected with *tag-60(zh93)* and *erm-1(tm677)*. The genetic data indicates that the two factors regulate the LET-23 pathway in a more complex manner.

3.3.6 ERM-1::CFP is localized to the basolateral membrane of the VPCs (D. Kradolfer)

Work by David Kradolfer from our lab suggests that ERM-1 is not exclusively localized to the apical compartment of all tubular epithelia, as stated by Göbel et al. (2004). The

translational reporter of *erm-1* included the endogenous promoter and the *erm-1a* cDNA. Transgenic worms harbouring this reporter have been shown to rescue the lethality associated with *erm-1(tm677)* mutants. These rescued lines were nevertheless very sick, indicating that either the C-terminal CFP interferes with ERM-1 function, or that overexpression of ERM-1 gives similar phenotypes as reducing its activity. The subcellular localization of the fusion protein was similar as reported by Göbel et al. with one important exception: a closer look at the developing vulva revealed that in several lines, ERM-1::CFP was specifically localized to the basolateral compartment of the primary and secondary vulval cells (Figure 3.18, arrows). Some fraction of the fusion protein might also be localized at the apical junctions (Figure 3.18, arrowheads). These preliminary results extend the data gained by Göbel et al. (2004), where they reported exclusive apical localization of ERM-1::CFP in the late L4 stage of vulval development.

3.3.7 ERM-1::CFP associates with LET-23 (D. Kradolfer, E. Fröhli)

The striking subcellular localization of ERM-1::CFP in the VPCs lead to the hypothesis that ERM-1 could be an inhibitor of the inductive pathway associated with LET-23. To test this possibility, D. Kradolfer and E. Fröhli performed biochemical experiments, where LET-23 was immunoprecipitated from mixed staged worm lysate of *erm-1(tm677); zhEx[erm-1::cfp]* animals, and probed with αGFP on Western Blot. Interestingly, a band around 100kDa was observed which accounts for the ERM-1 (~66kDa) fused to CFP (~30kDa). These results indicated that ERM-1::CFP is part of a complex with LET-23.

Moreover, immunoprecipitation of TAG-60 lead to the coprecipitation of ERM-1::CFP, supporting the idea of TAG-60 and ERM-1 forming a complex. Further biochemical experiments performed by D. Kradolfer and E. Fröhli showed that TAG-60 did not coimmunoprecipitate with LET-23, indicating that TAG-60 is not associated with LET-23, but rather forms a distinct complex with ERM-1 of unknown function. Since the αTAG-60-1 antibody might not recognize TAG-60c and TAG-60d, it is not clear if these isoforms would associate with LET-23 or not.

3.4 Discussion

C. elegans vulval development is an established system to study LET-23/EGFR signalling and its role in cell fate determination and organogenesis (Sternberg 2005). One of the areas of interest of our lab is the trafficking of the EGF-receptor and its impact on cell fate specification. This study deals with the attempt to characterize putative regulators of LET-23/EGFR localization.

PDZ domain containing proteins are known to be conserved scaffolds that organize signalling complexes, cell junctions and specialized plasma membrane domains (Fanning and Anderson 1999). In particular, the PDZ proteins LIN-7, LIN-2 and LIN-10 in *C. elegans* are thought to form a tripartite complex that bind to the C-terminal tail of LET-23 *via* the PDZ domain of LIN-7 and hence target it to the basolateral membrane of the VPCs (Simske et al. 1996, Kaech et al. 1998, Whitfield et al. 1999).

Most of the 4.1 band protein family share an N-terminally located FERM domain (Bretscher et al. 2002). It is a protein interaction module shown to bind transmembrane proteins or PDZ-domain containing scaffolds (Bretscher et al. 2002). Some FERM-domain proteins, such as the ERMs, contain a C-terminal F-actin binding site (Bretscher et al. 2002). As reported for the cystic fibrosis transmembrane conductance regulator (CFTR) and the β2 adrenergic receptor, the ERMs act as a bridge to the cortical cytoskeleton *via* the PDZ protein EBP-50 (Bretscher 1999).

A previous RNAi screen performed by A. Stetak targeted all uncharacterized genes that encode PDZ-domains and FERM-domains in *C. elegans*. In order to assess whether downregulation of these genes would have an impact on the LET-23 pathway, the *let-60(n1046gf)* allele was used as a sensitised background. Two genes, *frm-8* and *tag-60* were found as candidate suppressors of the *let-60(n1046gf)* Muv phenotype. Furthermore, RNAi of both *frm-8* and *tag-60* in the RNAi hypersensitive background *rrf-3(pk1426)* appeared to affect the loclization of the LET-23 receptor to intracellular punctae and the apical junctions of the VPCs (A. Stetak, personal communication). We hypothesized that the low penetrant defect was possibly due to inefficient downregulation by RNAi. In order to study the function of *frm-8* and *tag-60*, we generated deletion mutants by screening 6 deletion libraries in total. The isolated deletion mutants *frm-8(zh67)* and *tag-60(zh93)* were superficially wild-type.

3.4.1 *frm-8* is unlikely a regulator of the LET-23 pathway

The *frm-8(zh67)* allele was isolated to further characterize the funciton of this gene product. The *zh67* deletion removes 1'677bp containing the 4th, the 5th and parts of the 6th exon of the a-isoform. The *zh67* deletion covers part of the PDZ and the FERM domain, which is likely to reduce FRM-8 function regarding the PDZ and FERM activity. To date, it is not known if the *zh67* allele results in a truncated protein or not. However, the putative translated FRM-8 proteins would lack most of the FERM domain and the whole uncharacterized C-terminus, as *zh67* results in a frame-shift leading to a premature STOP codon. Although the nature of the *zh67* has not been studied extensively, it is very likely to strongly reduce FRM-8 activity. The generation of other alleles of *frm-8* would be necessary to deduce the effect of the *zh67* on the *frm-8* gene activity. This option was not feasible because of time restrictions.

Interestingly, *frm-8(zh67)* seemed to have an impact on LET-23 localization as depicted in figure 3.2 D. 30-40% of the *frm-8(zh67)* animals showed LET-23 at intracellular punctae and the basolateral membrane facing the both primary sister cells in the 2-cell stage. Also in the 4-cell stage it was possible to observe aberrant LET-23 localization, as in 5% of the animals only 3 out of 4 cells showed expression of LET-23.

Despite its effect on LET-23 localization, the *frm-8(zh67)* allele did not show significant genetical interaction with *let-60(n1046gf)*, and only weakly suppressed the *lin-2(n105)* Vulvaless phenotype. Also, the expression level of the early 1° cell fate marker *egl-17::cfp* in *zh67* did not show significant changes in expression. Taken together, these results suggest no major role of FRM-8 in the inductive pathway. Since the nature of the *frm-8(zh67)* allele has yet to be determined, it is possible that *zh67* represents a weak hypomorphic allele and may thus be redundant with other regulators of vulval development. However, this is unlikely since no synthetic phenotype on the level of vulval development and LET-23 localization were found by downregulation of all available FERM-encoding genes by RNAi in a *frm-8(zh67)* background. Similar experiments were performed previously by others, where combinatorial RNAi by injection was performed using a mixture of ten different dsRNAs of FERM-genes (*frm-(1-6)*, *frm-8*, *frm-10*, *ptp-1* and *nfm-1*) but failed to show any obvious phenotypes (van Fürden et al. 2004). Further genetic epistasis using mutants of all FERM-genes might uncover more cryptic functions of this gene family.

The finding that transcriptional GFP reporters showed expression in the pharynx, the intestine, excretory system, ventral nerve cord, some unidentified cells but not in the vulval cells, implied that a putative role of FRM-8 as a regulator of the LET-23 pathway would be

cell-nonautonomous. This would rule out a model where FRM-8 bridges LET-23 to the cortical cytoskeleton of the VPCs.

In consideration of the facts presented in this study, the gene *frm-8* might not directly regulate the LET-23 pathway during vulval development and hence the investigation of *frm-8* was not continued.

3.4.2 TAG-60 may be the *C. elegans* orthologue of EBP-50 and NHE-RF2

EBP-50 and NHE-RF2 are closely related proteins harbouring each two PDZ domains and a less characterized C-terminus. It has been shown in various reports that these proteins serve as scaffolds of signal transduction complexes at the plasma membrane (Bretscher et al. 2000, Weinman et al. 2006). In particular, the PDZ domains have been demonstrated to bind to transmembrane proteins and their regulators or effectors (Bretscher et al. 2000, Weinman et al. 2006). The very C-terminus was shown to harbour an interaction interface for FERM-domains (Finnerty et al. 2004). TAG-60, although only showing 28% sequence similarity to EBP-50 at the sequence level, harbours the same domain architecture as EBP-50/NHERF1 and NHERF2/E3KARP. The *tag-60* locus encodes five different isoforms, from which three have two PDZ domains and two isoforms only show one PDZ domain. All isoforms share almost the same C-terminus and all isoforms have been confirmed by cDNAs. As no paralogue of TAG-60 has been found and predicted so far, it is possible that TAG-60 may be the sole *C. elegans* homologue of the EBP-50 family of proteins.

3.4.3 TAG-60 might be involved in LET-23 retention at the basolateral membrane of the VPCs

This study proposes TAG-60 as a regulator of vulval development. In the preceding RNAi screen, downregulation of *tag-60* suppressed the Muv phenotype of *let-60(n1046gf)* and mislocalized LET-23 in the primary cells to intracellular punctae and the apical junctions (A. Stetak, personal communication). Deletion libraries were set up and screened for deletions in the *tag-60* locus. The *zh93* deletion was isolated after screening 6 deletion libraries and covers parts of the 5th exon, the whole exons 6 and 7 and parts of the 8th exon of *tag-60a*. The *zh93* deletion spans 1’564bp and is an “in-frame” deletion, which means that a truncated protein is likely to be expressed. Unfortunately, the deletion does not cover any predicted protein domains. Hence, no good prediction of how the deletion affects the protein function can be deduced. However, *tag-60(zh93)* animals are superficially wild-type and undergo normal vulval development.

The *tag-60(zh93)* mutants displayed intracellular accumulation of LET-23 in the VPCs in 40% of the cases, in contrast to wild-type animals, which show predominant basolateral localization of LET-23 (Figure 3.6). This result indicates that TAG-60 might be involved in the regulation of LET-23 localization at the basolateral membrane. Interestingly, Lazar et al. (2004) found a similar effect of EBP-50 on human EGFR trafficking. They could demonstrate that the first PDZ domain of EBP-50 directly binds to a DSFL sequence in the C-terminus of EGFR. Moreover they found that this interaction is needed for the inhibition of the ligand induced endocytosis of EGFR at the plasma membrane. In this event, they showed that the interaction between EGFR and EBP-50 occurs at the plasma membrane and that EBP-50 is not cointernalized with EGFR upon activation with EGF, indicating that EBP-50 is involved in the retention of EGFR at the plasma membrane of COS-7 cells. Unfortunately, Lazar et al. (2004) did not investigate the role of the ERM-binding C-terminus of EBP-50 in this process. In contrast to these results, Cao et al. (1999) found that EBP-50 interacts with the β2-adrenergic receptor in HEK293 cells and that it is not involved in retention but rather in the recycling of the receptor back to the plasma membrane.
Given these findings, I propose that TAG-60 is involved in a retention or recycling mechanism (or both) of LET-23 at the basolateral membrane of the VPCs.

3.4.4 The *tag-60(zh93)* allele interacts genetically with the LET-23 pathway

The *tag-60* gene was identified by RNAi as a suppressor of the *let-60(n1046gf)* Muv phenotype (A. Stetak, personal communication). Unfortunately, the *tag-60* locus (Chr. IV: 4.05cM) is too close to the *let-60* locus (Chr. IV: 5.21cM) to build a double mutant with a reasonable effort. As a substitute experiment to confirm the findings by RNAi, the *gaIs36* integrated transgene was used. *gaIs36* contains heat-shock inducible *mpk-1* and *mek-2*, which is reported to show a strong Muv phenotype after heat-shock (Lackner et al. 1994). Although the Muv phenotype was not as strong as reported by Lackner et al. (1994), no significant change in average induced VPCs was observed in a *tag-60(zh93)* background. Nonetheless, the data from the pilot RNAi screen suggested that downregulation of *tag-60* results in reduced overall LET-23 signalling. Therefore the weak *lin-2(n105)* mutant was tested in combination with *tag-60(zh93)* for an enhancement of its Vulvaless phenotype, but surprisingly *tag-60(zh93)* was found to have a suppressive effect on *lin-2(n105)*. Consistently, also the strong Vulvaless phenotype of *lin-2(n397)* was suppressed by *zh93*, but not the Vulvaless alleles *lin-7(e1413)* and *lin-10(e1439)*. These results indicate that *tag-60* acts genetically upstream of *lin-7* and *lin-10* and in parallel to or downstream of *lin-2*.

Additionally, it was found that *tag-60(zh93)* suppressed the Vulvaless phenotypes of *sem-5(n2019), let-23(sy10)* but not *let-23(sy1)*. Since the *sem-5(n2019)* allele does not completely abolish *sem-5* function, it is not possible to place *tag-60* genetically with *sem-5*. However, the genetic interaction between the *sy10* and *sy1* alleles of *let-23* is of very high interest. *sy1* is a C to T alteration resulting in a LET-23 variant lacking the distal six C-terminal amino acids (Aroian et al 1994). As previously mentioned, the very C-terminus of LET-23 is crucial for the interaction with LIN-7 and hence, animals homozygous for *let-23(sy1)* show an apically mislocalized receptor. The *sy10* allele is a point mutation in the extracellular first cystein rich domain of LET-23 which renders it to a receptor with strongly reduced activity (Aroian et al. 1994). Conclusively, the regulation of the LET-23 pathway by TAG-60 seems to be dependent on the C-terminus of LET-23.

Many mutants of negative regulators of the LET-23 pathway show wild-type vulval development, but result in a Muv phenotype when combined with a mutant of another attenuator (Yoo et al. 2004). In contrast to this assumption, the combination of *tag-60(zh93)* with previously characterized mutants of negative regulators such as *gap-1(ga133), sli-1(sy143), unc-101(sy108), dpy-23(e840), dep-1(zh34)* did not show a Muv or other synthetic phenotype whatsoever (figure 3.7). An explanation for this finding could be that the different negative regulators do not functionally overlap with TAG-60 and hence, no synthetic effect can be generated by removing both genes.

Interestingly, the expression levels of the early primary cell fate marker *egl-17::cfp* was found to be reduced in *tag-60(zh93)* animals. This result indicates that the LET-23 pathway is attenuated in the primary cells of *tag-60(zh93)* animals, which appears to be in conflict with the suppression of the *lin-2(lf)* Vulvaless phenotypes. However, it is still possible that there is more LET-23 signalling activity in the secondary cells of *tag-60(zh93)* animals. So far, there is no data supporting this notion. Alternatively, enhanced LIN-12 Notch signalling in the secondary cell lineage might be the cause for the suppression of the *lin-2(lf)* Vulvaless phenotypes by promoting the secondary fate in P5.p and P7.p. In wild-type animals at the time of induction, the LIN-12 protein is expressed in all VPCs but is downregulated in the primary lineage following induction (Shaye and Greenwald, 2005). Therefore, it is possible that LIN-12 persists in the primary cells of *tag-60(zh93)* animals, which would account for the reduction of the 1° cell fate marker *egl-17::cfp* expression in the primary cells themselves. Preliminary data supports this model, as the *lip-1::gfp* secondary cell fate marker was found to be mis-expressed in the primary vulval lineage until the L4 stage of vulval development (data not shown). Since *lip-1* is a direct transcriptional target of LIN-12, examination of the

LIN-12::GFP translational reporter can be used to assess whether indeed LIN-12 has delayed degradation in the 1° cell lineage of *tag-60(zh93)* animals. Accordingly, the same effect in the secondary vulval lineages could account for the suppression of Vulvaless mutants by *tag-60(zh93)* as discussed above. Enhanced activity of the LIN-12 Notch pathway (e.g. by interfering with LIN-12 degradation) could lead to increased secondary cell fate specification of P5.p and P7.p.

Involvement of TAG-60 in the LIN-12 Notch pathway can be additionally tested by combination of *tag-60* alleles with mutants of LIN-12. According to the hypothesis formulated above, it would be possible that LIN-12 activity is enhanced in *tag-60(zh93)* animals. Therefore it would be interesting to test, whether *tag-60(zh93)* is able to enhance the defects associated with partial gain-of-function alleles of *lin-12*.

3.4.5 *zh93* is a dominant allele of *tag-60*

In order to identify the molecular nature of the *zh93* allele, genetic experiments were performed in the *lin-2(n397)* sensitized background. This study has shown that animals heterozygous for *tag-60(zh93)* suppress the number of average induced VPCs in a *lin-2(n397)* background, meaning that *tag-60(zh93)* represents a dominant allele of *tag-60*.

In order to determine whether *zh93* is a gain-of-function or a reduction-of-function mutation, downregulation of *tag-60* by RNAi was our first approach of choice. If RNAi against *tag-60* in a *lin-2(lf)* background suppressed the Vulvaless phenotype, this would indicate a reduction-of-function nature of the *zh93* allele. In contrast, if RNAi of *tag-60* in a *tag-60(zh93); lin-2(n397)* background would bring the induction index back to *lin-2(n397)* single mutants level, this would speak for a gain-of-function nature of *zh93*. Unfortunately, RNAi of *tag-60* in neither the *lin-2(n397)* nor the *tag-60(zh93); lin-2(n397)* background showed any significant change. However, *tag-60* RNAi in *tag-60(zh93); lin-2(n397)* animals resulted in a weak suppression of the induction index with a not significant P-value of 0.057 (Table 3.2, row 6). Since this experiment was only peformed once and because the suppression of the vulval index was at the border of significance, it is advisable to repeat the RNAi experiments and score a larger number of animals.

More genetic experiments need to be performed to assess whether *zh93* represents a reduction or a gain-of-function allele. Therefore, all available *tag-60* alleles can be tested in a *lin-2(lf)* background to assess whether they suppress the Vulvaless phenotype and if so, to which extent. Additional testing of trans-heterozygotes of the different *tag-60* alleles with a deficiency covering the *tag-60* locus will provide more information about the nature of the

tag-60 alleles. The proposed genetic experiments and the comparison of all available *tag-60* alleles are crucial to correctly interpret the epistatic analysis and to draw a model of TAG-60 function during vulval development.

3.4.6 A cell non-autonomous role of TAG-60 during vulval development?

The expression patterns of various transcriptional GFP reporters for the different *tag-60* isoforms were analyzed by C. Gurnot. A reporter construct containing 6 kb of upstream sequence of the ATG of the a isoform drove GFP expression in the pharynx, the intestine and some unidentified cells in the head and tail. A very similar GFP expression pattern was found by analyzing a reporter with 3kb upstream sequence of the *tag-60e* isoform. In contrast, no GFP expression was found in reporters harbouring 2 kb upstream sequence of the *tag-60b* isoform. These results indicate that the e isoform might use an alternative promoter for its expression, lying upstream of its ATG, within the large intron of all the other isoforms. Moreover it is possible that the immediate upstream sequence of the *tag-60b* isoform might not contain promoter elements, but rather uses the promoter elements of the *tag-60a*, c and d isoforms for its transcription. No expression of GFP was observed in the vulval cells in all transgenic lines analyzed, indicating that either *tag-60* is acting from another tissue distant from the vulva, or that the GFP reporters did not contain all the necessary regulatory elements to represent the endogenous expression pattern.

Rabbit antibody sera against two distinct peptides were generated. The epitope for αTAG-60-1 is located within the *zh93* deletion and possibly recognizes isoforms TAG-60a, b and e. Only half of this peptide is present in isoform TAG-60d and only one third in isoform TAG-60c (figure 3.9 A). Thus, it is not clear if the antibody recognizes the TAG-60c and TAG-60d isoforms. However, immunostaining experiments with αTAG-60-1 show expression of the epitope in the intestinal cells and the pharynx throughout development. The expression in the pharynx persisted when staining *tag-60(zh93)* animals while intestinal staining was lost, indicating that the expression in the intestine is indeed specific for TAG-60. The pharynx expression in *tag-60(zh93)* is different from the one recorded in wild-type worms, indicating that another epitope is recognized in addition to TAG-60 in the pharynx. No expression was observed in the vulval cells in the early developmental stages. However, in the early L4 stage when the vulval cells start to invaginate, αTAG-60-1 seems to recognize TAG-60 in the developing uterine tissue and in all vulval cells. The signal from the uterus is more pronounced compared to the vulval cells, where the expression is very low in most analyzed animals. The subcellular localization of TAG-60 in the vulval cells was observed in

unidentified intracellular compartments. It is possible, that TAG-60 is expressed in the early stages of vulval development (e.g. at the time of induction), but at a level that makes it undetectable by the immunostaining approach. Another issue is that the antibody αTAG-60-1 might not recognize all TAG-60 isoforms and therefore it remains inconclusive whether the recorded expression pattern is representing the endogenous expression.

The epitope of the second antibody αTAG-60-2 is located at the very N-terminus of the TAG-60e isoform, and is present in all predicted isoforms. Immunostaining experiments using αTAG-60-2 showed an expression pattern similar to that of the glutamate receptor *glr-1* (Maricq et al. 1995), as it showed signals in the nerve ring and in dotted structures along the ventral nerve cord. However, these signals were not sensitive to the *zh93* deletion, as immunostaining of *tag-60(zh93)* showed a superficially similar expression and localization of TAG-60 compared to wild-type animals. Analyzing αTAG-60-2 in the recently received *tag-60* mutants *tm3501* and *ok2292* could tell if this expression pattern is true and complements the TAG-60 expression pattern observed with αTAG-60-1. Interestingly, The PDZ protein LIN-10 has been reported to be involved in the localization of GLR-1::GFP to postsynaptic structures of interneurons (Rongo et al. 1998). Both, mutants in *glr-1* and *lin-10* have been demonstrated to be defective in the nose-touch response (Rongo et al. 1998). Assuming that the neuronal TAG-60 expression pattern recorded with aTAG-60-2 is true, it might be interesting to test whether TAG-60 is involved in localizing transmembrane proteins in the interneurons. However, it is still unknown if *tag-60* mutants display a nose-touch response or other neurological defects.

EBP-50 has been shown to inhibit ligand induced endocytosis of EGFR by a direct interaction of PDZ domain 1 with the C-terminus of EGFR (Lazar et al. 2004). Furthermore, EBP-50 has been shown to regulate retention or recycling of different kinds of transmembrane proteins by direct interaction (reviewed in Bretscher et al. 2000, Weinman et al. 2006). Since we observed mislocalized LET-23 in the primary vulval cells in *tag-60(zh93)* animals our working model was that TAG-60 functions cell-autonomously in the VPCs to regulate vulval development. Both, transcriptional GFP reporter analysis and immunostaining experiments do not provide any indications of TAG-60 expression in the VPCs at the time of induction and hence we cannot exclude a cell-nonautonomous function of TAG-60. Vulval development has been repeatedly shown to be influenced by other tissues as the hypodermal syncitium hyp7 (Cui et al. 2006) and neurons (Battu et al. 2003). Battu et al. (2003) showed that the G-protein coupled receptor (GPCR) SRA-13 is expressed in chemosensory neurons and that it negatively regulates vulval induction. The expression pattern of SRA-13 indicated a cell-

nonautonomous role in vulval development. Since human EBP-50 has been shown do bind and regulate the localization of GPCRs (Weinman et al. 2006), it is possible that TAG-60 functions in the neurons to regulate vulval development by interacting with GPCRs and hence regulating their localization.

3.4.7 TAG-60a::YFP fusion proteins localize to plasma membrane compartments

To address the cell autonomy of TAG-60 during vulval development, minigenes under the control of different tissue specific promoters were generated and introduced into *tag-60(zh93); lin-2(n397)* animals. The minigenes consisted of the *tag-60a* cDNA and the *yfp* sequence. The *opt-2* promotor was used to express the minigene construct specifically in the intestine and showed exclusive apical localization of the fusion protein, similar to what was found in the TAG-60 immunostaining experiments. This result indicated that the YFP did not interfere with TAG-60a localization in the intestinal cells. Minigene expression in all epithelial cells was driven by the *vab-9* promotor and showed predominant apical localization of TAG-60a::YFP, but also basolateral localization in some animals. The localization of TAG-60a::YFP in this construct could not be assessed in the early stages of vulval development, as the simultaneous expression in the uterine tissue was much stronger and hence masked the signals originating from the VPCs. The minigene reporter construct under the vulval specific element of the *lin-31* promotor showed very weak expression of TAG-60a::YFP on the whole plasma membrane and the junctions of the VPCs. Alltogether, it was found that TAG-60a::YFP is preferentially associated with plasma membrane compartments in a cell-type specific manner.

The TAG-60a::YFP fusion proteins were tested for their ability to alter the average number of induced VPCs of *tag-60(zh93); lin-2(n397)* double mutants. None of the established transgenic lines significantly affected the vulval induction of *tag-60(zh93); lin-2(n397)*. Several explanations could account for this observation. First, the constructs harboured a C-terminally fused YFP, which theoretically could interfere with TAG-60 function. Second, only the *tag-60a* isoform was used in these experiments. It is possible that another or several *tag-60* isoforms act in concert to regulate vulval development. Third, the transgenic lines constitute of an extrachromosomal array, which is mosaic in its expression and might account for the lack of rescue.

In order to address these issues, a 17kb PCR fragment of the genomic *tag-60* locus was generated and introduced into *tag-60(zh93); lin-2(n397)* animals. One transgenic line showed a significant enhancement of the vulval induction of *tag-60(zh93); lin-2(n397)*. The remaining

four analyzed lines did not alter the vulval induction. This result is to be interpreted very carefully, as normally at least three independent transgenic lines should show the same effect to substantiate the result. Since only one transgenic line showed an enhancement in vulval induction, the indications for *tag-60(zh93)* representing a gain-of-function allele are weak. Similar experiments with different genomic clones have to be performed in the future to reproduce these findings.

The experiments presented in this paragraph were performed before *tag-60(zh93)* was determined to be a dominant allele. In retrospective, providing additional *tag-60* copies to the putative gain-of-function allele *zh93* would in theory enhance the suppressive effect on the *lin-2(n397)* Vulvaless phenotype. However, *zh93* could also represent other types of dominant variants, such as a neomorphic allele, which has not been ruled out so far. As mentioned above, comparison of all available *tag-60* alleles in *trans* to a deficiency is indispensable for the future in this project. Once a reduction-of-function allele of *tag-60* is confirmed and its defects determined, I suggest to systematically analyze all isoforms for their ability to rescue these defects. Ubiquitous expression of the *tag-60* isoforms with a heat-shock promoter would be used in a first step. If one construct results in a rescue, tissue specific expression of the corresponding *tag-60* isoform needs to be performed to assess the cell autonomy. Considering the neuronal expression pattern reported with αTAG-60-2, it would be interesting to additionally test a neuron-specific promoter in the rescue constructs.

If however, several *TAG-60* isoforms are needed in concert to fulfil TAG-60 function, combinations of the heat-shock constructs have to be tested for rescue activity.

3.4.8 The *tag-60* locus encodes more than 5 different isoforms

The antibody αTAG-60-1, which recognizes an epitope encoded within the *zh93* deletion, was tested in Western Blot experiments. It was found that in mixed stages of wild-type animals a band of around 80kDa is recognized by this antibody, which is missing in *tag-60(zh93)* samples. None of the annotated TAG-60 proteins have a size of 80kDa. Hence, this result indicates that either the TAG-60 proteins are being post-translationally modified or that other not annotated isoforms of TAG-60 exist. There are additional indications that the latter possibility might be true. The assumption was that the first three exons of the *tag-60a* isoform would be spliced together with *tag-60b*, which would account for the 80kDa protein found in the Western Blot experiment. Therefore, a forward primer within the first exon of *tag-60a* and a reverse primer within the first exon of *tag-60b* were tested together in a PCR reaction on whole worm cDNA templates. Indeed, the two primers amplified the expected sequence,

which indicates the existence of an additional isoform encoded within the *tag-60* locus. So far the attempt to clone the whole cDNA of the putative novel isoform failed.

It is not clear why the Western Blot experiments only showed one specific band for TAG-60. The worm lysates used in this experiment originated from mixed staged worm cultures and therefore it might be advisable to synchronize the worm cultures and analyze the lysates in a time course experiment. It is possible that some TAG-60 isoforms are only expressed in specific stages of *C. elegans* development and maybe are expressed at a low level. Since vulval induction and patterning is initiated at the late L2 stage, the time-course experiment might tell which isoforms are expressed at this time-point and which might be involved in the regulation of vulval development.

3.4.9 ERM-1 and TAG-60 might form a complex

Since the putative human homologue of TAG-60 has been demonstrated to bind to ERM-like proteins (Finnerty et al. 2004), we analyzed the mutant allele *erm-1(tm677)* in respect to its function during vulval development and LET-23 localization. Indications for a TAG-60/ERM-1 complex in *C. elegans* were collected in this study and by others: First, ERM-1 and TAG-60 physically interacted in yeast-2-hybrid experiments (Li et al. 2004). Second, apical TAG-60 localization in intestinal cells was abrogated in erm-1 RNAi (Vidal RNAi clone) animals (figure 3.14 B, C). Lastly, D. Kradolfer and E. Fröhli demonstrated that ERM-1::CFP is coimmunoprecipitated with TAG-60 (unpublished results).

3.4.10 ERM-1 is a putative regulator of LET-23 retention or recycling at the basolateral membrane of the VPCs

The *erm-1* gene was a candidate in the preceding targeted RNAi screen (using the Ahringer library RNAi clones), but did not show any defects compared to the *erm-1(tm677)* allele (A. Stetak, personal communication). *erm-1* is an essential gene and is needed for morphogenesis of tubular epithelia (Göbel et al. 2004). It was shown that the *erm-1(tm677)* allele represents a "null" mutant, as placing *tm677* in *trans* to a deficiency did not increase the severity of the defects observed in *tm677* homozygous animals (Göbel et al. 2004).

LET-23 seemed to be mislocalized to intracellular punctae in *erm-1(tm677)* animals, similarly to the defects observed in *tag-60(zh93)* animals. In both cases, the identity of the intracellular compartments, which are positive for LET-23, are unknown.

EBP-50 and ERM proteins have been repeatedly demonstrated to form a link between the peripherical actin cytoskeletion and plasma membrane proteins, and in this way regulate their

localization and activity (Bretscher et al. 2002). Taken together, the indications of a *C. elegans* TAG-60/ERM-1 complex and the effect of *tag-60(zh93)* and *erm-1(tm677)* on LET-23 localization led to the working model, where TAG-60 and ERM-1 act together to regulate LET-23 localization in the VPCs. Since both single mutants *tag-60(zh93)* and *erm-1(tm677)* display wild-type induction, it is likely that LET-23 is normally targeted to the basolateral membrane, but is not efficiently retained or recycled in these animals.

3.4.11 ERM-1 is a novel negative regulator of vulval development

Epistasis experiments were performed to study the genetic interactions of *erm-1(tm677)* with mutants of components of the inductive pathway. Interestingly, *erm-1(tm677)* significantly enhanced the Multivulva phenotype of *let-60(n1046gf)* animals. As mentioned above, *tm677* was determined to be a "null" mutation (Göbel et al. 2004). Therefore, the enhancement of the *let-60(n1046gf)* Muv phenotype indicated that *erm-1* encodes a negative regulator of vulval development. Consistently, *erm-1(tm677)* was able to suppress the Vulvaless phenotypes of *lin-2(n397)*, *lin-7(e1413)* and *lin-10(e1439)*.

Additional genetic experiments performed by D. Kradolfer, showed that *erm-1(tm677)* could suppress the Vulvaless phenotype of *let-23(sy1)*, encoding the LET-23 variant lacking the six C-terminal amino acids (Aroian et al. 1994). This result demonstrated that the regulation of vulval development by ERM-1 is independent of the distal C-terminus of LET-23. D. Kradolfer also found that regulation of vulval development by ERM-1 seems to be dependent on LIN-3 EGF and LIN-45 Raf, since *erm-1(tm677)* did not alter the vulvaless phenotypes of *lin-3(e1417*) and *lin-45(sy96)* mutants. So far, no "null" mutant of the core LET-23 pathway was tested, which would genetically place *erm-1* in the inductive pathway. *mpk-1(0)* alleles are the only mutants of the core inductive pathway that do not result in lethality (Lackner and Kim 1998). The combination *erm-1(tm677); mpk-1(0)* would help to place *erm-1* either up- or downstream of *mpk-1*.

Comparison of the genetic data collected with the *tag-60(zh93)* and the *erm-1(tm677)* mutants is difficult because of the unknown molecular nature of the *tag-60(zh93)* allele. Assuming that *zh93* encodes a dominant-negative form of TAG-60, it is possible that TAG-60 acts as an attenuator of vulval development. However, the model of the TAG-60/ERM-1 complex negatively regulating vulval development would then be challenged. *tag-60(zh93)* suppressed the *lin-2(n397)*, but not the *lin-7(e1413)* and *lin-10(e1439)* Vulvaless phenotypes, suggesting that TAG-60 and ERM-1 do not regulate vulval development as one sole functional unit, but as part of differently composed protein complexes. As mentioned before, different *tag-60*

alleles have to be tested in genetic experiments to characterize TAG-60 and its general role in vulval development.

However, biochemical experiments performed by D. Kradolfer and E. Fröhli demonstrated that ERM-1::CFP but not TAG-60 is coimmunoprecipitated with LET-23. Therefore, ERM-1 might be associated with LET-23 and inhibit the inductive pathway in a TAG-60 independent mechanism. ERM-1 is the sole orthologue of Ezrin, Radixin and Moesin in *C. elegans* (Göbel et al. 2004). However, the *nfm-1* gene product is the putative *C. elegans* orthologue of the human ERM-like protein Merlin/Nf2 (Göbel et al. 2004). Merlin, together with EBP-50, was reported to be involved in contact dependent inhibition of EGFR (Curto et al. 2007, Cole et al. 2008). EGFR bound to EBP-50 and Merlin is thought to be localized to specialized microdomains, which inhibit receptor activation and internalization (Curto et al. 2007, Cole et al. 2008). Similarly, it is possible that in *C. elegans* TAG-60 inhibits LET-23 in a Merlin dependent mechanism. However, the fact that TAG-60 is not coimmunoprecipitated with LET-23 speaks against this theory. In addition, NFM-1 function during vulval development cannot be investigated, as the mutants die as L1 larvae and alternative *nfm-1* RNAi (Ahringer clone) seems to be not effective.

3.4.12 ERM-1::CFP is localized to the basolateral membrane of the VPCs (D. Kradolfer)

To study the subcellular localization of ERM-1 a translational ERM-1::CFP fusion protein was constructed under the control of its endogenous promoter (D. Kradolfer, unpublished results), as reported by Göbel et al. (2004). *erm-1(tm677)* harbouring the ERM-1::CFP encoding transgene were viable, indicating that the ERM-1::CFP fusion protein was functional. In contrast to the findings of Göbel et al. (2004), ERM-1::CFP localized to the apical compartment of all tubular epithelia with one exception. ERM-1::CFP appeared to be localized exclusively at the basolateral membrane of the P5.p, P6.p and P7.p lineages during early vulval development. This result is consistent with the defects in LET-23 localization found in *erm-1(tm677)* animals and with the biochemical experiments, which indicate that ERM-1 is associated with LET-23. So far it was not tested if ERM-1::CFP fusion protein is able to revert the effects of *erm-1(tm677)* on the Vulvaless phenotypes of loss-of-function alleles of *lin-2, lin-7* or *lin-10*.

3.4.13 Putative mechanisms for ERM-1 function during vulval development

Genetic experiments clearly indicate that ERM-1 is a novel attenuator of vulval development. Further epistatic experiments have to be performed to genetically place *erm-1* in the inductive

pathway. However as stated above, ERM-1 might associate with LET-23 and thus regulate LET-23 localization. At the moment we cannot exclude the possibility of ERM-1 regulating the inductive pathways by other mechanisms. Additionally, the cell-autonomy of ERM-1 was not *per se* investigated. Vulva-specific expression of ERM-1::CFP in *erm-1(tm677); lin-2(n397)* has to be performed to assess this question.

3.4.13.1 Models for *C. elegans* ERM-1 activation

Krieg and Hunter (1992) found Ezrin as a putative phosphorylation target of human EGFR. Following stimulation of A431 cells by EGF, Ezrin was predominantly phosphorylated at residues Tyr145 and Tyr353. Subsequent *in vitro* kinase assays demonstrated that EGFR directly phosphorylates Ezrin at the mentioned residues (Krieg and Hunter 1992). As shown in figure 3.12 (blue dots), the residues Tyr145 and Tyr353 are not conserved in *C. elegans* ERM-1. Nevertheless, it is possible that ERM-1 is a phosphorylation target of LET-23 and that these putative phophorylation events could acivate ERM-1 or modulate its activity (figure 3.19). ERM proteins have been demonstrated to switch from the globular inactive state to the extended active state by phosphorylation of a conserved threonine in the C-terminus (Bretscher et al. 2002, figure 3.12 red dot). Because of the high sequence conservation between *C. elegans* ERM-1 and human Ezrin and Moesin (figure 3.12), it is likely that the activation mechanism is conserved as well (figure 3.19). Therefore, LET-23 might only modulate ERM-1 activity. ERM-1 variants, with mutated candidate phosphorylation sites could be introduced into *C. elegans*, followed by the investigation of their effects on vulval induction. For example, substitution of threonins (or serines, tyrosines) by alanine (or phenylalanine) would abolish phosphorylation. On the other hand, substitution with phosphomimicking amino acids could also serve to dissect the mechanism of ERM-1 function during vulval development. Additionally, expression of epitope tagged dominant negative ERM-1 constructs in loss-of-function mutants of *lin-2*, *lin-7* or *lin-10* could uncover the mechanism of ERM-1 function.

3.4.13.2 Putative ERM-1 effectors

ERM-1 could act as a direct inhibitor of LET-23 (figure 3.19) by linking the receptor to the peripherical cytoskeleton, as was proposed for human EGFR and Merlin/Nf2 (Curto et al. 2007, Cole et al. 2008). *erm-1(tm677)* suppressed the *let-23(sy1)* Vulvaless phenotype, indicating that the ihibition of vulval development by ERM-1 is independent of the distal C-terminus of LET-23. It is possible that ERM-1 directly interacts with LET-23 or *via* an

unknown factor. Interaction studies by yeast-2-hybrid or *in vitro* binding assays have to be performed to assess these questions. It would be furthermore interesting to test, whether the localization of ERM-1::CFP is sensitive to the *let-23(sy1)* or *lin-2(n397)* background, where LET-23 is displayed on the apical surface of the VPCs. It is possible that in these Vulvaless mutants ERM-1::CFP shows similar mislocalization compared to LET-23.

Other hypothetical effectors of *C. elegans* ERM-1 could be components of the RHO-1 pathway (figure 3.19). The RhoGEF (Guanine nucleotide exchange factor) ECT-2 was found to positively regulate vulval induction *via* RHO-1 (Canevascini et al. 2005). Although not providing a mechanism, Speck et al. (2003) demonstrated that *D. melanogaster* Moesin acts antagonistically to the Rho pathway *in vivo*. Therefore, a possible model constitutes of ERM-1 as a negative regulator of the RHO-1 signalling pathway (figure 3.19), and thus indirectly attenuates the inductive pathway. Ubiquitous expression of a dominant negative variant of RHO-1 (Canevascini et al. 2005) in *erm-1(tm677); lin-2(n397)* animals would test this possibility.

3.5 Methods

3.5.1 General methods and alleles

Standard methods were used to maintain and manipulate *C. elegans* (Brenner 1994). The *C. elegans* Bristol srain (N2) was used as the wild-type reference strain. The mutations used in this study are listed below by their linkage group.

LGI: *lin-10(e1439)* (Whitfield et al. 1999), *erm-1(tm677)* (Göbel et al. 2004), *unc-101(sy108)* (Lee et al. 1994).
LGII: *let-23(sy1)* (Aroian et al. 1994, Hajnal et al. 1997), *let-23(sy10)* (Aroian et al. 1994), *lin-7(e1413)* (Simske et al. 1996); *dep-1(zh34)* (Berset et al. 2005).
LGIII: *frm-8(zh67)* (this study)
LGIV: *tag-60(zh93)* (this study), *tag-60(ok297), let-60(n1046gf)*
LGX: *lin-2(n105)* (Hoskins et al. 1996), *lin-2(n397)* (Hoskins et al. 1996); *sem-5(n2019)* (Clark et al. 1992), *sli-1(sy143)* (Jongeward et al. 1994), *gap-1(ga133)* (Hajnal et al. 1997), *dpy-23(e840)* (Pan et al. 2007).
Integrated transgenic arrays: *arIs92[egl-17::cfp; tax-3::gfp]* (Yoo et al. 2004), *gaIs36[hs-mpk-1(+); EF1alpha-D-mek(gf); unc-30(+)*] (Lackner and Kim, 1998).
Extrachromosomal transgenic arrays: *zhEx308.1[Plin-31::tag-60a::yfp, lin-48::gfp]* through *zhEx308.3*, *zhEx309.1[Pvab-9::tag-60a::yfp, lin-48::gfp]* through *zhEx309.3*, *zhEx310.1[Popt-2::tag-60a::yfp lin-48::gfp]* through *zhEx310.2*, *zhEx312.1[tag-60 genomic fragment, sur-5::dsRed]*
Rearrangements: *hT2[bli-4(e937) let-?(q782) qIs48]* (I;III)

3.5.2 Buffers

Worm lysis buffer (WLB)
50mM KCl
10mM Tris pH8.2
2.5mM $MgCl_2$
0.45% NP-40
45% Tween-200
0.01% Gelatine

20mg/ml Proteinase K

1xPBS

Instamed 9.55g/l PBS Dulbecco w/o Ca^{2+}, Mg^{2+} (Biochrom AG)

Paraformaldehyde

100mg Paraformaldehyde

+ 450µl H_2O

+ 0.5µl 12M NaOH

vortex

incubate at 60°C for about 10min (vortex after every 2min)

+ 5µl 1M HCl

+ 50µl 10xPBS

2xRFB (always keep at -20°C)

160mM KCl

40mM NaCl

20mM Na_2EGTA

10mM Spermidine HCl

30mM Na PIPES pH7.4

50% Methanol

1xTTB

100mM Tris HCl, pH7.4

1mM EDTA

0.1% Triton X-100

100x BO_3 buffer

5M H_3BO_3

2.5M NaOH

(pH should not be lower than 9.5)

4xBO_3 buffer

Dilute 100x BO_3 buffer 1:25

0.01% Triton X-100

ABA buffer

2% bovine serum albumin (BSA) in 1x PBS-T

Mowiol

Mowiol 4-88	2.4g
Glycerol	6g
H_2O	6µl
0.2M Tris pH8.5	12µl
DABCO	2.5% (w/v)

3.5.3 RNA-interference

The Ahringer RNAi library is based on bacterial *E.coli* strains HT115(DE3), that produce dsRNA against specific *C. elegans* genes (Kamath et al. 2003; Kamath and Ahringer, 2003). The gene specific sequence within the plasmid L4440 is flanked by T7 promoters. Production of dsRNA by the bacteria is hence inducible by IPTG (Isopropyl β-D-1-thiogalacotpyranoside). An alternative high-throughput RNAi rescource was generated by the Vidal laboratory (Rual et al. 2004).

RNAi clones were grown for 5 hours in 2xTY at 37°C and subsequently seeded on NGM plates (3g/l NaCl, 2.5g/l tryptone, 17g/l agar, 5µg/ml cholesterol, 1mM $MgSO_4$, 1mM $CaCl_2$, 1mM KPO_4) containing 1mM IPTG and 50 µg/ml ampicillin. Seeded RNAi plates were incubated at room temperature for 24 hours. L4 larvae were aliquoted onto the RNAi plates and allowed to grow at 20°C. The next generation was analyzed at the indicated stages.

3.5.4 Purification of polyclonal TAG-60 antibodies

To characterize TAG-60 expression, we assigned “Zymed laboratories” (now part of Invitrogen Inc.), with the production of rabbit polyclonal anitsera against TAG-60 peptides. “Peptide 1” (NSAYQYKESSTAYD) was used for the purification of αTAG-60-1 and “peptide 2” (LPRLAELNKGTPD) was used for the purification of αTAG-60-2.

Peptides (2mg) were coupled to NHS(N-hydroxysuccinimide)-activated sepharose columns (HiTrap, GE Healthcare) as described by the manufacturer. 1ml of antiserum was diluted 1:10

in 10mM Tris-HCl (pH 7.5). Remaining cellular debris was removed by centrifugation. Antisera were passed three times through the column. Washing buffer (10mM Tris / 500mM NaCl / pH7.5) was used to remove unspecific bound molecules. Elution of antibodies was performed using 100mM Glycine (pH2.5) and pH was neutralized using 1M Tris (pH 8.0). Handling and storage of the column was performed as described by the manufacturer (GE Healthcare).

3.5.5 Whole-mount immunostaining

Immunostaining was used to visualize expression and localization of LET-23 and TAG-60. Monoclonal and polyclonal antibodies recognizing LET-23 have been generated and used by our laboratory before this study (Stetak et al. 2006). The immunostaining method used in this study is based on the protocol established by Finney and Ruvkun (1990).

One 6cm dish full of mixed staged worms was washed with 1xPBS and transferred into an eppendorf tube. The worm suspension was washed with 1xPBS until the remaining bacteria was removed and the supernatant was clear. The spinning steps in this protocol are henceforth performed at 2'000rpm for 1min. The volume was adjusted to 450µl. If the worms were being processed on another day, 500µl of 2xRFB buffer (-20°C) was added. The tubes were then inverted several times and subsequently frozen in liquid nitrogen. Further storage of the tubes was done at -70°C. The samples have been reported to be stable for months.

Fixation

After adding the 2xRFB-buffer, 50µl of the fixating agent paraformaldehyde (1% end concentration) was added. Afterwards the tubes were subjected to 3 rounds of freeze-thaw cracking in liquid nitrogen to allow the paraformaldehyde to penetrate the cuticle of the worms. Thawing was done with handwarm tapwater. Fixation was done by incubating the tubes for 30min at 4°C on a rocker. The fixation reaction was stopped by washing the worms 3 times with 1xTTB.

Permeabilization

During the permeabilization reactions, the cuticle of the worms is processed to allow the antibodies to penetrate. Therefore the disulfide bonds of the cuticle collagen were reduced by rocking the tubes with 1ml 1xTTB, 40µl Triton X-100 (10%) and 10µl β-Merkaptoethanol for 6h at 37°C. In order to finish the reaction, the worms were washed 2 times with 4xBO_3 buffer.

The following two reactions were performed to modify and seal the reduced disulfide bonds. First, the worms were treated with a solution consisting of 990µl of 4xBO_3 buffer and 10µl of DTT (1M) for 15min rocking at RT. The reaction was stopped by 2 washes with 4xBO_3 buffer. Afterwards, the worms were incubated in 990µl 4xBO_3 buffer with 10µl H_2O_2 for 15min. This oxidation step was stopped by 2 washes with 4xBO_3.

The permeabilized worms were treated with 1ml of the blocking ABA-buffer for 15min rocking at RT, in order to minimize unspecific binding of the antibodies. Primary antibodies were diluted in 200µl ABA-buffer and then added to the worms. Incubation was done rocking overnight at 4°C. On the next day, the solution with the primary antibody was removed with one quick and 3 washes (15min rocking at RT) of PBS-T. The secondary antibodies were diluted 1:100 in 200µl of ABA-buffer. Worms were incubated with secondary antibodies for 2h rocking at RT. As the fluorophores coupled to the antibodies are light-sensitive, this step had to be performed in the dark. For this purpose, the tubes were wrapped in aluminium foil. Henceforth, all steps were carried out in the dark.

Staining of DNA

In some cases it was of interest to visualize the nuclei. This was done by staining the DNA with the Hoechst (Sigma) dye. Worms were incubated with 1ml PBS-T plus 1µl of Hoechst dye (10mg/ml) for 5min rocking at RT. Two subsequent washes with PBS-T of 5min at RT were concluding the staining protocol.

Mounting

After the last washing step, the supernatant was removed as much as possible, which corresponded to an approximate final end volume of 20µl. This worm suspension was mixed with 20µl of Mowiol and then immediately distributed on 2 drops on one slide. The drops were covered carfully with a coverslip using forceps. The mounted samples were dried overnight at RT in the dark. Long term storage was done at 4°C.

3.5.6 Scoring the VPC induction index

Worms were analyzed at the L4 stage. The induction index I is the average number of induced VPCs (P3.p-P8.p) of a certain worm strain. In the wild-type reference strain N2, only P5.p, P6.p and P7.p are induced which accounts for an induction index of 3. A worm population that shows an induction index of $0 \leq I < 3$ is underinduced and is therefore called “Vul”

(Vulvaless). Overinduced animals have an induction index of $3 < I \leq 6$ and are termed “Muv” (Multivulva).

3.5.7 Generation of *C. elegans* gene knockout libraries

Synchronisation and mutagenesis of worms

In order to create and isolate deletion mutants of *frm-8* and *tag-60*, we constructed six knockout libraries. Large numbers of N2 worms were grown on OP50 and gravid adults were collected with sterile M9 buffer. Remaining bacteria was washed off with sterile M9-buffer. The worms were subsequently bleached and transferred onto empty NGM-plates. Surviving eggs hatched overnight at 20°C and stopped development because of lack of food. On the next day the synchronized L1 worms were transferred onto NGM-plates containing OP50. After two days at 20°C the synchronized animals reached L4 stage and hence were collected with sterile M9 buffer. Remaining bacteria was washed away with M9-buffer. The final volume of worm suspension was 2ml. We used the mutagen EMS (ethyl methane sulfonate) to generate small DNA lesions. 30µl of EMS was diluted in 2ml of sterile M9 by inverting the tube several times. The diluted EMS was then transferred into the tube with the worm suspension. The total volume of the new worm suspension was 4ml and the end EMS concentration was 75mM. The mutagenesis was performed during 4h at RT by rocking the tube. Afterwards, the EMS was eliminated with 3 washes of M9 buffer. The volume of the worm suspension was adjusted to approximatively 0.5ml and the worms were subsequently transferred onto NGM-plates with OP50. The worms were kept at 20°C overnight and then distributed by 5 worms per plate. In total we constructed six different libraries of different proportions. Our smallest library contained 5x5x96 and our largest 3x20x96 (3 worms per plate instead of 5) mutagenized worms, respectively.

Collection of samples from the worm populations

The worms were allowed to produce progeny for the next 7 days at 20°C. The different plates represent different complex populations of mutagenized worms. In order to screen these populations a sample was taken by applying 1ml of Q-H_2O onto the plate and transferring 200µl of worm suspension into 96 well plates. The 96 well plates were spun for 1min at 2000rpm and 150µl of supernatant was removed from each well. 50µl of 2x WLB and 1µl Proteinase K (60µg/µl) were added to the remaining 50µl of worm suspension. Worms were lysed at 60°C for 3h. Subsequent inactivation of Proteinase K was performed at 95°C for

10min. For the first screening round, we generated pools of the bulk lysates. Of every 96well plate, each row was pooled separately by mixing 20µl of each sample into a new well. These pools were then transferred into eppendorf tubes for Phenol/Chloroform-purification.

Purification of genomic DNA derived from worm pools

Each pool had a volume of 12x20µl=240µl. 260µl of TE-buffer was added to a final volume of 500µl for better handling. The first purification step was done by adding 500µl PCI (Phenol/Chloroform/Isoamylalcohol) solution. After a thorough vortex step, the eppendorf tubes were spun for 2min at maximum speed. The upper (aqueous) phase was transferred to a new eppendorf tube and the step with the PCI solution was repeated. In the next step, the isolated aqueous phase was mixed with 500µl of CI (Chloroform/Isoamylalcohol) solution, thoroughly vortexed and again spun for 2min at maximum speed. The upper phase was again isolated and after all these purification steps, the starting volume of 500µl was reduced to an approximate volume of 400µl. The reason for this reduction lies in the interphase. Between the lower (organic solution) phase and the upper (aqueous) phase cellular debris accumulated. It was of particular importance to not transfer this debris to the successive purification step, meaning that it was only possible to recover approximatively 95% of the aqueous phase in each step.

A further purification step was done by ethanol precipitation as follows: We added 1/10 Vol. of 3M Sodiumacetate (pH5.2) and 2 Vol. of EtOH (100%) to the 400µl of DNA solution, inverted the tubes several times and incubated them at -70°C for 2h. The precipitated DNA was spun at 4°C for 10min and the resulting supernatant was removed by carefully inverting the tubes. The eppendorf tubes were carefully tipped on a towel to remove remaining ethanol. Afterwards, another ethanol precipitation step was performed with 2 Vol. of EtOH (70%). The tubes were inverted several times and spun at 4°C for 10min. The supernatant and remaining ethanol was removed as described above. Additionally we tried to remove persisting ethanol around the DNA pellet with the P200 pipette. The pellets were subsequently dried on air for 20min. To dissolve the DNA pellets, 40µl of TE-buffer were added and incubated at 40°C for 30min on a shaker. Another way to dissolve the DNA was to incubate the tubes overnight at 4°C. In some cases it was not possible to dissolve the DNA completely. Our optimization experiments showed that the DNA was too concentrated for the PCR screening. The DNA samples were therefore diluted 1:20 by transferring 10µl of each eppendorf tube to a 96 well plate and adding 190µl of TE-buffer.

3.5.8 Screening the *C.elegans* gene knockout-libraries

A nested PCR based assay to screen for small deletions

Before generating the knockout-library, we optimized a nested PCR assay, which covered approximatively 3kb of our genes of interest. As we were performing large scale PCR assays on a complex mix of genomic DNA as template, we chose nested PCR because of its increased sensitivity and specificity. The PCR screening was therefore done in two parts: the first PCR was performed with the two outer primers (henceforth called "outer reaction") and the purified DNA-pool-samples as templates. The second PCR was done with the two inner primers (henceforth called "inner reaction") and 0.1µl of the first PCR as a template. All PCRs were done in duplicates to show reproducibility of any band. As the WT band size was around 3kb, any smaller band would indicate a deletion in this region. The primers used to screen for the *frm-8* and the *tag-60* deletions are shown in following table.

Gene	Primer	Description
frm-8	OPG13 TTTGAAAATTGATATCTCGCTC	forward primer outer reaction
frm-8	OPG14 AATTGTTCAGCTATCTAACAAG	forward primer inner reaction
frm-8	OPG15 AAATGATCGAAACCTAGTCATG	reverse primer outer reaction
frm-8	OPG16 TTAAATTGAAGCTGACAACGAG	reverse primer inner reaction
tag-60	OPG5 CTTGCAAGGTAGGTGCAGATAATG	forward primer outer reaction
tag-60	OPG6 GCATAGATAAGTAATCGGAGTATC	forward primer inner reaction
tag-60	OPG7 CACTAGTCGAGCTTGCTGCATATC	reverse primer outer reaction
tag-60	OPG8 CCATTGCTCAATGGAGATGGTTG	reverse primer inner reaction

Isolation of deletion mutants

Once a reproducible band shorter than 3kb was found by screening the DNA pools, we had to identify the original worm plate that might harbour the deletion mutant. Every DNA pool represented the DNA lysates of one complete row of a 96 well plate (12 samples per row). We therefore performed the nested PCR as described above. The only difference was that these lysates were not Phenol/Chloroform purified. Once one well gave the same PCR band as from

the pool, we identified the worm plate. The worms on this plate were already starved at this time-point. The positive plate was chunked onto six new NGM-plates with OP50 and incubated at 20°C overnight. The worms were redistributed on fresh NGM-plates with food. This sib selection was done, by putting 20 worms on each plate. We used always at least 200 plates at this step. If the impression was that there are still a lot of worms on the chunked plates, we optionally used up to 300 plates. The following steps were done as described for the construction of the library. The worms were allowed to grow at 20°C until they were starved (5-7 days), followed by taking a sample as described above. The differences are, that during the sib selection steps we never pooled nor purified the bulk lysates. The nested PCR assay was done as described before. Once a positive plate was found again, the plate was chunked and a new sib selection round started. For every round we decreased the complexity of the worm populations, meaning that we put always less worms on the plates. Following numbers of worms were used in the different subsequent sib selection rounds: 10, 5, 2 and 1.
To genotype the isolated deletions, novel PCR assays were designed and optimized, which were easier and faster to handle than the nested PCR from the screen. We designed PCR assays with 3 primers, from which one was a "poison" primer located within the deletion. These assays are described in the next paragraph.

3.5.9 Genotyping PCR assays

Genotyping was performed in most cases by 2 primers flanking the correspondent deletion and one primer lying within the deletion. All genotyping PCR reactions were done with the Invitrogen Taq Polymerase in 25 µl reactions. The composition of the reaciton mix is shown in following table.

Ingredient	Volume
Invitrogen reaction buffer (10x)	2.5µl
dNTP mix (2mM of each nucleotide)	3.0µl
Primer 1 (2uM)	2.5µl
Primer 2 (2uM)	2.5µl
Primer 3 (2uM)	2.5µl
$MgCl_2$ (50mM)	1.0µl
Invitrogen Taq Polymerase	0.1µl
Q-H_2O	10.0µl
Template	1.0µl

In the cases where only two flanking primers were used, the volume of the third primer was compensated with Q-H_2O. Single worm lysates (SWLs) were used as a template for genotyping PCRs. One SWL was produced by lysing 1 worm in 10µl of WLB. The following tables show the PCR-programs and primers used to genotype different deletion alleles. The shaded fields indicate the cycling of the correspondent PCR program.

tag-60(zh93) (deletion)

Time	**Temp. [°C]**
2min	95
30sec	95
30sec	58
2min	72
5min	72
forever	12
cycling: 30x	

Primers	**Sequence**
OPG98	TGGAGTTGCATATGCATCGTATGC
OPG102	ACAGAGAATTGTTGGAGTAAATGG
OPG104	GATGATGAGTTTGAGAGTGTTGC
WT bands	**Deletion band**
1046bp	312bp
1877bp	

frm-8(zh67) (deletion)

Time	**Temp. [°C]**
2min	95
30sec	95
30sec	60
1min	72
5min	72
forever	12
cycling: 30x	

Primers	**Sequence**
OPG58	ATATTGCAGTCGTAGGCGACCTGTTGGAC
OPG59	GACGAGTAGGATAAGCCTGCTGAGGC
OPG60	ACCATGGGCGTCATGGAGATGTCG
WT bands	**Deletion band**
1088bp	765bp
2642bp	

erm-1(tm677) (deletion)

Time	**Temp. [°C]**
2min	95
30sec	95
30sec	58
1.5min	72
3min	72
forever	12
cycling: 30x	

Primers	**Sequence**
OPG135	TGATCTCTATCTTGGTGTCGATGC
OPG136	AACACATTACTCGATATCGAGGCG
OPG137	CAATTGCAATTGCTTGAGTTGAGC
WT bands	**Deletion band**
698bp	339bp
1310bp	

gap-1(ga133) (deletion)

Time	**Temp. [°C]**
2min	95
40sec	95
40sec	55
1min	72
5min	72
forever	12
cycling: 30x	

Primers	**Sequence**
OPG182 (S1C)	CTGTTATCCCCTATTTTAGTGG
OPG183 (S1D)	CTCTTGCTGGATCCACTTCAC
WT band	**Deletion band**
500bp	190bp

rrf-3(pk1426) (deletion)

Time	**Temp. [°C]**
2min	95
40sec	95
40sec	58
40sec	72
3min	72
forever	12
cycling: 30x	

Primers	**Sequence**
rrf3 del up1	
rrf3 del up2	
rrf3 del dn	
WT band	**Deletion band**
320bp	500bp

gaIs36 (integrated transgene)

Time	**Temp. [°C]**
2min	95
30sec	95
30sec	58
1min	72
5min	72
forever	12
cycling: 35x	

Primers	**Sequence**
OAH159	GCAAAAGGAGGGCGACTCAC
OAH160	TTTCCCGAAGTGTCCGTTGAC
WT band	**Deletion band**
-	Between 500bp and 650bp

let-60(n1046gf) (point mutation / use OAS604 for sequencing)

Time	**Temp. [°C]**
2min	95
30sec	95
30sec	58
30sec	72
2min	72
forever	12
cycling: 30x	

Primers	**Sequence**
OAS596	GGTAATGACGGAGTACAAGCTTG
OAS604	GTTTCAATTTGCTCCCACCACATG
WT band	
appr. 400bp	

lin-2(n397) (deletion)

Time	**Temp. [°C]**
2min	95
30sec	95
30sec	58
2min	72
5min	72
forever	12
cycling: 35x	

Primers	**Sequence**
L5.1	CGCCTATGAAATCTCAGTTT
L12.2	CGCGCATTTTCATAATTGCG
WT band	**Deletion band**
9’373bp	appr. 2’000bp

lin-2(n105) (point mutation)

Time	**Temp. [°C]**
2min	95
30sec	95
30sec	58
30sec	72
1min	72
forever	12
cycling: 30x	

Primers	**Sequence**
L1.1	CCTACGCTCGAGAACAAATA
L1.2	GTGGAAAAACCCCAGGTTTT
WT band	**Deletion band**
600bp	

3.5.10 DNA constructs

Transgenes were produced using the PCR fusion technique (Hobert 2002). Following primers were used for the DNA constructs encoding the TAG-60a::YFP translational fusion proteins:

Primer	Description
OPG299 ATGGTGCACATTCCGAGCGACGTG	*tag-60a* cDNA forward
OPG303 TTACATGTTGCTGACCAATTGATAC	*tag-60a* cDNA reverse
OPG307 CGAGAAGTATCAATTGGTCAGCAACAT GATGAGTAAAGGAGAAGAACTTTTCACTGG	*yfp::unc-54*(3'UTR) forward
FireVector D AAGGGCCCGTACGGCCGACTAGTAGG	*yfp::unc-54*(3'UTR) reverse
FireVector D* GGAAACAGTTATGTTTGGTATATTGGG	*yfp::unc-54*(3'UTR) reverse nested
OAS522 CAATCAAGAATAGAACTAACCTCTC	*vab-9* promoter forward
OAS523 CAAAGACAGCCTGTCTTTCTCAG	*vab-9* promoter forward nested
OPG306 CACGTCGCTCGGAATGTGCACCAT TTTGTCCCTTGAAGAGGATCTCTCG	*vab-9* promoter reverse
OIR150 CTATGCCATGGAGGTCTTCG	*opt-2* promoter forward
OIR151 CGAATGGCGGAGGACCTCG	*opt-2* promoter forward nested
OPG308 CACGTCGCTCGGAATGTGCACCATA GTGGCGATACTGACGAGGAATGAGC	*opt-2* promoter reverse
OPG309 ACGAGGAGCGGTGGTGTGGCCAGC	*lin-31* promoter forward
OPG310 TCAACCGTGCGATCGAGCGGCACC	*lin-31* promoter forward nested
OPG311 CACGTCGCTCGGAATGTGCACCAT ACACACGTAAAACGTGATACTTCG	*lin-31* promoter reverse

The DNA constructs (end concentration estimated to 10 ng/µl) were injected into gonads of *tag-60(zh93); lin-2(n397)* animals together with carrier DNA (pBS-KS$^-$, 100 ng/µl) and a coinjection marker (*lin-48::gfp*, 30 ng/µl).

Following primers have been used to amplify 3 overlapping fragments of the *tag-60* locus, which were stiched together using the PCR fusion technique (Hobert, 2002).

Primer	Description
OPG107 TGTCTACAAATGTACATAACGGCG	Reaction 1 forward
OPG317 AGTTTTAATCAGATTTCAATCGCC	Reaction 1 reverse
OPG111 GCTTGTGATCTCTGAAGAAGGAGC	Reaction 2 forward
OPG322 ATCAGTCTTCTGTGCTCAATGAGC	Reaction 2 reverse
OPG114 CATTGAAACGCATCTTGTAATCCG	Reaction 3 forward
OPG320 TATCACGAACAACTTCTAGGAGCC	Reaction 3 reverse
OPG108 GTGCTTGTTTTGGCGTGTCAGCCG	Fusion reaction forward
OPG319 ATCGTTTGTACTCTGTTTACTGGC	Fusion reaction reverse

The genomic *tag-60* fragment was injected into gonads of *tag-60(zh93); lin-2(n397)* animals together with carrier DNA (pBS-KS$^-$, 100 ng/µl) and a coinjection marker (*sur-5::dsRed*, 25 ng/µl).

3.5.11 Quantification of *egl-17::cfp* expression

Large amounts of gravid adult worms containing the arIs92 transgene (Yoo et al. 2004) were bleached on NGM plates without food. The survived eggs hatched overnight at 20°C. The synchronized population of L1 larvae were tranferred on plates with food and allowed to grow at 20°C until the 1-cell stage (28h), the 2-cell stage (32h) and the 4-cell stage (36h) respectively. The worms were mounted on a slide with an agarose pad (4% in Q-H_20) and immobilized with Azide-solution (25mM). The focal plane was adjusted to the center of the nuclei of the primary VPCs in the DIC channel and a picture was taken. Then the microscope settings were changed to detect CFP and a picture was taken. In order to quantify the expression levels of the *egl-17* reporter, the blue nuclear signal was selected using the magic wand tool and the mean fluorescence intensity was measured for each picture. For the 2- and 4-cell stage, the mean intensity of all nuclei together was measured. Aquirement of the DIC

and fluorescence pictures was done with the Openlab software (Improvision Inc.). Quantification of fluorescence intensity was done with the Volocity software (Improvision Inc.).

3.5.12 Lifespan assay

A total amount of 100 L4 larvae was distributed on 10 NGM plates. Every second day the worms from one plate were transferred onto a fresh plate. The reason for this transfer was first, to avoid any confusions with the F1 generation and second, to avoid any fungal contaminations which might have appeared after several days of incubation at 20°C. During the transfer steps, the state of the worms was scored. The worms were either stated as “alive”, “dead”, “bursted”, “bag” or “censored”. A worm was censored, if it was not found anymore (e.g. it escaped from the plate). The censored worms were later not accounted into the statistical analysis (Kaplan-Meier).

3.5.13 Protein alignments

Protein sequence alignments were performed with the ClustalX 2.0.9 software. The layout of the alignment was optimized with the BioEdit software (Ibis Biosciences).

3.5.14 Western Blot

One 6cm NGM plate full of mixed stage worms was washed with Q-H2O and the worms transferred into an eppendorf tube. Remaining bacteria was removed by additional washes with Q-H2O. The supernatant was removed and the remaining worm pellet was resuspended in 200ul of 2xSDS loading buffer and subsequently boiled at 95°C for 5min. Total protein concentration was measured using the Weizmann-Schaffner test. Between 10 and 20ug of total protein were separated on a SDS-PAGE and afterwards blotted onto a PVDF membrane. To avoid unspecific binding of the antibodies, the membrane was blocked with 5% milk in TBS-T. Afterwards, the primary antibody was diluted in the blocking solution and applied onto the membrane overnight at 4°C. Excess antibody was removed by six washes of 10min with TBS-T rocking at RT. Secondary antibodies conjugated with horse radish peroxidase were diluted 1:10’000 in 5%milk in TBS-T and applied onto the membrane for 1h at RT. The same washing conditions were used as to remove the excess primary antibodies at this step.

Activation of the horse radish peroxidase was done by applying the ECL (GE Healthcare) onto the membrane for 4min.

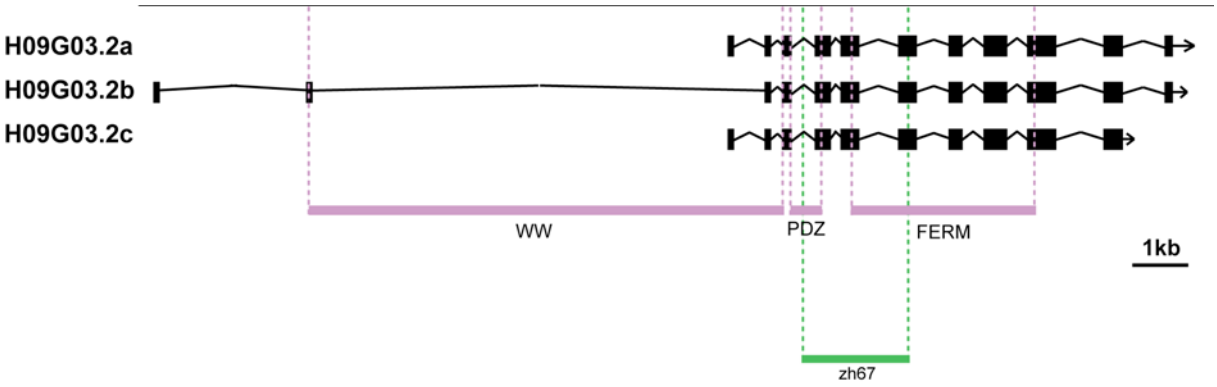

Fig. 3.1: *frm-8* (H09G03.2) gene model.
Schematic representation of the *frm-8* gene model. Three different isoforms are predicted and partially confirmed by cDNAs. All three isoforms encode a WW, a PDZ and a FERM domain. The *zh67* deletion was generated (this study) and spans 1'677bp removing parts of the PDZ and parts of the FERM domain. A putative truncated protein would be generated as *zh67* leads to a frame shift and results in a premature STOP codon within the FERM domain encoding sequence.

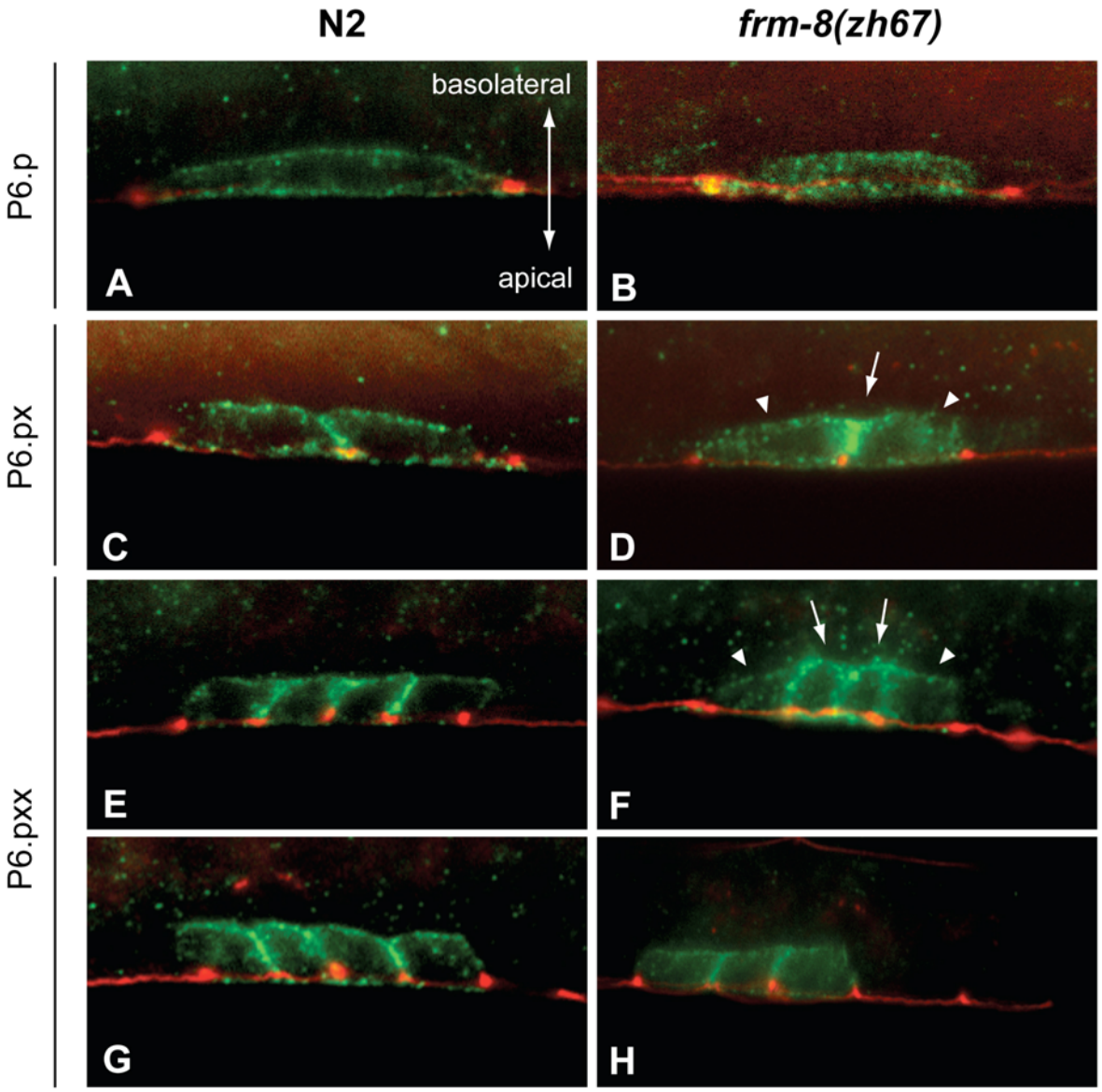

Fig. 3.2: LET-23 localization in *frm-8(zh67)* animals.
Immunofluorescence pictures of LET-23 (green) and AJM-1 (red) of wild-type animals (A, C, E, G) compared to *frm-8(zh67)* animals (B, D, F, H). *frm-8(zh67)* seems to show mislocalized LET-23 in the primary vulval lineage throughout the early steps of vulval development. At the 1-cell stage, *frm-8(zh67)* seems to have more LET-23 in intracellular punctae and less at the basolateral membrane (B) compared to the wild-type control (A). In the 2-cell stage of *frm-8(zh67)* animals, LET-23 was predominantly expressed on the basolateral membrane facing the corresponding sister cell (D, arrow), compared to the residual basolateral membrane (D, arrowheads). This effect had a penetrance of 30-40% compared to wild-animals which showed in almost all cases even distribution on the basolateral membrane of the P6.px cells (C). In 50% of *frm-8(zh67)* 4-cell stage animals, P6.pap and P6.ppa showed more LET-23 expression (F, arrows) than in the two distal P6.p descendants (F, arrowheads), compared to wild-type animals, where all P6.p descendants appear to have equal amount of LET-23 respectively (E). In 5% of the *frm-8(zh67)* animals, 3 (H) compared to 4 VPCs (G) in wild-type animals were positive for LET-23 at the P6.pxx stage.

Row	Genotype	n	VPC index	P
1	*WT*	many	3.0	
2	*frm-8(zh67)*	many	3.0	
3	*let-60(n1046gf)*	46	3.5	
4	*let-60(n1046gf); frm-8(zh67)*	41	3.4	>=0.05[†]
5	*lin-2(n105)*	25	0.9	
6	*lin-2(n105); frm-8(zh67)*	27	1.1	<0.05[@]

Table 3.1: Epistasis experiments with *frm-8(zh67)*.
The *frm-8(zh67)* allele does not genetically interact with *let-60(n1046gf)*, but suppresses very weakly the *lin-2(n105)* Vulvaless phenotype. All strains containing the temperature sensitive *lin-2(n105)* allele were grown at 25°C. All the other strains were grown at 20°C. Statistical significance was determined with the Mann-Whitney U test. [†]compared to row 3. [@]compared to row 5.

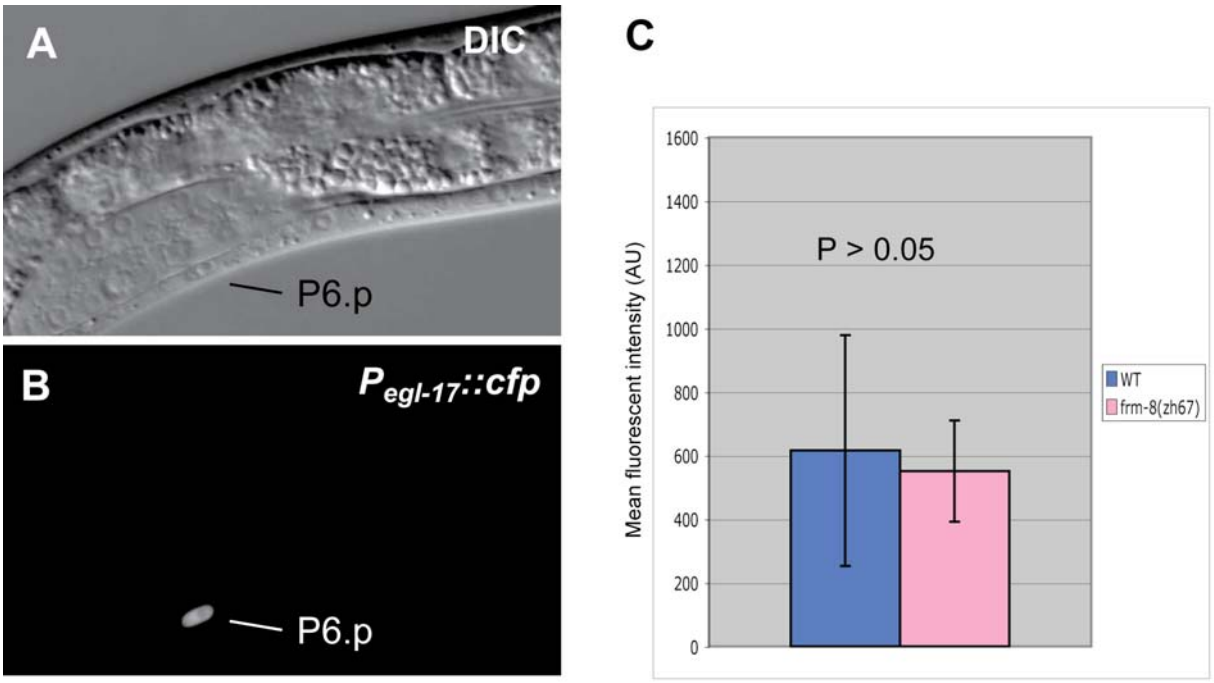

Fig. 3.3: *egl-17::cfp* expression analysis in *frm-8(zh67).*
Animals harbouring the *arIs92[egl-17::cfp]* transgene in a wild-type or *frm-8(zh67)* background were analyzed at the 1-cell stage of vulval development. A) DIC picture was taken focusing on the center stage of the nucleus of P6.p. B) *egl-17::cfp* expression was determined by selecting the area of the P6.p nucleus and the average fluorescence intensity was measured. C) *frm-8(zh67)* animals do not show a significant change in *egl-17::cfp* expression in P6.p compared to wild-type animals. y-axis: fluorescence intensity (arbitrary units). Statistical significance was determined with the two-tailed Student's *t*-test.

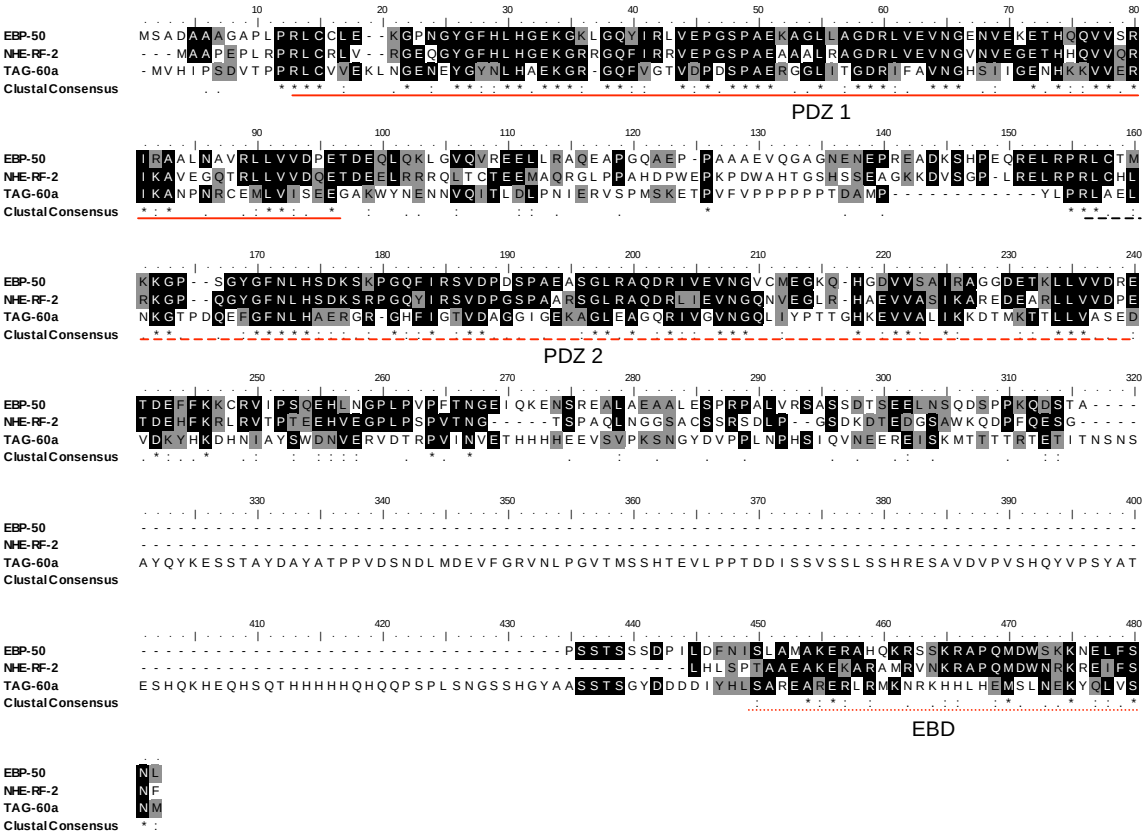

Fig. 3.4: Protein alignment of EBP-50, NHE-RF-2 and TAG-60a.
ClustalX software was used to perform a multiple alignment of TAG-60a and its putative human orthologues. Regions of high identity/similarity are found in the first PDZ domain (red line) and the second PDZ domain (red dashed line). Similarities are also found at the carboxy-terminus, the ERM-binding domain (EBD) of EBP-50 and NHE-RF-2 (red dotted line). Black boxes symbolize identical and grey boxes similar amino acids respectively.

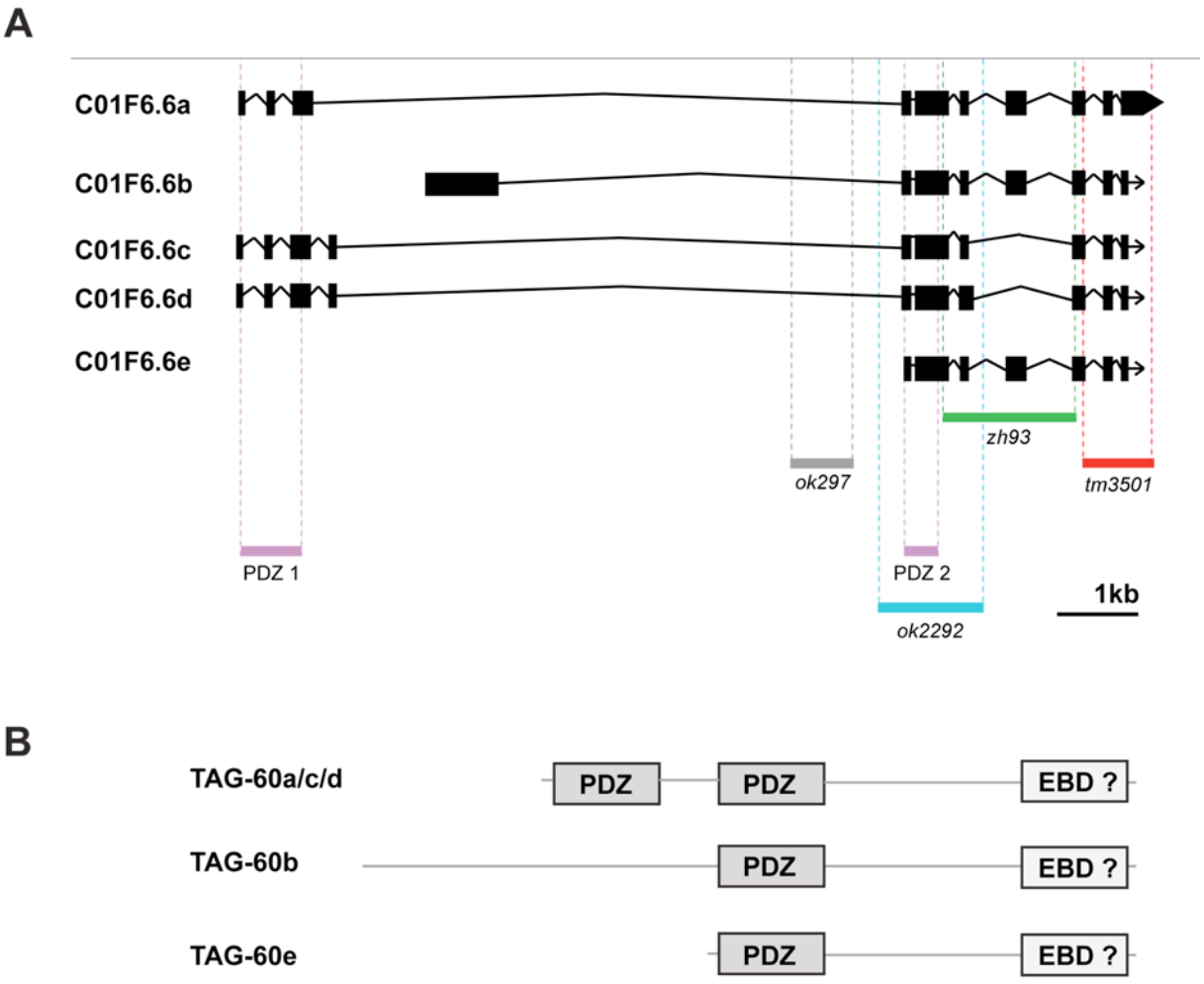

Fig. 3.5: *tag-60* (C01F6.6) gene model.
A) Schematic representation of the *tag-60* gene model. In total five different isoforms have been confirmed by cDNA. The main allele used in this study is *zh93*, which was generated in our laboratory. zh93 is an in-frame deletion of 1'565 bp, which covers sequences that do not encode predicted domains. The *ok297* deletion removes 724bp within intronic sequences. The alleles *tm3501* and *ok2292* were recently generated and remove 953bp and 1'117bp respectively. *tm3501* covers the STOP codon and parts of the 3'UTR of all isoforms. *ok2292* covers the second predicted PDZ domain. B) The putative proteins encoded by the *tag-60* locus have either two PDZ domains (isoforms a, c and d), a large uncharacterized N-terminus and one PDZ domain (isoform b) or one PDZ domain (isoform e). All isoforms share a putative ERM-binding domain at the distal carboxy-terminus.

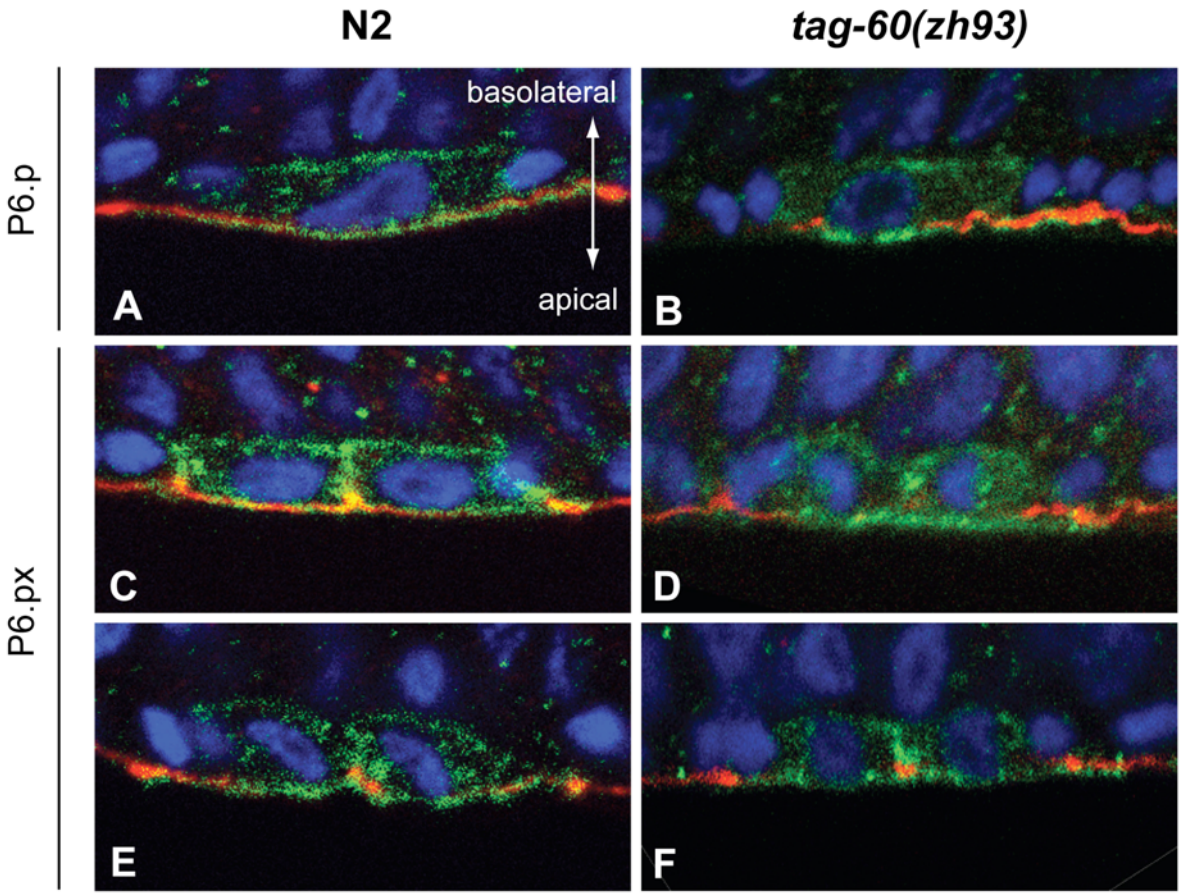

Fig. 3.6: LET-23 localization in *tag-60(zh93)* animals.
Immunofluorescence pictures of LET-23 (green) and AJM-1 (red) of wild-type animals (A, C, E) and *tag-60(zh93)* animals (B,D, F). At the 1-cell stage (P6.p), a subtle shift of LET-23 from the basolateral membrane to intracellular punctae was observed in *tag-60(zh93)* (B) compared to wild-type animals, where predominant basolateral LET-23 localization was detected (A). This effect got more pronounced in the 2-cell stage (P6.px), where LET-23 largely accumulated in the intracellular space in 40% of *tag-60(zh93)* animals (D, F). In most cases of wild-type animals (90%), the predominant basolateral localization of LET-23 got very pronounced (C), whereas in approximatively 10% of the animals intracellular accumulated LET-23 was detected (E). Representative pictures were acquired with a confocal laser scanning microscope. Determination of the penetrance of the effects on LET-23 was performed with epifluorescence microscopy.

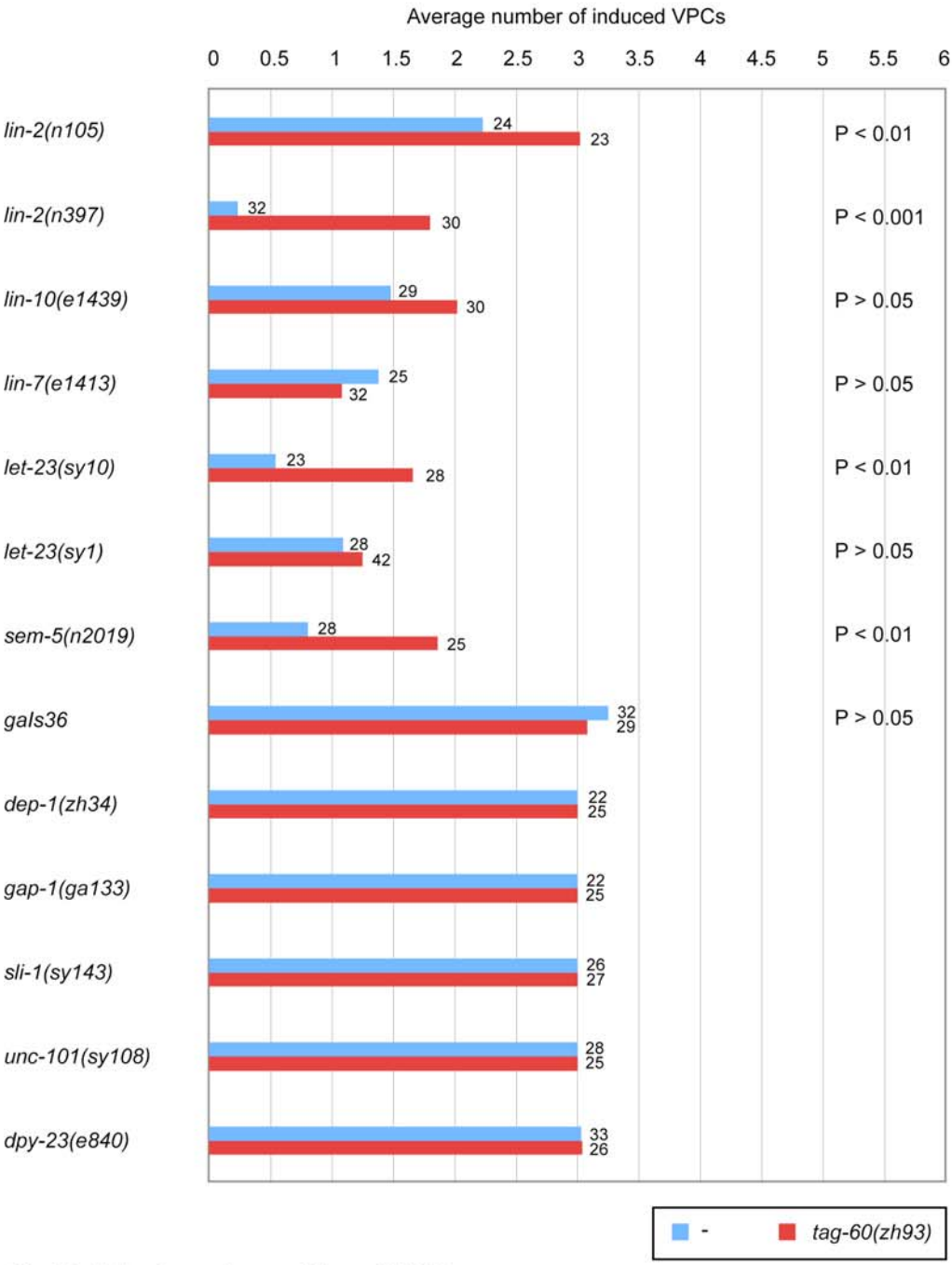

Fig. 3.7: Epistasis experiments with *tag-60(zh93)*.
The *tag-60(zh93)* allele was combined with mutants of regulators and core components of the LET-23-pathway (shown on the y-axis) and the average number of induced VPCs was scored (x-axis). Blue bars indicate the data of the single mutants indicated on the x-axis and the red bars indicate the data of the double mutant combination with the *tag-60(zh93)* allele. Sample sizes are indicated at the top of the bars. gaIs36 is an integrated transgenic array consisting of heat shock inducible *mpk-1* and *mek-2* (Lackner et al. 1994). All strains were grown at 20°C. The strains containing gaIs36 were heat shocked at 33°C for 5 minutes at the L1 stage. Statistical significance was determined with the Mann-Whitney U Test.

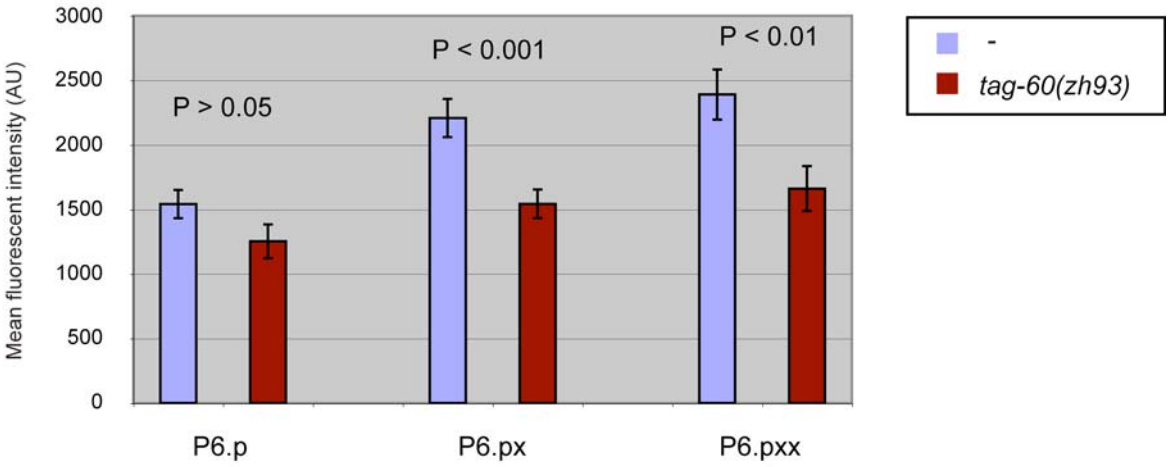

Fig. 3.8: *egl-17::cfp* expression analysis in *tag-60(zh93)*.
The expression of the nuclear *arIs92[egl-17::cfp]* integrated transgene was compared between the wild-type background (blue bars) and the *tag-60(zh93)* background (red bars). Average fluorescence intensity (arbitrary units on the y-axis) was measured from all nuclei of the primary lineage at the 1-cell stage (P6.p), the 2-cell stage (P6.px) and the 4-cell stage (P6.pxx) as indicated on the x-axis. In the 2- and 4-cell stage, *tag-60(zh93)* animals show a 20-30% reduction of *egl-17::cfp* expression in the primary lineage compared to wild-type animals. Statistical significance was determined with the two-tailed Student's *t*-test.

Row	Genotype	RNAi clone	n	VPC index	P
1	*lin-2(n397)*	vector	33	0.14	
2	*lin-2(n397)*	*tag-60* #1	29	0.17	0.44 (1)
3	*lin-2(n397)*	*tag-60* #2	24	0.15	0.38 (1)
4	*tag-60(zh93); lin-2(n397)*	vector	28	1.55	<0.001(1)
5	*tag-60(zh93); lin-2(n397)*	*tag-60* #1	27	1.15	0.096 (4)
6	*tag-60(zh93); lin-2(n397)*	*tag-60* #2	26	1.06	0.057 (4)

Table 3.2: Determination of the molecular nature of the *tag-60(zh93)* allele by RNAi.
tag-60 RNAi by feeding was performed in either *lin-2(n397)* or *tag-60(zh93); lin-2(n397)* animals. Both *tag-60* RNAi clones #1 and #2 harbour the tag-60a cDNA and originate from the Vidal RNAi library. None of the RNAi experiments could significantly alter the average number of induced VPCs compared to the vector control experiments. Only the two vector controls are highly significantly different as expected. Statistical significance was determined using the Mann-Whitney U test. Numbers in brackets indicate, to which row the VPC index was compared to for statistical analysis.

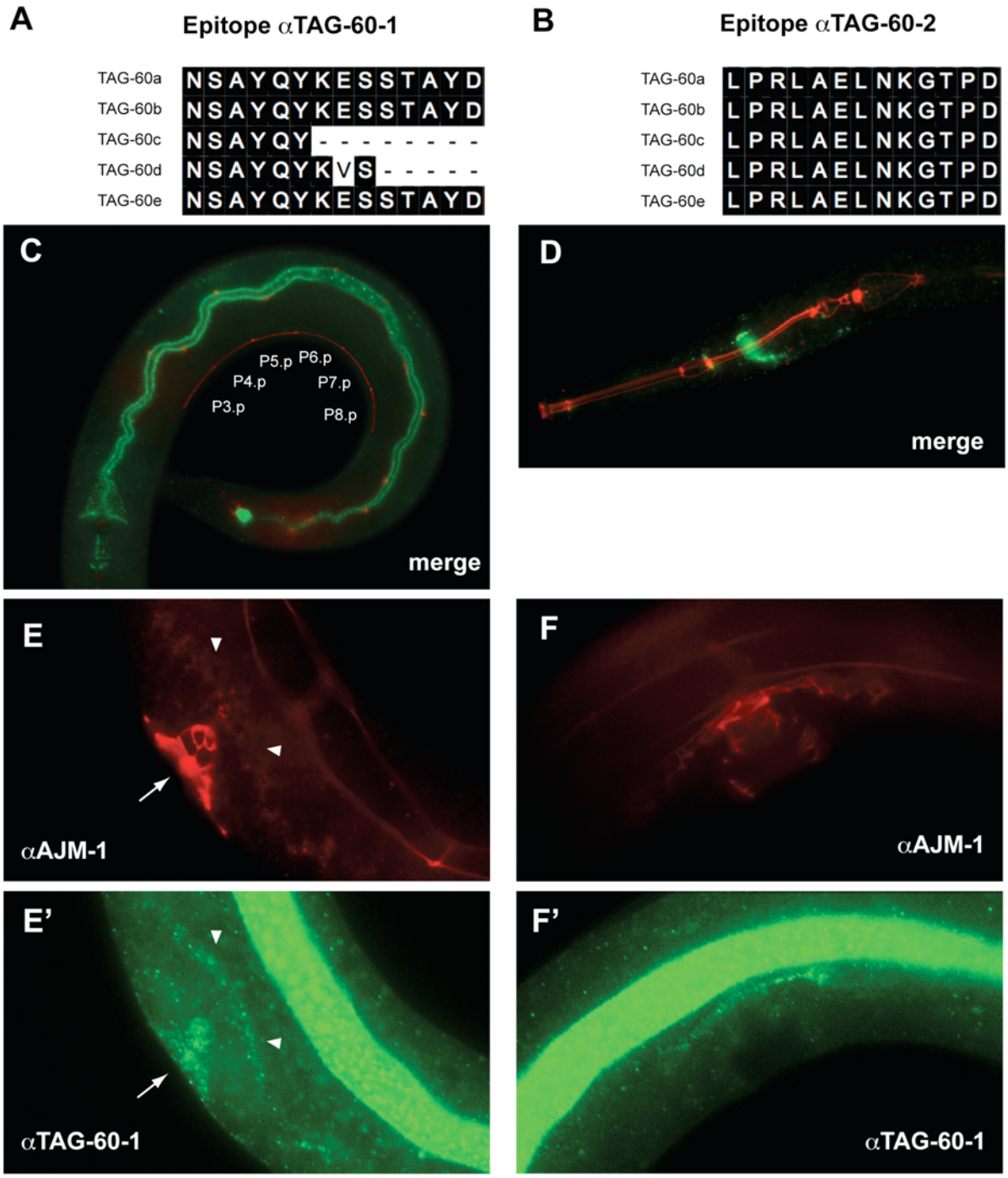

Fig. 3.9: TAG-60 expression analysis.
Two different TAG-60 peptides were used to raise two different rabbit antisera. The peptide NSAYQYKESSTAYD is encoded within the region covered by *zh93* and is present in the TAG-60 isoforms a, b and e. A degenerated version of this peptide is present in isoforms c and d (A). The antibody raised with this peptide (αTAG-60-1) shows high level of expression in the pharynx and the intestine (C, green: αTAG-60-1, red: AJM-1). The peptide LPRLAELNKGTPD is present in all TAG-60 isoforms (B) and exhibits TAG-60 expression in the nerve ring (D, green: αTAG-60-2, red: AJM-1) and what appears to be the ventral nerve cord (data not shown). The antibody αTAG-60-1 showed additionally weak TAG-60 expression in the developing uterus (arrowheads) and vulva (arrow) at the early L4 stage (E, E') which fades at the middle of the L4 stage (F, F'). No expression was observed in the VPCs at the early steps of vulval development (C). The signals originating from the intestine, uterus and vulva were sensitive to the *zh93* deletion (data not shown), indicating that these signals originate from TAG-60 proteins.

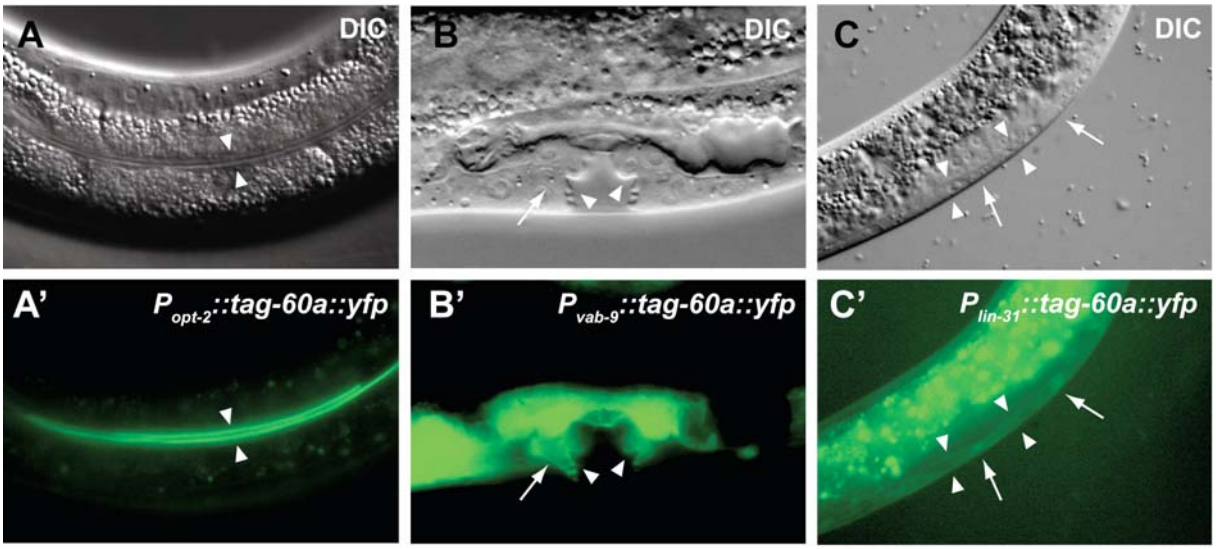

Fig. 3.10: Subcellular localization of TAG-60a::YFP fusion proteins.
TAG-60a::YFP fusion proteins were expressed with either the *opt-2* (A, A'), *vab-9* (B, B') or *lin-31* (C, C') promotor. The *opt-2*, *vab-9* and *lin-31* promotors drive expression in the intestine, epithelia tissues and the VPCs, respectively. The TAG-60a minigene expressed in the intestine localizes exclusively to what appears to be the apical plasma membrane compartment of the intestinal cells (A'). The TAG-60a::YFP fusion protein expressed under the control of the *vab-9* promotor appears to be expressed stronger in the uterus than in the vulval tissue and therefore masks the vulval signal at the early stages of vulval development, but seems to localize to the apical (B', arrowheads) and basolateral membrane (B', arrow) compartments. Intracellular signal might be a side effect from the overexpression of the construct. Very weak signals were detected from the TAG-60a::YFP fusion protein expressed by the *lin-31* promotor, which seems to localize at the plasma membrane (C', arrowheads) and the junctions (C' arrows).

Row	Ex. Array	Type	n	VPC index	P
1	-	-	32	1.77	
2	*zhEx309.1*	$P_{vab\text{-}9}$*::tag-60a*::YFP	44	1.60	
3	*zhEx309.2*	$P_{vab\text{-}9}$*::tag-60a*::YFP	39	2.10	
4	*zhEx309.3*	$P_{vab\text{-}9}$*::tag-60a*::YFP	48	1.83	
5	*zhEx310.1*	$P_{opt\text{-}2}$*::tag-60a*::YFP	42	1.52	
6	*zhEx310.2*	$P_{opt\text{-}2}$*::tag-60a*::YFP	36	2.17	
7	*zhEx308.1*	$P_{lin\text{-}31}$*::tag-60a*::YFP	31	1.76	
8	*zhEx308.2*	$P_{lin\text{-}31}$*::tag-60a*::YFP	49	1.73	
9	*zhEx308.3*	$P_{lin\text{-}31}$*::tag-60a*::YFP	40	2.10	
10	*zhEx312.1*	*tag-60* genomic	35	2.60	$<0.01^{\dagger}$
11	*zhEx312.2*	*tag-60* genomic	20	1.98	
12	*zhEx312.3*	*tag-60* genomic	52	1.83	
13	*zhEx312.4*	*tag-60* genomic	35	1.97	
14	*zhEx312.5*	*tag-60* genomic	24	1.60	

Table 3.3: The effects of tag-60 transgenes on the vulval induction of *tag-60(zh93); lin-2(n397)*.
tag-60 minigenes consisting of either the *vab-9* (epithelial tissue, rows 2, 3, 4), *opt-2* (intestine, rows 5, 6) and *lin-31* (VPCs) promotors combined with the *tag-60a* cDNA and c-terminal encoded YFP were introduced into *tag-60(zh93); lin-2(n397)* animals. All the minigenes variants harboured the standardized *unc-54* 3'UTR. No significant change of VPC induction was observed (rows 2-9) compared to animals without transgene (row 1). Additionally, a 17kb PCR fragment containing the genomic *tag-60* locus, covering 5.8kb upstream of the ATG of the a isform and 1kb of 3'UTR region, was introduced into *tag-60(zh93); lin-2(n397)* animals. One established line showed a significant increase of vulval induction to 2.6 (row 10) compared to the control animals (row 1). Four addtional lines did not show a significant change in vulval induction (rows 11-14). Statistical significance was assessed with the Mann-Whitney U test.

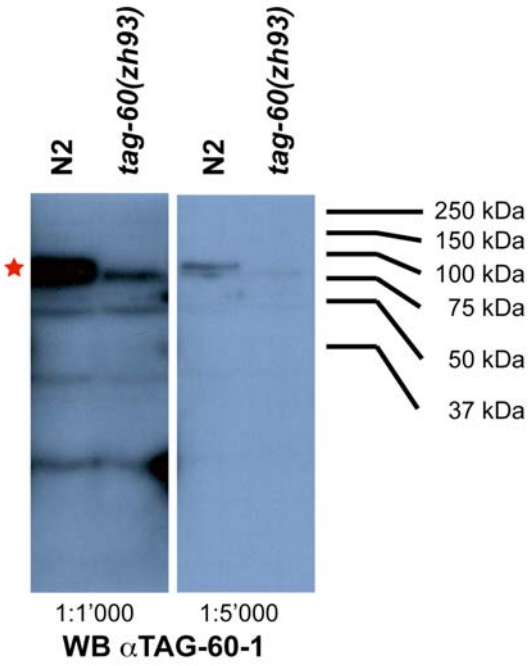

Fig. 3.11: TAG-60 detection in Western Blot experiments. Mixed staged worm cultures of wild-type and *tag-60(zh93)* were lysed in 2xSDS loading buffer and separated on a 12% SDS-PAGE. The antibody αTAG-60-1 (figure 3.9 A, C, E' and F') was used to detect TAG-60 proteins in two dilutions, 1:1'000 and 1:5'000 respectively. Since the epitope for αTAG-60-1 lies within the *zh93* deletion, only one detected band of around 80kDa corresponded to a TAG-60 protein (red star), as it was only detectable in the wild-type lysates, but not in the *tag-60(zh93)* lysates. Therefore, the other detected bands are not considered to represent TAG-60 proteins.

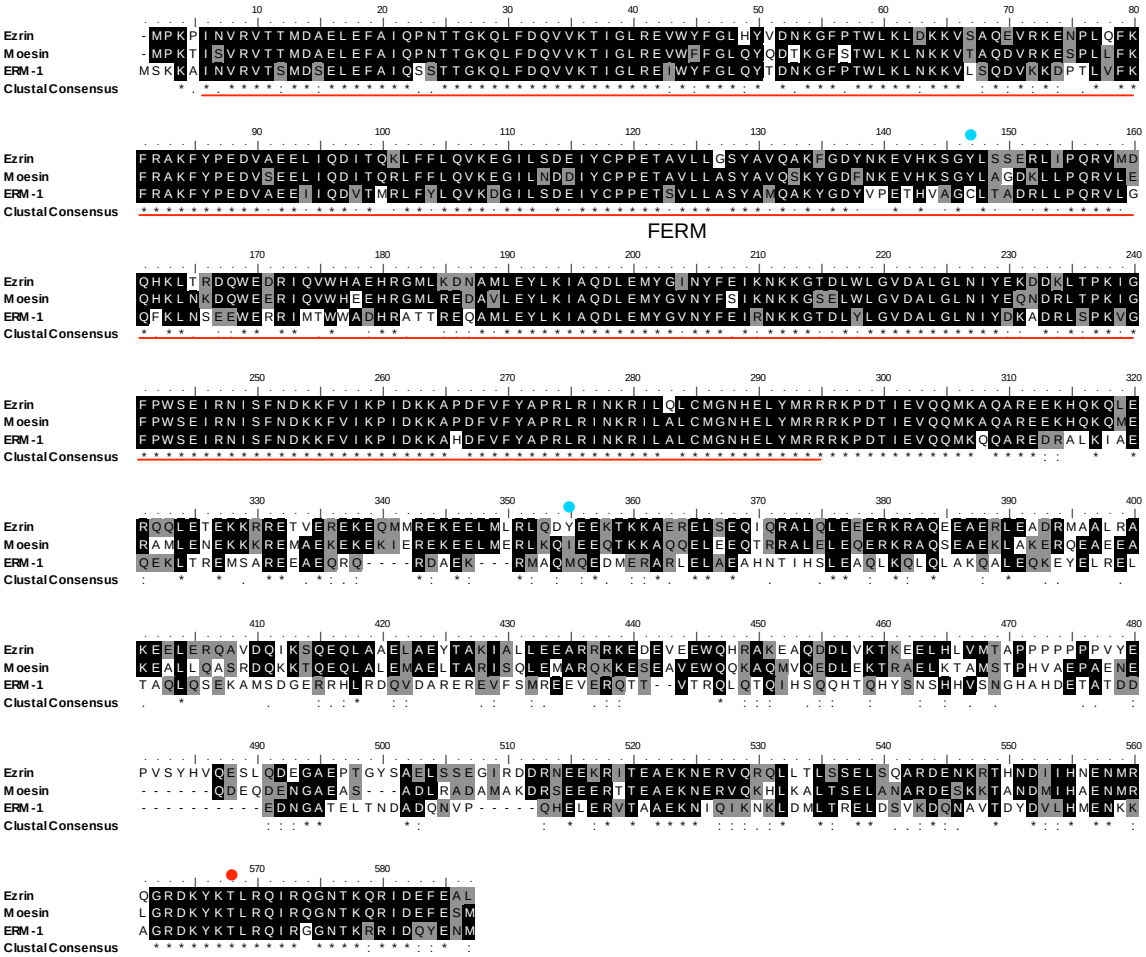

Fig. 3.12: ERM-1 is the *C. elegans* orthologue of human Ezrin, Radixin and Moesin.
ClustalX protein alignment of Ezrin, Moesin and ERM-1 shows high levels of conservation in the N-terminal FERM-domain (N-ERMAD, N-terminal ERM association domain, red line) and lower levels of conservation in the C-ERMAD (C-terminal ERM association domain). Radixin is a protein highly similar to Ezrin and Moesin and is not shown in this alignment. Blue dots indicate tyrosine residues of Ezrin that have been shown to be phosphorylated by EGFR (Krieg and Hunter 1992). Red dot indicates threonine residue of Ezrin and Moesin that has been shown to activate ERM proteins when phosphorylated (reviewed in Bretscher et al. 2002). Black boxes indicate identical amino acids and grey boxes indicate similar amino acids.

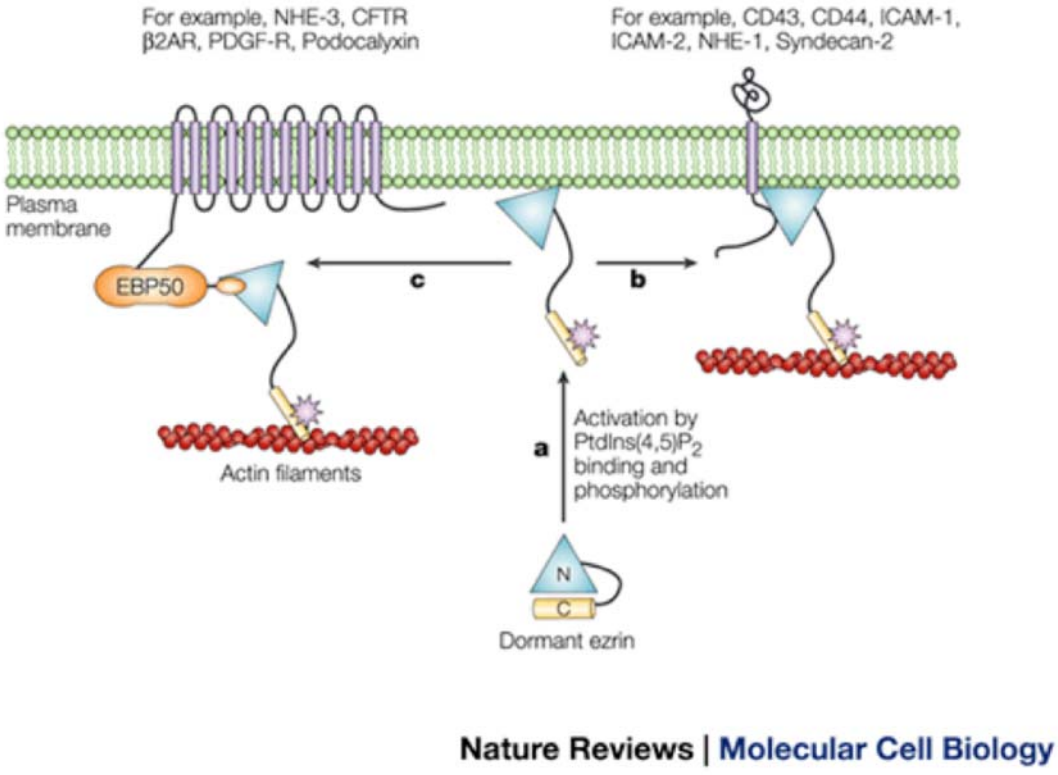

Fig. 3.13: Model of the ERM protein activation (Bretscher et al. 2002).
In the inactive (dormant) state of Ezrin, the FERM domain is masked by the C-ERMAD (C-terminal ERM association domain). Phosphorylation of T567 in the C-terminus of Ezrin in concert with PtdIns(4,5)P_2 binding to the FERM domain renders Ezrin to the extended, active state (a). The FERM domain either interacts directly with transmembrane proteins (b) or indirectly via scaffolds like EBP-50/NHERF1 or E3KARP/NHERF2 (c). The C-terminus of Ezrin additonally harbours an interaction interface for F-actin.

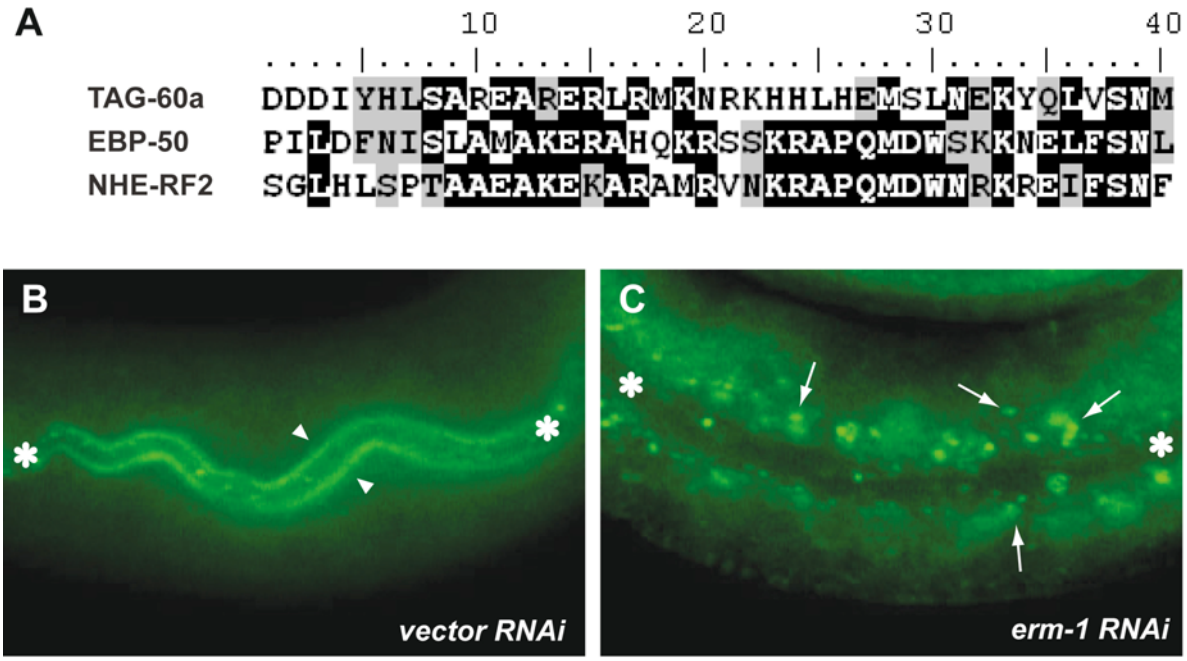

Fig. 3.14: TAG-60 localization in the intestine is dependent on ERM-1.
ClustalX protein alignment of the distal C-terminus of TAG-60a, EBP-50/NHE-RF1 and NHE-RF2/E3KARP reveals a low level of sequence similarity (A). Black boxes indicate identical amino acids and grey boxes indicate similar amino acids. Throughout development, TAG-60 localization in the intestinal cells was dependent on ERM-1. wild-type animals were subjected for RNAi of either empty vector (B) or *erm-1* (C) and subsequently immunostained with αTAG-60-1. The evident exclusive apical localization of TAG-60 in the control animals (B, arrowheads) is lost in 100% of *erm-1* RNAi animals (C), where TAG-60 seems to be mislocalized to subapical intracellular compartments (C, arrows). Asteriks in B and C indicate the lumen of the intestine on either side of the picture.

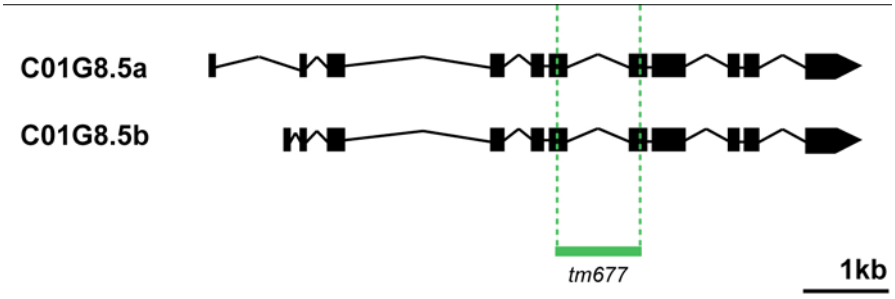

Fig. 3.15: *erm-1* (C01G8.5) gene model.
The *erm-1* locus encodes at least 2 isoforms, which differ only in their first exon. The *tm677* deletion covers 972bp and affects both isoforms in the same way. Göbel et al. (2004) rationalize that *tm677* represents a "null" allele, since transheterozygots of *erm-1(tm677)* over a deficiency does not enhance the defects associated with *erm-1(tm677)* homozygous animals.

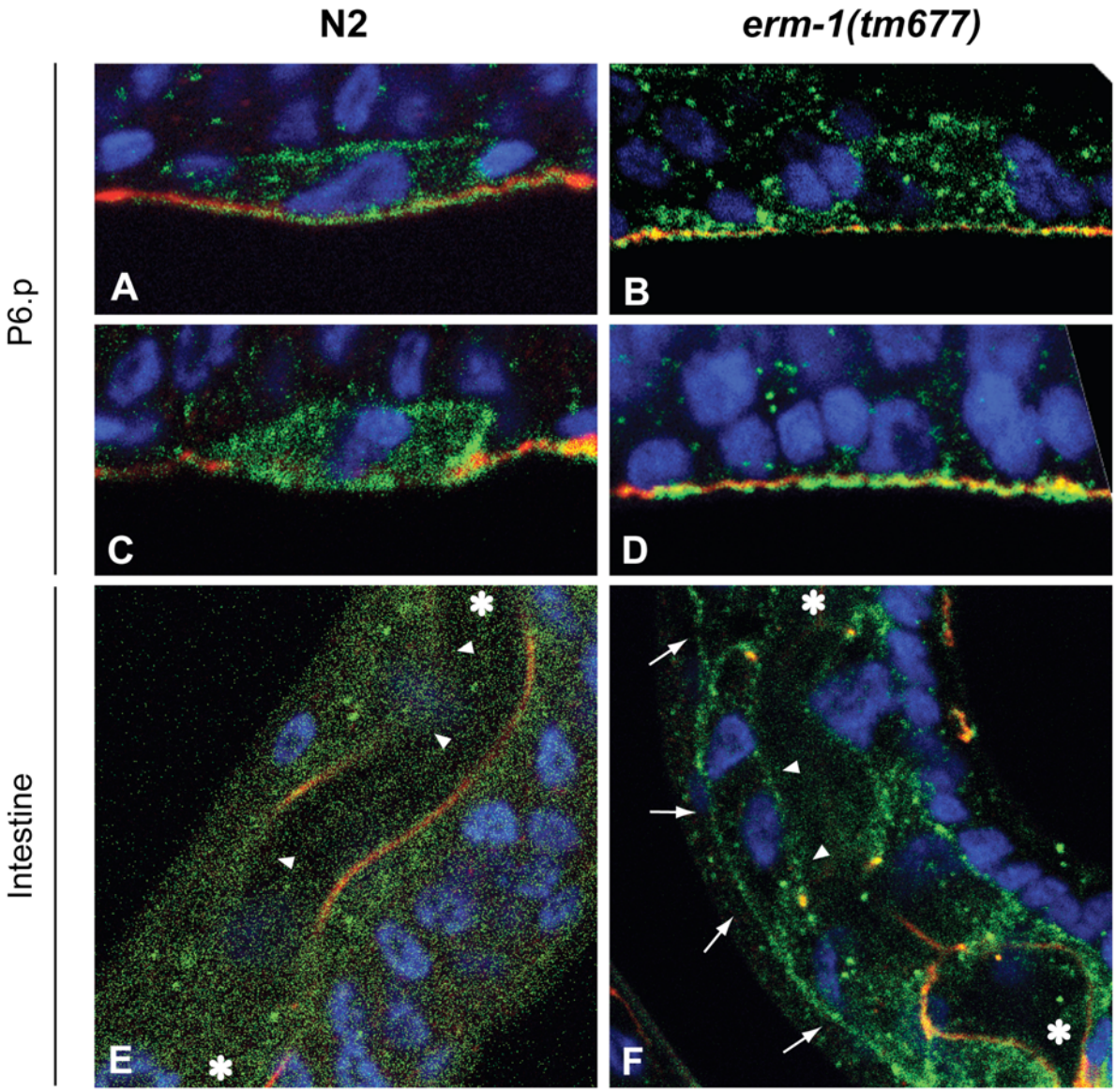

Fig. 3.16: Immunostaining of LET-23 in *erm-1(tm677)* animals.
Wild-type and *erm-1(tm677)/unc-63(x18) dpy-5(e61)* (and segregants) animals were subjected for immunostaing of LET-23. At the 1-cell stage *erm-1(tm677)* animals show mislocalized LET-23 to intracellular punctae (B, D), while wild-type animals show predominant basolateral LET-23 localization (A, C). Homozygosity of *erm-1(tm677)* was determined by screening for worms, which show basolaterally mislocalized LET-23 in intestinal cells (F, arrows). In control animals, LET-23 is weakly expressed on the apical side of intestinal cells (E, arrowheads). Asteriks indicate the lumen of the intestin on either side of the picture. LET-23 is shown in green, AJM-1 is shown in red and DNA is visualized with DAPI (blue).

Row	Genotype	n	VPC index	P
1	*WT*	many	3.0	
2	*erm-1(tm677)*	many	3.0	
3	*let-60(n1046gf)*	23	3.4	
4	*erm-1(tm677)/+; let-60(n1046gf)*	29	3.5	$<0.05^{\dagger}$
5	*erm-1(tm677); let-60(n1046gf)*	26	5.1	$<0.001^{@}$
6	*gap-1(ga133)*	many	3.0	
7	*erm-1(tm677); gap-1(ga133)*	24	3.0	

Table 3.4: Preliminary epistasis experiments with *erm-1(tm677)*.
erm-1(tm677) animals show a wild-type vulval induction (row 2). However, the *erm-1(tm677)* allele significantly enhances the Multivulva phenotype of *let-60(n1046gf)* animals (rows 3, 4, 5). In contrast, *erm-1(tm677)* does not result in overinduction when combined with *gap-1(ga133)* (rows 6, 7). Statistical significance was determined using the Mann-Whitney U test. †compared to row 3. $^{@}$compared to row 4.

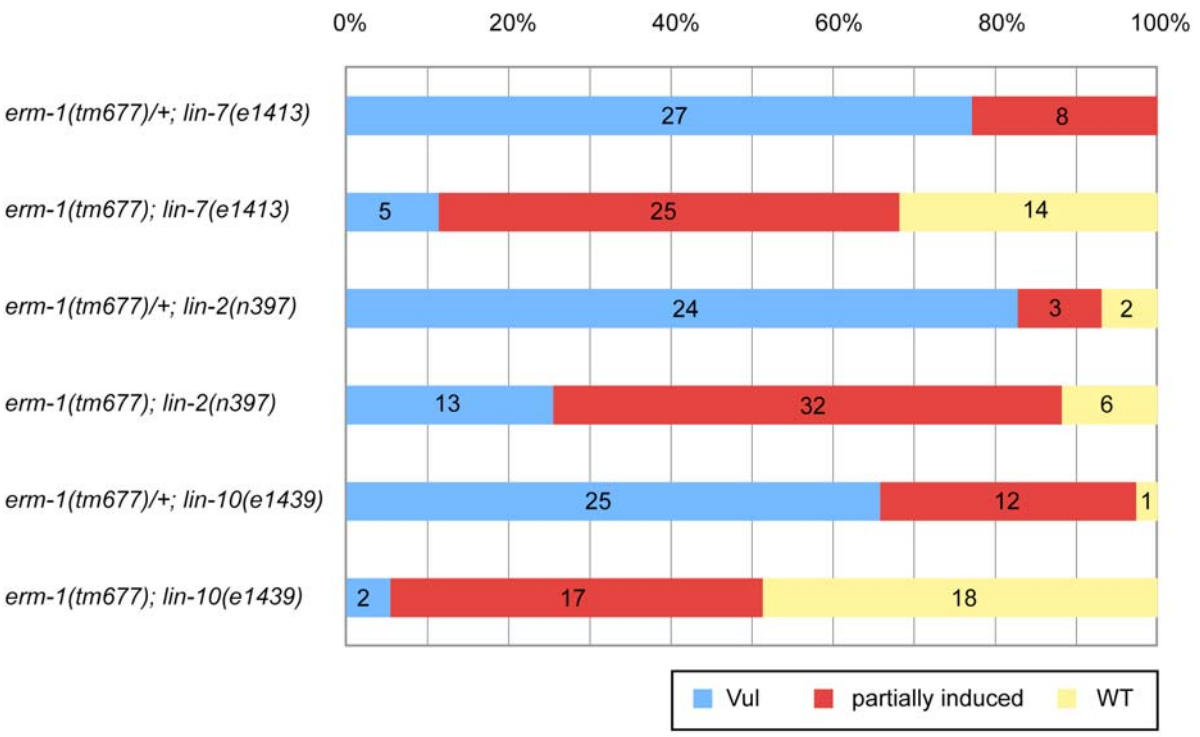

Fig. 3.17: *erm-1(tm677)* suppresses the Vulvaless phenotypes of *lin-7(lf)*, *lin-2(lf)* and *lin-10(lf)*.
erm-1(tm677) was combined with the loss-of-function alleles *lin-7(e1413)*, *lin-2(n397)* and *lin-10(e1439)*. Since *erm-1(tm677)* results in larval lethality in the F2 generation, *erm-1(tm677)* strains are maintained with the balancer hT2, a chromsosomal translocation from chromosome I to III. The hT2 balancer is marked with a *myo-2::gfp* construct, which results in a GFP positive pharynx. For the genetical analysis shown in this graph, *erm-1(tm677)* homozygous animals were compared to *erm-1(tm677)*/hT2, which are assumed to be *erm-1(tm677)*/+. Numbers of scored animals are indicated within the bars.

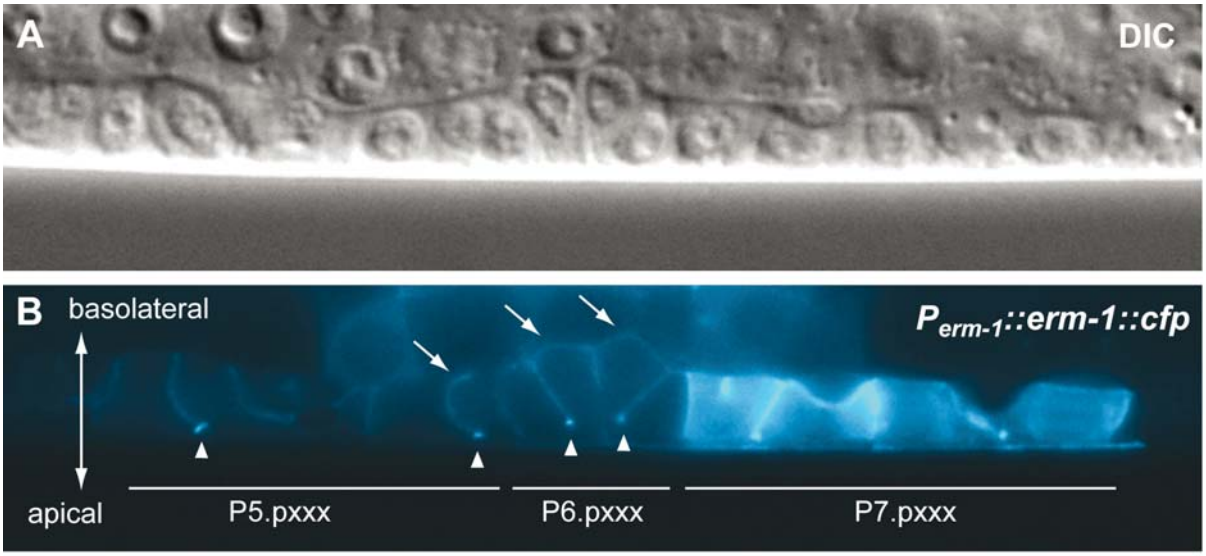

Fig. 3.18: ERM-1::CFP localizes to the basolateral membrane of vulval cells (provided by D. Kradolfer).
erm-1(tm677) associated lethality was rescued with a minigene *erm-1* construct constituting of its endogenous promotor, the cDNA of *erm-1a* and the *cfp* sequence followed by the *unc-54* 3'UTR. Throughout the early steps of vulval develpment (A, 4-cell stage), ERM-1::CFP appeared to display basolateral localization in the vulval cells (B, arrows). A fraction of ERM-1::CFP could be localized to the apical junctions (B, arrowheads).

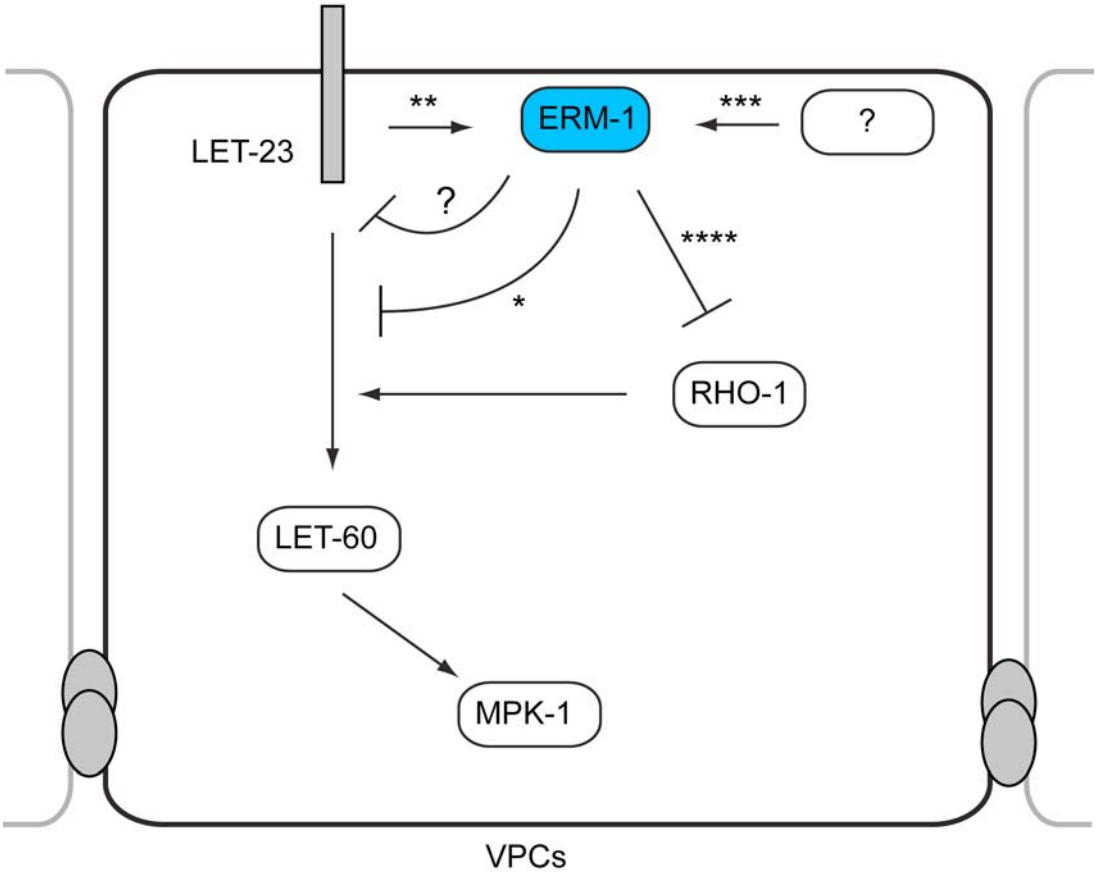

Fig. 3.19: Model of ERM-1 as a negative regulator of vulval development.
The genetic data collected in this study indicates that ERM-1 is a novel attenuator of vulval development (*). However, it is not clear yet if ERM-1 only affects the inductive, but also other pathways (*). The basolateral ERM-1::CFP subcellular localization and the association of ERM-1::CFP with LET-23 in immunoprecipitation experiments (D. Kradolfer and E. Fröhli, unpublished results) indicate that ERM-1 regulation of vulval development occurs at the level of LET-23. Consistently, LET-23 is mislocalized to intracellular punctae in *erm-1(tm677)* animals, indicating that ERM-1 plays a role in basolateral LET-23 retention or recycling. Ezrin, the human homologue of ERM-1, was shown to be a direct phosphorylation target of EGFR (**; Krieg and Hunter, 1992). However, the phosphorylated tyrosin residues are not conserved in ERM-1 (figure 3.12). Several kinases have been proposed to activate ERM proteins in higher organisms, by phosphorylating a conserved threonine residue in the C-terminus (***; figure 3.12; Bretscher et al. 2002). Speck et al. (2003) demonstrate that *D. melanogaster* Moesin acts antagonistically to Rho GTPases (****). *C. elegans* RHO-1 was demonstrated to positively regulate the inductive pathway at the level of or upstream of SOS-1 (Canevascini et al. 2005).

4. Part II: A forward genetic screen for *gap-1(lf)* interactors

4.1 Introduction

4.1.1 GAP-1 is a negative regulator of the EGFR/Ras/MAPK pathway

The evolutionary conserved EGFR/Ras/MAPK pathway has been implicated in processes such as cell differentiation and proliferation (Yarden and Sliwkowski, 2001). Intensity and timing of the signal is tightly regulated on many levels of the signalling cascade. The Ras proto-oncogene is the founding member of the Ras superfamily of small GTPases, which have been proven to act as central switches in various signalling pathways (Bollag and McCormick, 1991). The analogy of a "switch" arose from the fact that GTPases exist in both active (GTP bound) or inactive (GDP bound) states. Ras harbours a low intrinsic GTPase activity, which allows it to hydrolyse the bound GTP molecule and therefore to inactivate itself. GTPase activating proteins (GAPs) do not possess any enzymatic activity themselves but rather increase the intrinsic GTPase activity of their target GTPases (Bollag and McCormick, 1991). Hence, GAPs are negative regulators of Ras signalling, since the enhanced turnover of GTP to GDP results in the inactivation of Ras.

So far, four sub-families of RasGAP proteins have been found in humans: the Gap1 (*gap-1* in *C. elegans*), synGAP (*gap-2*), p120 RasGAP (*gap-3*) and the Neurofibromin 1 (no orthologue predicted in *C. elegans*) family. All are inhibitors of Ras, but differ in their tissue specificity (Stetak et al. 2008).

gap-1, in addition to *gap-3*, is the major negative regulator of *let-60/ras* during vulval development (Stetak et al. 2008). *gap-1* loss-of-function animals show elevated levels of inductive signal in the VPCs but undergo normal vulval development (Hajnal et al. 1997, Yoo et al. 2004). Removal of additional negative regulators of the EGFR/Ras/MAPK pathway in *gap-1(lf)* animals may result in ectopic induction and hence in a Muv phenotype. This observation is in accordance with the general belief that the inductive signal has to pass a certain threshold to result in a cell fate transformation of the 3° VPCs. Many other mutants of negative regulators of the EGFR/Ras/MAPK pathway with similar properties like *gap-1(lf)* alleles have been identified in *C. elegans*: single mutants of *dep-1* or *lip-1* result in elevated levels of inductive signalling, but undergo wild-type vulval development (Berset et al. 2005, Berset et al. 2001).

4.1.2 Rationale of the forward genetic screen

The property of *gap-1* and *lip-1* loss-of-function alleles to render VPCs susceptible to abnormal development have been exploited in forward genetic screens in the past. Those alleles served as sensitized backgrounds in order to identify additional regulators of the EGFR/Ras/MAPK pathway by means of a visible Muv phenotype (Canevascini et al. 2005, Walser et al. 2006, Berset et al. 2005). Two types of genes are expected to be isolated in such a screen: genes encoding negative regulators of the EGFR/Ras/MAPK pathway that act redundantly with *gap-1* (Figure 4.1 A), and – although for less obvious reasons - genes which are involved in the regulation of basolateral localization of LET-23. Why mutations in the latter genes cause a Muv phenotype when combined with a *gap-1 (lf)* allele can be explained on the basis of the gradient distribution of secreted LIN-3/EGF ligand: In the wild-type situation LET-23 of P6.p sequesters most of the AC-derived LIN-3 ligand, whereas the flanking VPCs receive lower LIN-3 levels. In mutants where the majority of LET-23 is mislocalized to the apical compartment of the VPCs, the same amount of LIN-3 is still produced, but it is no longer predominantly sequestered by P6.p. Consequently, more LIN-3/EGF is able to reach the distal VPCs and LET-23 activation on these cells is increased. In a *gap-1(lf)* background, the threshold for the inductive signal to induce a cell fate transformation of the 3° cells is thus passed (Figure 4.1 B). Proof of principle for this model comes from the finding that the Vul phenotype of loss-of-function alleles of *lin-7*, *lin-2* and *lin-10*, in which LET-23 is mislocalized to the apical compartment of the VPCs (Kaech et al. 1998, Whitfield et al. 1999), is not only rescued but overinduced in combination with a *gap-1(lf)* allele (Hajnal et al. 1997).

4.2 Results

4.2.1 Isolation of six mutant alleles

To perform the described screen, *gap-1(ga133)* worms were synchronized and then mutagenized at the L4 stage, after which these animals were allowed to lay eggs. The F1 generation was heterozygous for any mutation and hence did not show a phenotype (assuming a recessive mutation). These F1 animals were singled out and allowed to lay eggs. As shown in figure 4.2, the F2 generation was screened for the Muv phenotype, which is expected to appear in approximatively 25% of the progeny of a single F1 animal. As the same screen settings were previously applied (Canevascini et al. 2005, Walser et al. 2006, Stetak et al. 2008), we seeked to isolate mutations that might give rise to sterility or a late lethal phenotype in addition to the Muv phenotype. By screening for those more complex phenotypes, previously uncharacterized genes might be identified. Once a plate with Muvs was found, unhealthy mutants were maintained by picking worms with wild-type appearance that segregated mutant worms. In this study, 1400 F1 plates were screened for Muv animals. Out of 15 strains displaying a Muv phenotype, only six were considered for further analysis, as the remaining strains had a highly variable or very low penetrant phenotype. The mutants *zh78*, *zh94*, *zh95*, *zh96*, *zh98* and *zh99* were chosen for characterization and mapping.

Preliminary characterization of the isolated mutants was performed by two means: First, visualization of LET-23 using whole mount immunostaining to determine if LET-23 localization was affected, and second, the assessment of whether the Muv phenotype is due to a synthetic interaction between *gap-1(ga133)* and the *zh* alleles. The mutants were grouped according to their effect on LET-23 localization. Group I consists of the alleles *zh96* and *zh98* and represent mutants that display mislocalized LET-23. Group II contains the alleles *zh94*, *zh95*, *zh99* and *zh78*, which show normal localization of LET-23 in the VPCs.

Mapping was performed in most cases by automated FLP (Fragment Length Polymorphism, (Zipperlen et al. 2005, figure 4.13 A) and SNP (Single Nucleotide Polymorphism) assays. Additionally, deficiency mapping and classical three-factor crosses were used to confirm the FLP and SNP-mapping results. Once the region of the mutation was confined to a few 100 genes, candidates were determined by consulting the “Manchester RNAi dataset” (see chapter 5) or by literature search. The “Manchester RNAi dataset” consists of a list of candidate genes that were obtained in a preliminary genome-wide RNAi screen for Muv animals in a *rrf-3(pk1426); gap-1(ga133)* background. It was assumed that downregulation of the candidates in the sensitized background phenocopied the mutants found in the forward genetic screen

presented in this section. The last step in the mapping process was to confirm a candidate gene by either a complementation assay or by sequencing the coding regions of the candidate.

4.2.2 *zh96* is a novel allele of *lin-2*

The allele *zh96* was found to cause a highly penetrant synthetic Muv phenotype (Fig. 4.3 A) with *gap-1(ga133)*. Besides the ectopic induction of VPCs, no other obvious defects were detected. The strain was first maintained heterozygous for *zh96* because homozygous animals were sick and had reduced fertility. Therefore the strain was outcrossed 4 times, which resulted in normal fertility.

Interestingly, whole-mount staining of mixed stages of *zh96; gap-1(ga133)* animals uncovered apically mislocalized LET-23 in the VPCs of all animals (Fig. 4.3 B, arrowheads). This strongly resembles the phenotypes of loss-of-function alleles of *lin-7*, *lin-2* or *lin-10*. As shown in figure 4.3 C, Tier1 FLP-mapping results show a clear linkage of *zh96* to the X chromosome. Two FLP-assays, namely ZHX-11 and ZHX-13, show that of 16 different recombinants more than 80% had Bristol DNA. These results exclude *lin-7* (LG II) and *lin-10* (LG I) as candidates. Detailed FLP-mapping on chromosome X placed *zh96* on the right arm of chromosome X between the assays ZHX-12 (11’464’550bp / 3.85cM) and ZHX-05 (13’288’921bp / 11.98cM), restricting *zh96* to 360 predicted candidate genes (figure 4.3 D). One of these genes encodes the previously characterized membrane associated guanylate kinase (MAGUK) LIN-2 (Hoskins et al. 1996, Kaech et al. 1998). Therefore, the coding regions of the *lin-2* gene were sequenced in *zh96*, and a C to T transition was found in exon 19 of *lin-2a*. This resulted in a Q700STOP nonsense mutation that is located to the C-terminally encoded GUK domain. The kinase activity of this domain has previously been shown not to be involved in LET-23 localization (Hoskins et al. 1996). Nevertheless, C-terminally located premature STOP codons in *lin-2* mutants can interfere with LIN-2 function towards LET-23 localization, as has been shown for the *lin-2(n105)* allele (A. Stetak, personal communication). Indeed, *zh96* failed to complement the *lin-2(n105)* allele, as the trans-heterozygous animals were egg-laying defective and forming bags of worms. *zh96* thus represents an allele of *lin-2* and hence validates the rationale of the *gap-1(lf)* screen.

4.2.3 *zh98* is a novel allele of *lin-7*

The *zh98; gap-1(ga133)* animals displayed a strong *gap-1(ga133)*-dependent Muv phenotype (data not shown). The fertility of these animals was normal and therefore this mutant was not backcrossed at first. *zh98; gap-1(ga133)* completely mislocalized LET-23 to the apical

compartments of the VPCs similar to *lin-2(zh96)* and the previously described *lin-2(lf)*, *lin-7(lf)* and *lin-10(lf)* alleles (Figure 4.4 A, Simske et al. 1996, Kaech et al. 1998, Whitfield et al. 1999). As shown in figure 4.4 B, the Tier1 FLP-mapping results show a clear linkage to chromosome II, since over 80% of 16 recombinant lysates had Bristol DNA at the assay ZH2-01. In the Tier2 mapping experiments 4 assays distributed along the whole chromosome II were chosen and run on 48 different recombinant lysates. As shown in figure 4.4 C, 11 recombinants showed Hawaii DNA from the left side until ZH2-27 (10'527'682bp / 3.06cM) and 1 recombinant until ZH2-12 (14'045'121bp / 22.35cM). These results strongly indicated that *zh98* was located on the right arm of chromosome II. It was further possible, that *zh98* was very close to the assay ZH2-12, as we obtained only one Hawaii recombinant at this position. Indeed, *lin-7* is located very close to this FLP-assay (14'349'309bp / 22.9cM) and hence was the best candidate in this region. Confirming this hypothesis, the transheterozygote with the *lin-7(e1413)* allele failed to complement *zh98*. By sequencing the coding regions of *lin-7*, a C to T transition in exon 4 was found which results in a premature STOP codon. The Q208STOP transition is located just before the PDZ domain, which is responsible for the interaction with, and correct basolateral localization of, LET-23. Thus, *zh98* represents an allele of *lin-7* and is together with *lin-2(zh96)* emphasizing the correct rationale of the screen as positive controls.

4.2.4 *zh94* is a novel allele of the Ras inhibitor *gap-3*

The double mutant *zh94; gap-1(ga133)* showed a strong Muv phenotype (figure 4.5 A, Stetak et al. 2008), which was fully dependent on *gap-1(ga133)*. The isolated mutant after mutagenesis was very sick and showed reduced fertility, even following four rounds of backcrosses. *zh94; gap-1(ga133)* showed predominant basolateral expression of LET-23 in the VPCs (figure 4.5 B), hence *zh94* likely encodes a negative regulator of the inductive signalling pathway.

The Tier1 FLP-mapping results were at first not conclusive, as many of the assays showed Bristol DNA between 50-70% and only ZH1-03 (4'557'221bp / -0.98cM) over 70% of 16 recombinant lysates (figure 4.5 C). To confirm this linkage to chromosome I, two different FLP-assays on the distal ends of the chromosome were probed with the same 16 recombinant lysates: As shown in figure 4.5 D, ZH1-16 (470'031bp / -19.02cM) showed Bristol DNA in over 80% of the cases, in contrast to ZH1-24 (13903448bp / 22.19cM), which showed Bristol DNA in slightly more than 50% of the cases. These results strongly indicated that *zh94* was located on the distal left arm of chromosome I.

The Tier2 mapping results were at first also not conclusive: after analyzing 144 recombinant lysates (accounts for 1.5 96well plates), the region of *zh94* was bordered by the FLP-assays ZH1-16 (470'031bp / -19.02cM) and ZH1-10a (1'724'899bp / -13.32cM). The assay in between, ZH1-17 (1'038'236bp / -17.34cM), showed Bristol DNA in all recombinant lysates probed (figure 4.6 A). This finding could be due to two reasons: either *zh94* was located very close to ZH1-17, so that the recombination event between the two loci would be very unlikely, or the mapping strain Hawaii; *gap-1(ga133)* was not suitable for mapping in this particular region. To test the second theory, the mapping strain Hawaii; *gap-1(ga133)* was analyzed with the same FLP-assays shown in figures 4.6 A and 4.6 B, which are distributed along the whole first left third of chromosome I. Interestingly, the mapping strain showed Hawaii DNA in all FLP assays but ZH1-17 (data not shown). This error most likely was caused during the generation of this mapping strain, where the *gap-1(ga133)* allele was crossed six times into Hawaii background. Further investigation of this phenomena showed that other research groups also experienced challenges mapping mutations in this part of the *C. elegans* genome (Stephan Gysi, personal communication). In order to bypass the incomplete Hawaii background of our generated mapping strain, the mapping crosses were then repeated with pure Hawaii worms. Tier2 FLP-mapping was performed with the same assays as in figure 4.6 A, this time using the new recombinant lysates (figure 4.6 B). The results of this experiment confirmed the finding that the mapping strain was corrupt and that recombination can happen on the location of ZH1-17, indicating that *zh94* was bordered either between the FLP-assays ZH1-17 and ZH1-10a or between ZH1-10a and ZH1-25 (figure 4.6 B). The first region consists of 80 predicted genes, from which *smo-1* has been shown to exhibit a Muv phenotype with *gap-1(lf)* (G. Poulin, personal communication). Additionally, the genes *gsa-1*, *dapk-1* and Y92H12BR.8 were found to be positives in the Manchester RNAi dataset. Sequencing of the coding regions of *gsa-1* did not show any aberrations. The second possible region, between ZH1-10a and ZH1-25, encodes 71 predicted genes from which *gap-3* was a candidate gene studied at that time in our lab. Transheterozygous *zh94/gap-3(ga139) ; gap-1(ga133)* animals showed that *gap-3(ga139)* failed to complement *zh94*, and subsequent sequencing of the *gap-3* cDNA of *zh94; gap-1(ga133)* animals uncovered a point mutation at the beginning of the last exon (figure 4.7 A). *zh94* results in a Q to STOP exchange at position 872 within the predicted RasGAP domain (figure 4.7 B). The *gap-3(ga139)* allele is the same type of point mutation as in *zh94* but is located further N-terminally within the RasGAP-domain. The fact that both *ga139* and *zh94* perturb the

inhibitory domain of the GAP-3 protein and both alleles are synthetic Muv with *gap-1(ga133)* strongly indicates that *zh94* represents a novel allele of *gap-3*.

gap-3 encodes the only predicted p120 Ras GAP family member in *C. elegans*. The *gap-3(ga139)* allele was found in an independent forward genetic screen with a *gap-1(ga133)* sensitized background. This allele was mapped and characterized by A. Stetak in our lab. It was shown that *gap-3* encodes a negative regulator of the EGFR/Ras/MAPK signalling pathway, acting redundantly with *gap-1* and *gap-2*. These 3 RasGAPs were tested for their tissue specificity by analyzing the correspondent mutants and their effect on Ras-mediated processes during *C. elegans* development and behaviour (Stetak et al. 2008). Reduction-of-function alleles of *let-60/ras* have defects in excretory duct cell specification, sex myoblast migration, specification of the P12 cell fate, pachytene exit during miosis in the germline, vulval development and chemotaxis (Sundaram 2006). Mutants of *gap-1*, *gap-2* and *gap-3* were tested for their ability to suppress the defects provoked *by let-60(rf)*. All three GAPs seem to have redundant functions during sex myoblast migration and chemotaxis (Stetak et al. 2008, figure 4.7 C).

The *gap-3(zh94)* allele from this study was additional proof that a mutation in the RasGAP domain of GAP-3 interferes with the inhibitory function towards LET-60, since rescue experiments of the *gap-3(ga139); gap-1(ga133)* with a minigene of *gap-3* did not succeed (A. Stetak, personal communication). Altogether, both alleles *ga139* and *zh94,* as well as *gap-3* RNAi, in a *gap-1(ga133)* background resulted in a Muv phenotype and hence established GAP-3 as a negative regulator of LET-60 mediated processes.

4.2.5 *zh95* is a putative allele of *lin-13*

The double mutant *zh95; gap-1(ga133)* was maintained heterozygous for *zh95* since the homozygous double mutant showed a maternally rescued fertility but the F2 animals were 100% sterile. The Muv phenotype was only partially dependent on *gap-1(ga133)* since *gap-1(ga133)* heterozygousity was enough to result in ectopic inductions at 20°C. Not only the sick phenotype but also the level of ectopic induction seemed to be less in the F1 (I = 3.58 / 53% Muv) than in the F2 generation (I = 5.5 / 100% Muv) (figure 4.8 A). Additionally, *zh95; gap-1(ga133)* worms showed a dramatic decrease of intestinal cell size, aberrant DTC migration and gonad morphology defects. All the described defects persisted after backcrossing the strain 4 times.

In whole mount immunostaining of *zh95; gap-1(ga133)* mixed stage animals, LET-23 was found to be predominantly expressed at the basolateral compartment of the VPCs (figure 4.8

B). This indicates that *zh95* rather represents a gene that encodes a negative regulator of the inductive pathway.

Tier1 FLP-mapping results positioned *zh95* to chromosome III, since the two FLP-assays ZH3-07 (2'328'170bp / -14.68cM) and ZH3-11 (11'399'237bp / 9.26cM) detected more than 80% and 90% of Bristol DNA from 16 independent recombinant lysates respectively (figure 4.8 C).

Further mapping using the Tier2 FLP-assays determined the region for *zh95* between the assays ZH3-05a (7'772'487bp/-0.59cM) and ZH3-32 (8'691'426bp/-0.20cM), which harboured 241 predicted genes. This result had to be interpreted with care because out of 256 analyzed samples only one recombinant from the left and three recombinants from the right side are defining this region. For some unknown reason the mapping crosses with Hawaii did not result in many recombinants in that particular region. Out of the 241 predicted genes, four were found in the Manchester RNAi dataset and were tested as candidates for *zh95* by different approaches: *rfp-1* by complementation analysis, and *apc-2*, *gsto-1* and ZK652.6 by sequencing the coding regions. However, all tests turned out to be negative and hence render these genes unlikely candidates for *zh95*.

The lysates of the four informative recombinants were further analyzed by fine-mapping. Eight different SNPs distributed along the considered area further restricted the mapping region. Shown in figure 4.8 D are the results of the fine-mapping with the SNPs: only the lysate of recombinant #247 showed Hawaii DNA as far as the SNP (uCE3-1047) at position 7'938'720bp / -0.48cM. Between this SNP and the FLP assay ZH3-05a 37 genes are located. Considering the low number of informative recombinants though, final proof for the accuracy of the resulting region was still missing.

In order to confirm the region of *zh95* found by FLP and SNP mapping, we used 3 different overlapping deficiencies, which in total span the region from ZH3-05a (-0.59cM) to ZH3-32 (-0.20cM). Mapping with deficiencies can be an easy and fast way to determine the region of a certain mutation, but it has to be borne in mind that the breakpoints of the deficiencies are often unknown or roughly estimated. The ends of the deficiencies used in this study were assumed to be correct as annotated on www.wormbase.org (figure 4.9 A): sDf128 (from -0.61cM to -0.56cM), nDf20 (from -0.57cM to -0.13cM) and nDf22 (from -0.28cM to -0.13cM). The different deficiencies were put in *trans* to *zh95* in a *gap-1(ga133)* background. Unfortunately, all three deficiencies complemented *zh95*, indicating that the *zh95* mutation lies outside the region covered with the deficiencies.

Since the FLP- and deficiency mapping results were contradictory, a classical mapping strategy was applied. Three-factor mapping was chosen as an alternative approach, where two flanking mutations with visible phenotypes are used. Since the location of *zh95* was only estimated by FLP-mapping (around -0.50cM), the choice of these markers had to be optimized first. On the left side, *dpy-17(e164)* was chosen, which is located at -2.15cM. *unc-69(e587)* at the position 2.31cM was chosen for the right side. The two markers were put *trans* to *zh95* in a *gap-1(ga133)* background and the next generation was screened for Unc-nonDpy (Figure 4.9 B). These recombinants were singled out and their phenotypic segregation pattern was scored. The presence of Unc-nonDpys indicates that the recombination event occurred between the *dpy* and the *unc* mutation. If the recombination were between the *dpy* marker and *zh95*, one would expect Unc-nonDpys and Dpy-Uncs in the progeny, whereas if the recombination were between *zh95* and the *unc* marker, Unc-nonDpys, Dpy-Uncs and Unc-Muvs would be expected. With this method, one can estimate the genetic location of *zh95* by calculating the ratio of the two segregation groups. In this study only the Unc-nonDpy recombinants were considered, because some of the Dpy-nonUnc recombinants were sterile, which might be due to an unknown genetic interaction. As shown in figure 4.9 B, 16 Unc-nonDpy recombinants were found to segregate Unc-nonDpys, Dpy-Uncs and Unc-Muvs and only 8 segregated Unc-nonDpys and Dpy-Uncs. The ratio between the segregation groups located *zh95* closer to *dpy-17* than to *unc-69*, namely to an estimated genetic location of -0.66cM. This genetic position was outside the region determined by FLP-mapping, to the left of the assay ZH3-05a (-0.59cM).

Close to this position, two previously characterized negative regulators of the inductive pathway can be found: the synMuv genes *lin-13* (-0.63cM) and *lin-37* (-0.8cM) (Fay and Yochem, 2007). *lin-13* encodes a protein of 2248 amino acids containing multiple zinc fingers of the C2H2 type and a LXCXE retinoblastoma binding motif (Meléndez and Greenwald, 2000). With respect to vulval development, LIN-13 was found to be a synMuv B protein acting together with LIN-35/Rb to inhibit the inductive pathway. Interestingly, Meléndez and Greenwald (2000) furthermore showed that the null phenotype of *lin-13* is temperature sensitive, meaning that single mutants show a Muv phenotype at 25°C, but at lower temperatures only in combination with a mutation in another negative regulator of the inductive pathway (e.g. a synMuv A). Meléndez and Greenwald hypothesize that the process in which *lin-13* is functioning is temperature sensitive, rather than the mutant gene product. To test whether *zh95* might be an allele of *lin-13*, the dependency of *gap-1(ga133)* for the Muv phenotype was assessed at 25°C. Similar to the results obtained by Meléndez and

Greenwald, *zh95* seemed to exhibit a Muv phenotype independently of *gap-1(ga133)* at 25°C. This result suggests that *zh95* is an allele of *lin-13*, as such temperature sensitive synthetic phenotypes are considered to be very rare. Sequencing or complementation assays were not performed due to time restrictions.

Mutations in *lin-37* are not likely to result in a synthetic Muv phenotype together with *gap-1(lf),* since *lin-37* is part of the synMuv B class of genes, whose mutants generally do not genetically interact with *gap-1(lf)* (Fay and Yochem, 2007). However, further complementation experiments need to be performed to rule out *lin-37* or other candidates being affected by *zh95.*

4.2.6 *zh99* affects the gene encoding LET-19, a mediator subunit

The double mutant *zh99; gap-1(ga133)* was found to be 64% Muv (figure 4.10 A) and 100% sterile. However, the Muv phenotype was determined to be independent of *gap-1(ga133),* rendering this mutant to a lower priority in this study. Moreover, *zh99* showed a protruding vulva phenotype (Pvl) in 100% of the cases, which was also independent of *gap-1(ga133)*. Interestingly, 16% of the overinduced animals showed a rather rare phenotype, as the posterior Pn.p cells (P9.p, P10.p, P11.p) seemed to have divided one round before fusing with hyp7. In one case, even P9.p was induced and formed an invagination. In wild-type animals it is known that expression of the Hox-factor LIN-39 protects the VPCs from fusion to hyp7. It is assumed that in the Pn.p cells, which fuse to hyp7, the expression of *lin-39* is repressed by the canonical wnt-signalling pathway (Yoda et al. 2005). Additionally, the immunostaining of LET-23 showed basolateral localization (figure 4.10 B, arrowheads), suggesting that *zh99* likely encodes a negative regulator of the inductive pathway. Considering these findings, *zh99* encodes a gene involved in the process of cell fusion and hence negatively regulates vulval fates.

By coincidence, it was also found that *zh99; gap-1(ga133)* males exhibit male tail development defects. As shown in figure 4.10 C-F, *zh99; gap-1(ga133)* animals have degenerated rays and spicules. These kinds of defects are also found in mutants that misexpress other hox factors, such as MAB-5 in specific cells of the male tail (Yoda et al. 2005).

FLP-mapping showed a clear linkage of *zh99* to chromosome II with a slight bias to the right arm, as in Tier1 the assay ZH2-05 showed Bristol DNA in over 90% and the assay ZH2-09 in 100% of 16 analyzed recombinant lysates (figure 4.11 A). Further FLP-mapping on chromosome II confined *zh99* to a region bordered by the FLP-assays ZH2-20

(8'612'029bp/0.83cM/ 1 recombinant) and ZH2-09 (11'359'409bp/3.44cM/ 2 recombinants). As only 3 informative recombinants have been found by analyzing a total of 192 recombinant lysates (accounts for 2x96well plates) the determined region might not be accurate.

In order to confirm the FLP-mapping results, deficiencies were used to narrow down the region of *zh99*. Fortunately, Sigurdson et al. (1984) characterized a plethora of different deficiencies on chromosome II. Putting the deficiencies in trans to *zh99* showed that mnDf89, mnDf16, mnDf29 and mnDf83 complemented the *zh99* defects. In contrast mnDf66, mnDf85 and mnDf80 failed to complement *zh99* and resulted in sterile animals with Pvl phenotype (figure 4.11 B). The smallest positive deficiency used was mnDf80, which covers chromosome II from 0.86cM to 0.91cM, harbouring 59 genes. One of these genes was *let-19* (also known as *mdt-13*), which was determined to be a good candidate after literature review. The *let-19(os33)* mutant has been shown to result in a Muv phenotype and sterility, and *os33* failed to complement *zh99*.

Moreover, the *let-19(hd135)* allele was shown to have on average 2.3 ± 0.9 extra VPC divisions per animal (Clayton et al. 2008). Clayton et al. furthermore found that *let-19* was involved in VPC quiescence. Earlier studies by Yoda et al. (2005) demonstrated that *let-19* encodes the orthologue of the human MED13/TRAP240 protein. This protein is a component of the Mediator complex, a multicomponent complex that can regulate transcription in a positive or negative manner, depending on the cellular context (Kornberg 2005).

4.2.7 *zh78* is a putative allele of *lin-1*

The double mutant *zh78; gap-1(ga133)* was strongly Muv (figure 4.12 A) and very sick even after four rounds of backcrossing in the *gap-1(ga133)* background. Nevertheless it was possible to maintain the strain homozygous for *zh78*. The strong Muv phenotype was determined to be not dependent on the *gap-1(ga133)* allele. Hence, *zh78* was a mutant with lower priority during this study.

Visualizing LET-23 by immunostaining showed that the receptor is predominantly expressed on the basolateral plasma membrane of the vulval cells. Additionally LET-23 was expressed in unidentified vulval cells besides P6.p descendants (figure 4.12 B). Hence, *zh78* most likely abrogates the function of a negative regulator of the inductive pathway.

FLP-mapping of *zh78* showed a clear linkage to chromosome IV with a slight bias to the left arm, as 100% of 16 recombinant lysates showed Bristol DNA in the assay ZH4-05 and around 95% of the lysates in the assay ZH4-10a (figure 4.12 C). Tier2 FLP-mapping on the left arm of chromosome IV confined the region for *zh78* between the assays ZH4-05 (1'740'251bp/-

15cM) and ZH4-16 (4’581’704bp/0.48cM) (figure 4.12 D). This region contains 517 predicted genes. Since in this particular experiment the resolution of the automated FLP-mapping approach was not exploited, the analyzed samples should be assessed with FLP assays within the region between ZH4-05 and ZH4-16. Most likely more recombinant lysates would have to be analyzed in order to determine a reliable region.

Among the genes from the determined region, we suspect *lin-1* being a very good candidate for *zh78*, as it is a well-characterized negative regulator of vulval fates. LIN-1 is a nuclear protein and target of MPK-1 in the VPCs. Before induction, LIN-1 represses vulval fates together with LIN-31. Once MPK-1 phosphorylates this complex, LIN-1 and LIN-31 dissociate from each other and their repressing function is abolished (Tan et al. 1998).

Mutants of *lin-1* exhibit a very strong Muv phenotype which is independent of *gap-1(lf)*. Considering the high phenotypic similarity of *lin-1* alleles with *zh78*, we wished to perform a complementation assay with the previously characterized allele *lin-1(n304)* (Beitel et al. 1995). Unfortunately the crosses were unsuccessful, most probably because both *lin-1(lf)* and *zh78* animals are very sick. Therefore, the coding regions of *lin-1* were sequenced (except exon 5, where sequencing failed for unknown reasons) but no mutation was found. Hence, it is not clear, which gene is affected by *zh78*. Further mapping experiments need to be performed to reduce the putative region determined by FLP-mapping and to propose and test further candidate genes.

4.2.8 Summary

In this study, six mutant strains exhibiting a Muv phenotype were isolated from a forward genetic screen in the *gap-1(ga133)* background. The characterization and mapping of these mutants are summarized in Table 4.1.

4.3 Discussion

The second approach to find regulators of LET-23 during vulval development was based on forward genetics. An EMS mutagenesis screen was performed in a *gap-1* loss-of-function background and strains with a Multivulva phenotype were isolated. The same setting was already used to exclusively find mutants that are homozygous fertile (Canevascini et al. 2005, Walser et al. 2006, Stetak et al. 2008, personal communication A. Hajnal). In order to find uncharacterized components of vulval development, this study's goal was to additionally screen for mutants that are homozygous sick or sterile. In total, 15 mutant lines were isolated and six (*zh78*, *zh94*, *zh95*, *zh96*, *zh98* and *zh99*) were chosen for further characterization, as the other lines showed either a very variable or a very low penetrant phenotype.

4.3.1 A *gap-1(lf)* enhancer screen can reveal factors involved in LET-23 localization

Two mutants *zh96* and *zh98* seemed to affect genes involved in the localization of LET-23, as immunostaining of the receptor in the respective *gap-1(lf)* double mutant showed predominant apical expression of LET-23. Interestingly, *zh98* was homozygous fertile when isolated after mutagenesis. In contrast, *zh96* was homozygous sterile when isolated, but turned out to be fertile after 4 rounds of outcrossing with *gap-1(ga133)* animals. This finding suggested that during mutagenesis other mutations besides *zh96* were generated, which affected the animal's fitness. These other mutations were "eliminated" by the outcrossing procedure. FLP-mapping soon showed that *zh96* is located in the same region as *lin-2* on the X chromosome. Sequencing the exons of the *lin-2* gene in *zh96* animals revealed a C to T transition, which exchanges Q700 with a premature STOP. Similarly, *zh98* turned out to be an allele of *lin-7*. These results emphasize the rationale of the screen and serve as positive controls. Unfortunately, the remaining 4 mutant lines did not show mislocalized LET-23, but rather ectopic basolateral expression in the VPCs. The ectopic expression of LET-23 indicates a cell fate transformation from tertiary/secondary to primary vulval fate. Altogether, these findings show that *zh78*, *zh94*, *zh95* and *zh99* might encode negative regulators of the LET-23 pathway. During the first steps of characterization it was found that the Muv phenotype in *zh94* and *zh95*, but not in *zh78* and *zh99* was dependent on *gap-1(ga133)*. Nevertheless, the characterization and mapping of these mutants was continued, as identifying novel negative regulators of the inductive pathway would be of high interest.

4.3.2 *zh94* is a mutant allele of the conserved RasGAP gene *gap-3*

The double mutant *zh94; gap-1(ga133)* showed a Muv phentoype, which was completely dependent on *gap-1(ga133)*. These animals also had reduced fertility and none of the observed phenotypes changed after outcrossing the mutant in *gap-1(ga133)* animals. LET-23 localization in these animals seemed to be predominantly on the basolateral compartment, indicating that *zh94* abrogates the function of a negative regulator of the inductive pathway.

The FLP-mapping of *zh94* was at first misleading, as the mapping strain Hawaii; *gap-1(ga133)* was not suitable to map mutations on the left arm of chromosome I. We analyzed the DNA composition of the Hawaii; *gap-1(ga133)* strain on the left arm of chromosome I and found Bristol DNA at the position of ZH1-17. It is not exactly known, why this specific part of the genome was not exchanged by Hawaii DNA. This selection event might indicate that worms harbouring Bristol DNA around the loci of ZH1-17 are fitter than those with Hawaii DNA. Similarly, Seidel et al. (2008) found a genetic incompatibility locus between Bristol and Hawaii, also located on the left arm of chromosome I, but this does not cover the region of the FLP assay ZH1-17. These findings indicate that there might be several such incompatibility loci between Bristol and Hawaii. Thus, the generation of mapping strains constituting Hawaii DNA in a sensitized background generated in a Bristol background can lead to misinterpretations during the mapping procedure. Therefore, in order to map *zh94*, pure Hawaii animals were used in the crossing scheme as shown in figure 4.13 B.

One of the candidates in this region was the gene *gap-3*, previously described by our group (Stetak et al. 2008). Indeed, complementation analysis showed that *gap-3(ga139)* failed to complement *zh94* in a *gap-1(ga133)* background. Furthermore, it was found that the *gap-3* cDNA of *zh94* animals harboured a point mutation at the beginning of the last exon, resulting in a premature STOP codon within the RasGAP domain of GAP-3 (Q872STOP, figure 4.7 A and B). The *gap-3(ga139)* allele encodes a similar point mutation within the RasGAP domain (Q844STOP, figure 4.7 B). Both, *gap-3(ga139)* and *zh94* showed a similar effect when combined with *gap-1(ga133)* as shown by Stetak et al. (2008): in *gap-3(ga139); gap-1(ga133)* double mutants, the VPC induction index was determined to be 4.03 (n=35), compared *to zh94; gap-1(ga133)* animals with an average indcution of 3.79 (n=31). These results strongly indicated that *zh94* is a loss-of-function allele of the RasGAP activity of GAP-3.

GAP-3 is the *C. elegans* orthologue of the human p120-type RasGAP, an inhibitor of LET-60 RAS redundant to two other RasGAPs, *gap-1* and *gap-2*. The three RasGAPs have different tissue specificities, assessed by the potential of the *gap*-mutants to suppress phenotypes

caused by *let-60(rf)* alleles. In this way it was determined that GAP-3 is the main inhibitor of LET-60 during germ cell development, where it regulates the exit of the germ nuclei from the pachytene stage. Furthermore, it was shown that *gap-3* plays a minor role in other processes such as vulval development, sex myoblast positioning, P12.p specification and excretory duct cell specification. LET-60 RAS is also involved in behavioural processes such as chemosensation, in which all three *gap* genes seem to contribute equally in the inhibition of LET-60 (Stetak et al. 2008). The main *gap-3* allele used by Stetak et al. (2008) is *ga139*. *zh94* was used to support the finding that the *gap-3* gene encodes a negative regulator of LET-60, as rescue experiments with a *gap-3* minigene introduced into *gap-3(ga139); gap-1(ga133)* animals did not show any effect (A. Stetak, personal communication).

4.3.3 *zh95* is a putative allele of *lin-13*

As shown in figure 4.8, *zh95; gap-1(ga133)* animals showed a highly penetrant Muv phenotype at 20°C. LET-23 localization in these double mutants was predominantly basolateral in the VPCs. Therefore *zh95* was classified as a putative negative regulator of the EGFR/Ras/MAPK pathway.

The mapping of *zh95* turned out to be accompanied by contradicting results, as the FLP approach determined a region on chromosome III between the FLP assays ZH3-05a and ZH3-32 (figure 4.8 D). In contrast, 3 different overlapping deficiencies spanning this region complemented the *zh95; gap-1(ga133)* Muv phenotype (figure 4.9 A), indicating that *zh95* lies outside this region. The region assessed by the FLP-approach was based on only three informative recombinants, which renders this region to a rather poor reliability. For an unknown reason, only few Hawaii recombinants were obtained in this region of chromosome III. Therefore, another mapping approach was used. Classical three-factor mapping placed *zh95* at the genetic position of -0.66cM. This position lies outside of the region determined by FLP-mapping, left from ZH3-05a (-0.59cM). Three-factor mapping was thus consistent with the findings by the deficiency mapping and showed that the results obtained by FLP-mapping are not reliable, most likely because of the lack of a higher number of informative recombinants.

Around the genetic position -0.66cM, two candidates were found by literature search: *lin-37* and *lin-13* (Fay and Yochem, 2007). Both candidates are previously characterized synMuv genes found to negatively regulate the LET-23 pathway. Interestingly, Meléndez and Greenwald (2000) found that loss-of-function alleles of *lin-13* exhibited a peculiar temperature sensitivity, as *lin-13(lf)* animals exhibit a wild-type phenotype at 15°C, but

develop a Muv phenotype at 25°C. Considering these findings, *zh95* was assessed for this temperature sensitive phenomenon. Indeed, *zh95* seemed to exhibit a Muv phenotype independent of *gap-1(ga133)* at 25°, in contrast to 20°C, where the Muv phenotype was dependent on *gap-1(ga133)*. To our knowledge, this kind of temperature sensitivity is a rather seldom phenomenon, which was not studied further. However, this phenotypic resemblance between *zh95* and *lin-13* alleles makes *lin-13* a very likely candidate for the *zh95* allele. So far no further experiments were performed to show that this is really the case. Complementation analysis with previously characterized alleles of *lin-13* would be the approach of choice, as sequencing the cDNA of *lin-13* (6'747bp) would be costly and very time consuming.

lin-13 encodes a protein with various zinc-fingers of the C2H2 type. Meléndez and Greenwald (2000) show that LIN-13 harbours a LIN-35/Rb binding motif, and they hypothesize that this complex is part of the synMuv B branch, which antagonizes the inductive pathway. Interestingly, as the loss-of-function mutations are concerned, Meléndez and Greenwald hypothesize that not these mutations themselves, but rather the process in which LIN-13 is involved seems to be temperature sensitive.

4.3.4 *zh99* is most likely an allele of *let-19/mdt-13*

zh99; gap-1(ga133) animals exhibited a 100% penetrant Pvl, a 64% penetrant Muv (figure 4.10 A) and a 100% penetrant sterility phenotype. It was found that the vulval phenotypes were independent of *gap-1(ga133)*, which rendered this mutant to a lower priority of characterization and mapping within this study. LET-23 localization appeared to be predominantly on the basolateral plasma membrane compartment of the VPCs, indicating that *zh99* affects a negative regulator of the LET-23 pathway (figure 4.10 B). By coincidence it was found that *zh99; gap-1(ga133)* exhibited male tail developmental defects, as the rays were degenerated or missing (figure 4.10 D) and the spicules were missformed (figure 4.10 F) compared to the control animals (figure 4.10 C and E respectively).

FLP-mapping showed a clear linkage to chromosome II (figure 4.11 A) but did not reveal enough information to determine a subchromosomal region of good confidence. Therefore, deficiencies were used to confirm this region and to increase the resolution of mapping. Sigurdson et al. (1984) established and characterized a plethora of deficiencies on chromosome II. The smallest deficiency used (mnDf80) harbours 59 genes from which *let-19* was found as a candidate by literature search. *let-19* encodes a subunit of the Mediator complex, which is known to regulate transcription of target genes by influencing the activity of the RNA polymerase (Kornberg 2005). Clayton et al. (2008) showed that LET-19 is

important for cell-cycle arrest of the VPCs prior to induction. Removing *let-19* activity resulted in 2.3±0.9 extra VPC divisions per animal on average. Furthermore, Yoda et al. (2005) found that the *let-19(mn19)* allele showed fusion defects of Pn.p cells, that usually fuse to the hypodermal syncitium hyp7. As indicated in chapter 4.2.6, *zh99* worms showed an increased number of posterior Pn.p cells. In one animal even P9.p was induced, leading to the conclusion that the fusion of the posterior Pn.p cells was disturbed. Considering the similarity of the defects described for *let-19* alleles and *zh99*, a complementation assay was performed, which showed that *zh99* most likely represents an allele of *let-19*. Since *zh99* was not a mutant of high priority, the time consuming and costly sequencing of the *let-19* cDNA (8'589bp) was not considered.

Given the facts collected by Yoda et al. (2005) and Clayton et al. (2008), LET-19 controls the cell-cycle arrest of the VPCs and the fusion of all Pn.p cells to hyp7, rather than inhibiting the LET-23 pathway directly. The model is that unfused Pn.p cells stay competent to receive and process the inductive signal originating from the AC. *gap-1(lf)* thus renders unfused VPCs sensitive to be induced by the AC.

4.3.5 *zh78* might be an allele of *lin-1*

zh78 was found to exhibit a strong Muv phenotype, which was independent of *gap-1(ga133)* (figure 4.12 A). Therefore, *zh78* was a mutation with a relatively low priority for characterization and mapping. LET-23 localization was assessed by immunostaining and found to be predominantly basolateral in the VPCs, indicating that the affected gene might encode a negative regulator of the LET-23 pathway.

FLP-mapping placed *zh78* on the left arm of chromosome IV to a region harbouring 517 predicted genes (figure 4.12 A and B). No further mapping experiments were performed because of the low priority of *zh78* and time restrictions. However, the previously characterized negative regulator of vulval induction *lin-1* was found in the interval mentioned above. Since *lin-1* loss-of-function alleles show a very strong Muv phenotype independently of *gap-1(lf)* it is possible that *zh78* represents an allele of *lin-1*. Complementation crosses with the *lin-1(n304)* allele failed most probably because the animals were very sick. Sequencing the coding regions of *lin-1* (except exon 5) in *zh78* animals did not reveal any mutations. In order to map *zh78*, it might be useful to repeat the complementation analysis with *lin-1(n304)*, since among the 517 genes no other obvious candidate genes are found. Assuming that *zh78* is not an allele of *lin-1*, it would be worth to continue the mapping of this mutant, as it seems to be an important negative regulator of vulval development.

However, it is very unlikely that *zh78* defines an uncharacterized inhibitory gene, as most negative regulators exhibiting a phenotype as single mutants have probably already been found. We assume that new regulators of vulva development might only be found by screening in sensitized backgrounds for a synthetic phenotype.

4.3.6 Concluding remarks

In this chapter, a forward genetic screen for synthetic Multivulva animals in a *gap-1(ga133)* background was presented. Six mutant strains were isolated, characterized and mapped. The novel alleles *lin-2(zh96)* and *lin-7(zh98)* showed apically mislocalized LET-23 in the VPCs and validated the concept of the forward genetic screen in a *gap-1(lf)* background.

Additionally, the novel allele *gap-3(zh94)* was isolated, which supported the previous findings of A. Stetak with the *gap-3(ga139)* allele. GAP-3 was found to be a negative regulator of LET-60 mediated processes, redundantly with GAP-1 and GAP-2 (Stetak et al., 2008).

The mutant *zh95* exhibited a temperature sensitive synthetic Muv phenotype with *gap-1(ga133)*. Similar findings by Meléndez and Greenwald (2000) highly suggest *lin-13* as a candidate for *zh95*. Complementation analysis has to be performed to confirm this notion.

zh99 was found to exhibit a Muv phenotype independently of *gap-1(ga133)*. Hence, the characterization of this mutant had a lower priority within this study. *let-19* is a very likely candidate for the *zh99* mutation, as *let-19(os33)* failed to complement *zh99*. However, the sequencing of the *let-19* locus was not performed, mainly because of time restrictions.

Another mutant, which showed a Muv phenotype independent of *gap-1(ga133),* was *zh78*. The FLP-mapping approach was not exploited to full extend. However, the mapping experiments position *zh78* on the left arm of chromosome IV. A prominent negative regulator in this region is *lin-1*. Unfortunately, the complementation crosses failed and have to be repeated.

In total, progeny of 1400 F1 animals (figure 4.2) were screened for a Muv phenotype. All mutants mapped represent previously characterized regulators of the inductive pathway (*zh96, zh98* and *zh94*) or genes involved in the regulation of the Pn.p cell fusion to hyp7 (*zh99*). It is clear that this screen was not saturated for various reasons: first, other known genetic interactors of *gap-1* such as *lin-10* (Hajnal et al. 1997) and *puf-8* (Walser et al. 2006), were not picked up in this screen. Second, the novel mutants of *lin-2, lin-7* and *gap-3* discovered in this screen were only single hits. Third, a preliminary genome-wide RNAi screen in *a gap-1(ga133)* background indicated the existence of many more genetic interactors of *gap-1* (See

chapter 5). Therefore, it is very likely that *gap-1(lf)* as a sensitized background in genetic screens has not been exploited to full extent yet.

4.4 Methods

4.4.1 Mutagenesis procedure for the forward genetic screen

EMS (ethyl methane sulfonate) is an alkylating agent, which can induce point mutations or small deletions in DNA molecules. *gap-1(ga133)* worms were grown on ten 6cm petri dishes and bleached as soon as many adults were gravid. Synchronized eggs were transferred on NGM plates without food and let hatch o/n at 20°C. On the next day, the L1 larvae were transferred to NGM plates with OP50 bacteria and incubated for 2 days at 20°C. Animals were collected at the L4 stage with sterile M9 (figure 4.2, P0 generation). Worms were washed three times using sterile M9 and the final volume of the suspension was set to 2ml. Spinning steps were always performed at 1'000rpm for 2 minutes. In parallel, a 100mM EMS solution in 2ml sterile M9 was generated. After dissolving the viscous EMS in the M9 buffer, the solution was transferred to the worm suspension. Worms in EMS solution were incubated for 4 hours at room temperature while rocking. After mutagenesis, the worms were washed at least 3 times with sterile M9 to remove remaining EMS. The final volume was set to 1ml and the worm suspension was distributed on 10 NGM plates with OP50 and kept overnight (at least 12 hours) at 20°C.

4.4.2 Organization of mutagenized worms and screening

100 mutagenized P0 animals were distributed on 10 NGM plates with OP50 (10 worms per plate) and kept for 3 days at 20°C until the F1 progeny reached the L4 stage (figure 4.2, F1 generation). In each mutagenesis round, 200-500 F1 animals were singled out on NGM plates with OP50 and subsequently incubated for 5 to 7 days at 20°C. The F2 generation (figure 4.2) was screened for animals with a Muv phenotype. Once a positive plate was determined, the strain was maintained by picking 12 wild-type looking worms, which were either +/+ or mutant/+. Muv animals that were fertile were maintained homozygous and sick animals were maintained heterozygous. In total, the progeny of 1400 F1 plates were analyzed.

4.4.3 Automated FLP mapping

An automated high-throughput mapping method based on fragment length polymorphisms (FLPs) was established at the University of Zurich (Zipperlen et al. 2005). This approach uses sequence polymorphisms called InDels (small insertions or deletions), which appear to be unique for certain wild-type isolates of *C. elegans*. The laboratory wild-type background originates from a Bristol isolate (N2). For this mapping approach we use additionally the

Hawaii isolate (CB4856). Zipperlen et al. (2005) established PCR assays, which can differentiate between Bristol and Hawaii DNA at specific loci along all the 6 chromosomes of *C. elegans* (figure 4.13 A). Physical and genetic positions of the FLP-assays can be found in Zipperlen et al. (2005).

Mutant hermaphrodites, generated in a Bristol background, were crossed with Hawaii males, and wild-type F1 cross-progeny were isolated. Self-progeny exhibiting the mutant phenotype were lysed for genotyping. Different classes of recombinants can be recovered from these crosses as indicated in figure 4.13 B. The loci that were positive for Hawaii DNA are therefore excluded as a putative region for the corresponding mutation. Tier1 experiments determine the chromosomal linkage by analyzing 16 recombinant lysates with 2 FLP-assays per chromosome. The assay with the highest percentage of Bristol DNA would therefore indicate the chromosome on which the mutation was generated. Tier2 experiments determine the sub-chromosomal region by analyzing at least 48 recombinant lysates with 8 FLP-assays of choice. Depending on the mutant that was being mapped, variable amounts of recombinants were generated and analyzed.

This study deals with Muv phenotypes that are synthetically generated when combined with the *gap-1(ga133)* mutation. In order to increase the frequency of recombinants exhibiting a Muv phenotype, a modified mapping strain was used by crossing *gap-1(ga133)* into the Hawaii strain in 6 subsequent rounds. This Hawaii; *gap-1(ga133)* strain was found to work for the mapping of *zh78*, *zh96* and *zh98*, but could not be used for the left arm of chromosome I due to residual Bristol DNA in this region.

4.4.4 Manual SNP-mapping

Single nucleotide polymorphisms were used during the mapping process of *zh95*. The SNPs were chosen from www.wormbase.org and correspondent PCR assays were established to amplify and sequence the loci. The SNPs used to map *zh95* on chromosome III and the corresponding primers are listed below.

SNP	Genetic position	Primers
pkP3048	-0.58 cM	OPG273 TCTTACAAAGCTAACGTGTAACGC OPG274 GATATAGGAACGTGGAAACTTACG
CE3-166	-0.57 cM	OPG271 CGGTTCCGAATTTCAATTGGATCG OPG272 AGTAAGAGGAGTCACCATCAATCG
uCE3-1047	-0.48 cM	OPG269 TTCGCTAAATCCTACGGGGCACCG OPG270 TCCATTCGAAATCCTTCACCAGCC
snp_C14B9	-0.38 cM	OPG267 GTTAGTATGCTGACCACCACTACG OPG268 TGACAGATGAAACGTTGCATATGC
snp_C50C3	-0.37 cM	OPG265 ATCGACAACATCAGAATGGCTTCG OPG266 ACATCAAGCATACCGAATGCGTCG
snp_F09G8	-0.35 cM	OPG263 TCTTGCTTCATTACCAGGATCAGC OPG264 AGACTGACTGACAATCATTGGTGC
CE3-171	-0.27 cM	OPG261 GTAAGCTTCAAGCATTCCAGCGGC OPG262 TTTGCAGCTCACCAACGAGGATGC
oxP1	-0.26 cM	OPG259 ACCTTTTGGAACTTCAATCCGACG OPG260 TTGTGCTGTAGAAGTCGTTGGTCG

4.4.5 Alleles

LGI: *gap-3(ga139)*

LGII: *let-19(os33), lin-7(e1413)*

LGIII: *dpy-17(e164), unc-69(e587), rfp-1(ok572)*

LGIV: *lin-1(n304)*

LGX: *gap-1(ga133), lin-2(n105)*

Rearrangements: *hT2[bli-4(e937) let-?(q782) qIs48]* (I;III)

mIn1[mIs14 dpy-10(e128)] (II)

4.4.6 Whole-mount immunostaining

See chapter 3.5.5

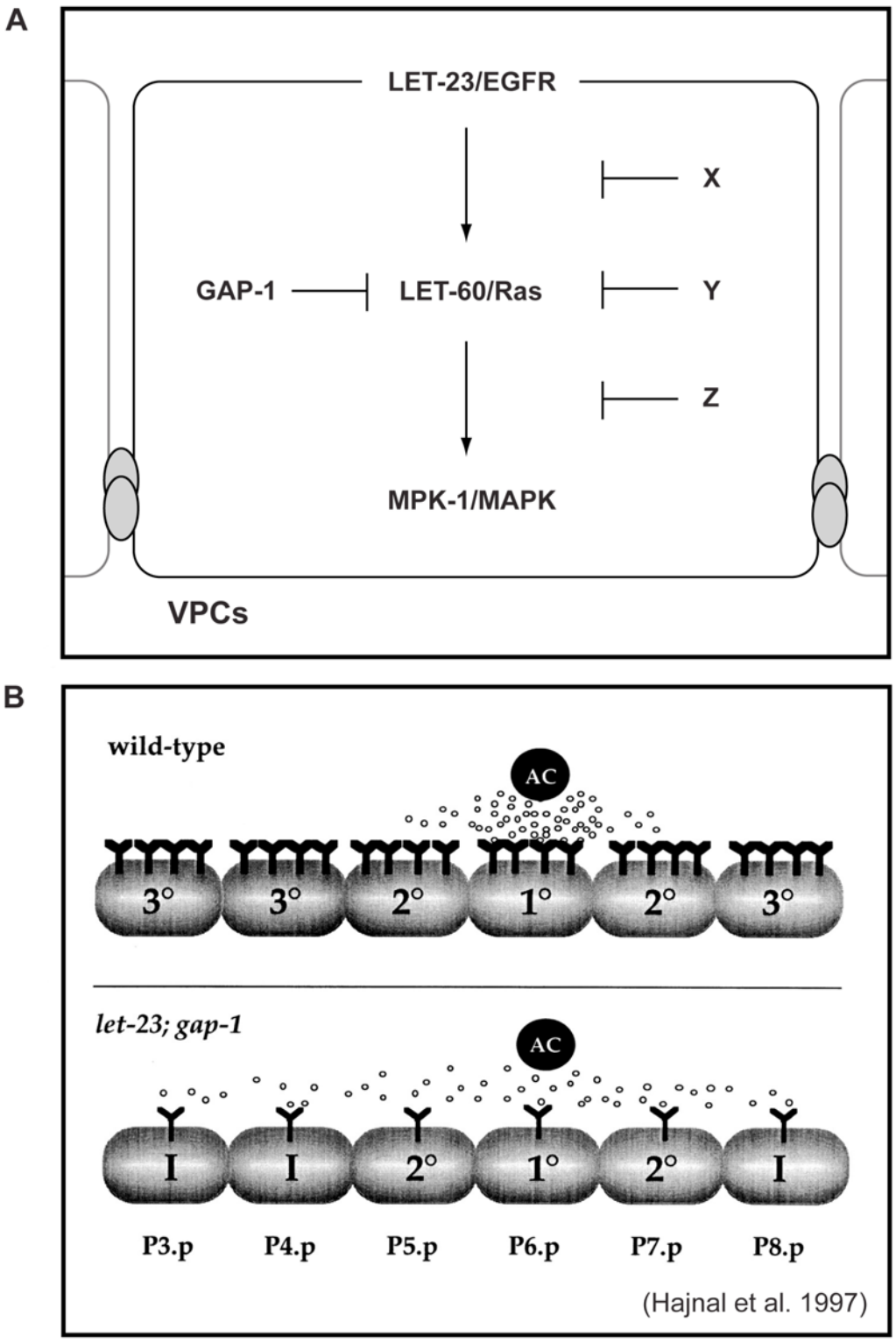

Fig. 4.1: Rationale of the forward genetic screen in a *gap-1(lf)* background.
A) *gap-1(lf)* animals have increased LET-60/Ras signalling but exhibit a wild-type phenotype. The combination with a reduction-of-function mutant of a hypothetical negative regultor (e.g. X,Y or Z) can elevate the inductive singalling and overcome the threshold to induce a Multivulva phenotype (Hajnal et al. 1997, Yoo et al.2004).
B) Mutants, which (partially) mislocalize LET-23/EGFR (Y-shaped sructures in the scheme) in the VPCs exhibit a Vulvaless phenotype. The combination of those mutants with *gap-1(lf)* can lead to a Multivulva phenotype. Since LET-23/EGFR of P6.p does not sequester most of the LIN-3/EGF ligand in this situation, LET-23/EGFR on distal VPCs can be activated. Additional loss of LET-60/Ras ihibition by *gap-1(lf)* alleles may lead to ectopic inductions and hence to a Multivulva phenotype (Hajnal et al. 1997).

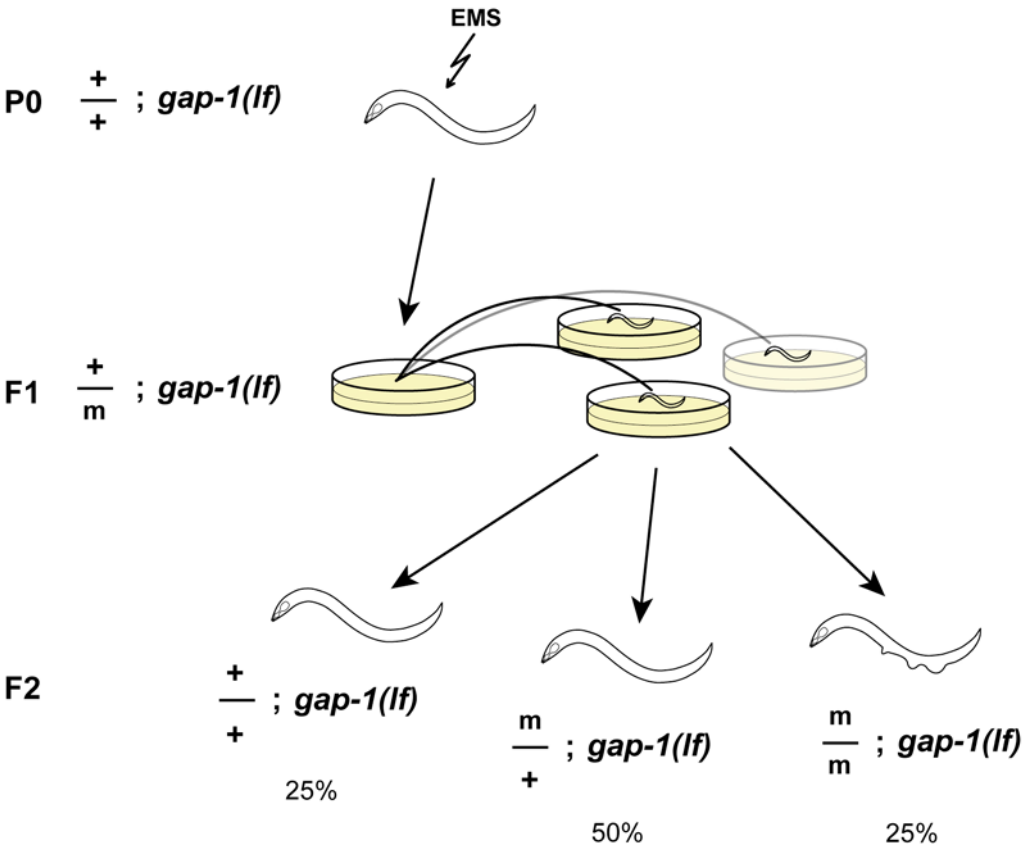

Fig. 4.2: Schematic representation of the forward genetic screening procedure. *gap-1(ga133)* worms were synchronized and mutagenized at the L4 stage (P0 generation). Self progeny, which are heterozygous for any mutation, were singled out (F1 generation). The next generation (F2) was screened for animals with a Multi-vulva phenotype. The highest expected penetrance for a Muv phenotype caused by a recessive mutation was 25% and the rest of the population was expected to exhibit a wild-type phenotype (50% would be mutant/+ and 25%.+/+). Scheme provided by Raphael Sacher.

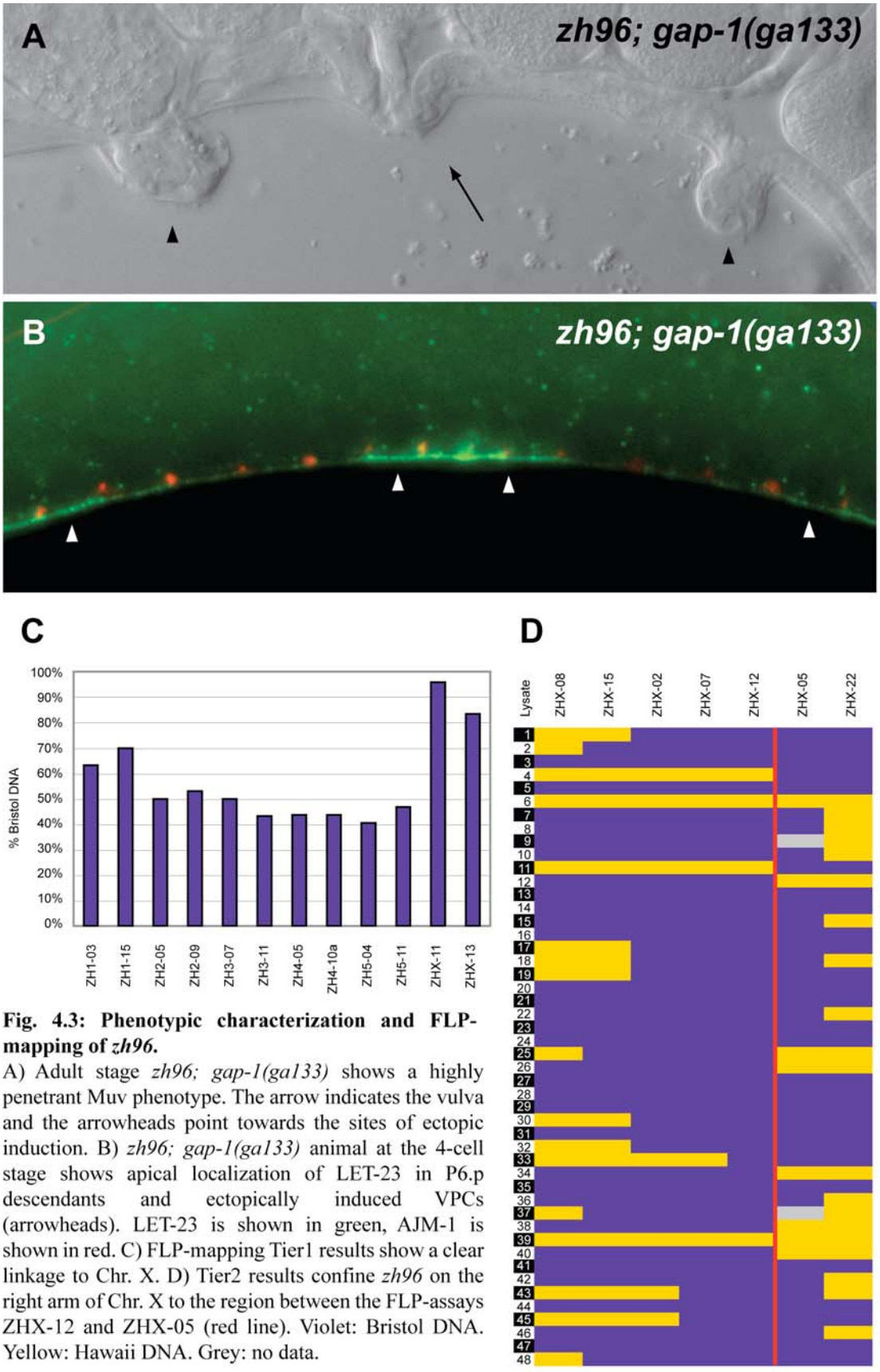

Fig. 4.3: Phenotypic characterization and FLP-mapping of *zh96*.

A) Adult stage *zh96; gap-1(ga133)* shows a highly penetrant Muv phenotype. The arrow indicates the vulva and the arrowheads point towards the sites of ectopic induction. B) *zh96; gap-1(ga133)* animal at the 4-cell stage shows apical localization of LET-23 in P6.p descendants and ectopically induced VPCs (arrowheads). LET-23 is shown in green, AJM-1 is shown in red. C) FLP-mapping Tier1 results show a clear linkage to Chr. X. D) Tier2 results confine *zh96* on the right arm of Chr. X to the region between the FLP-assays ZHX-12 and ZHX-05 (red line). Violet: Bristol DNA. Yellow: Hawaii DNA. Grey: no data.

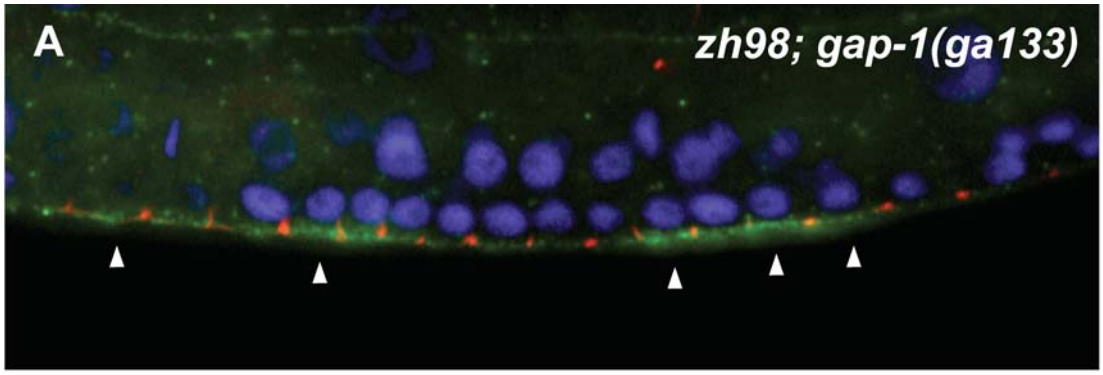

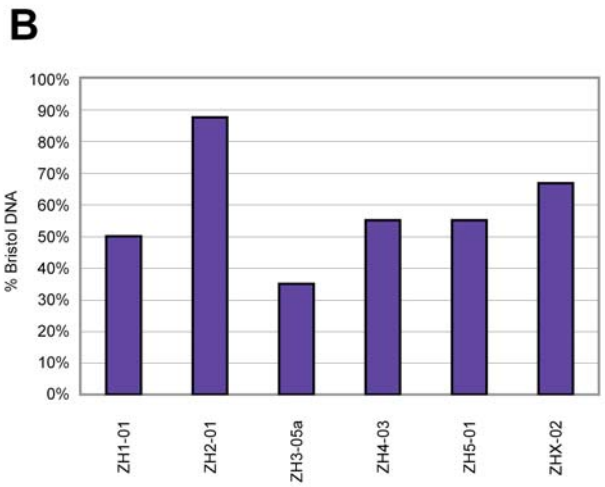

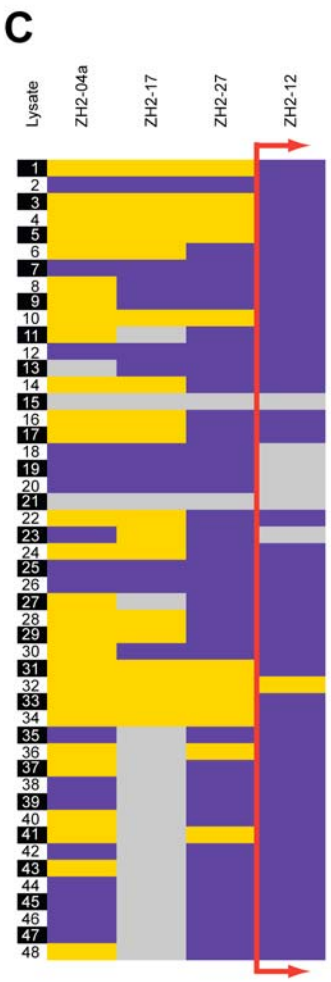

Fig. 4.4: Phenotypic characterization and FLP-mapping of *zh98*.
A) *zh98; gap-1(ga133)* animal at the 4-cell stage shows apical expression of LET-23 in the vulval cells, as indicated by the arrowheads. LET-23 is shown in green, AJM-1 is shown in red and DNA is shown in blue. B) FLP-mapping Tier1 results show a clear linkage to Chr. II. C) Tier2 results confine *zh98* on the very distal part of the right arm of Chr. II (between the red line and the right end of Chr. II). Violet: Bristol DNA. Yellow: Hawaii DNA. Grey: no data.

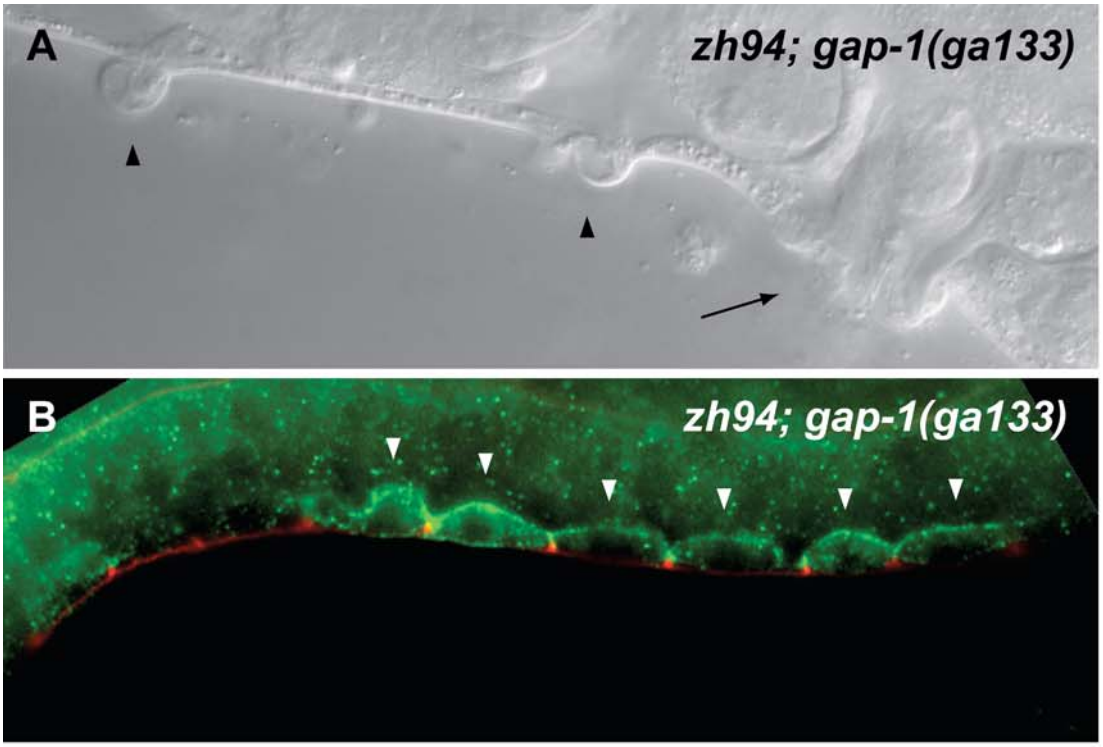

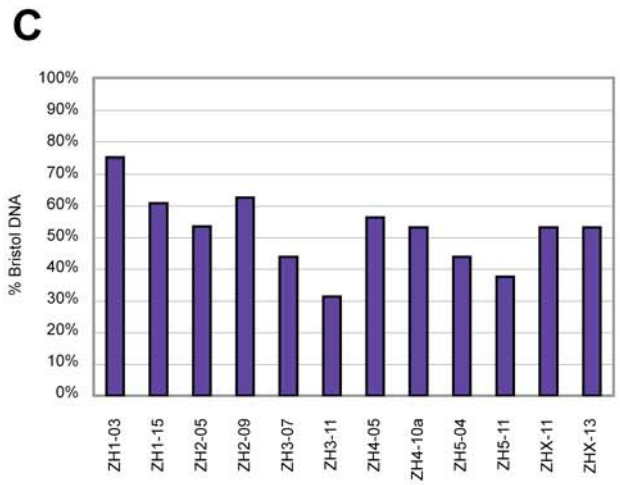

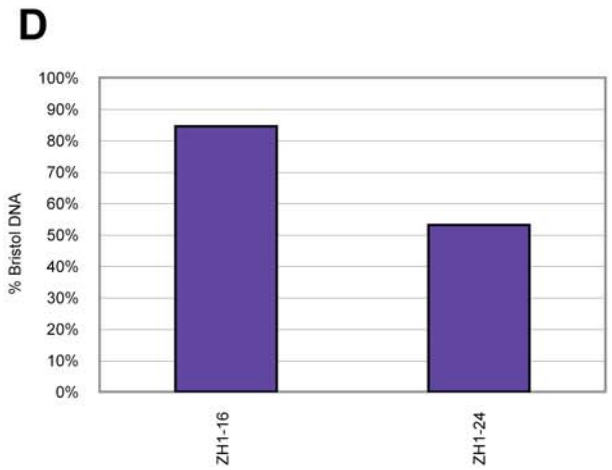

Fig. 4.5: Phenotypic characterization and FLP-mapping of *zh94*.
A) Adult stage *zh94; gap-1(ga133)* shows a Muv phenotype. The arrow indicates the everted vulva and the arrowheads point towards the sites of ectopic induction. B) *zh94; gap-1(ga133)* animal at the 2-cell stage shows predominant basolateral expression of LET-23 in the vulval cells, as indicated by the arrowheads. C) FLP-mapping Tier1 results show a probable linkage to Chr. I. D) Tier1 experiments with 2 different FLP-assays located on the distal arms of Chr. I show a clear linkage to the left arm.

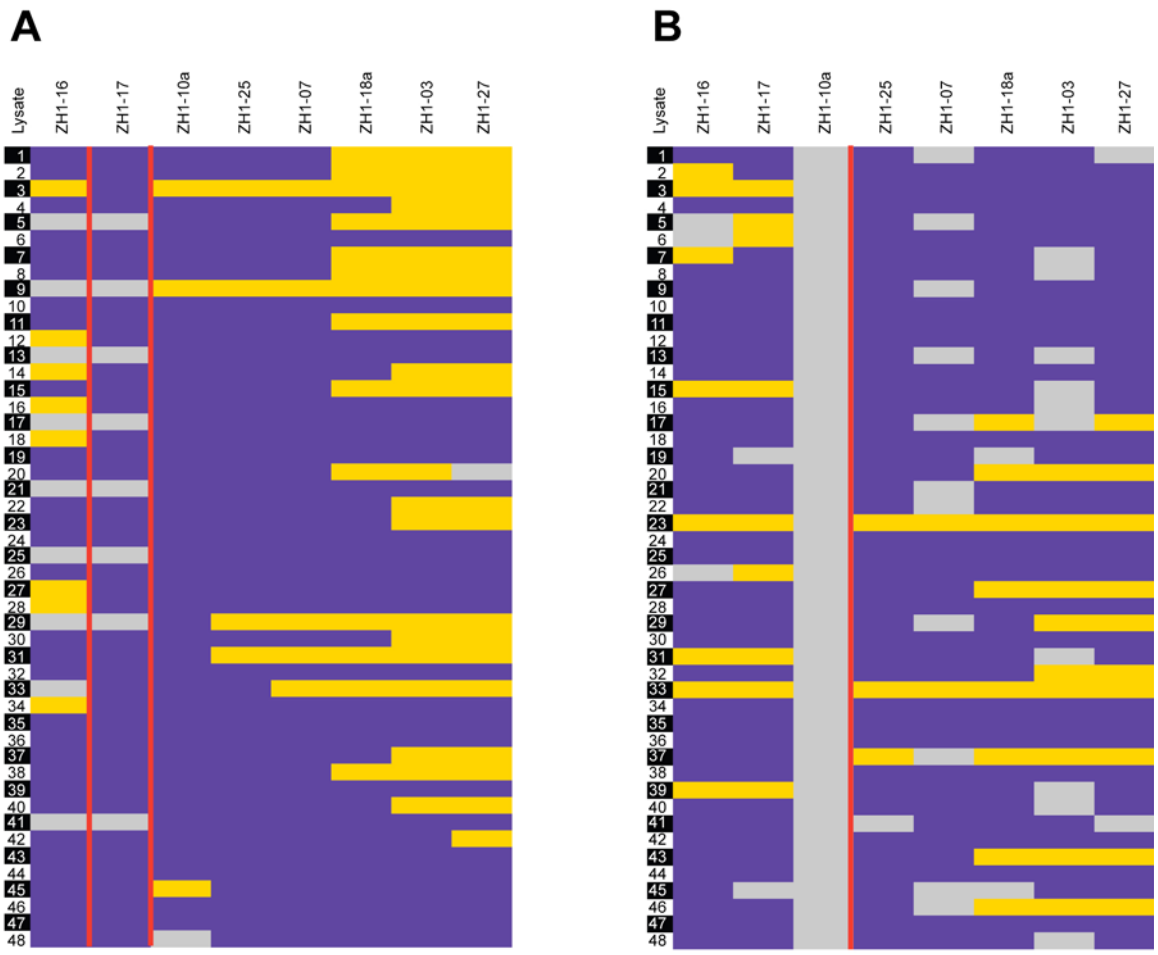

Fig. 4.6: Tier2 FLP-mapping of *zh94*

A) Crosses for mapping performed with Hawaii; *gap-1(ga133)* confine the region of zh94 on the left arm of Chr. I between the FLP-assays ZH1-16 and ZH1-10a (between the red lines). B) Crosses for mapping performed with Hawaii only are more accurate, as the region for *zh94* is confined between the FLP-assays ZH1-10a and ZH1-25. Violet: Bristol DNA. Yellow: Hawaii DNA. Grey: no data.

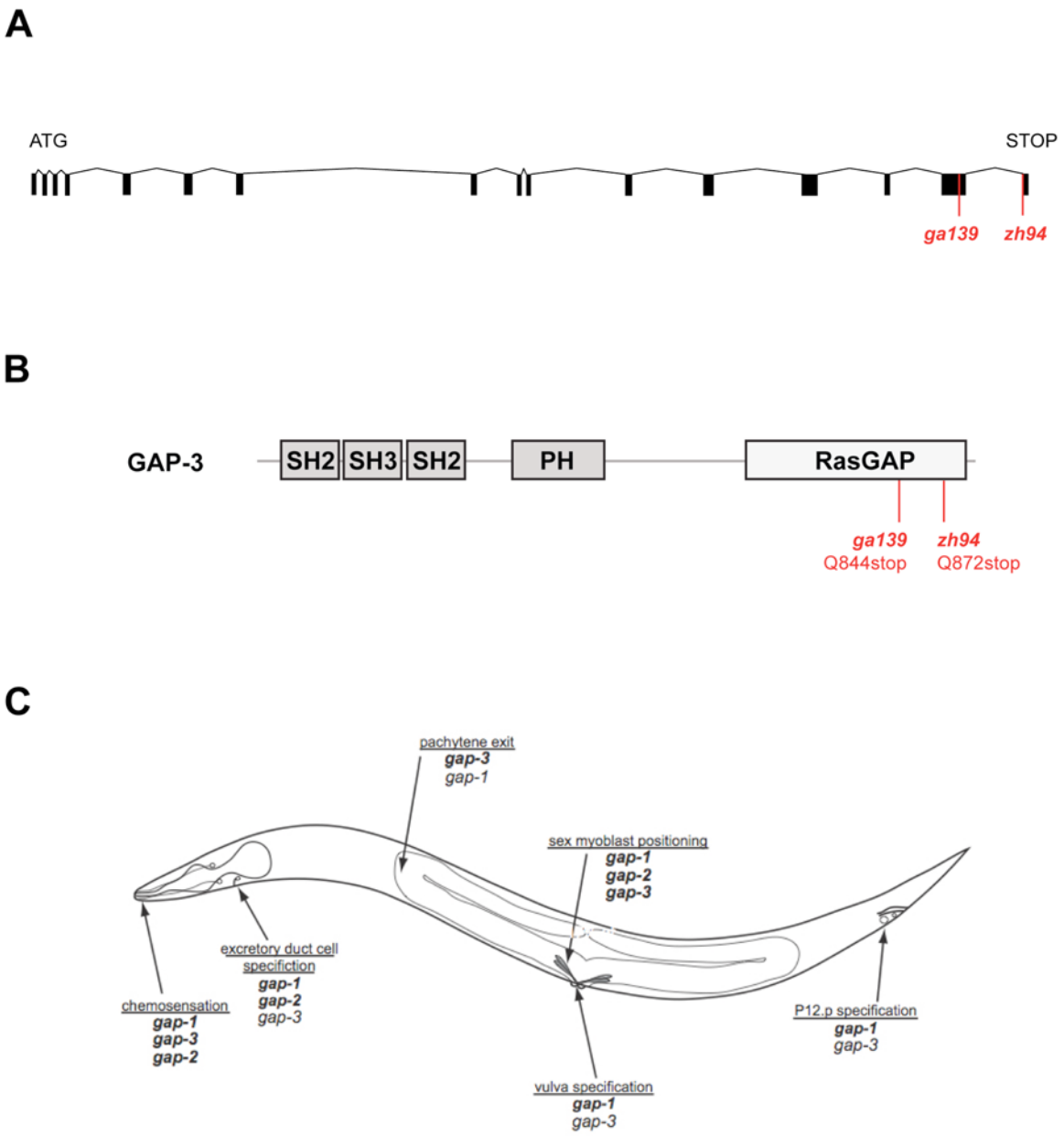

Fig. 4.7: *zh94* is a novel allele of *gap-3*
A) Gene model of *gap-3*. The two mutant alleles *ga139* and *zh94* are indicated in red. B) Protein domains of GAP-3. The N-terminal SH3-domain is flanked by two SH2-domains. A PH-domain is predicted in the center part of GAP-3. Both alleles, *ga139* and *zh94*, are affecting the C-terminal RasGAP domain and encode a premature STOP codon instead of a glutamine (Q). SH = Src-Homology. PH = Pleckstrin Homology. RasGAP = Ras GTPase Activating Protein. C.) Tissue specificity of the redundant RasGAPs *gap-1*, *gap-2* and *gap-3*. The GAPs with a high level of contribution are shown in bold (Stetak et al. 2008).

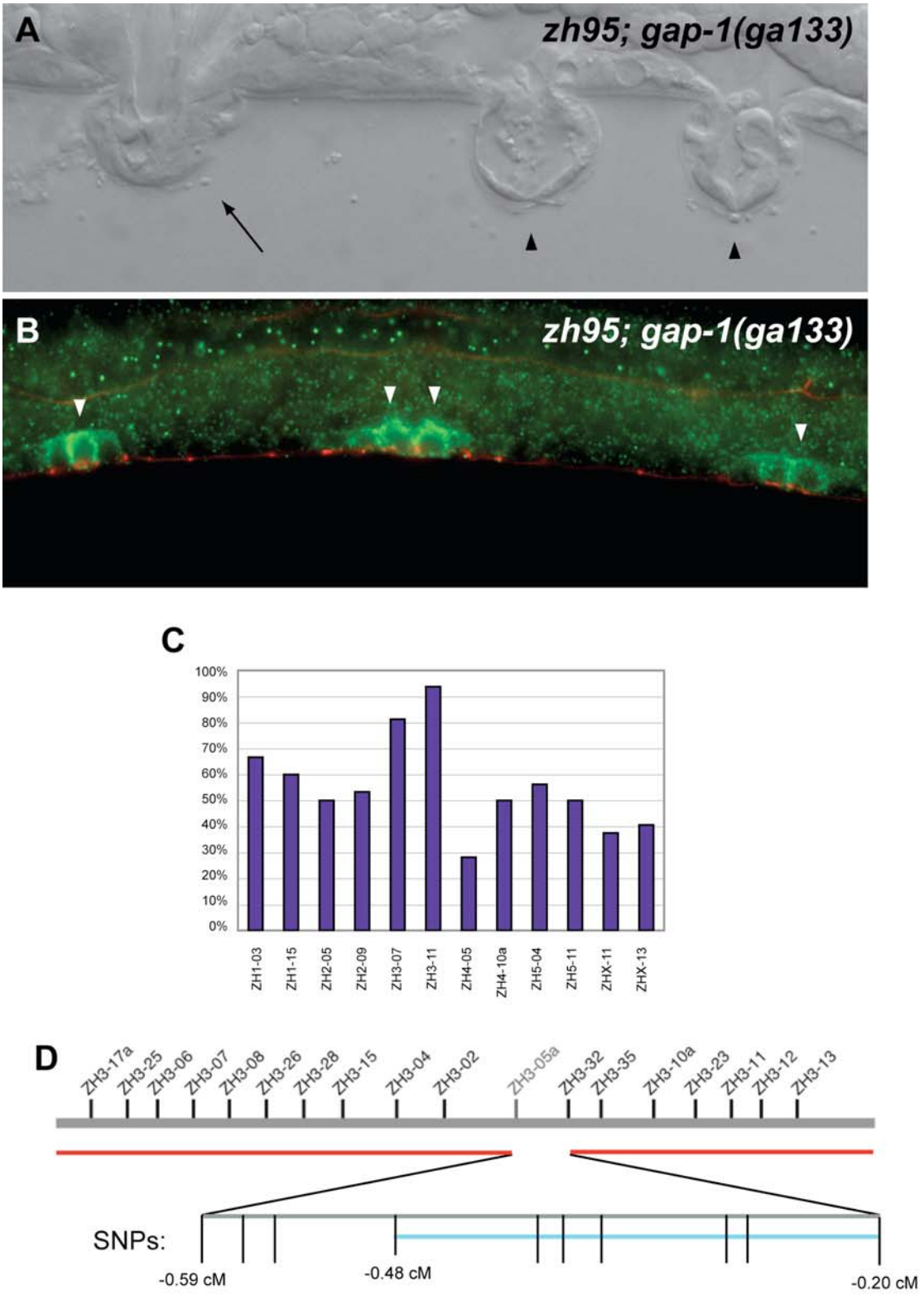

Fig. 4.8: Phenotypic characterization and FLP-mapping of *zh95*.
A) Adult stage *zh95; gap-1(ga133)* shows a highly penetrant Muv phenotype. The arrow indicates the everted vulva and the arrowheads point towards the sites of ectopic induction. B) *zh95; gap-1(ga133)* animal at the 4-cell stage shows predominant basolateral expression of LET-23 in in the vulval cells, as indicated by the arrowheads. LET-23 is shown in green and AJM-1 is shown in red. C) FLP-mapping Tier1 results show a clear linkage to Chr. III. D) Tier2 FLP mapping results confine *zh95* to the region between the FLP-assays ZH3-05a and ZH3-32 (red lines). Finemapping with SNPs (Single Nucleotide Polymorphisms) is indicated below. One recombinant lysate showed Hawaii DNA until the SNP at position -0.48cM (blue line). Scheme of Chr. III adapted from Zipperlen et al. (2005).

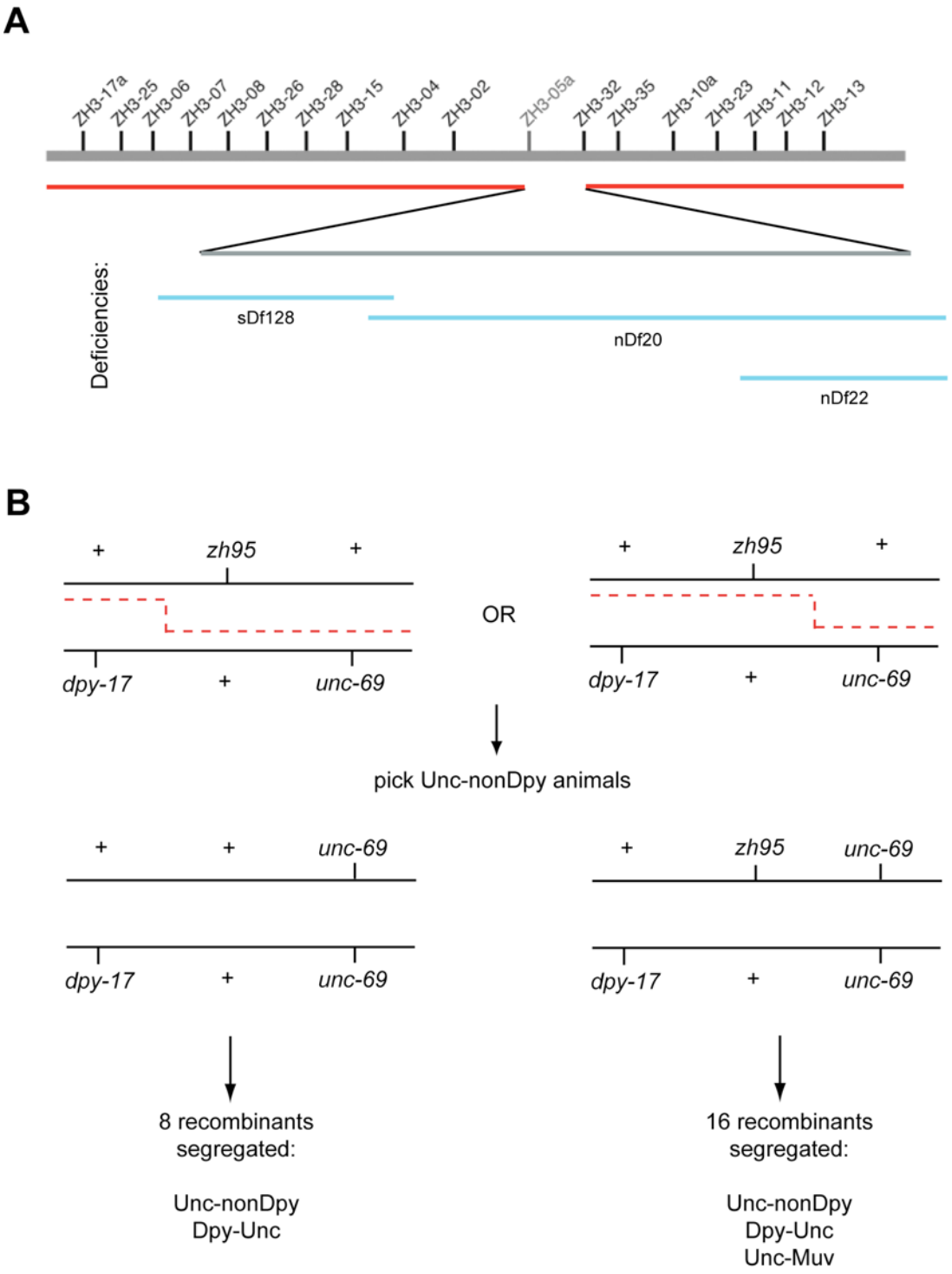

Fig. 4.9: Deficiency- and three-factor-mapping of *zh95*.
A) Deficiency mapping of *zh95*. Deficiencies sDf128, nDf20 and nDf22 were placed in *trans* to *zh95* in a *gap-1(ga133)* background. All deficiencies complemented *zh95*. B) Three-factor mapping of *zh95*. Two flanking recessive mutations with obvious phenotypes, *dpy-17(e164)* and *unc-69(e587)*, were put in *trans* to *zh95* in a *gap-1(ga133)* background. The two relevant recombination situations are indicated in red. Depending on if the recombination happens between *dpy-17* and *zh95* or between *zh95* and *unc-69*, different segregation patterns are expected. The ratio between these two recombination situations corresponds to the ratio of the genetical distances between one marker and *zh95* respectively.

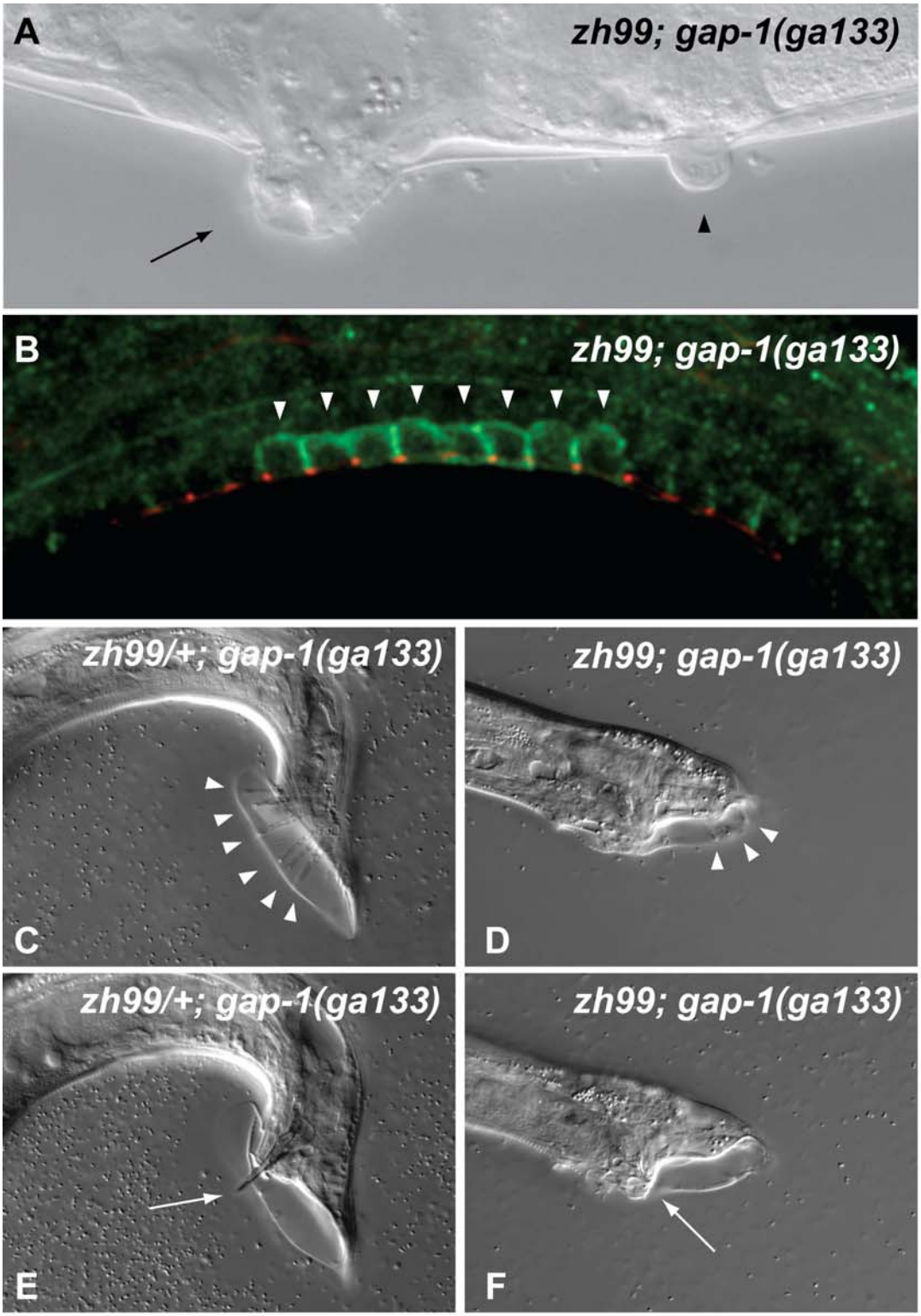

Fig. 4.10: Phenotypic characterization of *zh99; gap-1(ga133)*.
A) Adult stage *zh99; gap-1(ga133)* worms show a 100% penetrant Pvl phenotype (arrow) and a 64% penetrant Muv phenotype (arrowhead). B) *zh99; gap-1(ga133)* animals at the 4-cell stage show predominant basolateral expression of LET-23 in the vulval cells (arrowheads). LET-23 and AJM-1 are shown in green and red, respectively. Figures C-F show male tails of *zh99/+; gap-1(ga133)* (C and E) and *zh99; gap-1(ga133)* (D and F). Compared to the control (C), *zh99; gap-1(ga133)* animals have reduced number and degenerated male rays (D, arrowheads). Also the spicule (arrow) in *zh99; gap-1(ga133)* is degenerated (F) compared to the control (E).

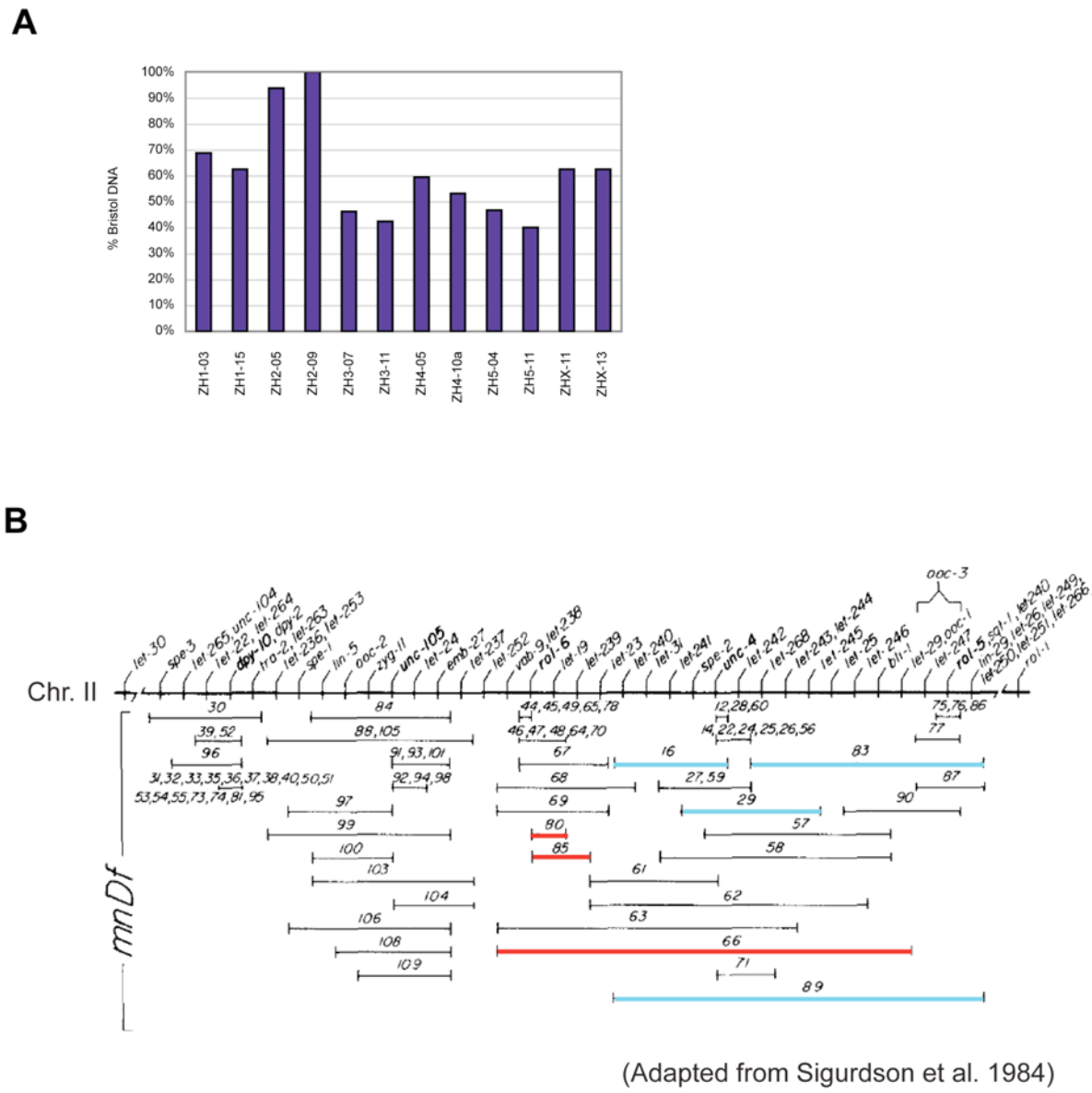

Fig. 4.11: Mapping of *zh99*.
A) FLP-mapping Tier1 results show a clear linkage to Chr. II. The percentage of animals with Bristol DNA is plotted on the y-axis and the different FLP-assays on the x-axis. B) Deficiency mapping of *zh99*. Schematic representation of a part of Chr. II with the available deficiencies and their positions are listed below. Several deficiencies were put in *trans* to *zh99* and assessed for a Pvl and sterility phenotype. mnDf89, mnDf16, mnDf29 and mnDf83 complemented *zh99* (Deficiencies marked with blue). mnDf66, mnDf85 and mnDf80 failed to complement *zh99* and resulted in sterile animals with Pvl (Deficiencies marked with red).

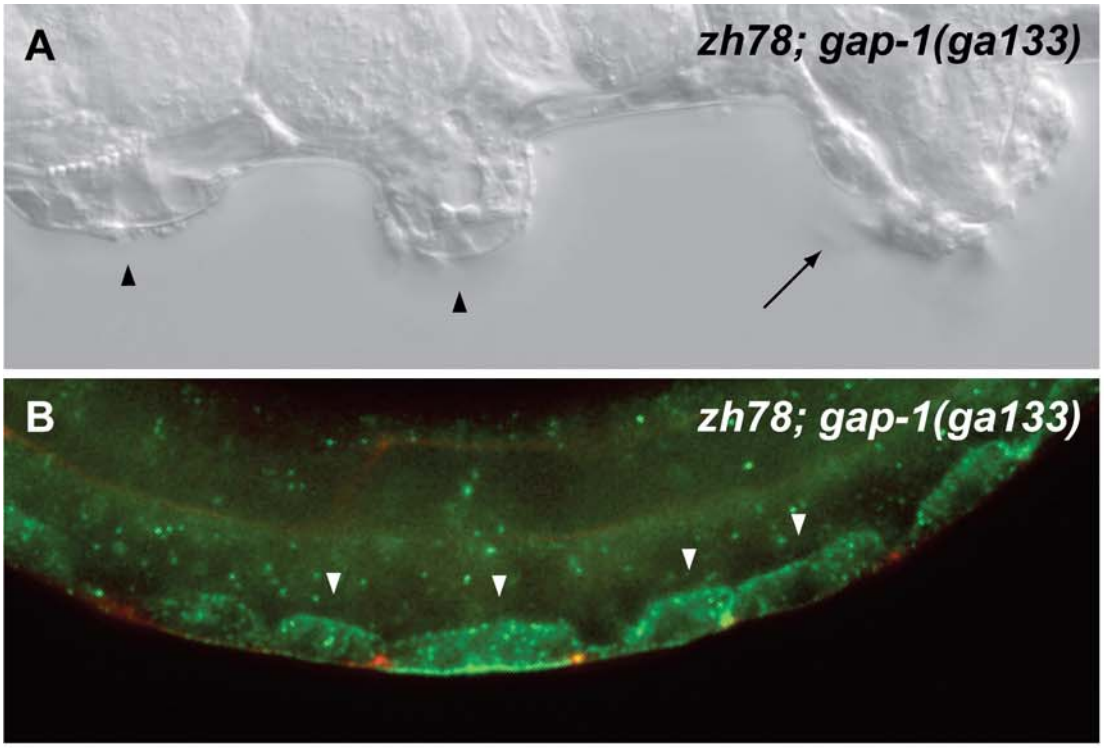

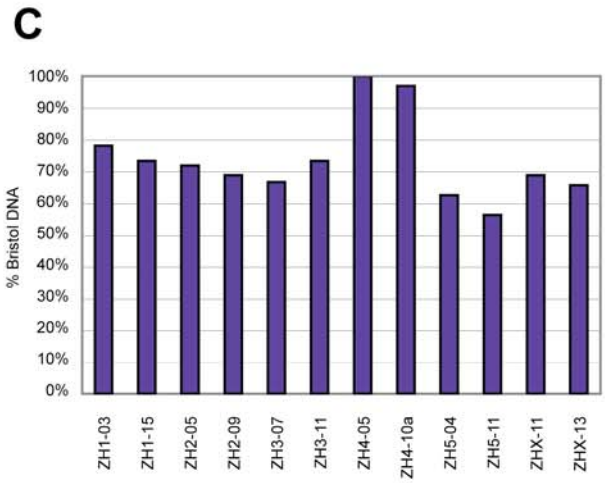

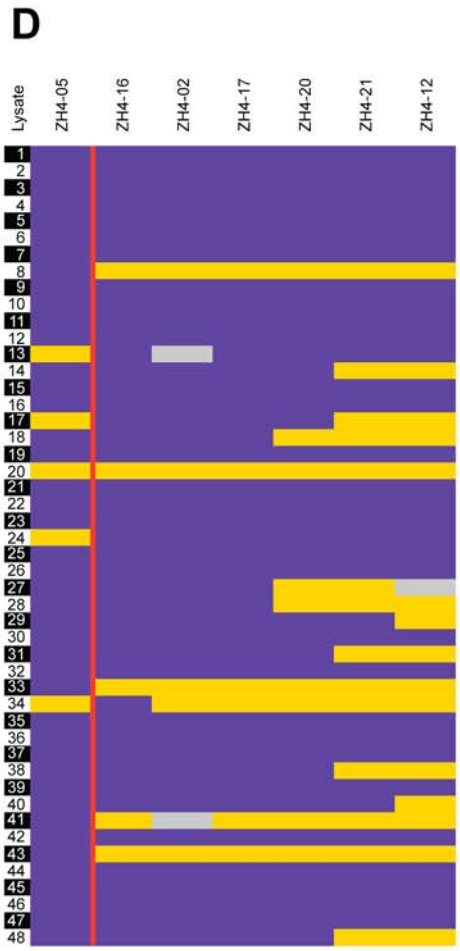

Fig. 4.12: Phenotypic characterization and FLP-mapping of *zh78*.
A) Adult stage *zh78; gap-1(ga133)* shows a highly penetrant Muv phenotype. The arrow indicates the everted vulva and the arrowheads point towards the sites of ectopic induction. B) *zh78; gap-1(ga133)* animal at the 1-cell stage shows predominant basolateral expression of LET-23 in the vulval cells, as indicated by the arrowheads. LET-23 is shown in green and AJM-1 is shown in red. C) FLP-mapping Tier1 results show a clear linkage to Chr. IV. The percentage of animals with Bristol DNA is plotted on the y-axis and the different FLP-assays on the x-axis. D) Tier2 results confine *zh78* to the left arm of Chr. IV to the region between the FLP-assays ZH4-05 and ZH4-16 (red line). Violet: Bristol DNA. Yellow: Hawaii DNA. Grey: no data.

Mutant	Muv dep. on *gap-1(lf)*	Mislocalized LET-23	Fertility	Back - crossed	LG	Candidates	Fails to complement	PM
zh96	yes	yes	fertile	4x	X	*lin-2**	*lin-2(n105)*	yes
zh98	yes	yes	fertile	0x	II	*lin-7**	*lin-7(e1413)*	yes
zh94	yes	no	partial fertile	4x	I	*smo-1** *gsa-1** *dapk-1* Y92H12BR.8 *gap-3**	*gap-3(ga139)*	yes
zh95	yes (20°C) no (25°C)	no	sterile	4x	III	*apc-2** *gsto-1** ZK652.6* *lin-37* *lin-13*	-	-
zh99	no	no	sterile	0x	II	*let-19*	*let-19(os33)*	-
zh78	no	no	partial fertile	4x	IV	*lin-1*†	-	-

Table 4.1: Summary of the phenotypic characterization and mapping of the six isolated mutants.
Characterization of the mutants *zh96*, *zh98*, *zh94*, *zh95*, *zh99* and *zh78* involved assessing the Multivulva phenotyp and its dependence on the *gap-1(ga133)* background, immunostaining of LET-23 and the fertility. The corresponding linkage groups (LG), as well as some of the candidates deduced by either RNAi or literature search are listed. Candidates, whose coding regions have been sequenced are indicated with an asterisk. †*lin-1* coding regions sequenced except exon 5. The alleles used for the complementation crosses are indicated. PM indicates whether a point mutation was found in the coding regions of the correspondent candidate.

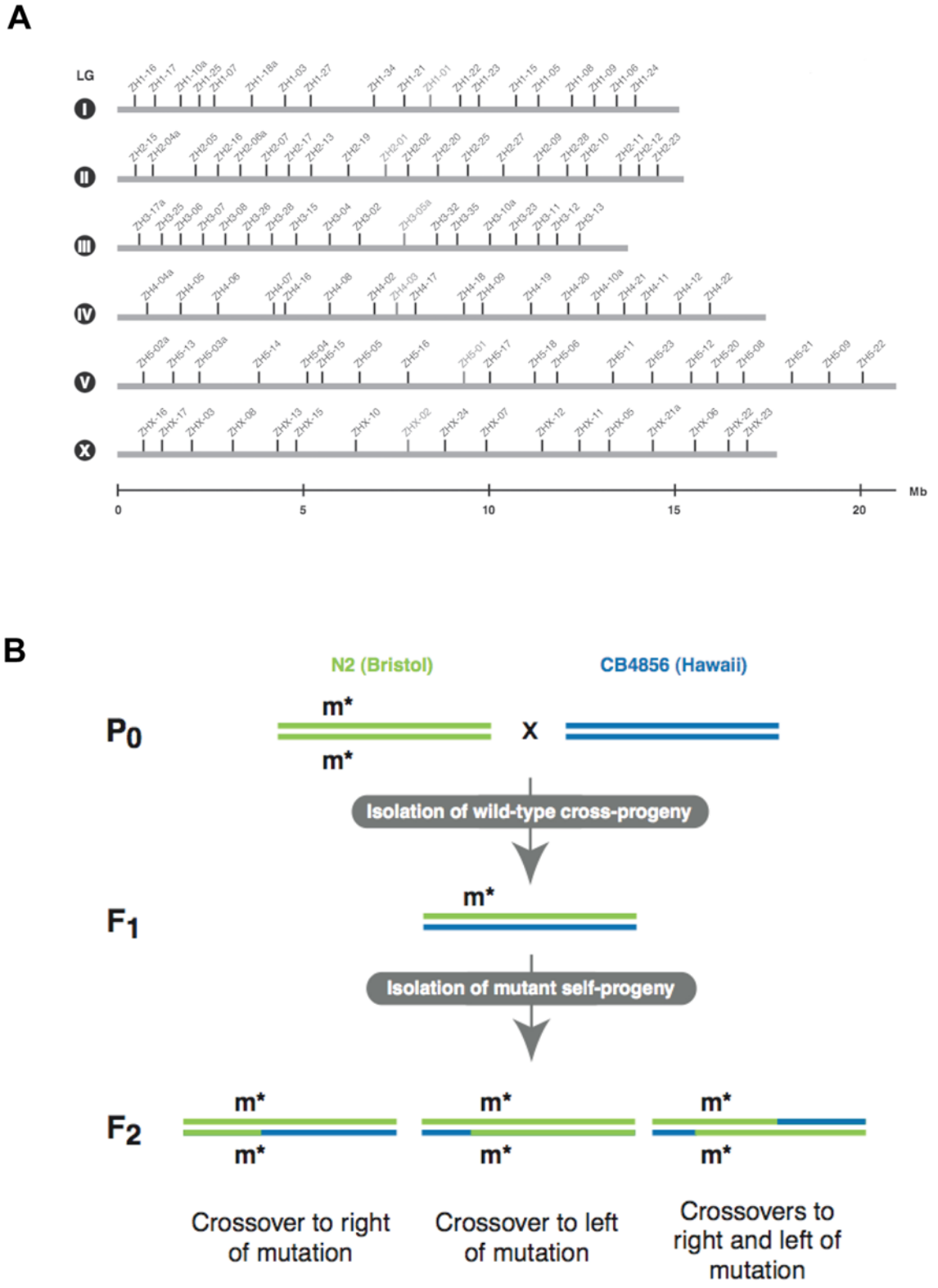

Fig. 4.13: FLP-mapping in *C. elegans* (Zipperlen et al. 2005)
A) Schematic representation of all six *C. elegans* chromosomes and the established FLP-assays to distinguish between Bristol and Hawaii DNA. B.) Simplified crossing scheme to produce Bristol-Hawaii recombinants used to map any mutation "m". Schemes from Zipperlen et al. (2005).

5. Part III: A preliminary genome-wide RNAi screen in a *gap-1(lf)* background

5.1 Introduction

5.1.1 RNAi is a powerful reverse genetics tool

Craig Mello and Andrew Fire discovered RNA interference (RNAi) and established it as a genetic tool in *C. elegans* for *in vivo* gene silencing (Fire et al. 1998). Providing cells with dsRNA of a certain targeted gene initiates its degradation (Fire et al. 1998). They were rewarded with the Nobel Prize in Physiology or Medicine in the year 2006.

The Ahringer laboratory was interested in using RNAi for high-throughput screening and established a large library of 16'757 bacterial clones, each of which possessed a plasmid with a unique sequence targeting in total approximatively 86% of the predicted genes in *C. elegans* (Kamath et al. 2003). This sequence was flanked by the T7 promotor and hence the production of dsRNA of the corresponding sequence was inducible by IPTG. By feeding *C. elegans* with the dsRNA-producing bacteria, the downregulation of the targeted gene can be accomplished (Kamath and Ahringer 2003). The RNAi library made it possible to systematically analyze the function of genes on a genomic level (Kamath et al. 2003). Since then, many different laboratories have been successfully using the Ahringer RNAi library in genome-wide screens (Kamath et al. 2003, Simmer et al. 2003, Poulin et al. 2005, Hamilton et al. 2005). However, RNAi seems not to be completely effective, as some RNAi clones did not show any effect compared to the corresponding mutant phenotypes (Kamath et al. 2003). Sijen et al. (2001) and Simmer et al. (2003) reported that mutations in the gene *rrf-3* render the animals hypersensitive for RNAi, thereby increasing the potential of the technique to analyze gene function.

5.1.2 Rationale of the preliminary genome-wide RNAi screen presented in this study

The RNAi screen presented in this section underlies the same rationale as described in chapter 4.1. The allele *gap-1(ga133)* was used as a sensitized background to screen for Multivulva animals. Downregulation of other attenuators of the EGFR/Ras/MAPK pathway or regulators of LET-23 localization in *gap-1(ga133)* animals can result in the synthetic Muv phenotype (see figure 4.1).

Two lines of interest were followed during this project: first, the RNAi experiments that result in a Muv phenotype would constitute a list of candidate genes, which would aid the mapping process of the mutants isolated in the forward genetic screen presented in chapter 4 of this study. Second, to our knowledge nobody ever performed an RNAi screen on a genome-wide level in a *gap-1(lf)* background. It was therefore of great interest to determine if the forward genetic screens in a *gap-1(lf)* background were saturated or not and to exploit and compare the two different genetic approaches. On the other hand, it is clear that mutagenesis screens can lead to very specific alleles of genes, which might render them constitutivly active or just inactivate a certain domain of a gene product. These kinds of genetic interactions would not be found in an RNAi screen, as the downregulation of the target gene affects the total gene activity. Nevertheless, mutations which totally inactivate a certain essential gene activity cannot be maintained, but might be uncovered in an RNAi approach, where downregulation of some genes might not be fully efficient.

5.2 Results

The RNAi screen presented in this section was performed in collaboration with the Poulin laboratory in Manchester. The resulting candidate lists are called the "Manchester Dataset" henceforth. The Ahringer library clones of chromosomes I, II and III were fed to *rrf-3(pk1426); gap-1(ga133)* animals at the L4 stage and the progeny was screened for a Multivulva phenotype under the dissecting microscope. In total, 8'718 RNAi experiments were performed and screened and the positive experiments were grouped into three classes. "Muv>4" constitutes the high confidence class, as more than four Multivulva (Muv) animals were scored. "Muv2-4" were determined to be the class of middle confidence, as only two to four Muvs were scored per plate. The third class was called "Muv1", which constituted all clones, where only one Muv animal was observed and hence represented the low confidence class.

5.2.1 Thirty-six candidates constitute the high confidence class

From the 8'718 RNAi experiments, thirty-six were part of the "Muv>4" class, which are listed in Table 5.1. This class of positives was of high confidence for various reasons: first, the penetrance of the Muv phenotype was often in a striking range (20% or higher, data not shown). Second, within this list previously characterized genetic interactors of *gap-1* were found. For example, the *puf-8* (Table 5.1, row 22) gene product was shown to regulate the temporal competence of the VPCs (3° cell fusion to hyp7 delayed) and consequently *puf-8(zh17); gap-1(ga133)* animals exhibited a synthetic Muv phenotype (Walser et al. 2006). Downregulation of *fbf-1* and *fbf-2* (Table 5.1, rows 19, 20) was also found to cause a highly penetrant Muv phenotype in a *gap-1(ga133)* background. In contrast, neither *fbf-1(ok91); gap-1(ga133)* nor *fbf-2(q738); gap-1(ga133)* were reported to exhibit a Muv phenotype (Walser et al. 2006). The explanation for the findings in the RNAi screen is that both *fbf-1* and *fbf-2* share over 90% identity on the nucleotide level and RNAi against either gene would downregulate both *fbf*'s. Accordingly, 94% of the *fbf-1(ok91) fbf-2(q704); gap-1(ga133)* triple mutants displayed a Muv phentoype (Walser et al. 2006). The fact that *puf-8*, *fbf-1* and *fbf-2* were identified in the RNAi screen presented in this study, validates the rationale of the screen.

5.2.2 The *rrf-3(pk1426); gap-1(ga133)* background results in many false positives

209 RNAi experiments showed two to four Muvs, and 916 showed one Muv per plate. These findings indicated at first sight that approximatively 10% of the *C. elegans* genes would genetically interact with *gap-1*. This finding is unlikely to be true and hence control experiments were performed. First, 96 RNAi experiments from the screen were repeated twice (96well plate #49 of the Ahringer library). Indeed, most of the positives from the category "Muv2-4" and "Muv1" were not reproducible. Only the positives from the "Muv>4" class were clearly reproducible and hence represent the category of high confidence. It is still possible that some of the RNAi experiments from both "Muv2-4" and "Muv1" categories represent true positives, but since the penetrance is that low (in average 100 worms per plate), repetition experiments would be needed to determine them. Repetition of all positives from the categories of low confidence was not feasible due to time restrictions.

It was hypothesized, that the combination of the *rrf-3(pk1426)* with the *gap-1(ga133)* allele might be the cause of the high frequency of false positives. In order to test this possibility, the double mutant *rrf-3(pk1426); gap-1(ga133)* was scored for Muvs on NGM-plates with OP50 ("RNAi off"). Indeed, scoring 8'674 *rrf-3(pk1426); gap-1(ga133)* animals revealed a very low penetrant Muv phenotype. Of the 8'674 scored animals, two were Muv, two Pvl, two showed general body morphology defects and nine exhibited the "roller" phenotype. This low Muv penetrance might not be a problem if one conducts a few RNAi experiments. However, in a large-scale context as this high-throughput RNAi screen, it can generate a high rate of false positives. Assuming that in average 100 worms are scored in each RNAi experiment, 9'600 animals would be present in 96 experiments. Comparing these numbers to the Muv penetrance of *rrf-3(pk1426); gap-1(ga133)* makes it clear that roughly two to three "Muv1" observations are possible within 100 RNAi experiments. G. Poulin and K. Fisher performed further control experiments, where the *rrf-3(pk1426); gap-1(ga133)* double mutant was tested on either 96 RNAi experiments targeting *gfp* and 96 RNAi experiments targeting *dpy-2* ("RNAi on"). Consistent with our findings from the main screen, eleven and eight experiments were determined to be of the "Muv1" class in the *gfp* and *dpy-2* RNAi respectively. One additional experiment targeting *dpy-2* was of the "Muv2-4" category. Alltogether, these results demonstrate that the *rrf-3(pk1426); gap-1(ga133)* is the likely cause for the high number of false positives in our screen.

5.3 Discussion

A preliminary genome-wide RNAi screen for Multivulva animals was performed in the *gap-1(ga133)* background. All clones for targets on chromosomes I, II and III of the Ahringer RNAi library were screened (Kamath et al. 2003). Of the 8'718 RNAi experiments, Thirty-six constitute the high confidence list of positives (Table 5.1). Within these 36 candidates, *puf-8, fbf-1* and *fbf-2* were previously characterized genetic interactors of *gap-1* (Walser et al. 2006). Most of these 36 candidates did show a Muv phenotype dependent on *gap-1(ga133)* in repetition experiments (G. Poulin, personal communication). Furthermore, some of these candidates were downregulated in wild-type animals harbouring the early 1° cell fate marker *egl-17::cfp* (transgene *arIs92*, Yoo et al. 2004). In wild-type worms *egl-17::cfp* is only expressed in the P6.p lineage during early vulval development. In contrast, downregulation of some of the high confidence candidates (Table 5.1) resulted in *egl-17::cfp* expression in the P5.p or P7.p lineages (G. Poulin, personal communication). These findings indicate, that the rationale of the genetic screens in a *gap-1(lf)* background is valid, and that it is possible to find new attenuators of the inductive pathway. However, the positive genetic interactions found with RNAi should be tested with mutants of the corresponding genes.

As stated above, one of the reasons this screen was performed was to generate a candidate list of genetic interactors of *gap-1*, which would serve as a mapping aid for the mutants isolated in the forward genetics screen (chapter 4). The mutants *lin-2(zh96)* (LG X) and *lin-7(zh98)* (LG II) were already mapped before the RNAi screen was performed. In retrospective, the candidate list obtained by the RNAi screen was not of great help to map the remaining mutants, since *let-19* RNAi did not show any effects and the RNAi clones for *gap-3* (LG I) and *lin-13* (LG III) were not present in the Ahringer library. The *zh78* mutation was placed on chromosome IV by FLP-mapping, a chromosome which was not covered in this RNAi screen. So far, it is not clear if some of the 36 candidates encode proteins that are involved in LET-23 localization. Repetitions of these RNAi experiments with subsequent immunostaining of LET-23 or using a LET-23::GFP reporter might answer this question. However, since both RNAi and immunostaining of LET-23 are techniques with variable effectiveness, it is important to construct the corresponding double mutants and analyze those for LET-23 localization.

Once the genetic interaction with *gap-1(lf)* is validated by mutants, one can start to compare the forward (chapter 4) and reverse genetic approach (chapter 5) and test, whether they are biased or not. Confirming some of the positive candidates found by RNAi would indicate that

the forward genetic screens in *gap-(lf)* sensitized backgrounds are not saturated yet, since to our knowledge only *puf-8* of the thirty-six candidates was found in a mutagenesis screen (Walser et al. 2006). From these thirty-six candidates, two are discussed below in more detail.

5.3.1 The candidate gene *cdc-37*

The gene *cdc-37* was among the thirty-six high confidence positives from the RNAi screen (Table 5.1). CDC-37 is the *C. elegans* orthologue of the human co-chaperone of Hsp90. Beers and Kemphues (2006) reported that RNAi of *cdc-37* causes polarity defects in the early embryo, most likely because it affects the localization of the PAR-proteins. The proteins PAR-1 and PAR-2 localize to the posterior cortex of the one-cell embryo and the PAR-3/PAR-6/PKC-3 complex localizes to the anterior cortex (Goldstein and Macara, 2007). These PAR-proteins are involved in the establishment and maintenance of polarity in many different cell types (Goldstein and Macara, 2007). Furthermore, Xu et al. (2001) showed that human ErbB2 associates with Hsp90 and that this interaction is necessary for ErbB2 stability. They suggest that Hsp90 is needed for receptor maturation and function. It is therefore possible that *C. elegans* CDC-37, maybe in concert with a heat shock protein, is involved in LET-23 maturation and trafficking to the basolateral membrane. Hence, I propose CDC-37 as a candidate regulator of LET-23 localization.

5.3.2 The candidate gene F43G9.1

The gene F43G9.1 encodes the alpha subunit of the isocitrate dehydrogenase (IDH). RNAi against F43G9.1 exhibited a reproducible synthetic Multivulva phenotype in a *gap-1(ga133)* background and expression of the 1° cell-fate marker *egl-17::cfp* in the P5.p and P7.p lineage in a wild-type background (G. Poulin, personal communication). These results indicate that the alpha subunit of *C. elegans* IDH represents a novel negative regulator of the inductive pathway. Sara Vassalli, a former Ph.D student from our lab, determined that F43G9.1 is needed for anchor cell invasion into the vulval tissue at the late L3 stage (S. Vassalli, personal communication). This *fos-1* mediated migration event initiates the development of the cellular structures that connect the adult vulva to the uterus (Sherwood et al. 2005, Rimann and Hajnal 2007). RNAi against F43G9.1 in animals harbouring the anchor cell marker *cdh-3::cfp* abrogated the anchor cell invasion into the vulval tissue (S. Vassalli, personal communication). So far, there is no direct molecular link between the cell-fate specifications of the vulval tissue and the AC invasion process.

IDH is an enzyme of the citric acid cycle and catalyzes the oxidative carboxylation of isocitrate to α-ketoglutarate (Parsons et al. 2008). In this reaction, nicotinamide adenine dinucleotide phosphate (NADPH) is generated as a byproduct, which is thought to be involved in the control of oxidative damage (Lee et al. 2002). Unfortunately, there is no mutant available to reproduce the data collected with RNAi. However, it is unclear how a metabolic enzyme might be involved both vulval cell fate specification and anchor cell migration. It is possible but highly speculative that the gene product of F43G9.1 harbours two independent activities, one being the dehydrogenase activity and an additional one with unknown function.

Interestingly, Parsons et al. (2008) reported that the human IDH1 gene was mutated in 12% of analyzed glioblastoma multiforme (GBM) samples (n=149). In all cases, the arginine at position 132 was mutated, which is localized to the isocitrate binding site (Xu et al. 2004). To date it is not clear what consequences result through alterations in the IDH1 gene and the associated role in tumour formation or progression.

5.3.3 Screening the remaining three chromosomes IV, V and X

Because of time restrictions, we screened only the RNAi clones of chromosomes I, II and III and found 36 high confidence candidates. Most of these candidates have not been yet validated with genetic mutants. Nevertheless, preliminary experiments with the cell fate marker *egl-17::cfp* performed by K.Fisher and G. Poulin (personal communication) highly support the rationale of the screen.

The combination of the *rrf-3(pk1426)* and *gap-1(ga133)* was an unfortunate choice, since it is very likely the cause of the high frequency of false positives in the RNAi screen. The very low penetrant Muv phenotype observed in the double mutant indicate that these two genes interact genetically with each other. Therefore, future screens in sensitised backgrounds should be performed without *rrf-3(pk1426)* to avoid the high number of false positives.

The data collected in the genome-wide RNAi screen performed by Kamath et al. (2003) indicated that the different chromosomes harbour unique features. RNAi experiments resulting in postembryonic phenotypes were enriched on chromosome II, whereas clones on chromosome III resulted in more nonviable phenotypes compared to experiments on other chromosomes. Similarly, chromosome V seemed to contain fewer essential genes (Kamath et al. 2003). Taking these observations into account, it would make sense to continue the RNAi screen in a *gap-1(lf)* background on chromosomes IV, V and X. In order to reduce the number

of false positives, it would be advisable to avoid the RNAi hypersensitive background *rrf-3(pk1426)*.

5.4 Methods

5.4.1 RNAi screen setup

The experimental procedure was adapted from Kamath and Ahringer (2003). RNAi plates consisting of NGM agar including 25 μg/ml carbenicillin and 1mM IPTG were poured and dried for 7-10 days at room temperature. RNAi bacterial clones were grown for 6-8 hours at 37°C in LB-miller medium and subsequently spotted on the RNAi plates. Induction of the dsRNA production was performed by incubating the RNAi plates for 24 hours at room temperature. *rrf-3(pk1426); gap-1(ga133)* animals were synchronized with hypochloride solution. L1 larvae were allowed to grow on OP50 until the L4 stage at 20°C for 2 days. Then, the L4 animals were aliquoted onto the RNAi plates and allowed to grow at 22°C for 4 days. Every RNAi plate was screened for Multivulva animals on three subsequent days.

Row	Plate	Well	Sequence name	Public name	Function
1	1	H9	K12C11.4	*dapk-1*	signalling
2	3	B5	K03E5.3	*cdk-2*	cell cycle
3	4	A10	F55C7.7	*unc-73*	signalling
4	4	E12	C43E11.10	*cdc-6*	DNA replication
5	5	E4	C10H11.9	*let-502*	signalling
6	7	E11	T19B4.6	*unc-40*	signalling
7	7	G10	C32F10.5	*hmg-3*	chromatin
8	10	D3	C37A2.4	*cye-1*	cell cycle
9	10	H1	F15C11.1	*sem-4*	signalling
10	11	B1	K10D3.5	(H37N21.1)	signalling
11	14	A7	F43G9.1	-	metabolism
12	15	A9	W06D4.1	*hgo-1*	metabolism
13	15	B5	W10D5.3	*gei-17*	sumo ligase
14	15	H5	F30A10.10	-	ubiquitin processing
15	25	E4	C37A5.10	-	uncharacterized
16	26	C1	Y54E5A.5	-	uncharacterized
17	32	C6	W08F4.8	*cdc-37*	chaperone
18	32	G10	C08G5.6	-	uncharacterized
19	46	C3	H12I13.a	*fbf-1*	translation
20	46	C12	F21H12.5	*fbf-2*	translation
21	47	C7	C56E6.3	-	uncharacterized
22	49	C5	C30G12.7	*puf-8*	translation
23	50	B1	B0495.2	-	signalling
24	50	D4	T05A6.1	*cki-1*	cell cycle
25	52	E4	T01B7.6	-	uncharacterized
26	58	G4	F07A11.6	*din-1*	RNA binding
27	69	F8	R13G10.1	*dpy-27*	chromatin
28	70	B2	E03A3.4	*his-70*	chromatin
29	72	G11	T10F2.3	*ulp-1*	ubiquitin protease
30	74	A2	F54E7.4	*par-3*	signalling
31	75	H4	T26A5.7	*set-1*	chromatin
32	76	D2	K07E12.1	*dig-1*	extra cell matrix
33	81	B4	ZK637.7	*lin-9*	chromatin
34	81	F1	F02A9.6	*glp-1*	signalling
35	86	E1	C18D11.4	*rsp-8*	splicing
36	87	B10	Y49E10.6	*his-72*	chromatin

Table 5.1: List of genes within the „Muv>4“ high confidence category.
In the RNAi screen with the Ahringer clones from chromosome I, II and III, 36 experiments showed more than 4 Muvs per plate. Plate and Well indicate the position of the RNAi clone within the library.

6. General discussion

The aim of this study was to isolate and characterize novel proteins involved in *C. elegans* LET-23 EGFR localization. The predominantly basolateral localization of LET-23 in the VPCs is crucial for correct induction of vulval development (Kaech et al. 1998). In particular, each of the three PDZ proteins LIN-7, LIN-2 and LIN-10 were found to be essential for this process. Loss-of-function mutants of *lin-7*, *lin-2* and *lin-10* show apically mistargeted LET-23 in the VPCs and hence result in a highly penetrant Vulvaless phenotype (Kaech et al. 1998, Withfield et al. 1999). Similar phenotypes were reported for the *let-23(sy1)* mutant, which encodes a LET-23 variant lacking the distal C-terminus (Aroian et al. 1994, Kaech et al. 1998). LIN-7, LIN-2 and LIN-10 interact with each other *in vitro* and the PDZ domain of LIN-7 binds the distal C-terminus of LET-23 (Kaech et al. 1998). These findings lead to the current model of basolateral LET-23 localization in the VPCs, where the tripartite complex consisting of LIN-7, LIN-2 and LIN-10 bind to LET-23 and ensure its correct targeting (Kaech et al. 1998). Despite the fact that LIN-7, LIN-2 and LIN-10 bind each other simultaneously *in vitro* (Kaech et al. 1998), each of these proteins display distinct subcellular localizations within the VPCs. LIN-7::GFP was found to be associated with the apical junctions (Simske et al. 1996). Immunostaing of overexpressed LIN-2 showed basolateral localization (A. Hajnal, personal communication). LIN-10 localized to perinuclear structures in immunostaining experiments (Withfield et al. 1999). These findings raise new questions about the mechanism of LET-23 targeting. So far, no other components were found to be involved in the LET-23 targeting mechanism and it is not clear how proper localization is achieved.

Regulatory processes after LET-23 targeting to the basolateral membrane involve the protein EPS-8, a positive regulator of vulval induction. Stetak et al. (2006) showed that EPS-8 can bind directly to LIN-2. However, *eps-8(lf)* animals display LET-23 accumulated in intracellular punctae and wild-type vulval induction. These findings indicate that LET-23 is correctly targeted to the basolateral membrane in *eps-8(lf)* animals and that EPS-8 is involved in retention or recycling mechanisms of LET-23. However, the molecular mechanism of EPS-8 function is not clear yet.

In order to investigate LET-23 localization and the underlying molecular mechanisms, we sought for novel components using different genetic approaches.

6.1 The candidate based approach to find regulators of LET-23 localization

A preceding candidate RNAi screen targeting genes endocing PDZ- or FERM-domains performed by A. Stetak in our laboratory identified *frm-8* and *tag-60* as putative regulators of LET-23 localization. In order to substantiate the results obtained by RNAi, deletion mutants were generated and stained for LET-23. It has to be noted that immunostaining of LET-23 resulted in highly variable expression compared with other antibodies used in this study (αAJM-1 and αTAG-60-1). It is likely that the epitope of the LET-23 antibody becomes instable after fixation and permeabilization treatments. It was observed that identical worm samples were immunostained for LET-23 at the same day but resulted in high quality differences. Therefore, immunostaining of LET-23 was not the only criteria to decide whether or not to follow a candidate gene. Genetic interaction with the inductive pathway was used to test a role in vulval development.

frm-8(zh67) animals showed intracellular accumulation of LET-23 but only weak genetic interaction with *lin-2(n105)*. However, *egl-17::cfp* expression in the 1° cells of *frm-8(zh67)* animals was not significantly different compared to wild-type animals and downregulation of other FERM-domain encoding genes in a *frm-8(zh67)* background did not result in a synthetic phenotype. Considering these findings, the project was not continued. It is possible that *frm-8* plays a minor role in vulval development, which might be only visible in combination with more complex sensitized backgrounds (e.g. more than two mutations). It is also possible that FRM-8 acts redundantly with other proteins that do not harbour a FERM-domain or that RNAi of other FERM domain genes was not effective.

The *tag-60(zh93)* deletion mutant was isolated after screening six different deletion libraries, which were performed in a time-frame of about one year. It is unclear why no positive deletion mutants were found in earlier screens. Colleagues that screened the same libraries did not find their target gene deletions. Therefore, it is possible that the mutagenesis was not performed properly. However, the subsequent performed forward genetic screen, which involved a similar mutagenesis step (50mM instead of 75mM EMS), produced many different mutant strains. A possible explanation why no *tag-60* allele was found earlier is that the null mutants of *tag-60* might be inviable. Genetic experiments involving other *tag-60* alleles and a deficiency covering the *tag-60* locus are underway to assess this possibility.

Most of the experiments in this study were performed with the *tag-60(zh93)* allele. *zh93* is an in-frame deletion, which does not remove any sequences encoding known domains. It was found that in *tag-60(zh93)* animals mRNAs of the *tag-60* locus are produced and that these mRNAs were shorter than in wild-type animals, corresponding to the size of the *zh93* deletion. Hence, it is likely that in *tag-60(zh93)* animals truncated proteins are being produced. We determined that the *tag-60(zh93)* allele is dominant, but the question whether it represents a reduction-of-function or a loss-of-function allele remains open. Therefore, it is difficult to interprete the results obtained with the *tag-60(zh93)* allele and to draw a model at this time, but the analysis of the recently obtained alleles *tag-60(tm3501)* and *tag-60(ok2292)* should answer this question.

In immunostaining experiments of *tag-60(zh93)* mutants we found that LET-23 is accumulated in intracellular compartments. The genetic interactions of *tag-60(zh93)* with components of the inductive pathway neither supports nor contradicts the finding of LET-23 mislocalization. The suppression of the *lin-2(n397)* and also the *let-23(sy10)* and *sem-5(n2019)* Vulvaless phenotypes by *tag-60(zh93)* demonstrates that *tag-60(zh93)* animals have elevated inductive or lateral signalling. On the other hand, *tag-60(zh93)* animals show 20-30% reduced *egl-17::cfp* expression in the 1° cell lineage, indicating a reduction of LET-23 signalling activity. It is therefore likely that TAG-60 might also have effects on the 2° cells and that TAG-60 might be involved in multiple signalling pathways.

Since we only analyzed the *tag-60(zh93)* allele, it is possible that all the observed effects are allele-specific and might not represent general *tag-60* features. It is also possible that a closely cis-linked mutation is responsible for the observations presented in this study. As already mentioned before, it is indispensable to analyze and compare all available *tag-60* alleles. Assuming that the results presented here are specific for *tag-60*, we can conclude that TAG-60 is a regulator of vulval development, which is involved in LET-23 localization.

Expression analysis with αTAG-60-1 antibodies in immunostaining experiments showed that TAG-60 is expressed in the vulval cells at the L4 stage, when the vulval tissue starts to invaginate. At this time point, the vulval induction and patterning events are already completed. The genetic data supports the notion of TAG-60 being involved in the induction process. However, no TAG-60 expression was observed in the VPCs at the time of induction, where TAG-60 was detected mainly in the intestine and the pharynx. The putative human homologue of TAG-60, EBP-50, has been shown to directly bind EGFR and inhibit ligand induced endocytosis (Lazar et al. 2004). So far, we cannot exclude a cell-nonautonomous model, where TAG-60 might regulate vulval development by a distant tissue. However, it is

also possible that TAG-60 is expressed at low levels in the VPCs at the time of induction, which are not detectable by the αTAG-60-1 antibody. Additionally, the αTAG-60-1 antibody might not recognize all TAG-60 isoforms.

Three possible models for TAG-60 function

Since the molecular nature of *tag-60(zh93)* has not been determined so far, the interpretation of the results and the resulting model of TAG-60 function is highly speculative. The similarity between TAG-60 and the human orthologue EBP-50 suggests a similar function of both proteins. EBP-50 was shown to bind directly to EGFR in human tissue culture cells and hence controls the localization of EGFR (Lazar et al. 2004). Therefore the model where TAG-60 acts cell-autonomously in the vulval cells to regulate LET-23 is favourable. Assuming that *zh93* represents a reduction-of-function allele (e.g. haploinsufficient, dominant negative) the genetic data would indicate that TAG-60 is a negative regultor of vulval development (figure 6.1 A). Mislocalization of LET-23 to intracellular punctae in *tag-60(zh93)* would indicate that TAG-60 is either an inhibitor of LET-23 internalization or promoting LET-23 recycling or degradation. Similarly, EBP-50 was found to inhibit ligand-induced endocytosis of EGFR (Lazar et al. 2004). The data shown in this study do not support or disprove this model. TAG-60 was not detected in the VPCs at the time of induction, which could be due to low levels of TAG-60 expression within the vulval cells undetectable by immunostainig. If present in the VPCs, TAG-60 could bind to ERM-1 and form a molecular linker between LET-23 and the cortical cytoskeleton. *tag-60(zh93)* and *erm-1(tm677)* animals show similar genetic interactions with mutants of the LET-23 pathway, supporting the idea of both proteins being involved in the same process (figure 6.1 A). Similarly, human EBP-50 was found to physically interact with the ERM-like protein Merlin and to link EGFR to detergent insoluble compartments (Curto et al. 2007; Cole et al. 2008). However, *erm-1(tm677)* suppressed the Vulvaless phenotypes of *lin-7(e1413)* and *lin-10(e1439)*, whereas *tag-60(zh93)* did not. This difference could indicate that TAG-60 function, in contrast to ERM-1, is somehow dependent on LIN-7 and LIN-10. A possible interpretation would be that TAG-60 acts redundantly with another PDZ-domain protein in ERM-1-mediated LET-23 localization and regulation of vulval development (figure 6.1 A).

Assuming that *tag-60(zh93)* represents a gain-of-function allele (e.g. constitutive active), this would indicate that *C. elegans* TAG-60 has the opposite function to that described for its human orthologue EBP-50. In this case, TAG-60 would promote LET-23 internalization or inhibit LET-23 recycling and/or degradation. The genetic data would then indicate that TAG-

60 is a positive regulator of vulval induction, since *tag-60(zh93)* was able to suppress significantly the *lin-2(n397)* Vulvaless phenotype. On the other hand, *tag-60(zh93)* did not suppress the Vulvaless phenotypes of either *lin-7(e1413)* or *lin-10(e1439)*, indicating that TAG-60 function is dependent on LIN-7 and LIN-10 but not on LIN-2. The proteins LIN-7, LIN-2 and LIN-10 were shown to be necessary for initial basolateral targeting of LET-23 in the VPCs (Kaech et al. 1998). It was furthermore shown that LIN-2, together with EPS-8, is involved in LET-23 retention at the basolateral membrane (Stetak et al. 2006). It is possible that LIN-7, LIN-10 and TAG-60 are involved in LET-23 trafficking after the initial LET-23 targeting event, similar to what was shown for LIN-2 and EPS-8 (Stetak et al. 2006). If *tag-60(zh93)* was indeed a gain-of-function allele, the model of TAG-60 regulating vulval development together with ERM-1 would be rejected. *erm-1(tm677)* is a null allele (Göbel et al. 2004) and has similar genetic interactions as *tag-60(zh93)*. Therefore, TAG-60 and ERM-1 would have opposite regulatory effects on vulval development (figure 6.1 B). In this case, ERM-1 might be linked to LET-23 by another PDZ-domain protein or might bind directly to LET-23 (figure 6.1 B), as was shown for other transmembrane proteins (Bretscher et al. 2002). ERM-1 would thus link LET-23 to the cortical cytoskeleton independently of TAG-60 (figure 6.1 B).

At the time of vulval induction, TAG-60 was detected in the intestine but not in the vulval cells using immunostaining. The similarity between TAG-60 and human EBP-50 speaks for a cell-autonomous model. However, it is also possible that TAG-60 functions within the intestinal cells to regulate vulval development. To our knowledge, there is no known example, where a factor from the intestine influences vulval induction. However, it is known that surrounding tissues such as the hypodermis (hyp7) are involved in regulating the development of the vulva (Cui et al. 2006). LET-23 is also expressed in intestinal cells and localizes to the apical membrane compartment (figure 3.16 E, arrowheads). TAG-60 and ERM-1 share the subcellular localization of LET-23 within the intestinal cells (figure 6.2). The function of LET-23 and TAG-60 in the intestine is unknown. Our data do not exclude a model where intestinal LET-23 together with TAG-60 and ERM-1 regulate vulval development cell non-autonomously (figure 6.2). In *erm-1(tm677)* animals, intestinal LET-23 is not localized exclusively on the apical side (lumenal side) of the intestinal cells as in wild-type animals (figure 3.16 E, arrowheads), but LET-23 is rather distributed on the whole plasma membrane (figure 3.16 F, arrows). The anchor cell in the somatic gonad secretes the LIN-3 EGF protein, which activates LET-23 in the VPCs (Hill and Sternberg, 1992; Aroian and Sternberg, 1991). It is possible that LIN-3 in the extracellular space can diffuse and reach tissues other than the

vulva. Therefore, a model is possible where ERM-1, maybe in concert with TAG-60, localizes LET-23 to the apical membrane of intestinal cells, rendering it inactive to LIN-3 produced by the anchor cell on the basolateral side (figure 6.2). By removing ERM-1, LET-23 might be activated by basolateral LIN-3. In the hypodermis, the synMuv pathways function to repress LIN-3 production in a cell-autonomous manner (Cui et al. 2006). By removing certain combinations of synMuv factors, the hypodermis produces LIN-3, leading to ectopic vulval induction (Cui et al. 2006). It is possible that a similar mechanism takes place in the intestine, where active LET-23 might induce the production of LIN-3 or another growth factor (figure 6.2). Excess LIN-3 in *erm-1(tm677)* mutants would account for the suppression of the Vulvaless phenotype observed in mutants such as *lin-2(n397)*. So far, the localization of LET-23 in the intestine of *tag-60(zh93)* animals is unknown and hence it is not clear if TAG-60 would work in concert with ERM-1 or not.

Investigation of ERM-1 was part of this study because it is a putative binding partner of TAG-60. The fact that the human homologues directly interact (Finnerty et al. 2004) and that the *C. elegans* proteins bind in yeast-2-hybrid experiments (Li et al. 2004) were the basis for this project. In this study, we provide further evidence for the existence of a TAG-60/ERM-1 complex. First, TAG-60 localization in the intestinal cells is dependent on ERM-1 and second, ERM-1::CFP could be coimmunoprecipitated with TAG-60 (D. Kradolfer and E. Fröhli, unpublished results).

Experiments with the *erm-1(tm677)* allele show similar genetic interactions with the EGFR pathway as *tag-60(zh93)*. The *tm677* allele represents a null allele of *erm-1* (Göbel et al. 2004), which suppresses the Vulvaless phenotypes of *lin-2*, *lin-7* and *lin-10* loss-of-function alleles and enhances the *let-60(n1046)* gain of function Multivulva phenotype. Therefore, ERM-1 is a novel negative regulator of vulval development.

This study presents further results, which indicate that the regulation of vulval development by ERM-1 occurs at the level of LET-23. Immunostaining experiments showed that LET-23 in the VPCs of *tm677* animals is mislocalized to intracellular compartments. Consistently, ERM-1::CFP is localized to the basolateral membrane compartment of the VPCs and could be coimmunoprecipitated with LET-23 (D. Kradolfer and E. Fröhli, unpublished results). However, it is not clear if ERM-1 is acting upstream of downstream of LET-23. The human homologue of ERM-1, Ezrin, was shown to be activated by threonine phosphorylation in the C-terminus (Bretscher et al. 2002). On the other hand, EGFR was found to directly phosphorylate Ezrin *in vivo* and *in vitro* and therby modulate Ezrin activity (Krieg and

Hunter, 1992). The tyrosine residues of Ezrin that were phosphorylated by EGFR are not conserved in *C. elegans* ERM-1, and hence it is not clear whether LET-23 kinase activity is necessary for ERM-1 function.

NFM-1 is the putative *C. elegans* homologue of Nf2/Merlin, which was shown to be involved in contact-dependent inhibition of EGFR in tissue culture cells, by linking the receptor to insoluble membrane compartments and hence render it inactive and blocking its internalization (Curto et al. 2007, Cole et al. 2008). Since Nf2/Merlin is a protein closely related to the ERM family (Bretscher et al. 2002), it is possible that LET-23 is an effector of ERM-1 at the plasma membrane and inhibits its activity similarly to what was shown for Nf2/Merlin and EGFR. Other possible effectors of ERM-1 are components of the RHO-1 pathway, which positively regulates the inductive pathway in the VPCs (Canevascini et al. 2005). Speck et al. (2003) showed that *D. melanogaster* Moesin antagonizes the Rho pathway *in vivo*. Therefore it is possible that this is also the case for *C. elegans* ERM-1. Since the genetic studies presented here do not include any "null" mutation of a core component of the inductive pathway, we cannot place *erm-1* genetically in this pathway. Therefore, ERM-1 could act at any level of the inductive pathway. Further genetic experiments have to be performed to pinpoint the level, at which ERM-1 functions during vulval development.

One of the questions that arose during this study is, why genes like *tag-60* and *erm-1* have not been identified before in forward genetic screens for regulators of vulval development. We present evidence that TAG-60 and ERM-1 regulate vulval development during the induction and patterning processes. *erm-1* is an essential gene and mutations affecting its activity have dramatic effects on the viability of the animals. Therefore, the probability is low to find *erm-1* mutations in a forward genetic screen. This clearly emphazises the importance of candidate based and RNAi approaches. Furthermore, *erm-1(tm677)* animals show pleiotropic defects, which complicate the analysis of this mutant. It is important to note that *erm-1(tm677)* animals display severe morphological defects of all tubular epithelia (Göbel et al. 2004), which makes it difficult to properly analyze *erm-1* function during vulval induction. The *tag-60(zh93)* mutants seem to be undistinguishable from wild-type animals.

Loss-of-function mutants of *lin-2*, *lin-7* or *lin-10* show apically mislocalized LET-23 and hence display a high penetrant Vulvaless phenotype (Kaech et al. 1998). However, the combination of those mutants with a *gap-1(lf)* allele results in a Multivulva phenotype (Hajnal et al. 1997). This genetic interaction formulated the rationale of the forward genetic screen presented in this study. The *tag-60* and *erm-1* mutants analyzed in this study showed

intracellular accumulation of LET-23 in the VPCs. The fact that in these mutants vulval induction is executed as in wild-type animals, leads to the conclusion that LET-23 is targeted correctly to the basolateral membrane and that both TAG-60 and ERM-1 might be involved in the retention or recycling of LET-23. Both *tag-60(zh93)* and *erm-1(tm677)* do not show a synthetic Muv phenotype when combined with *gap-1(lf)*, indicating that not all mutants that mislocalize LET-23, genetically interact with *gap-1(lf)*. Consistently, *eps-8* was found in a candidate-based approach to be a positive regulator of vulval development (Stetak et al. 2006). *eps-8(lf)* animals showed intracellular accumulation of LET-23 in the VPCs but did not result in a Muv phenotype in combination with *gap-1(lf)* (Stetak et al. 2006, A. Stetak personal communication). Therefore, from a genetical point of view, it would be impossible to find regulators of LET-23 localization such as TAG-60, ERM-1 and EPS-8 in a forward genetic screen using *gap-1(lf)* as a sensitized background.

Immunostaining of LET-23 turned out to have variable efficiencies. In order to substantiate the findings presented in this study, we wish to reproduce these results with a LET-23::GFP fusion protein. Our laboratory recently succeeded to construct a LET-23::GFP variant, which is sensitive to loss-of-function mutations of *lin-2*, where it was mislocalized to the apical plasma membrane compartment (J. Escobar, personal communication). Unfortunately, the LET-23::GFP did not rescue the induction defects of *let-23(sy1)* (J. Escobar, personal communication). However, this translational LET-23 reporter might facilitate the study of TAG-60 and ERM-1 regarding LET-23 localization. In addition, it would be possible to use the LET-23 reporter as a tool in future screens for proteins involved in LET-23 localization (J. Escobar, personal communication).

6.2 The forward genetic approach to find regulators of LET-23 localization

At the beginning of this study, the generation of deletion mutants for *frm-8* and *tag-60* was very time consuming, as especially for the *tag-60* allele no deletion was found at first. Since it was unclear whether the deletion screens would be successful, we decided to start a parallel backup project. A forward genetic screen for Multivulva animals in a *gap-1(ga133)* sensitized background was started to find regulators of LET-23 localization, such as LIN-2, LIN-7 and LIN-10. The same rationale was already used before to screen for fertile mutants (A. Hajnal, personal communication). In order to identify novel factors, the screen was performed with a focus on mutants with more complex phenotypes such as late lethality and sterility. In addition to proteins involved in LET-23 localization, we hoped to find novel attenuators of vulval development. Six mutant lines were isolated from 2'800 mutagenized genomes. Two of them turned out to apically mislocalize LET-23 and were found to represent novel alleles of *lin-2* and *lin-7*. The remaining four mutants showed predominantly basolateral LET-23 localization and hence represented putative negative regulators of vulval development. *zh94* turned out to be an allele of GAP-3, an inhibitor of LET-60/Ras (Stetak et al.2008). The discovery and study of *gap-3(zh94)* was used to substantiate the previous characterization of the *gap-3(ga139)* allele (Stetak et al. 2008). The three remaining mutants turned out to exhibit a Multivulva phenotype, which is independent of the *gap-1(lf)* allele: *zh99* is likely to be an allele of *let-19*, a gene encoding a subunit of the mediator complex (Yoda et al. 2005, Clayton et al. 2008), and the location of *zh95* (candidate gene *lin-13*; Melendez and Greenwald, 2000) and *zh78* was not yet determined. For this backup project, 1400 clones were analyzed and only three mutant lines were found to be synthetic Muv with *gap-1(lf)*. The fact that we found *lin-2* and *lin-7* once but not *lin-10* makes clear that the screen is not saturated yet.

6.3 The large-scale RNAi screen in a *gap-1(lf)* background

In colaboration with the Poulin laboratory in Manchester, we peformed a large-scale RNAi screen of chromosomes I, II and III using the Ahringer RNAi feeding library (Kamath et al. 2003). The idea was to generate a list of candidate genetic intarctors of *gap-1*, which would facilitate the mapping of the mutants isolated during the forward genetic screen. Thirty-six candidate genes showed a high-confidence synthetic Muv phenotype in a *gap-1(lf)* background. Unfortunately, this list of candidates was not useful for the mapping process of the mutants. It turned out that the RNAi clones for *gap-3* and *lin-13* (candidate gene affected by *zh95*) are not present in the Ahringer library. Additionally, RNAi against *let-19* did not have any defects.

The previously characterized attenuators of vulval development *puf-8, fbf-1* and *fbf-2* (Walser et al. 2006) were found, which validated the rationale of the screen. Additionally, the thirty-six candidates might include novel genetic interactors of *gap-1*, which still have to be analyzed in detail. Deletion mutants of the candidates have to be used to substantiate the RNAi results and to confirm the genetic interactions. The candidate genes could encode regulators of LET-23 localization or attenuators of vulval development. The LET-23::GFP reporter (J. Escobar, personal communication) could be used to answer this question. Assuming that most of the new candidates are true, it would be interesting to continue this project and to screen the remaining chromosomes IV, V and X. It appears that the RNAi screen can reveal a different set of genetic *gap-1* interactors, compared to previously performed forward genetic screens.

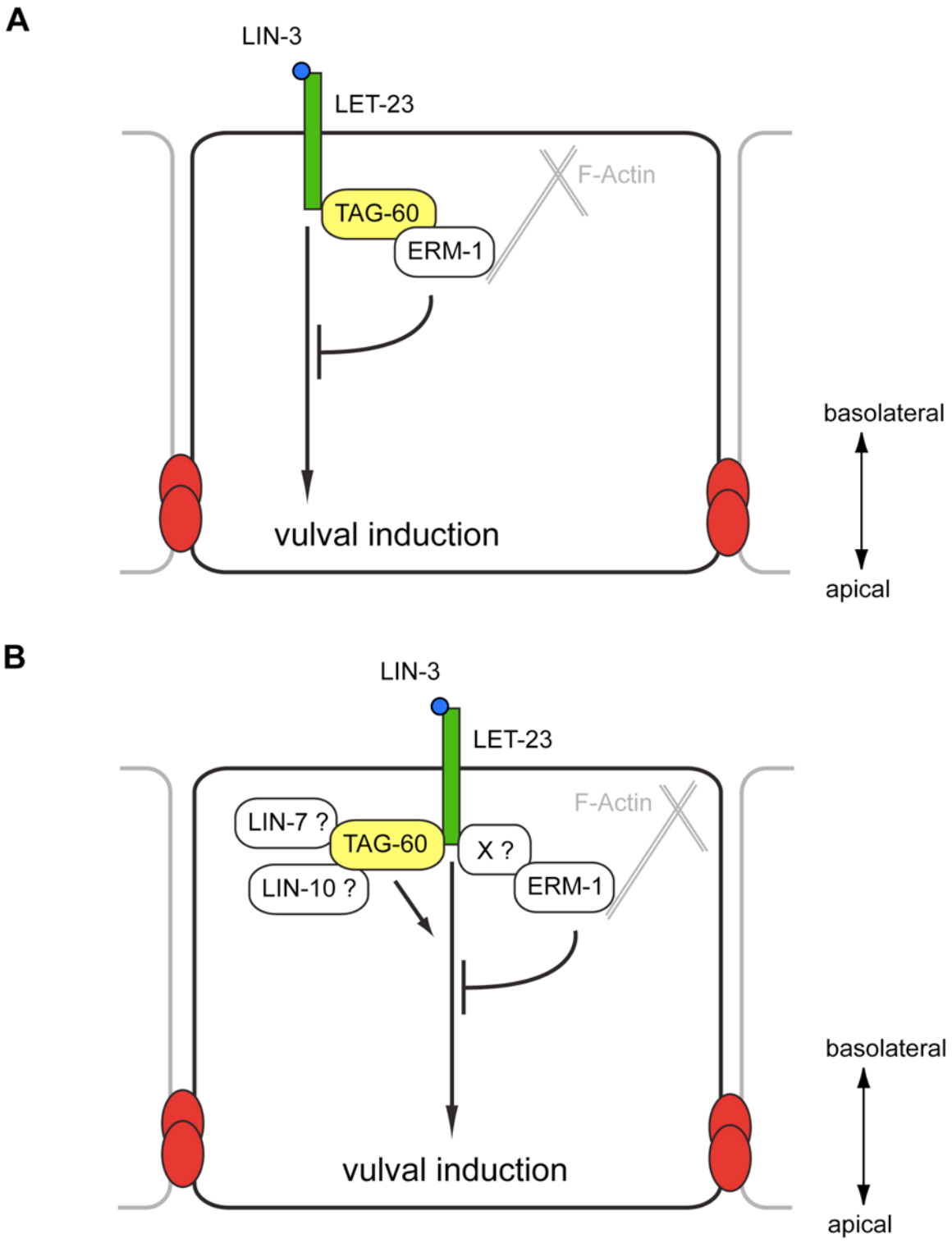

Fig. 6.1: Cell autonomous models of TAG-60/ERM-1 function
Hypothetical models for TAG-60 function, based on the results collected with *tag-60(zh93)*. Two different assumptions were made, where *zh93* either represents a reduction-of-function (A) or a gain-of-function (B) allele. A)Similar genetic interactions of *tag-60(zh93)* and *erm-1(tm677)* suggest that both gene products are involved in the same process to negatively regulate vulval induction. In both mutant animals, LET-23 is mislocalized to intracellular punctae. TAG-60 and ERM-1 possibly form a complex that links LET-23 to the cortical cytoskeleton. B) The similar genetic interactions of *tag-60(zh93)* and *erm-1(tm677)* indicate that both gene products do have opposite functions during vulval development, ERM-1 being a negative and TAG-60 being a positive regulator of vulval induction. ERM-1 might bind directly or indirectly (putative protein X) to LET-23 and link it to the cortical cytoskeleton. The genetic data collected with *tag-60(zh93)* indicates that TAG-60 function is dependent on LIN-7 and LIN-10.

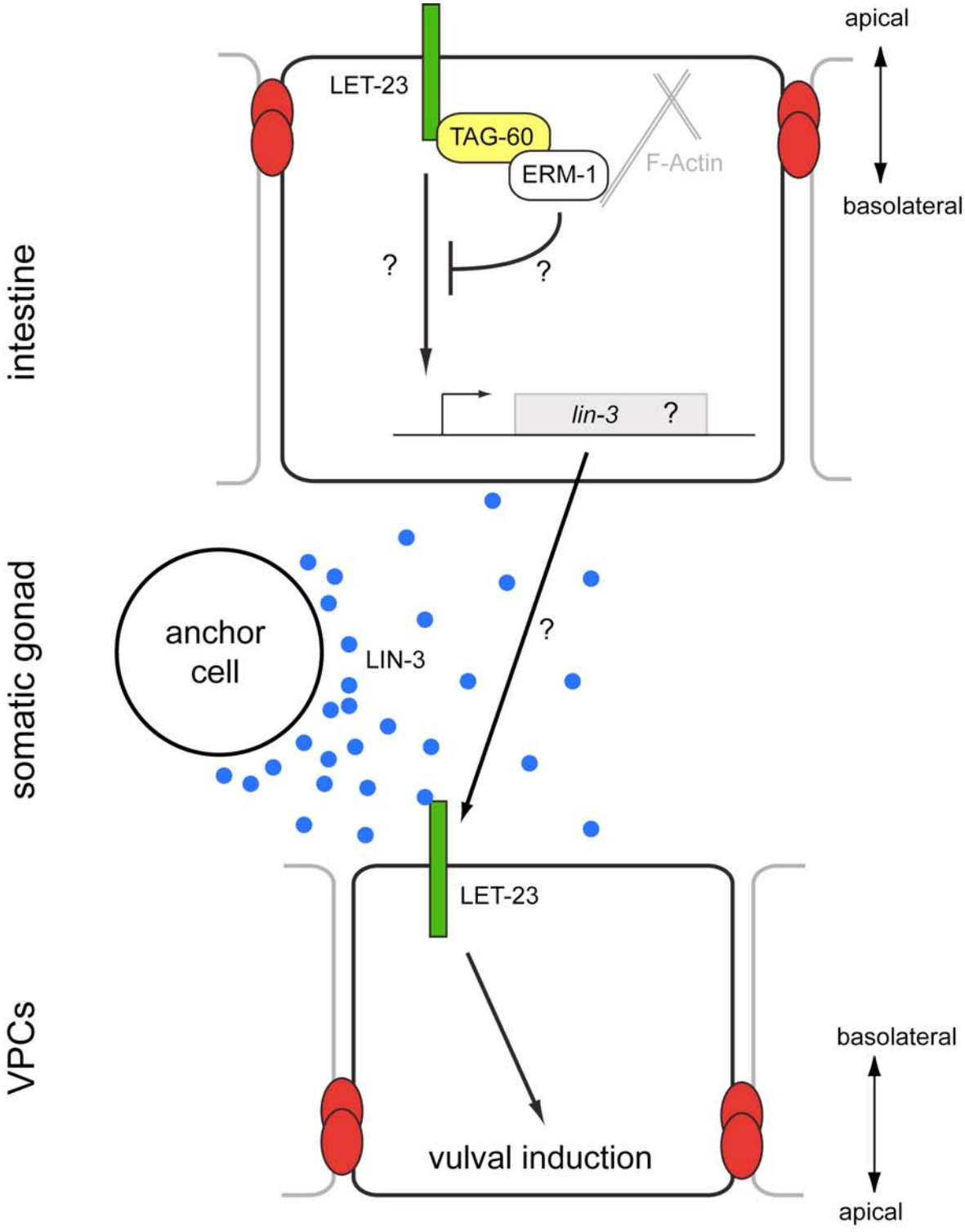

Fig. 6.2: Cell non-autonomous model of TAG-60/ERM-1 function
In the intestine, LET-23, TAG-60 and ERM-1 are exclusively localized to the apical compartment. The LIN-3 producing anchor cell faces the basolateral compartments of the intestinal and the vulval cells. Basolateral LET-23 in the VPCs is activated by LIN-3 produced by the anchor cell. LET-23 in the intestine might be excluded from the basolateral compartment by the action of TAG-60 and ERM-1, which might link the receptor to the cortical cytoskeleton. In *erm-1(tm677)* animals, intestinal LET-23 is localized all around the plasma membrane, which might induce the production of LIN-3. Excess LIN-3 might activate LET-23 on the VPCs.

7. References

AROIAN, R. V., LESA, G. M. & STERNBERG, P. W. (1994) Mutations in the Caenorhabditis elegans let-23 EGFR-like gene define elements important for cell-type specificity and function. *Embo J,* 13**,** 360-6.

AROIAN, R. V. & STERNBERG, P. W. (1991) Multiple functions of let-23, a Caenorhabditis elegans receptor tyrosine kinase gene required for vulval induction. *Genetics,* 128**,** 251-67.

BATTU, G., HOIER, E. F. & HAJNAL, A. (2003) The C. elegans G-protein-coupled receptor SRA-13 inhibits RAS/MAPK signalling during olfaction and vulval development. *Development,* 130**,** 2567-77.

BAULIDA, J., KRAUS, M. H., ALIMANDI, M., DI FIORE, P. P. & CARPENTER, G. (1996) All ErbB receptors other than the epidermal growth factor receptor are endocytosis impaired. *J Biol Chem,* 271**,** 5251-7.

BEERS, M. & KEMPHUES, K. (2006) Depletion of the co-chaperone CDC-37 reveals two modes of PAR-6 cortical association in C. elegans embryos. *Development,* 133**,** 3745-54.

BEITEL, G. J., CLARK, S. G. & HORVITZ, H. R. (1990) Caenorhabditis elegans ras gene let-60 acts as a switch in the pathway of vulval induction. *Nature,* 348**,** 503-9.

BEITEL, G. J., TUCK, S., GREENWALD, I. & HORVITZ, H. R. (1995) The Caenorhabditis elegans gene lin-1 encodes an ETS-domain protein and defines a branch of the vulval induction pathway. *Genes Dev,* 9**,** 3149-62.

BERRYMAN, M., FRANCK, Z. & BRETSCHER, A. (1993) Ezrin is concentrated in the apical microvilli of a wide variety of epithelial cells whereas moesin is found primarily in endothelial cells. *J Cell Sci,* 105 (Pt 4)**,** 1025-43.

BERRYMAN, M., GARY, R. & BRETSCHER, A. (1995) Ezrin oligomers are major cytoskeletal components of placental microvilli: a proposal for their involvement in cortical morphogenesis. *J Cell Biol,* 131**,** 1231-42.

BERSET, T., HOIER, E. F., BATTU, G., CANEVASCINI, S. & HAJNAL, A. (2001) Notch inhibition of RAS signaling through MAP kinase phosphatase LIP-1 during C. elegans vulval development. *Science,* 291**,** 1055-8.

BERSET, T. A., HOIER, E. F. & HAJNAL, A. (2005) The C. elegans homolog of the mammalian tumor suppressor Dep-1/Scc1 inhibits EGFR signaling to regulate binary cell fate decisions. *Genes Dev,* 19**,** 1328-40.

BOGUSKI, M. S. & MCCORMICK, F. (1993) Proteins regulating Ras and its relatives. *Nature,* 366**,** 643-54.

BOLLAG, G. & MCCORMICK, F. (1991) Regulators and effectors of ras proteins. *Annu Rev Cell Biol,* 7**,** 601-32.

BORG, J. P., MARCHETTO, S., LE BIVIC, A., OLLENDORFF, V., JAULIN-BASTARD, F., SAITO, H., FOURNIER, E., ADELAIDE, J., MARGOLIS, B. & BIRNBAUM, D. (2000) ERBIN: a basolateral PDZ protein that interacts with the mammalian ERBB2/HER2 receptor. *Nat Cell Biol,* 2**,** 407-14.

BRENNER, S. (1974) The genetics of Caenorhabditis elegans. *Genetics,* 77**,** 71-94.

BRETSCHER, A., CHAMBERS, D., NGUYEN, R. & RECZEK, D. (2000) ERM-Merlin and EBP50 protein families in plasma membrane organization and function. *Annu Rev Cell Dev Biol,* 16**,** 113-43.

BRETSCHER, A., EDWARDS, K. & FEHON, R. G. (2002) ERM proteins and merlin: integrators at the cell cortex. *Nat Rev Mol Cell Biol,* 3**,** 586-99.

BRONE, B. & EGGERMONT, J. (2005) PDZ proteins retain and regulate membrane transporters in polarized epithelial cell membranes. *Am J Physiol Cell Physiol,* 288**,** C20-9.

BURDINE, R. D., BRANDA, C. S. & STERN, M. J. (1998) EGL-17(FGF) expression coordinates the attraction of the migrating sex myoblasts with vulval induction in C. elegans. *Development,* 125**,** 1083-93.

CANEVASCINI, S., MARTI, M., FROHLI, E. & HAJNAL, A. (2005) The Caenorhabditis elegans homologue of the proto-oncogene ect-2 positively regulates RAS signalling during vulval development. *EMBO Rep,* 6**,** 1169-75.

CAO, T. T., DEACON, H. W., RECZEK, D., BRETSCHER, A. & VON ZASTROW, M. (1999) A kinase-regulated PDZ-domain interaction controls endocytic sorting of the beta2-adrenergic receptor. *Nature,* 401**,** 286-90.

CHANG, C., HOPPER, N. A. & STERNBERG, P. W. (2000) Caenorhabditis elegans SOS-1 is necessary for multiple RAS-mediated developmental signals. *Embo J,* 19**,** 3283-94.

CHEN, N. & GREENWALD, I. (2004) The lateral signal for LIN-12/Notch in C. elegans vulval development comprises redundant secreted and transmembrane DSL proteins. *Dev Cell,* 6**,** 183-92.

CHEN, Z. & HAN, M. (2001) C. elegans Rb, NuRD, and Ras regulate lin-39-mediated cell fusion during vulval fate specification. *Curr Biol,* 11**,** 1874-9.

CHISHTI, A. H., KIM, A. C., MARFATIA, S. M., LUTCHMAN, M., HANSPAL, M., JINDAL, H., LIU, S. C., LOW, P. S., ROULEAU, G. A., MOHANDAS, N., CHASIS, J. A., CONBOY, J. G., GASCARD, P., TAKAKUWA, Y., HUANG, S. C., BENZ, E. J., JR., BRETSCHER, A., FEHON, R. G., GUSELLA, J. F., RAMESH, V., SOLOMON, F., MARCHESI, V. T., TSUKITA, S., TSUKITA, S., HOOVER, K. B. & ET AL. (1998) The FERM domain: a unique module involved in the linkage of cytoplasmic proteins to the membrane. *Trends Biochem Sci,* 23**,** 281-2.

CLARK, S. G., CHISHOLM, A. D. & HORVITZ, H. R. (1993) Control of cell fates in the central body region of C. elegans by the homeobox gene lin-39. *Cell,* 74**,** 43-55.

CLARK, S. G., STERN, M. J. & HORVITZ, H. R. (1992) C. elegans cell-signalling gene sem-5 encodes a protein with SH2 and SH3 domains. *Nature,* 356**,** 340-4.

CLAYTON, J. E., VAN DEN HEUVEL, S. J. & SAITO, R. M. (2008) Transcriptional control of cell-cycle quiescence during C. elegans development. *Dev Biol,* 313**,** 603-13.

COLE, B. K., CURTO, M., CHAN, A. W. & MCCLATCHEY, A. I. (2008) Localization to the cortical cytoskeleton is necessary for Nf2/merlin-dependent epidermal growth factor receptor silencing. *Mol Cell Biol,* 28**,** 1274-84.

CONSORTIUM, T. C. E. S. (1998) Genome sequence of the nematode C. elegans: a platform for investigating biology. *Science,* 282**,** 2012-8.

COX, E. A. & HARDIN, J. (2004) Sticky worms: adhesion complexes in C. elegans. *J Cell Sci,* 117**,** 1885-97.

CUI, M., CHEN, J., MYERS, T. R., HWANG, B. J., STERNBERG, P. W., GREENWALD, I. & HAN, M. (2006) SynMuv genes redundantly inhibit lin-3/EGF expression to prevent inappropriate vulval induction in C. elegans. *Dev Cell,* 10**,** 667-72.

CURTO, M., COLE, B. K., LALLEMAND, D., LIU, C. H. & MCCLATCHEY, A. I. (2007) Contact-dependent inhibition of EGFR signaling by Nf2/Merlin. *J Cell Biol,* 177**,** 893-903.

DAI, J. L., WANG, L., SAHIN, A. A., BROEMELING, L. D., SCHUTTE, M. & PAN, Y. (2004) NHERF (Na+/H+ exchanger regulatory factor) gene mutations in human breast cancer. *Oncogene,* 23**,** 8681-7.

DU, J. & WILSON, P. D. (1995) Abnormal polarization of EGF receptors and autocrine stimulation of cyst epithelial growth in human ADPKD. *Am J Physiol,* 269**,** C487-95.

FANNING, A. S. & ANDERSON, J. M. (1999) Protein modules as organizers of membrane structure. *Curr Opin Cell Biol,* 11**,** 432-9.

FAY, D. S. & YOCHEM, J. (2007) The SynMuv genes of Caenorhabditis elegans in vulval development and beyond. *Dev Biol,* 306**,** 1-9.

FINNERTY, C. M., CHAMBERS, D., INGRAFFEA, J., FABER, H. R., KARPLUS, P. A. & BRETSCHER, A. (2004) The EBP50-moesin interaction involves a binding site regulated by direct masking on the FERM domain. *J Cell Sci,* 117**,** 1547-52.

FINNEY, M. & RUVKUN, G. (1990) The unc-86 gene product couples cell lineage and cell identity in C. elegans. *Cell,* 63**,** 895-905.

FIRE, A. Z. (2007) Gene silencing by double-stranded RNA. *Cell Death Differ,* 14**,** 1998-2012.

FRENCH, A. R., TADAKI, D. K., NIYOGI, S. K. & LAUFFENBURGER, D. A. (1995) Intracellular trafficking of epidermal growth factor family ligands is directly influenced by the pH sensitivity of the receptor/ligand interaction. *J Biol Chem,* 270**,** 4334-40.

GAUTREAU, A., LOUVARD, D. & ARPIN, M. (2000) Morphogenic effects of ezrin require a phosphorylation-induced transition from oligomers to monomers at the plasma membrane. *J Cell Biol,* 150**,** 193-203.

GOBEL, V., BARRETT, P. L., HALL, D. H. & FLEMING, J. T. (2004) Lumen morphogenesis in C. elegans requires the membrane-cytoskeleton linker erm-1. *Dev Cell,* 6**,** 865-73.

GOLDSTEIN, B. & MACARA, I. G. (2007) The PAR proteins: fundamental players in animal cell polarization. *Dev Cell,* 13**,** 609-22.

GREENWALD, I. (2005) LIN-12/Notch signaling in C. elegans. *WormBook***,** 1-16.

GUPTA, B. P., LIU, J., HWANG, B. J., MOGHAL, N. & STERNBERG, P. W. (2006) sli-3 negatively regulates the LET-23/epidermal growth factor receptor-mediated vulval induction pathway in Caenorhabditis elegans. *Genetics,* 174**,** 1315-26.

HAJNAL, A., WHITFIELD, C. W. & KIM, S. K. (1997) Inhibition of Caenorhabditis elegans vulval induction by gap-1 and by let-23 receptor tyrosine kinase. *Genes Dev,* 11**,** 2715-28.

HAMILTON, B., DONG, Y., SHINDO, M., LIU, W., ODELL, I., RUVKUN, G. & LEE, S. S. (2005) A systematic RNAi screen for longevity genes in C. elegans. *Genes Dev,* 19**,** 1544-55.

HAN, M., GOLDEN, A., HAN, Y. & STERNBERG, P. W. (1993) C. elegans lin-45 raf gene participates in let-60 ras-stimulated vulval differentiation. *Nature,* 363**,** 133-40.

HANOVER, J. A., WILLINGHAM, M. C. & PASTAN, I. (1984) Kinetics of transit of transferrin and epidermal growth factor through clathrin-coated membranes. *Cell,* 39**,** 283-93.

HELDIN, C. H. (1995) Dimerization of cell surface receptors in signal transduction. *Cell,* 80**,** 213-23.

HILL, R. J. & STERNBERG, P. W. (1992) The gene lin-3 encodes an inductive signal for vulval development in C. elegans. *Nature,* 358**,** 470-6.

HOBERT, O. (2002) PCR fusion-based approach to create reporter gene constructs for expression analysis in transgenic C. elegans. *Biotechniques,* 32**,** 728-30.

HOLBRO, T. & HYNES, N. E. (2004) ErbB receptors: directing key signaling networks throughout life. *Annu Rev Pharmacol Toxicol,* 44**,** 195-217.

HORVITZ, H. R., BRENNER, S., HODGKIN, J. & HERMAN, R. K. (1979) A uniform genetic nomenclature for the nematode Caenorhabditis elegans. *Mol Gen Genet,* 175**,** 129-33.

HORVITZ, H. R. & SULSTON, J. E. (1980) Isolation and genetic characterization of cell-lineage mutants of the nematode Caenorhabditis elegans. *Genetics,* 96**,** 435-54.

HOSKINS, R., HAJNAL, A. F., HARP, S. A. & KIM, S. K. (1996) The C. elegans vulval induction gene lin-2 encodes a member of the MAGUK family of cell junction proteins. *Development,* 122**,** 97-111.

HUNTER, T. & COOPER, J. A. (1981) Epidermal growth factor induces rapid tyrosine phosphorylation of proteins in A431 human tumor cells. *Cell,* 24**,** 741-52.

JONGEWARD, G. D., CLANDININ, T. R. & STERNBERG, P. W. (1995) sli-1, a negative regulator of let-23-mediated signaling in C. elegans. *Genetics,* 139**,** 1553-66.

KAECH, S. M., WHITFIELD, C. W. & KIM, S. K. (1998) The LIN-2/LIN-7/LIN-10 complex mediates basolateral membrane localization of the C. elegans EGF receptor LET-23 in vulval epithelial cells. *Cell,* 94**,** 761-71.

KAMATH, R. S. & AHRINGER, J. (2003) Genome-wide RNAi screening in Caenorhabditis elegans. *Methods,* 30**,** 313-21.

KAMATH, R. S., FRASER, A. G., DONG, Y., POULIN, G., DURBIN, R., GOTTA, M., KANAPIN, A., LE BOT, N., MORENO, S., SOHRMANN, M., WELCHMAN, D. P., ZIPPERLEN, P. & AHRINGER, J. (2003) Systematic functional analysis of the Caenorhabditis elegans genome using RNAi. *Nature,* 421**,** 231-7.

KATZ, W. S., HILL, R. J., CLANDININ, T. R. & STERNBERG, P. W. (1995) Different levels of the C. elegans growth factor LIN-3 promote distinct vulval precursor fates. *Cell,* 82**,** 297-307.

KORNBERG, R. D. (2005) Mediator and the mechanism of transcriptional activation. *Trends Biochem Sci,* 30**,** 235-9.

KORNFELD, K., GUAN, K. L. & HORVITZ, H. R. (1995) The Caenorhabditis elegans gene mek-2 is required for vulval induction and encodes a protein similar to the protein kinase MEK. *Genes Dev,* 9**,** 756-68.

KRIEG, J. & HUNTER, T. (1992) Identification of the two major epidermal growth factor-induced tyrosine phosphorylation sites in the microvillar core protein ezrin. *J Biol Chem,* 267**,** 19258-65.

LACKNER, M. R. & KIM, S. K. (1998) Genetic analysis of the Caenorhabditis elegans MAP kinase gene mpk-1. *Genetics,* 150**,** 103-17.

LACKNER, M. R., KORNFELD, K., MILLER, L. M., HORVITZ, H. R. & KIM, S. K. (1994) A MAP kinase homolog, mpk-1, is involved in ras-mediated induction of vulval cell fates in Caenorhabditis elegans. *Genes Dev,* 8**,** 160-73.

LAZAR, C. S., CRESSON, C. M., LAUFFENBURGER, D. A. & GILL, G. N. (2004) The Na+/H+ exchanger regulatory factor stabilizes epidermal growth factor receptors at the cell surface. *Mol Biol Cell,* 15**,** 5470-80.

LEE, J., JONGEWARD, G. D. & STERNBERG, P. W. (1994) unc-101, a gene required for many aspects of Caenorhabditis elegans development and behavior, encodes a clathrin-associated protein. *Genes Dev,* 8**,** 60-73.

LEE, S. M., KOH, H. J., PARK, D. C., SONG, B. J., HUH, T. L. & PARK, J. W. (2002) Cytosolic NADP(+)-dependent isocitrate dehydrogenase status modulates oxidative damage to cells. *Free Radic Biol Med,* 32**,** 1185-96.

LEVKOWITZ, G., WATERMAN, H., ZAMIR, E., KAM, Z., OVED, S., LANGDON, W. Y., BEGUINOT, L., GEIGER, B. & YARDEN, Y. (1998) c-Cbl/Sli-1 regulates endocytic sorting and ubiquitination of the epidermal growth factor receptor. *Genes Dev,* 12**,** 3663-74.

LI, S., ARMSTRONG, C. M., BERTIN, N., GE, H., MILSTEIN, S., BOXEM, M., VIDALAIN, P. O., HAN, J. D., CHESNEAU, A., HAO, T., GOLDBERG, D. S., LI, N., MARTINEZ, M., RUAL, J. F., LAMESCH, P., XU, L., TEWARI, M., WONG, S. L., ZHANG, L. V., BERRIZ, G. F., JACOTOT, L., VAGLIO, P., REBOUL, J., HIROZANE-KISHIKAWA, T., LI, Q., GABEL, H. W., ELEWA, A., BAUMGARTNER, B., ROSE, D. J., YU, H., BOSAK, S., SEQUERRA, R., FRASER, A., MANGO, S. E., SAXTON, W. M., STROME, S., VAN DEN HEUVEL, S., PIANO, F., VANDENHAUTE, J., SARDET, C., GERSTEIN, M., DOUCETTE-STAMM, L., GUNSALUS, K. C., HARPER, J. W., CUSICK, M. E., ROTH, F. P., HILL, D. E. & VIDAL, M. (2004) A map of the interactome network of the metazoan C. elegans. *Science,* 303**,** 540-3.

MARICQ, A. V., PECKOL, E., DRISCOLL, M. & BARGMANN, C. I. (1995) Mechanosensory signalling in C. elegans mediated by the GLR-1 glutamate receptor. *Nature,* 378**,** 78-81.

MELENDEZ, A. & GREENWALD, I. (2000) Caenorhabditis elegans lin-13, a member of the LIN-35 Rb class of genes involved in vulval development, encodes a protein with zinc fingers and an LXCXE motif. *Genetics,* 155**,** 1127-37.

MELLMAN, I. (1996) Endocytosis and molecular sorting. *Annu Rev Cell Dev Biol,* 12**,** 575-625.

MOGHAL, N. & STERNBERG, P. W. (2003) The epidermal growth factor system in Caenorhabditis elegans. *Exp Cell Res,* 284**,** 150-9.

MUTHUSWAMY, S. K., GILMAN, M. & BRUGGE, J. S. (1999) Controlled dimerization of ErbB receptors provides evidence for differential signaling by homo- and heterodimers. *Mol Cell Biol,* 19**,** 6845-57.

NEHRKE, K. (2003) A reduction in intestinal cell pHi due to loss of the Caenorhabditis elegans Na+/H+ exchanger NHX-2 increases life span. *J Biol Chem,* 278**,** 44657-66.

OLAYIOYE, M. A., NEVE, R. M., LANE, H. A. & HYNES, N. E. (2000) The ErbB signaling network: receptor heterodimerization in development and cancer. *Embo J,* 19**,** 3159-67.

PAN, C. L., BAUM, P. D., GU, M., JORGENSEN, E. M., CLARK, S. G. & GARRIGA, G. (2008) C. elegans AP-2 and retromer control Wnt signaling by regulating mig-14/Wntless. *Dev Cell,* 14**,** 132-9.

PARSONS, D. W., JONES, S., ZHANG, X., LIN, J. C., LEARY, R. J., ANGENENDT, P., MANKOO, P., CARTER, H., SIU, I. M., GALLIA, G. L.,

OLIVI, A., MCLENDON, R., RASHEED, B. A., KEIR, S., NIKOLSKAYA, T., NIKOLSKY, Y., BUSAM, D. A., TEKLEAB, H., DIAZ, L. A., JR., HARTIGAN, J., SMITH, D. R., STRAUSBERG, R. L., MARIE, S. K., SHINJO, S. M., YAN, H., RIGGINS, G. J., BIGNER, D. D., KARCHIN, R., PAPADOPOULOS, N., PARMIGIANI, G., VOGELSTEIN, B., VELCULESCU, V. E. & KINZLER, K. W. (2008) An integrated genomic analysis of human glioblastoma multiforme. *Science,* 321**,** 1807-12.

PEARSON, M. A., RECZEK, D., BRETSCHER, A. & KARPLUS, P. A. (2000) Structure of the ERM protein moesin reveals the FERM domain fold masked by an extended actin binding tail domain. *Cell,* 101**,** 259-70.

POULIN, G., DONG, Y., FRASER, A. G., HOPPER, N. A. & AHRINGER, J. (2005) Chromatin regulation and sumoylation in the inhibition of Ras-induced vulval development in Caenorhabditis elegans. *Embo J,* 24**,** 2613-23.

RIESE, D. J., 2ND & STERN, D. F. (1998) Specificity within the EGF family/ErbB receptor family signaling network. *Bioessays,* 20**,** 41-8.

RIMANN, I. & HAJNAL, A. (2007) Regulation of anchor cell invasion and uterine cell fates by the egl-43 Evi-1 proto-oncogene in Caenorhabditis elegans. *Dev Biol,* 308**,** 187-95.

RUAL, J. F., CERON, J., KORETH, J., HAO, T., NICOT, A. S., HIROZANE-KISHIKAWA, T., VANDENHAUTE, J., ORKIN, S. H., HILL, D. E., VAN DEN HEUVEL, S. & VIDAL, M. (2004) Toward improving Caenorhabditis elegans phenome mapping with an ORFeome-based RNAi library. *Genome Res,* 14**,** 2162-8.

SEIDEL, H. S., ROCKMAN, M. V. & KRUGLYAK, L. (2008) Widespread genetic incompatibility in C. elegans maintained by balancing selection. *Science,* 319**,** 589-94.

SHARMA-KISHORE, R., WHITE, J. G., SOUTHGATE, E. & PODBILEWICZ, B. (1999) Formation of the vulva in Caenorhabditis elegans: a paradigm for organogenesis. *Development,* 126**,** 691-9.

SHAW, R. J., PAEZ, J. G., CURTO, M., YAKTINE, A., PRUITT, W. M., SAOTOME, I., O'BRYAN, J. P., GUPTA, V., RATNER, N., DER, C. J., JACKS, T. & MCCLATCHEY, A. I. (2001) The Nf2 tumor suppressor, merlin, functions in Rac-dependent signaling. *Dev Cell,* 1**,** 63-72.

SHAYE, D. D. & GREENWALD, I. (2005) LIN-12/Notch trafficking and regulation of DSL ligand activity during vulval induction in Caenorhabditis elegans. *Development,* 132**,** 5081-92.

SHELLY, M., MOSESSON, Y., CITRI, A., LAVI, S., ZWANG, Y., MELAMED-BOOK, N., AROETI, B. & YARDEN, Y. (2003) Polar expression of ErbB-2/HER2 in epithelia. Bimodal regulation by Lin-7. *Dev Cell,* 5**,** 475-86.

SHERWOOD, D. R., BUTLER, J. A., KRAMER, J. M. & STERNBERG, P. W. (2005) FOS-1 promotes basement-membrane removal during anchor-cell invasion in C. elegans. *Cell,* 121**,** 951-62.

SIGURDSON, D. C., SPANIER, G. J. & HERMAN, R. K. (1984) Caenorhabditis elegans deficiency mapping. *Genetics,* 108**,** 331-45.

SIJEN, T., FLEENOR, J., SIMMER, F., THIJSSEN, K. L., PARRISH, S., TIMMONS, L., PLASTERK, R. H. & FIRE, A. (2001) On the role of RNA amplification in dsRNA-triggered gene silencing. *Cell,* 107**,** 465-76.

SIMMER, F., MOORMAN, C., VAN DER LINDEN, A. M., KUIJK, E., VAN DEN BERGHE, P. V., KAMATH, R. S., FRASER, A. G., AHRINGER, J. &

PLASTERK, R. H. (2003) Genome-wide RNAi of C. elegans using the hypersensitive rrf-3 strain reveals novel gene functions. *PLoS Biol,* 1**,** E12.
SIMSKE, J. S., KAECH, S. M., HARP, S. A. & KIM, S. K. (1996) LET-23 receptor localization by the cell junction protein LIN-7 during C. elegans vulval induction. *Cell,* 85**,** 195-204.
SIMSKE, J. S., KOPPEN, M., SIMS, P., HODGKIN, J., YONKOF, A. & HARDIN, J. (2003) The cell junction protein VAB-9 regulates adhesion and epidermal morphology in C. elegans. *Nat Cell Biol,* 5**,** 619-25.
SORKIN, A. & GOH, L. K. (2008) Endocytosis and intracellular trafficking of ErbBs. *Exp Cell Res,* 314**,** 3093-106.
SORKIN, A. & VON ZASTROW, M. (2002) Signal transduction and endocytosis: close encounters of many kinds. *Nat Rev Mol Cell Biol,* 3**,** 600-14.
SPECK, O., HUGHES, S. C., NOREN, N. K., KULIKAUSKAS, R. M. & FEHON, R. G. (2003) Moesin functions antagonistically to the Rho pathway to maintain epithelial integrity. *Nature,* 421**,** 83-7.
STERNBERG, P. W. (2005) Vulval development. *WormBook,* 1-28.
STERNBERG, P. W. & HORVITZ, H. R. (1986) Pattern formation during vulval development in C. elegans. *Cell,* 44**,** 761-72.
STETAK, A., GUTIERREZ, P. & HAJNAL, A. (2008) Tissue-specific functions of the Caenorhabditis elegans p120 Ras GTPase activating protein GAP-3. *Dev Biol,* 323**,** 166-76.
STETAK, A., HOIER, E. F., CROCE, A., CASSATA, G., DI FIORE, P. P. & HAJNAL, A. (2006) Cell fate-specific regulation of EGF receptor trafficking during Caenorhabditis elegans vulval development. *Embo J,* 25**,** 2347-57.
SUDOL, M. (1998) From Src Homology domains to other signaling modules: proposal of the 'protein recognition code'. *Oncogene,* 17**,** 1469-74.
SULSTON, J. E. & HORVITZ, H. R. (1977) Post-embryonic cell lineages of the nematode, Caenorhabditis elegans. *Dev Biol,* 56**,** 110-56.
SUNDARAM, M. V. (2006) RTK/Ras/MAPK signaling. *WormBook,* 1-19.
TAN, P. B., LACKNER, M. R. & KIM, S. K. (1998) MAP kinase signaling specificity mediated by the LIN-1 Ets/LIN-31 WH transcription factor complex during C. elegans vulval induction. *Cell,* 93**,** 569-80.
TSUKITA, S., YAMAZAKI, Y., KATSUNO, T., TAMURA, A. & TSUKITA, S. (2008) Tight junction-based epithelial microenvironment and cell proliferation. *Oncogene,* 27**,** 6930-8.
VAN FURDEN, D., JOHNSON, K., SEGBERT, C. & BOSSINGER, O. (2004) The C. elegans ezrin-radixin-moesin protein ERM-1 is necessary for apical junction remodelling and tubulogenesis in the intestine. *Dev Biol,* 272**,** 262-76.
WALSER, C. B., BATTU, G., HOIER, E. F. & HAJNAL, A. (2006) Distinct roles of the Pumilio and FBF translational repressors during C. elegans vulval development. *Development,* 133**,** 3461-71.
WEINMAN, E. J., HALL, R. A., FRIEDMAN, P. A., LIU-CHEN, L. Y. & SHENOLIKAR, S. (2006) The association of NHERF adaptor proteins with g protein-coupled receptors and receptor tyrosine kinases. *Annu Rev Physiol,* 68**,** 491-505.
WHITFIELD, C. W., BENARD, C., BARNES, T., HEKIMI, S. & KIM, S. K. (1999) Basolateral localization of the Caenorhabditis elegans epidermal growth factor receptor in epithelial cells by the PDZ protein LIN-10. *Mol Biol Cell,* 10**,** 2087-100.

WILEY, H. S. (2003) Trafficking of the ErbB receptors and its influence on signaling. *Exp Cell Res,* 284**,** 78-88.

WU, Y., HAN, M. & GUAN, K. L. (1995) MEK-2, a Caenorhabditis elegans MAP kinase kinase, functions in Ras-mediated vulval induction and other developmental events. *Genes Dev,* 9**,** 742-55.

XU, W., MIMNAUGH, E., ROSSER, M. F., NICCHITTA, C., MARCU, M., YARDEN, Y. & NECKERS, L. (2001) Sensitivity of mature Erbb2 to geldanamycin is conferred by its kinase domain and is mediated by the chaperone protein Hsp90. *J Biol Chem,* 276**,** 3702-8.

XU, X., ZHAO, J., XU, Z., PENG, B., HUANG, Q., ARNOLD, E. & DING, J. (2004) Structures of human cytosolic NADP-dependent isocitrate dehydrogenase reveal a novel self-regulatory mechanism of activity. *J Biol Chem,* 279**,** 33946-57.

YARDEN, Y. & SLIWKOWSKI, M. X. (2001) Untangling the ErbB signalling network. *Nat Rev Mol Cell Biol,* 2**,** 127-37.

YOCHEM, J., GU, T. & HAN, M. (1998) A new marker for mosaic analysis in Caenorhabditis elegans indicates a fusion between hyp6 and hyp7, two major components of the hypodermis. *Genetics,* 149**,** 1323-34.

YODA, A., KOUIKE, H., OKANO, H. & SAWA, H. (2005) Components of the transcriptional Mediator complex are required for asymmetric cell division in C. elegans. *Development,* 132**,** 1885-93.

YOO, A. S., BAIS, C. & GREENWALD, I. (2004) Crosstalk between the EGFR and LIN-12/Notch pathways in C. elegans vulval development. *Science,* 303**,** 663-6.

ZIPPERLEN, P., NAIRZ, K., RIMANN, I., BASLER, K., HAFEN, E., HENGARTNER, M. & HAJNAL, A. (2005) A universal method for automated gene mapping. *Genome Biol,* 6**,** R19.

8. Acknowledgements

My family deserves the biggest thank you for their great and constant support during the last four years. I am especially grateful to my parents and brother, who were a continuous source of unconditional help and steadiness.
I would like to thank Prof. Alex Hajnal for his supervision of this study. He gave me always a lot of freedom in the choice of my projects and allowed me to work independently. Also I would like to thank my former supervisor, Dr. Attila Stetak, who initiated the *frm-8* and the *tag-60* project.
I want to thank Prof. Moncia Gotta, Prof. Nancy Hynes and Dr. Gino Poulin, who monitored my progress during the last four years and provided me with lots of ideas as members of my thesis committee.
Additionally, I am very grateful for the help from Cécile Gurnot (summer student), David Kradolfer (master student) and Erika Fröhli, who were deeply involved in the *tag-60* and *erm-1* projects.

The deletion mutants isolated during this study, originated from deletion libraries, which were constructed in a joint-effort of various *C. elegans* researchers in Zurich: Erica Bogan, Dr. Claudia Couwenbergs, Marko Jovanovic, Gerhard Seisenbacher, Dr. Esther Zanin and Dr. Attila Stetak.

The FLP-mapping PCR assays of the mutants isolated in the forward genetic screen were performed by Matthias Bodmer and Martin Moser.

I would like to especially express my thanks to Dr. Gino Poulin, who organized the genome wide RNAi screen and introduced me to the world of high-throughput biology. Additionally, I would like to thank Kate Fisher and Dr. Gino Poulin, with whom I performed the RNAi screen and spent a great time in Manchester.

I am very grateful to Dr. Mark Pellegrino, Dr. Juan Escobar, Christina “Nina” Herrmann, Dr. Sara Vassalli, Dr. Ivo Rimann and Sarfarazhussain Farooqui for cross-reading different parts of my thesis and fruitful discussions.

I would like to thank all former and present members of the Hajnal and the Hengartner laboratory, which were always very helpful and who provided me with lots of input during our shared seminar. Special thanks goes to Erica Bogan, Dr. Lukas Neukomm and Stephan Gysi for their honest and direct comments regarding my projects.

Lastly, I want to thank Ivan Ostojic, who performed the statistics on the *tag-60* lifespan assay.

Zurich, March 2009